NONLINEAR DIGITAL COMPUTER CONTROL FOR THE STEAM GENERATOR SYSTEM IN A PRESSURIZED WATER REACTOR PLANT

by

JUNG IN CHOI

B.S. Seoul National University
(Feb. 1979)

M.S. Seoul National University
(Feb. 1981)

SUBMITTED TO THE DEPARTMENT OF NUCLEAR ENGINEERING
IN PARTIAL FULFILLMENT OF THE REQUIREMENTS
FOR THE DEGREE OF

DOCTOR OF PHILOSOPHY

at the

MASSACHUSETTS INSTITUTE OF TECHNOLOGY

August 1987

© JUNG IN CHOI

Signature of Author Signature redacted
Department of Nuclear Engineering
August 1987

Certified by Signature redacted
Professor John E. Meyer
Thesis Supervisor

Certified by Signature redacted
Professor David D. Lanning
Thesis Supervisor

Accepted by Signature redacted
Professor Allan F. Henry
Chairman, Department Graduate Committee

MASSACHUSETTS INSTITUTE OF TECHNOLOGY
DEC 15 1987
LIBRARIES
Archives

NONLINEAR DIGITAL COMPUTER CONTROL FOR THE STEAM GENERATOR SYSTEM IN A PRESSURIZED WATER REACTOR PLANT

by

Jung In Choi

Submitted to the Department of Nuclear Engineering on August 24, 1987, in partial fulfillment of the requirements for the degree of Doctor of Philosophy in Nuclear Engineering

ABSTRACT

Steam generator level control is complicated by thermal effects known as shrink and swell in a pressurized water reactor plant. The water level, measured in the downcomer, temporarily reacts in a reverse manner in response to water inventory changes. These complications are accentuated during start-up or low power conditions. Installed automatic control schemes often behave poorly and are replaced by human operators at low power. Either automatic or manual control gives a reactor trip rate which is found to be too high.

The objective of this research is to develop and evaluate a new controller to ensure a satisfactory automatic control for the steam generator water level from start-up to full power. It is assumed that the current analog control loop is replaced with digital computer control, expanding the range of possible solutions.

A pertinent nonlinear steam generator model is adopted to obtain physical ideas about steam generator dynamics, to develop a new control algorithm, and to substitute for actual plant testing. The simulation results are validated against actual plant data to provide support for model adequacy. A simplified linear model is also deduced through system identification for use in analytic evaluations.

The proposed approach for the new controller is to compensate the level measurement for shrink and swell. This is achieved by the use of two physically-based correction terms and an adaptive adjustment term. The first correction term compensates for a variation in the downcomer level using a calculated change of tube bundle mass. The second correction term accounts for tube bundle mass change that accompanies changes in steady-state operating variables such as power level. The third and final term is an adaptive adjustment to account for model imperfections.

A nonlinear digital observer is developed for calculating the tube bundle mass which is not directly measurable. The input measurements for the observer are the downcomer level, steam generator pressure, feedwater temperature, primary hot leg temperature, primary flow rate and primary pressure. The observer is found to be stable and on-line

applicable with micro-processors.

The proposed controller is evaluated by the various ways in conjunction with the simulation of an existing Westinghouse Type F steam generator. The effectiveness of the proposed correction terms is analytically evaluated and then confirmed with transient simulations. Finally, using a wide range of operating conditions, the performances of the controller are evaluated from the practical point of view. For a multi-ramp power increase from start-up to full power, the proposed controller shows good performances for the entire range. Water level settles down within 3 minutes after a single ramp increase (5% power increase in one minute) without any stability problem. Even at very low power the maximum overshoot is judged to be acceptable.

Thesis Supervisor: John E. Meyer
Title: Professor of Nuclear Engineering

Thesis Supervisor: David D. Lanning
Title: Professor of Nuclear Engineering

ACKNOWLEDGEMENTS

The author would like to express his deepest gratitude to his thesis supervisor, Professor John E. Meyer, for his endless support, guidance, concern and encouragement throughout the course of this research. The author would also like to deeply thank to his thesis co-supervisor, Professor David D. Lanning, for his steady care and invaluable advice.

The author wishes to express his heartful thanks to his wife, Hwa Young, for her devotional support with great patience. Thanks are also due to his daughter, Soyoun, for her encouragement with cuteness.

This research was supported through the Korean Government Scholarship. Special thanks are due to Professor M. Golay for additional financial support.

The author wants to thank to Mr. Paul Blanch, Mr. Nir Bhatt, Mr. Jeff Mahannah and other personnel of Northeast Utilities for their willingness to provide valuable information.

Also special thanks are due to:

- Every member of the Gate Bible Study Group for his/her prayer and care.
- Every member of N.E.D for his/her help and good fellowship during

the life at M.I.T

- Rachel Morton for her technical support in using computers.

- Marsha Levine for her assistance to obtain many technical information

Finally, the author dedicates his thesis to his mother, Jae Yong Yoon, missing her affection for him while in her life.

TABLE OF CONTENTS

page

Abstract 2

Acknowledgements 4

Table of Contents 6

List of Tables 9

List of Figures 10

Chapter 1. INTRODUCTION 16

1.1 Motivations 16

1.1.1 Steam Generator Water Level Control System 16

1.1.2 Digital Technology 19

1.2 Objectives 19

1.2.1 Controller Design 19

1.2.2 Steam Generator Modeling 20

1.3 Background Information 22

1.4 Organization of Thesis 26

Chapter 2. STEAM GENERATOR SYSTEM DESCRIPTION 35

2.1 System Overview 35

2.1.1 Steam Generator Internals 35

2.1.2 Associated Secondary Plant Components 36

2.2 Feedwater Flow Control System 39

2.2.1 Steam Generator Water Level Program 40

2.2.2 Steam Genrator Water Level Control System 42

2.3 Water Level Control Complications 47

2.3.1 "Shrink and Swell" Effects 47

2.3.2 Special Considerations for Low Power Operation ... 49

Chapter 3. Steam Generator Dynamic Model 56

3.1 Steam Generator Model Description 56

3.1.1 Model Regions 56

3.1.2 Secondary Side Model 57

3.1.3 Primary Side Model 76

3.1.4 Numerical Solution 80

3.2 Model Modification 103

3.2.1 Motivation 103

3.2.2 Modifications 105

3.2.3 Modified Equations 106

3.2.4 Modification Effects 110

3.2.5 Model Validation 114

3.3 A Chapter Summary 116

Chapter 4. Controller Design 136

4.1 Conventional Controller 136

4.1.1 Description of a "Conventional Controller" 136

4.1.2 Existing Control Problems 138

4.1.3 Simplified Steam Generator Level Model 142

4.2 Proposed Controller 147

4.2.1 Physically-Based Design Approach 148

4.2.2 Design for an Observer for Tube Bundle Mass.....155

4.2.3 Description of a "Proposed Controller" 160

4.3 A Chapter Summary 170

Chapter 5. Evaluation of Proposed Controller ·····194
5.1 Validation of Physical Ideas ·····194
5.1.1 Steam Generator Variables during Steady Operation ·····194
5.1.2 Steam Generator Variables during Transient Operation ·····196
5.1.3 Sensitivity Study of Correction Terms ·····199
5.2 Application of the Proposed Controller ·····210
5.2.1 Change in Power ·····210
5.2.2 Change in Reference Level ·····212
5.3 A Chapter Summary ·····213
Chapter 6. Summary, Conclusions and Recommendations ·····263
6.1 Summary ·····263
6.2 Conclusions ·····267
6.3 Recommendations ·····268
Appendix A Feed Pump Speed Control System ·····271
Appendix B Detailed Description for Measurements and Actuations ···275
Appendix C Geometric Model for the Steam Generator ·····290
Appendix D System Identification ·····299
Appendix E Stability Analysis of Linear System ·····307
Appendix F Practical Features ·····310
Nomenclatures ·····314
References ·····316

LIST OF TABLES

Table		page
1.1-1	Summary of unplanned automatic turbine/reactor trips in U.S. PWRs for the years 1979-1983 (OPEC DATA)	28
1.1-2	Breakdown of feedwater, condensate, and aux. feedwater trips in U.S. PWRs for the years 1979-1983 (OPEC DATA)	30
1.1-3	Summary of unplaned automatic turbine/reactor trips in U.S. LWRs for the first 6 months of 1984 (LER DATA)	31
1.1-4	Sources of LER failur events during Jan.-Jun. 1984	33
1.1-5	Breakdown of LER failur data for feedwater condensate, aux. feedwater and steam generator level control	34
3.1-1	Partial Derivatives of M_{TB} and E_{TB}	84
3.1-2	Property Derivatives	87
3.1-3	Partial Derivatives of M_R and E_R	88
3.1-4	Partial Derivatives for Eqs.3.1-31 and 3.1-32	89
3.1-5	Partial Derivatives for Eqs.3.1-45 and 3.1-46	91
3.1-6	Partial Derivatives of M_{TBC}	93
3.1-7	Components of matrix $\underline{\underline{A}}$	94
3.2-1	Partial Derivatives for M_{TB} and E_{TB} in the modified model	118
4.1-1	Simplified Model Parameters	172

LIST OF FIGURES

Figure		page
2.1-1	Schematic of steam generator internals	51
2.1-2	Schematic of feedwater and main steam system	52
2.2-1	Steam generator water level control system (from [B1])	53
2.3-1	A pictorial description of the "shrink and swell" phenomena	
	(a) Swell due to steam flow increase or feed flow decrease	54
	(b) Shrink due to feed flow increase or steam flow decrease	55
3.1-1	Primary side regions (from [S4])	98
3.1-2	Secondary side regions (from [S4])	99
3.1-3	Secondary side nomenclature (from [S4])	100
3.1-4	Notation for momentum equation	101
3.1-5	Primary side nomenclature (from [S4])	102
3.2-1	Specific volume profile in the modified model	123
3.2-2	Tube bundle regions in the modified model (a),(b),(c)	124
3.2-3	Specific volume profile change due to the steam flow step-up	125
3.2-4	Transient response of specific volumes to the steam flow step-up	126
3.2-5	Specific volume profile change due to the feed flow step-up	127
3.2-6	Transient response of specific volumes to the feed flow step-up	128
3.2-7	Modification effect in the level response to the steam flow step-up	129

3.2-8 Modifiaction effect in the level response to the feed flow step-up ····130

3.2-9 Modification effect in the controlled level response ····131

3.2-10 Calculated water level with plant data at 12 % power ····132

3.2-11 Feedwater flow input at 12 % power ····133

3.2-12 Calculated water level with plant data at 30 % power ····134

3.2-13 Feedwater flow input at 30 % power ····135

4.1-1 Schematic of the conventional controller ····173

4.1-2 Transient level responses to the power increase (10%→15%)

(a) With variation of level gain ····174

(b) With variation of integral time ····175

(c) With variation of flow gain ····176

4.1-3 Transient level responses to the power increase at the various power levels ····177

4.1-4 Transient level responses at the various power levels

(a) To the feed flow step-up ····178

(b) To the steam flow step-up ····179

4.1-5 Plant data for the feedwater and steam flow measurements ···180

4.1-6 Level response to the power increase (10%→15%) with a small gain and long integral time (K_p=65; and T_i=750 s) ····181

4.1-7 Block diagram for the level control system (P.I) ····182

4.2-1 Level response to the feed flow step-up at 5% power ····183

4.2-2 Decomposed ingredients of level response to the feed flow step-up at 5% power ····184

4.2-3 Mass responses to the feed flow step-up at 5% power ····185

4.2-4 Mass responses to the steam flow step-up at 5% power 186

4.2-5 (a) Internal energy responses to the feed flow step-up at 5% power 187

4.2-5 (b) Internal energy responses to the steam flow step-up at 5% power 188

4.2-6 Compensated level response by the tube bundle mass to the feed flow step-up at 5% power 189

4.2-7 Compensated level response by the tube bundle mass to the steam flow step-up at 5% power 190

4.2-8 Schematic of the proposed controller 191

4.2-9 Inherent tube bundle mass versus power 192

4.2-10 Inherent tube bundle mass versus primary hot-leg temperature 193

5.1-1 Steady-state variables 215

(a) Primary, steam , and feedwater temperatures

(b) Steam pressure

(c) Steam flow rate

(d) Tube bundle, riser, and downcomer mass

(e) Downcomer flow rate

5.1-2 Transient (12%→36%) input for the primary hot-leg temperature, feedwater temperature and steam flow 220

5.1-3 Transient (12%→36%) responses with the proposed controller 222

(a) Calculated power

(b) Steam pressure

(c) Tube bundle mass and downcomer mass

(d) Actual level and compensated level

(e) Feedwater and steam flows

5.1-4 (a) Root-Locus plot for α=0.0 (T_i=200 s; 10% power) ·····227

5.1-4 (b) Transient level response to the power increase (10%→15%) for α= 0.0 with K_p=428.9 and K_p=65 (T_i=200 s) ··228

5.1-5 (a) Root-Locus plot for α=0.0 (T_i=200 s; 50% power) ·····229

5.1-5 (b) Transient level response to the power increase (50%→55%) for α=0.0 with K_p=428.9 (T_i=200 s) ·····230

5.1-6 (a) Root-Locus plot for α=0.0 (T_i=200 s; 95% power) ·····231

5.1-6 (b) Transient level response to the power increase (95%→100%) for α=0.0 with K_p=428.9 (T_i=200 s) ·····232

5.1-7 (a) Root-Locus plot for α=1.0 (T_i=200 s; 10% power) ·····233

5.1-7 (b) Transient level response to the power increase (10%→15%) for α=1.0 with K_p=428.9 and K_p=1000 (T_i=200 s) ·234

5.1-8 Root-Locus plot for α=1.2 (α_m) (T_i=200 s; 10% power) ·····235

5.1-9 Root-Locus plot for α=1.35 (T_i=200 s; 10% power) ·····236

5.1-10 (a) Root-Locus plot for α=1.5 (T_i=200 s; 10% power) ·····237

5.1-10 (b) Transient level response to the power increase (10%→15%) for α=1.5 with K_p=428.9 and K_p=1000 (T_i=200 s) ·238

5.1-11 (a) Root-Locus plot for α=1.8 (α_t) (T_i=200 s; 10% power) ·····239

5.1-11 (b) Transient level response to the power increase (10%→15%) for α=1.8 (α_t) with K_p=428.9 (T_i=200 s) ·····240

5.1-12 (a) Root-Locus plot for α=3.5 (T_i=200 s;10% power) ·····241

5.1-12 (b) Transient level response to the power increase

(10%→15%) for α=3.5 with K_p=428.9 (T_i=200 s) ·····242

5.1-13 Transient level responses to the power increase (10%→15%) with K_p=428.9 for $1.0 \leq \alpha \leq 2.0$ (T_i=200 s) ·····243

5.1-14 (a) Root-Locus plot for α=1.5 with T_i=10 s (10% power) ·····244

5.1-14 (b) Transient level response to the power increase (10%→15%) for α=1.5 with K_p=428.9 and T_i= 10 s ·····245

5.1-15 Transient level response to the power increase (10%→15%) for $0.0 \leq \beta \leq 2.0$ (α=1.8; K_p=428.9;T_i=200 s) ·····246

5.2-1 Transient (5%→100%) input for the primary hot-leg temperature, feedwater temperature and steam flow ·····247

5.2-2 Transient (5%→100%) responses with the proposed controller ·····248

(a) calculated power

(b) narrow range water level

(c) feedwater flow rate

(d) steam pressure

(e) tube bundle, riser, and downcomer mass

(f) primary cold-leg temperature

(g) downcomer flow rate

5.2-3 Plant data

(a) percent power ·····256

(b) narrow range water level ·····257

5.2-4 Transient responses with the 33% to 44% level program

(a) narrow range water level ·····258

(b) tube bundle, riser, and downcomer mass ·····259

5.2-5 Transient level responses to the reference level step-up (100 mm) ····260

(a) at 10% power

(b) at 50% power

(c) at 95% power

A-1 Feed pump speed control system (from [B1]) ····274

B-1 Internals of differential pressure (D/P) sensor (from [B1]) 284

B-2 Steam generator level ranges (from [B1]) ····285

B-3 Internals of pressure sensors (from [B1]) ····286

B-4 Actuation with the main feedwater regulating valve (from [B1]) ····287

B-5 Actuation with the by-pass feedwater regulating valve (from [B1]) ····288

C-1 Steam generator geometrical representation ····296

C-2 Riser region model ····297

C-3 Riser region layout ····298

D-1 Decomposed ingredients of water level for the system identification ····302

(a) at 5% power

(b) at 10% power

(c) at 30% power

(d) at 50% power

(e) at 95% power

Chapter 1

INTRODUCTION

The objective of this research is to develop and evaluate a new controller for water level on the secondary side of a steam generator in a Pressurized Water Reactor (PWR) plant. The new controller is to ensure a satisfactory automatic control from start-up to full power.

As a development stage substitute for actual plant testing, a pertinent computer model for the steam generator is adopted. The model is used to evaluate the performance characteristics of the controller.

In this chapter, the motivation for the new controller development is discussed. The research objectives are then defined in more detail. Following this, a review of previous work is given. Finally, the organization of the remainder of the thesis is addressed.

1.1 Motivations

1.1.1 Steam Generator Water Level Control System

It is essential in a PWR plant to hold the steam generator water level between limits in order to ensure sufficient cooling of the reactor, to provide for good performance of the steam separators and dryers and also to eliminate all risks of hydrodynamic instability. So, if the water level is not maintained within reasonable bounds a reactor trip must be initiated. As a result, a good control system for the water level proves to be a major factor in overall plant

availability (Ref.[W1],[W2]).

During plant transients, the level control is complicated by the thermal reverse effects known as shrink and swell. Due to the presence of steam bubbles in the tube bundle region, the water level measured in the downcomer, temporarily reacts in a reverse manner to water inventory change. These phenomena are accentuated during start-up/low power conditions. At that situation, the only true indication for water inventory change is the relationship between steam flow and feed flow, which, however, is too uncertain to be used for control input. It is well-known that the control schemes traditionally provided do not permit satisfactory automatic level control during start-up/low power conditions. Unsatisfactory performance of automatic level control may either produce a reactor trip or require the operator to take manual control. Even for a skilled operator, it is very hard to react properly in response to the reverse level indications due to the shrink and swell effects.It is frequently observed that the operator's overreaction for restoring the level causes the reactor trip (Ref.[B1],[N1],[S1]).

The previous operating records for unplanned reactor trips illustrate these facts clearly. The results of the OPEC (Operating Plant Evaluation Code) data study (Ref.[S2],[S3]) on 47 U.S. PWR plants for 1979-1983 are depicted in Table 1.1-1 and Table 1.1-2. The largest single item in Table 1.1-1 is the feedwater, condensate system and auxiliary feedwater system (# 07), about 37 percent of the total number of trips. Table 1.1-2 shows the breakdown of the sources or

cause attributed areas of trips in this item. It should be noted that it is difficult to distinguish between the steam generator level control (# 073) and operator error (# 074) categories, which involved essentially the same problem. If combined, at 26 percent, these become the largest single item.

In addition, since the new licensee event report (LER) rule took effect in January of 1984 making reactor trip reports mandatory, more specific records could be obtained. LER data (Ref. [S2]) on reactor trips for the first six months of 1984 are listed in Table 1.1-3, Table 1.1-4 and Table 1.1-5. Despite the inclusion of BWR as well as PWR events, there is a striking similarity between the OPEC data in Table 1.1-1 and LER data in Table 1.1-3. The purpose of a search of LER data is to examine the effect of start-up and low power conditions in particular. In Table 1.1-4, it is noted that 24 of 42 start-up failures or about 60 percent, are originated from the feedwater, condensate and auxiliary feedwater system. As a breakdown of this category, Table 1.1-5 shows that 15 of 27 start-up failures, greater than half, are directly involved in the manual control of steam generator water level.

These obvious evidences from previous operation experiences give support to the urgent need for design improvement in the steam generator water level control system to reduce unplanned reactor trips. The intent of this study is that the troublesome manual control or the largely unsatisfactory automatic control during start-up/low power conditions is to be replaced by a new automatic controller which

can alleviated the existing problems.

1.1.2 Digital Technology

The evolution of powerful microprocessors and the emergence of cost-effective fault-tolerent computer system designs are warranting serious consideration of the application of digital technology to nuclear power plants (Ref.[E1]). The steam generator water level control system in a PWR plant is a prime candidate for application.

The current control system for the steam generator water level is performed by analog control loops which were designed using 10 to 20 years old technology. Efforts to find remedies for control problems associated with the steam generator water level control have been hindered by the limited capabilities of the current analog controller. The flexibility and computing power of digital controllers makes it possible to accommodate with highly sophisticated and advanced algorithms easily in the software. The range of possible algorithms and possible solutions to the previously identified problems is greatly expanded.

1.2 Objectives

1.2.1 Controller Design

The main objective of the research is to develop and evaluate a new controller which always ensures a satisfactory automatic control for the steam generator water level in a PWR plant.

The word "satisfactory" implies good performance in all of the following categories (Ref.[01]):

1) stability

2) capability, and

3) robustness.

We use the term "stability" to designate the controller attribute of the stable response. "Capability" implies a fast effective response in counteracting imposed disturbances. These are the major performance criteria for the controller. As the feedback gain of the controller decreases (or increases), the stability increases (or decreases) but the capability decreases (or increases). So there is a trade-off between these two performance indices. A big design challenge associated with them is the treatment of the shrink and swell effects at low power conditions.

The term robustness implies a measure of controller tolerance to sensor uncertainties, actuator disturbances and changes in component dynamics. At low power conditions, sensor uncertainties in steam flow and feed flow are very large, so the controller must be designed to mitigate or eliminate the dependence on these signals. To survive changes in dynamics, the controller must be provided with a pertinent adaptive scheme. It must also be insensitive to the adverse influences of model imperfections.

1.2.2 Steam Generator Modeling

A pertinent steam generator model is desired for the following

three purposes :

1) to give physical ideas about the steam generator dynamics;
2) to be used for direct incorporation in a controller if it runs fast enough (Ref.[S4],[R1]), and
3) to replace actual plant testing for early evaluation of the controller.

For these purposes, an existing steam generator model (by Strohmayer, Ref.[S4]) has been adopted. This model was originally aimed at higher load rather than lower load. As previously mentioned, particular attention must be paid to start-up or low power conditions for solving the control problems encounted by the current control scheme. So a secondary adopted objective has been to modify the existing steam generator model for the better simulation of the low power dynamics, especially the shrink and swell effects. These modifications must be evaluated by comparing calculation results to actual plant data. It is noted that the modified model should not impair the fast running capability originally provided to permit it to be used for direct incorporation in a controller.

Some of the features of the Strohmayer model (Ref. [S4]) are summarized as follows:

The model is developed using a first principles application of one dimensional conservation equations of mass, momentum, and energy. Two-phase flow is treated by using the drift-flux model. Two salient features of the model are the incorporation of an integrated

secondary-recirculation-loop momentum equation and the retention of all non-linear effects. The inclusion of the integrated loop momentum equation permits calculation of the steam generator water level. The use of a non-linear model, as opposed to linearized model, allows accurate calculation of steam generator conditions for transients with large changes from nominal operating conditions. The model is validated over a wide range of steady-state conditions and a spectrum of transient tests ranging from turbine trip events to a milder full-length control element assembly drop transient. The results of the validation effort indicate that the model is suitable for a broad range of operational transients. Execution speed of the model appears to be fast enough to achieve real time execution on a plant process computer.

1.3 Background Information

In spite of the practical impacts of the control problems in the steam generator water level of PWR plants, it is surprising that little literature exists relevant to those problems in the U.S . Meanwhile, in European countries, especially in France, the steam generator level control has been the subject of intensive studies and publications for many years. Some of them are summarized as follows :

1) The paper of Hocepied et al. (Ref. [H1]) provides a good description of problems associated with steam generator water level control. The paper also describes in some detail the systematic design of a controller water level. The systems so designed were installed on

the Belgian Doel-1 nuclear power plant (two-loop, 390 MWe) and were tested during the early operation of that unit in 1975. Results of the tests showed that automatic control was achieved from zero load to full load and that very large perturbations in load could be accommodated without trips. The paper ends with the statement that "the results obtained are applicable to the control of steam generators of all PWR power stations".

2) The paper of Gautier et al. (Ref. [G1]) describes a computer model of a recirculating U-tube steam generator and the way in which the model supplies insights into steam generator non-linear behavior. The model is assessed by comparing calculated results to plant data. Fessenheim-1 plant (880 MWe) data for a 10 % load step and for a full load rejection are shown as samples. The model is also applied to level controller design. The resulting controller incorporates modifications to an existing design by increasing the feedback gain markedly in the case of large level error signals. The modified version retains an existing variation in gain with power level (implemented by gain increase with increasing feedwater temperatures). The modification was tested at the Bugey-4 plant (900 MWe). From the description of the testing, "The entire test results appeared very encouraging and it is felt that the new design will, after future optimization through simulation techniques, substantially improve automatic level control at very low power levels."

3) The paper of Miossec et al. (Ref. [M1]) gives another good description of the problems of PWR steam generator low load level

control. By developing a numerical model, it allows a good representation of the steam generator internal physics and shows the variation of dynamics in relation with various parameters. It gives a simulation by the model for the dynamics of steam generator at low load (including shrink and swell effects) in the case of steam flow and feed flow step changes. It also describes the model utilization in setting the control parameters for actual plants. It concludes with the statement that "we have to improve the performance of the steam generator level controller beneath ten percent of load where we could have a bad estimation of the steam flow or feed flow."

4) The paper of Irving and Bihoreaux (Ref. [I1],[I2]) describes results of attempts to apply several new control techniques to steam generator water level control. An existing detailed steam generator model is first used to provide calculated results for some transients with small step changes in either steam flow or feed flow. Parameters are obtained through system identification codes to obtain a transfer function representation for a simplified steam generator model. This transfer function produces calculated results that agree with those of the detailed model. Six of seven parameters are found to be functions of steam flow; the seventh is a constant. The simplified model (transfer function for the steam generator dynamics) is used for the analysis of the drawbacks of the classical controllers. This model can be expressed in the state-space equations with four state variables. These equations are directly used for the controller design when combined with several new control techniques. Summarizing statements

indicated that "Only some of them have been checked successfully. Current studies are going on to discover the full implications of the new methods."

5) The paper of Parry et al. (Ref. [P1]) describes progress in steam generator level control in French PWR power plants. Extensive previous work is mentioned that validates steam generator computer models by comparision with data from three-loop 900 MWe plants. Additional excellent comparisions are presented that are based on 1984 data from the Paluel-1 plant (four-loop, 1300 MWe). Features of existing French analog level controllers described. The desirability of additional controller improvements is indicated by noting that 13 % of the cases of reactor trips are caused by steam generator level control. Ninety percent of these cases occured during operation under 30 % power. Plans are outlined for installing digital controllers on all new French four-loop plants. These controllers provide an expanded range of possible control solutions. They have been designed and optimized using the steam generator computer models. Controller features include : a) built-in capabilities to linearize valve control and to operate bypass and main feed valves with the same controller, b) smooth switching from steam flow measurement at high flow to steam flow estimation at low flow, c) similar but independent switching for the input feedwater flow signal, and d) more diverse capabilities for considering controller gains and time constants to be functions of process variables. A version of these digital controllers was installed in 1984 on the Dampierre-4 Unit (three-loop, 900 MWe).

Observed controller behavior indicated that "the first year of operation of the digital steam generator level control system has been fully satisfying. Some modifications will further improve its operation."

The lessons that we have learned from these previous studies are as follows :

1) Good controller designs are not easily achieved. Good progress is noted over the entire interval covered the decade starting in 1975. Yet level control problems are still responsible for too many plant trips.

2) Digital technology greatly expanded the range of possible solution and prompted the interest in control studies.

3) At low load, efforts to develop a good controller are still hindered by the lack of accuracies in steam flow or feed flow measurements. It is noted that the controller with less dependence on these flow measurements may be desirable.

4) A good steam generator model (well validated by using plant data) is an essential ingredient for good controller design.

5) Efforts for direct incorporation of the model into a controller can be based on off-line design calculations but those calculations do suffer from the disturbances of dynamics.

1.4 Organization of Thesis

In Chapter 2, the steam generator system in a PWR plant is

described. It includes the steam generator internals, associated secondary plant components and the steam generator water level control system. The complications of level control are discussed in more detail.

In Chapter 3, the steam generator dynamic model is described. First, the existing model is presented. And then associated with the shrink and swell effects, the modification of the model is described. Finally, the evaluation of the modified model is carried out, comparing caculated results with actual plant data.

In Chapter 4, first, the conventional controller for the steam generator water level is described and its problems are discussed. Then, details of new controller design are described.

In Chapter 5, performances of the new controller are evaluated. The research is summarized with conclusions and recommendations in Chapter 6. Additional details for the research are given in the appendices. Information about the computer program will be available in Ref.[C1].

Table 1.1-1 (Ref. [S2])

SUMMARY OF UNPLANED AUTOMATIC TURBINE/REACTOR TRIPS IN U.S. PWRS FOR THE TEARS 1979-1983 (OPEC DATA)

OPEC CODE	SYSTEM ORIGIN	TOTAL TRIPS	
01	UNDEFINED	14	(1.1%)
02	FUEL	8	(0.6%)
03	REACTOR COOLANT AND CONTROL ROD DRIVE SYSTEM	121	(9.5%)
04	STEAM GENERATOR	17	(1.3%)
05	CHEMICAL AND VOLUM CONTROL SYSTEM	2	(0.2%)
06	CONDENSER	14	(1.1%)
07	CONDENSATE FEEDWATER AND AUX. FEEDWATER SYSTEM	468	(36.7%)
08	MAIN STEAM	65	(5.1%)
09	MAIN TURBINE	156	(12.1%)
10	GENERATOR	73	(5.7%)
11	ELECTRICAL	141	(11.1%)
12	REACTOR PROTECTION SYSTEM	109	(8.6%)
13	AUXILIARY SYSTEM	8	(0.6%)
14	REFUELING AND/OR MAINTENANCE	2	(0.2%)
15	UTILITY GRID	42	(3.3%)
16	CIRCULATING WATER AND SERVICE WATER SYSTEM	17	(1.3%)

Table 1.1-1 (continued)

OPEC CODE	SYSTEM ORIGIN	TOTAL TRIPS	
19	SAFETY INJECTION	6	(0.5%)
20	STARTUP AND TRAINNING	1	(0.1%)
21	PAIRED UNIT IMPACT	1	(0.1%)
22	CONTAINMENT	8	(0.6%)
	TOTAL	1273	(100%)

Table 1.1-2 (Ref. [S2])

BREAKDOWN OF FEEDWATER, CONDENSATE, AND AUX FEEDWATER TRIPS IN U.S. PWRS FOR THE YEARS 1979-1983 (OPEC DATA)

OPEC CODE	AREA OR EQUIPMENT-CAUSE ATTRIBUED TO	TOTAL NO. OF TRIPS		EST. NO. OF CONTROL-RELATED TRIPS
071	FEEDWATER PUMP TRIPS TURBINE, PUMP, MOTOR FAILURE	107	(23 %)	90
072	FEEDWATER REGULATING, BYPASS VALVES AND CONTROLS AIR LINE BREAK	105	(22 %)	50
073	STEAM GENERATOR LEVEL CONTROL	79	(17 %)	79
074	OPERATOR ERROR (USUALLY IN STARTUP SG LEVEL CONTROL), MAINTENANCE ERROR	45	(9 %)	42
075	FEEDAWTER CONTROLS-OTHER	29	(6 %)	29
076	CONDENSATE SYSTEM - PUMP TRIPS OR SUCTION CLOGS, DEMIN, CONDENSER HOTSWELL STORAGE TANK LEVEL	22	(5 %)	10
077	FEEDWATER HEATER, DEAERATOR, DRAIN TANK LEVEL CONTROL	13	(3 %)	13
078	OTHER, MISCELLANEOUS	68	(15 %)	12
	TOTAL	468	(100%)	325

Table 1.1-3 (Ref. [S2])

SUMMARY OF UNPLANED AUTOMATIC TURBINE/REACTOR

TRIPS IN U.S. LWRS FOR THE FIRST 6 MOMTHS OF 1984 (LER DATA)

OPEC CODE	SYSTEM ORIGIN	TOTAL TRIPS	
01	UNDEFINED	0	(0.0%)
02	FUEL	0	(0.0%)
03	REACTOR COOLANT AND CONTROL ROD DRIVE SYSTEM	10	(6.6%)
04	STEAM GENERATOR	5	(3.3%)
05	CHEMICAL AND VOLUM CONTROL SYSTEM	0	(0.0%)
06	CONDENSER	5	(3.3%)
07	CONDENSATE FEEDWATER AND AUX. FEEDWATER SYSTEM	63	(41.5%)
08	MAIN STEAM	15	(9.9%)
09	MAIN TURBINE	18	(11.8%)
10	GENERATOR	8	(5.3%)
11	ELECTRICAL	8	(5.3%)
12	REACTOR PROTECTION SYSTEM	15	(9.9%)
13	AUXILIARY SYSTEM	0	(0.0%)
14	REFUELING AND/OR MAINTENANCE	0	(0.0%)
15	UTILITY GRID	3	(2.0%)
16	CIRCULATING WATER AND SERVICE WATER SYSTEM	0	(0.0%)

Table 1.1-3 (continued)

OPEC CODE	SYSTEM ORIGIN	TOTAL TRIPS	
19	SAFETY INJECTION	1	(1.3%)
20	STARTUP AND TRAINNING	0	(0.0%)
21	PAIRED UNIT IMPACT	0	(0.0%)
22	CONTAINMENT	0	(0.0%)
	TOTAL	152	(100%)

Table 1.1-4 (Ref. [S2])

SOURCES OF LER FAILURE EVENTS DURING JAN.-JUN. 1984

NO. OF FAILURES	SOURCE SYSTEM OR CATEGORY	STARTUP FAILURES	SHUTDOWN FAILURES	TEST FAILURES
51	FEEDWATER, CONDENSATE AUXILIARY FEEDWATER	24	2	3
5	CONDENSER	1	-	1
11	REACTOR PROTECTION	2	1	1
8	REACTOR COOLANT	4	-	-
7	TURBINE PROTECTION	-	-	2
9	TURBINE CONTROL	5	-	3
4	CONTROL ROL DRIVE	-	2	-
11	MAIN STEAM	-	-	6
4	ELECTRICAL	2	-	-
7	MAIN GENERATOR	1	-	-
3	EXTERNAL EVENTS	-	-	-
19	OPERATOR ERROR	3	2	6
13	MAINTENANCE ERROR	-	1	5
152	TOTAL	42	8	31

Table 1.1-5 (Ref. [S2])

BREAKDOWN OF LER FAILURE DATA FOR FEEDWATER

CONDENSATE, AUX. FEEDWATER, AND STEAM GENERATOR LEVEL CONTROL

TOTAL FAILURES	PROBLEM AREA OR SYSTEM	STARTUP FAILURES	CONTROL-RELATED FAILURES
5	REGULATING OR CONTROL VALVE FLOW OR OVERFEED	5	5
6	REGULATING VALVE FAILED SHUT, SHORTS, AIR SUPPLY OR POWER LOST	0	-
15	MANUAL FEED SG LEVEL TRIP	15	15
12	FEEDWATER PUMP CONTROL TRIP TURBINE OIL, LOGIC, LO SUCTION	4	12
3	POWER SUPPLY TO FEEDWATER PUMP	2	-
4	FEEDWATER HEATER LEVEL CONTROL	1	4
1	HEATER DRAIN PUMP	0	-
1	FEEDWATER PIPING OF VALVES	0	-
1	CONDENSATE PUMP	0	-
1	FEEDWATER FLOW TRANSMITTER	0	1
5	INTEGRATED CONTROL SYSTEM	0	5
1	AUX. FEEDWATER VALVE FAILED SHUT	0	-
55	TOTAL	27	42

Chapter 2

STEAM GENERATOR SYSTEM DESCRIPTION

In this Chapter, a basic description of the steam generator, steam system, and feed system as they pertain to the Steam Generator Water Level Control System is provided the background information. The complications of water level control are described in more detail. The features described are based on a current typical PWR plant (4-loop, 1150 MWe), which will be used as an example plant throughout the research (details may differ for other PWR plants).

2.1 System Overview

2.1.1 Steam Generator Internals

The schematic of Fig. 2.1-1 shows some representative features of steam generator internals in a PWR plant (Ref.[B1],[W2]).

Feedwater enters the steam generator from the steam plant, as indicated by the arrow "Feedwater In", through a normally submerged feed ring. This feedwater then mixes with liquid being discharged from liquid-vapor separation devices (this liquid is being recirculated and hence the steam generator is of the recirculating type). The liquid mixture flows downward through the annular "Downcomer" region. Various taps for differential pressure transmitters enter the downcomer region to sense water level for the Steam Generator Water Level Control System. After a turn at the bottom of the downcomer, the liquid is heated during an upward passage outside tubes in the "Tube Bundle"

region. The heat addition causes evaporation of some of the liquid and a two-phase mixture exits from the tube bundle and enters the "Riser". The liquid and vapor are partially separated by swirl vanes at the top of the riser; additional separation occurs in equipment near the top of the steam generator. The "Steam Out" arrow indicates the exit of vapor that is saturated and virtually dry (> 99.75 percent quality). That vapor travels to the steam plant for use in the main turbine and other auxiliaries.

The flow of liquid and vapor described above occurs on the secondary side (or shell side) of the steam generator. The heat addition is supplied by a higher pressure liquid flowing on the primary side (or tube side) of the steam generator. The passage of this liquid through the steam generator is indicated by the arrows "Hot Leg In" and "Cold Leg Out". The primary liquid flow path (up from the hot leg inlet, a semicircular turnaround, then down to the cold leg exit) is described by the term "U-tube steam generator".

2.1.2 Associated Secondary Plant Components

A number of secondary plant components influence on the Steam Generator Water Level Control System either directly or indirectly. A representative group of such components is shown schematically in Fig. 2.1-2. The illustrated components are parts of the feedwater system and the main steam system. They are located in three buildings (the "Containment Building", the "Main Steam Valve Building", and the "Turbine Building"); and they support four steam generators.

Starting near the upper left hand corner of Fig. 2.1-2, the steam going out the steam generator is next intentionally passed through a flow restrictor, "RST", which imposes additional system head loss. The head loss results in a differential steam pressure that is detected by pressure transmitters for steam flow measurement, "W_s". After the steam leaves the restrictor, its pressure is sensed by three pressure transmitters (not shown in Fig. 2.1-2) for the measurement of each steam generator pressure.

The steam travels in the steam line within the main steam valve building, where two types of valves are indicated. These are the "Safety Valves" to prevent excessive steam pressure and the Main Steam Isolation Valves, "MSIVs" that provide for isolating an individual steam generator from the remainder of the main steam system.

Next, the streams are piped to the turbine building, joined in a main steam header, then split for various purposes. Four of the split streams go to the main turbine (each passes through a Main Steam Valve, "MSV", and Main Control Valve, "MCV", which are active, respectively, during the important operations of turbine trip and load control). Two of the other split streams are sent to the Moisture Separator Reheaters, "MSR", for use in reheat operations at higher power levels. Finally, a split stream is available for sending stream directly to the condenser as a "Turbine Bypass" when the MSVs are closed. The point of split is called "Steam Dump System Bypass Header". This header cross-connects the steam lines of all four steam generators. Located on the header is a single pressure transmitter,

"P_s". The steam pressure causes the transmitter to develop a signal, which is used for automatic feed pump speed control and for the steam pressure mode of automatic steam dump operation.

During passage through the main turbines the energy of steam is extracted. After leaving the turbines, the steam enters the condensate system (not shown in Fig. 2.1-2). The condenste system condenses the steam to water at vacuum conditions in the main condenser. Condensate pumps return the water to the feedwater system restarting near the lower right hand corner of Fig. 2.1-2. Feedwater flow enters the suction side of the feedwater pumps. The top two pumps are operating; the remaining pump is available for use in other plant conditions. As the pumps discharge the feedwater, their discharge pressure "P_{fw}" is sensed by the pressure transmitter for the Feed Pump Speed Control System. The discharge streams from the pumps are joined, then are heated during passage through the tube sides of the three indicated feedwater heaters. Discharges from the heaters are gathered in a common line. The common line has branch lines that lead to each of the four steam generators. The feedwater is passed through a venturi to measure feedwater flowrate "W_{fw}" and then continues through the branch lines to a feedwater regulating valve. This valve automatically adjusts the rate of flow through the line in accordance with a positioning signal developed by the Steam Generator Water Level Control System. This valve can also be manually positioned. A bypass valve in a bypass line around the feedwater regulating valve allows feedwater flow control during low-power , low-flow condition. The

bypass valve has both automatic and manual flow control capability. Next, the feedwater flows to the Feedwater Isolation Valves (which isolate the feedwater system from the steam generator on a protective signal) then to the Feedwater System Check Valve (the final system component lying in the feedwater piping to the steam generator feed ring).

2.2 Feedwater Flow Control System

The Feedwater Flow Control System is used to adjust the flow of water to the steam generators either automatically or manually. Using it, the desired steam generator water level can be maintained to provide a proper heat sink for the Reactor Coolant System. Should the plant's situation require it, the Feedwater Flow Control System can automatically isolate feedwater from the steam generator inlets. The Feedwater Flow Control System is composed of two individual, but interdependent subsystems, the Steam Generator Water Level Control System and the Feed Pump Speed Control System.

The Steam Generator Water Level Control System computes a desired level of water in the steam generator that is based on turbine load. To maintain this desired level the Steam Generator Water Level Control System develops a control signal from various level- and flow-indicating parameters. This signal positions the feedwater regulating valve (and thus controls feed flow) for each of the four steam generators. This is the system under consideration in this research.

More details are presented in the following sections.

The Feed Pump Speed Control System is designed to complement the operation of the Steam Generator Water Level Control System. It computes a desired pump speed that is based on the total steam flow. To maintain this computed speed, a control signal is again developed. This signal functions to throttle steam flow to the feed pump turbine (and thus control feed pump speed). Variation of pump speed in this fashion results in reduced erosion of feedwater regulating valve flow control surfaces and improved feedwater regulating valve flow control (throttling) characteristics. The operation of this system is not considered in this research. Additional details for the Feed Pump Speed Control System can be found elsewhere (Ref. [B1],[S1]), as summarized in Appendix [A].

Isolation of normal feedwater flow to the steam generator as a protective function may be required for safe shutdown of both the Reactor Coolant System and the Main Feed System. Isolation is achieved by rapid (5 seconds) closure of each feedwater regulating valve and associated bypass line; along with individual downstream feedwater stop and check valves.

2.2.1 Steam Generator Water Level Program

There are several conditions which must be evaluated prior to choosing the optimum operational steam generator water level. These factors are :

1) The effects of shrink that may cause loss of level indication;

2) The effects of swell that may cause poor moisture separation performance and subsequent turbine damages; and

3) The influence on the magnitude of the peak containment building pressure achieved as a result of a complete blowdown of a steam generator's contents from a steam line rupture.

The first factor sets a lower bound for the programmed level. In other words, with programmed level above this lower bound, the chance that a sudden load rejection will result in shrink sufficient to cause a reactor trip on low-low water level is minimized. The second factor sets an upper bound for the programmed level. The swell produced by some specified step load increase (typically 10%) should not cause the downcomer level to backup into the moisture separators, ruining their effectiveness. The third factor also sets an upper bound on programmed level. A steam line break at hot zero power sets a limit on the maximum allowable steam generator fluid mass. If a steam line break were to occur inside the containment, the subsequent vapor release to the enclosed environment would cause building pressure to rise. The magnitude of this pressure rise is related to the amount of steam released, which would be, in turn, proportional to the steam generator fluid mass. It might seem unusual that limiting the maximum level at hot-zero power will set a maximum allowable steam generator fluid mass. The reason for this is that mass must increase in order for a fixed indicated water level to remain constant as power decreases from 100 percent to 0 percent.

For the Westinghouse model F-type steam generator in a typical

plant, the programmed level is set at 50 % water level for all power levels. It is said that all considerations previously addressed are satisfied with this program. Also the operator is to attempted to maintain at 50 % level when controlling steam generator water level in manual. Meanwhile, for the smaller steam generator of some other PWR plants, the steam generator level is programmed from 33 % level at zero power to 44 % level at twenty percent power and maintained at 44 % level up to full power (Ref.[W2]).

2.2.2 Steam Generator Water Level Control System

The Steam Generator Water Level Control System (Ref.[B1],[W3]), shown in Fig. 2.2-1, computes an electrical control signal that indirectly positions a pneumatically-operated feedwater regulating valve. By regulating feedwater with this valve, the control circuit maintains water level at the programmed level. For simplicity of discussion, only the control circuit and nomenclature associated with the NO. 1 steam generator are presented here and in Fig. 2.2-1.

The Steam Generator Water Level Control System compares actual downcomer water level to programmed water level. The difference between programmed and actual level forms what is called the "level error valve-positioning signal". A positive error signal (programmed > actual level) causes its feedwater regulating valve to open ; a negative error signal (programmed < actual level) causes the valve to move toward a closed position.

The Steam Generator Water Level Control System also compares

steam flow to feed flow. The difference between these values forms a second valve positioning signal known as the "flow error valve-positioning signal". A positive signal (steam flow > feed flow) causes the feedwater regulating valve toward an open position, while a negative signal (steam flow < feed flow) causes throttling down of the valve. The two basic error signals ("level error" and "flow error") determine a "total error" signal.

In Fig. 2.2-1 , detector "LT 519" (or its alternate "LT 551") measures actual downcomer water level. The measured level is lag adjusted prior to being compared with the programmed level. It is desirable during the initial stages of a transient to delay the actual downcomer level signal. This is because the effects of the shrink and swell, which are dicussed in more detail in the next section, mask what is actually happening to the fluid mass within the steam generator. Delaying the actual signal minimizes this disparity and allows the flow error to control the position of the feedwater regulating valve. At the same time, if a level error persists, the level-controlling feature will begin to dominate the total value-positioning signal. This built-in electronic delay automatically serves to dampen natural oscillations in steam generator water level.

The signal of this level program transmitter, like that of LT 519, is lag conditioned in plants with variable programmed level. However, since programmed level in our plant is assigned a constant value of 50 % , the programmed level is constant, too. Therefore the programmed level signal does not vary control circuit response.

A comparator is used to develop an error signal proportional to the difference between actual and programmed level. The output of this comparator serves as an input to a proportional-plus-integral (P.I) level controller. The proportional part of this signal conditioner is simply used to amplify the error signal. The integral portion makes the level error signal increasingly dominant the longer that a level error persists, continuously increasing its output as long as an error signal exists. The time constant associated with the integral portion of the P.I. level controller is very long, precluding an excessively rapid response of the Steam Generator Water Level Control System to level error.

Steam generator steam flow is sensed by FT 512. It is density-compensated using the electrical signal from PT 514 (or its alternate FT 513 / PT 515). Density compensation of steam flow is accomplished in a multiplication circuit that computes steam density based on a linear variation with steam pressure. This is expressed mathematically in the equations :

$$\text{Steam mass flow rate} = K\, P_{PT514}\, (\, \Delta P_{FT512}\,)^{1/2}$$

Actual steam flow rate is taken to be a function of the square root of the pressure differential. Additionally, a constant of proportionality must be electronically inserted into the steam flow rate equation to account for the flow to pressure drop relations based on the physical characteristics of the flow restrictor.

Steam generator feed flow rate is sensed by FT 510 (or its alternate, FT 511), which sends a signal indicative of the rate to a comparator. Transmitter FT 512 sends a signal indicative of steam flow rate to the same comparator. The comparator develops an error signal that is proportional to the difference between steam flow and feed flow. Along with level error, the flow error signal is sent directly to the total error controller.

The total error controller is a P.I controller. Again, the proportional portion is used solely for signal amplification. The major reason for incorporating integral action here is to ensure that feedwater regulating valve progressively opens as plant steam load increases. The use of a strictly proportional controller would produce a minimum electrical output when both level and flow errors were equal to zero. This, of course, would correspond to the fully closed position of the feedwater regulating valve -- obviously giving unacceptable flow setting at high power. Controller integration of input error insures that sufficient output signal strength exists even when the input error is zero. Proper setting of the integral time constant also enhances feed flow stability by minimizing control valve position overshoot. This total error signal is converted into a pneumatic valve-positioning signal using an eletropneumatic (I/P) converter. The output of the converter indirectly acts on the feedwater regulating valve diaphragm actuator, controlling valve position.

Detailed descriptions are contained elsewhere (Ref. [B1]) for the

components of measurements and actuations associated with the Steam Generator Water Level Control System. They are also summarized in Appendix [B].

Automatic and manual operations of steam generator water level are selected at the Automatic/Manual (A/M) Station. Note that this A/M Station is associated only with the steam generator total error controller. Neither remote adjustment of water level nor control of the level error circuit is possible. Operator adjustment of the steam generator automatic water level setpoint is not possible.

When the operator selects MANUAL on the A/M Station, he interrupts the output of the total P.I controller and replaces the output using two manual push bottoms, INCREASE and DECREASE. This enables the operator to vary the control signal directly that is sent to the associated feedwater regulating valve I/P converter.

The total error controller has been designed to produce smooth, "bumpless" transfer upon switching modes of operation. This is desirable in order to preclude large step changes in controller output when shifting back and forth between the manual and automatic mode. When the operator shifts to MANUAL, the signal to the respective I/P converter will remain at the value existing just prior to the transfer. At this time, the operator may change the control signal by pressing his manual push buttons. When the operator returns the controller to automatic operation, the controller output again assumes the value that existed just prior to the transfer. However, if an error exists between steam and feed flow, or actual level and

programmed level, the controller will begin adjusting its output as necessary. Depending on the magnitude of the errors involved, a large feed flow transient could occur. For this reason, the operator is instructed to insure that, prior to transfer from MANUAL to AUTOMATIC, steady-state conditions exist (steam flow equal to feed flow). He should also insure that actual steam generator water level is at the programmed value.

A bypass line with a bypass feedwater regulating valve is provided around each main feedwater regulating valve. This bypass valve is designed to operate at plant start up or low power conditions, which are conditions for which use of the main feedwater regulating valve gives a too sensitive relation between position and flow.

2.3 Water Level Control Complications

2.3.1 " Shrink and Swell " Effects

Steam generator water level control is complicated by phenomena known as the shrink and swell effects. The shrink and swell effects occur within the downcomer -- the sensing region for level measurement. The result of these effects is an apparent change in liquid mass that masks what is really happening to generator water inventory.

The shrink and swell can best be understood by observing fluid behavior in a steam generator during increasing and decreasing steam

flow conditions. As steam flow decreases because of turbine load reduction, the rate of steam removal from the steam generator drops below the rate of steam generation. In a saturated system, this imbalance results in a pressure rise which causes a rapid collapse of steam bubbles that exist in the liquid/vapor mixture in the tube bundle region. With the collapse of the steam bubbles, the volume taken up by the liquid/vapor mass suddenly decreases. Water mass from the downcomer moves into the vacated region, causing the indicated downcomer water level to "shrink", that is, to decrease. However, the fluid mass in the steam generator is actually increasing (feed flow > steam flow).

In the case where steam flow increases, excess steam removal results in a steam generator pressure decrease. The decrease causes expansion of the vapor portion of the liquid/vapor mixture in the tube bundle region. This sudden volume increase displaces water backup into the downcomer, causing the indicated water level to "swell" ; that is, to increase. However, now the actual fluid mass in the steam generator is actually decreasing (feed flow < steam flow).

The shrink and swell effects are also observed during increasing and decreasing feedwater flow, which is usually much colder than saturated recirculating liquid. As cold feedwater flow increases, the inlet enthalpy into the tube bundle region decreases so that the steam bubbles collapse causing the indicated downcomer water level to "shrink". Its result is the same, even though different in mechanism, as that of the steam flow decrease case. As the same token, the result

of the feed flow decrease case is the same as that of the steam flow increase case, causing the indicated downcomer water level to "swell".

The swell phenomena are pictorially described in Fig. 2.3-1 (a), and the shrink phenomena, in Fig. 2.3-1 (b).

2.3.2 Special Considerations for Low Power Operation

Water level at low power conditions is more susceptible to the shrink and swell effects for the following reasons :

1) Relative large fractional change in steam and feed flow rate; and ,

2) Cold feedwater (usually much colder than saturated recirculating liquid at low power conditions)

Because of shrink and swell, the only true indication of whether the amount of water is increasing or decreasing during a transient is the relationship between steam flow and feed flow. However, these flow measurements become too uncertain (perhaps meaningless) to use at low power condition with low flow rates.

Because of these difficulties, the current control schemes do not permit satisfactory automatic level control during low power conditions. Unsatisfactory performance of automatic level control may either produce a reactor trip or require the operator to take manual control. Even with a skilled operator, it is practically very hard for a human to react correctly to every important transient. The operator is apt to overreact to the shrink and swell effects and to cause reactor trips.

At low power, the low flow by-pass valves are used for fine actuation instead of the main feedwater regulating valves. Additional difficulties are faced by the operator when transferring control from the by-pass valve to the main regulating valve when increasing power or with the reverse transfer when decreasing power.

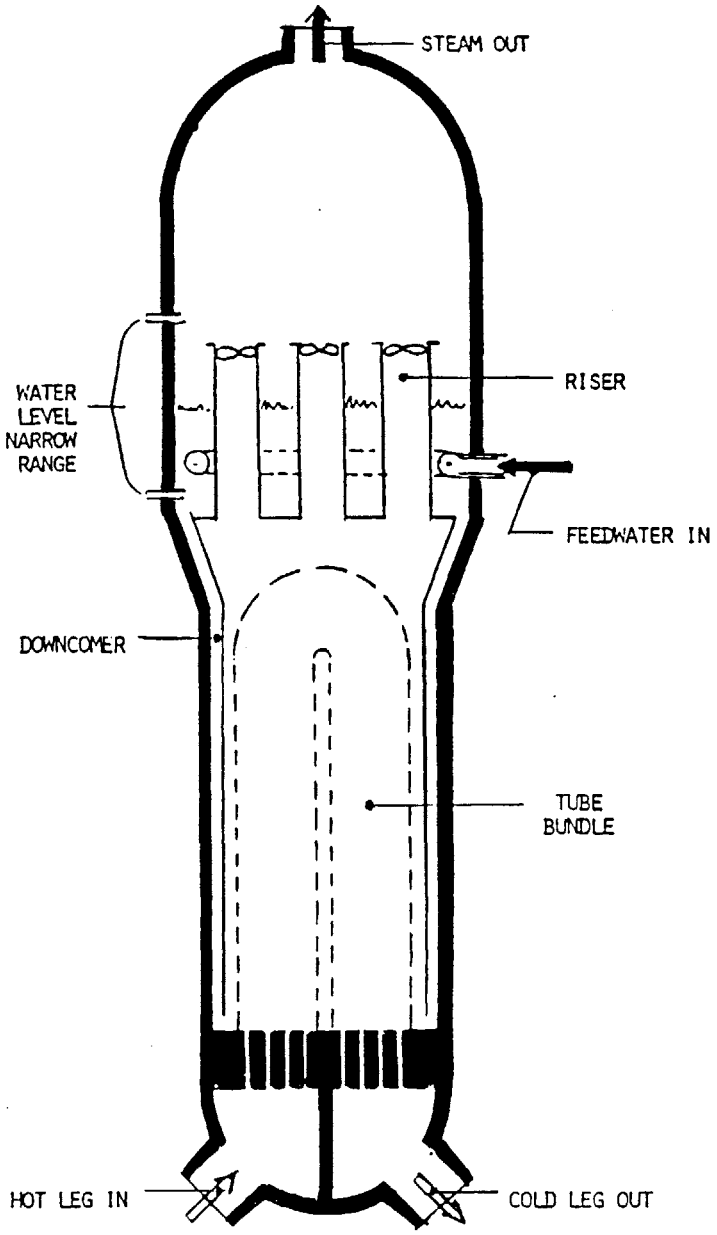

2.1-1 Schematic of steam generator internals

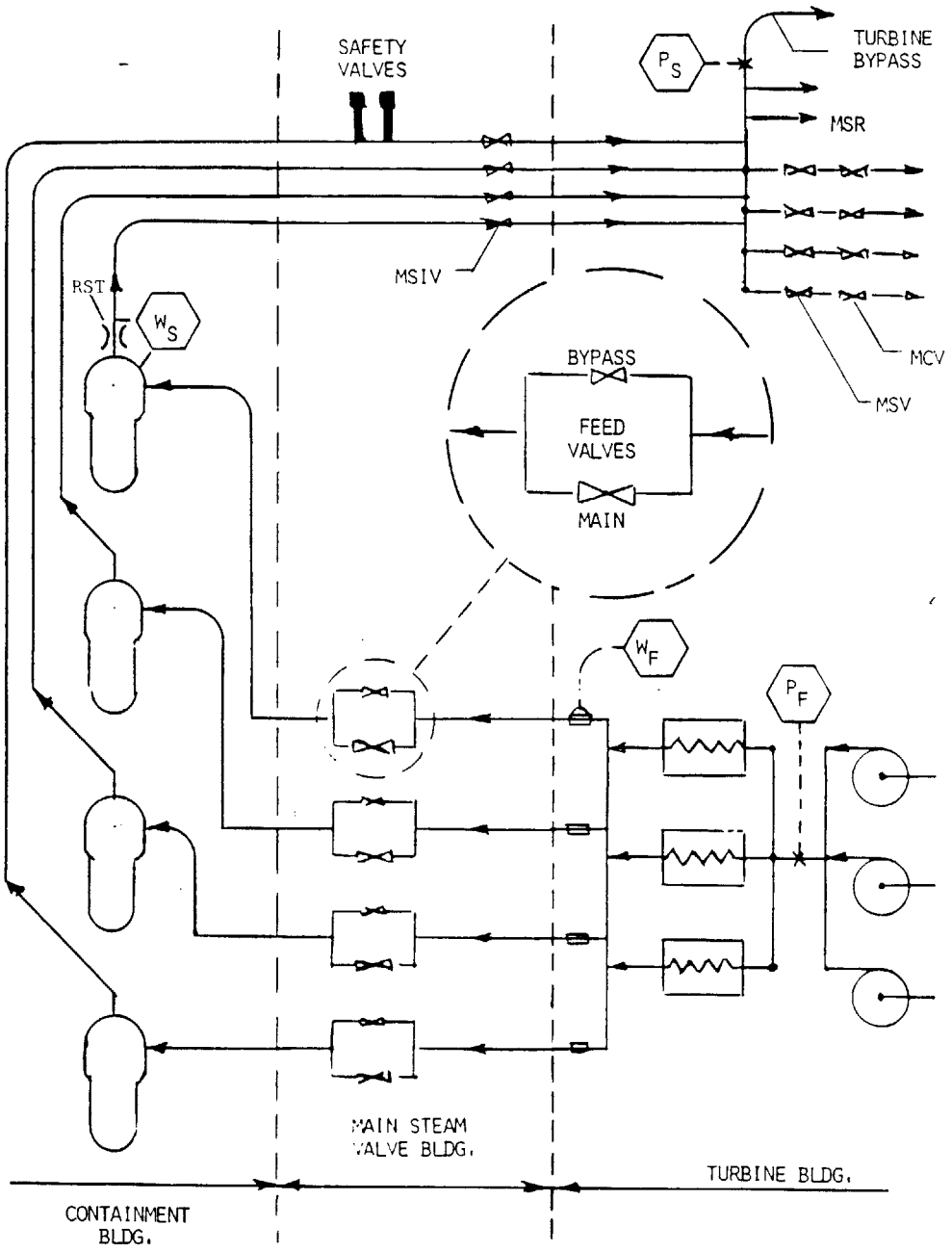

2.1-2 Schematic of feedwater and main steam system

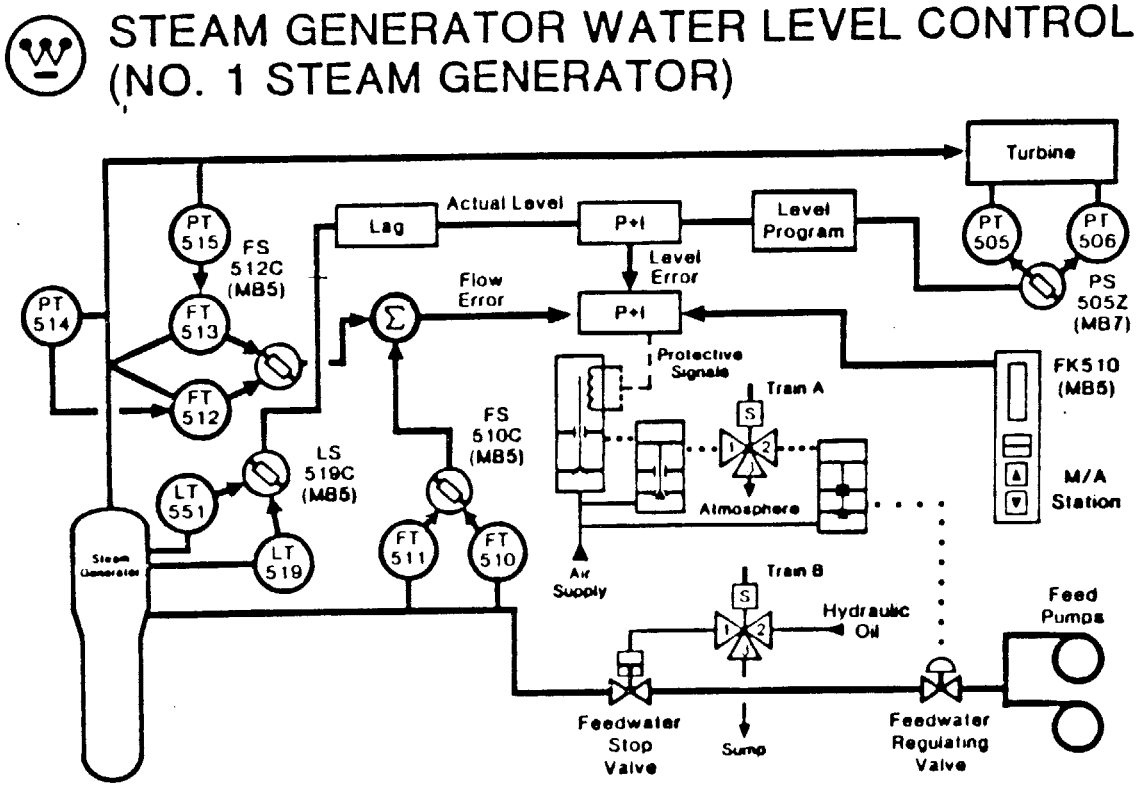

2.2-1 Steam generator water level control system (from [B1])

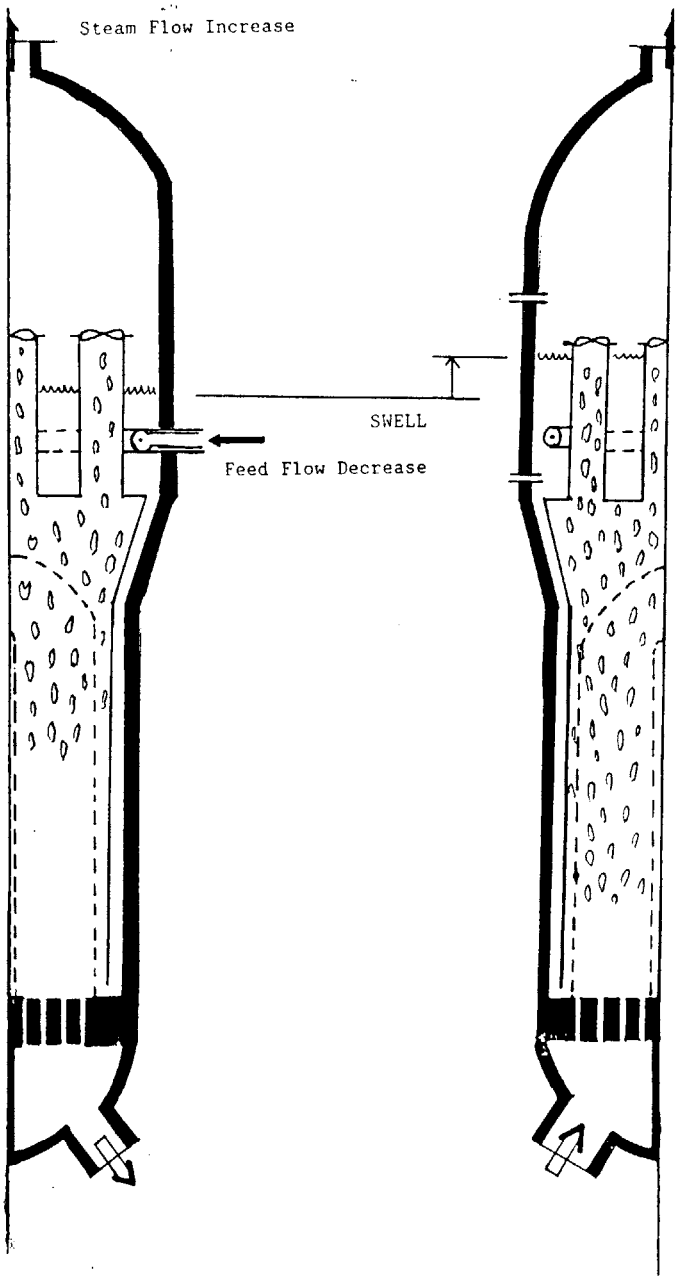

2.3-1 A pictorial description of the "shrink and swell" phenomena

(a) Swell due to steam flow increase or feed flow decrease

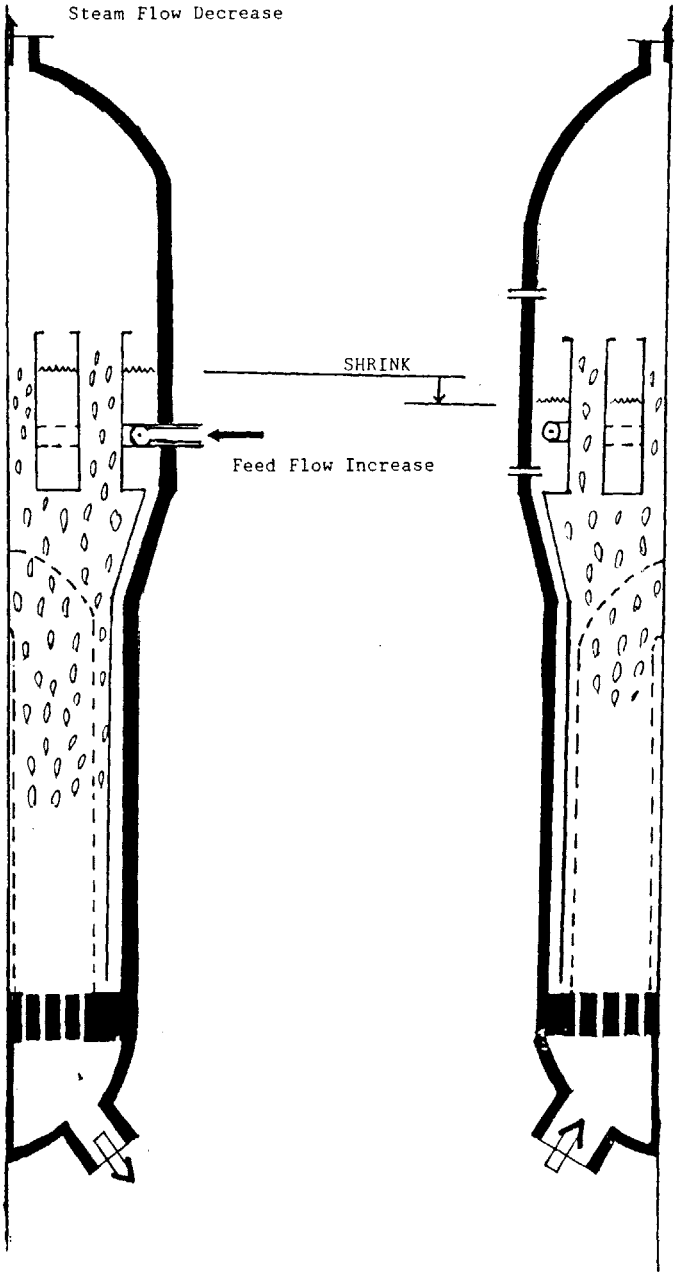

(b) Shrink due to feed flow increase or steam flow decrease

Chapter 3

STEAM GENERATOR DYNAMIC MODEL

An appropriate steam generator model is an essential tool for the design of a steam generator level controller. The steam generator model is to be used to obtain physical ideas about steam generator dynamics, develop a new control algorithm, and substitute for actual plant testing. When the model has a sufficiently fast-running capability to be real time executable, the direct incorporation of the model in a controller becomes possible. For these purposes, an existing steam generator model by Strohmayer (Ref. [S4]) is adopted and modified to improve its low power simulation capabilities.

3.1 Steam Generator Model Description

In this section, the existing steam generator model is described. And then, associated with steam generator low power dynamics, the modification of the model will be discussed in the following sections.

3.1.1 Model Regions

For modeling the steam generator system, it is necessary to divide the whole spatial domain into several regions as control volumes for which basic conservation equations are applied. It is very important to minimize the number of control volumes to achieve a fast-running model. These control volumes must be treated with care to keep sufficient accuracy for cases of interest. To specify the

different physical processes with accuracy, the regions are chosen to correspond to actual physical regions.

The steam generator model adopted in this work has three model control volumes (regions) on the primary side and four model control volumes (regions) on the secondary side. The primary side regions consist of the inlet plenum, the fluid volume within the tubes of the tube bundle, and the outlet plenum (Fig. 3.1-1). The four secondary regions are: the tube bundle region; the riser region; and the steam dome-downcomer, which is divided into a saturated volume and a subcooled volume (Fig. 3.1-2). The saturated and subcooled volumes have a movable interface, the position of which is an unknown variable. This moving boundary approach contributes to minimizing the number of regions as well as the order of the overall system.

3.1.2 Secondary Side Model

A schematic indicating the secondary side regions and variables of interest is shown in Fig. 3.1-3 (see nomenclature for variable identification). Governing mass and energy relations are obtained by applying the conservation equations of mass and energy to each region and by making suitable assumptions about the distribution of contents inside the region.

3.1.2.1 Tube Bundle Region

Applying the mass and energy equations to this region, we obtain

:

$$\frac{d\,M_{TB}}{d\,t} = W_o - W_r \qquad (3.1-1)$$

and

$$\frac{d\,E_{TB}}{d\,t} = W_o H_o - W_r H_r + q_B \qquad (3.1-2)$$

Linking these two equations by eliminating W_r , the equation is :

$$\frac{d\,E_{TB}}{d\,t} - H_r \frac{d\,M_{TB}}{d\,t} = W_o (H_o - H_r) + q_B \qquad (3.1-3)$$

To determine M_{TB} and E_{TB} , linear approximate profiles for specific volume $\bar{v}$ ($= 1/\bar{\rho}$) and internal energy $\bar{U}$ are used. That is :

$$\frac{1}{\bar{\rho}} = \left[\frac{1}{\bar{\rho}_r} - \frac{1}{\rho_o} \right] \frac{z}{L_{TB}} + \frac{1}{\rho_o} \qquad (3.1-4)$$

and

$$\bar{U} = (\bar{U}_r - U_o) z / L_{TB} + U_o \qquad (3.1-5)$$

Then the definitions of M_{TB} and E_{TB} yield :

$$M_{TB} = \int_0^{V_{TB}} \bar{\rho}\ dV = \left[\frac{V_{TB}\ \rho_o \bar{\rho}_r}{\rho_o - \bar{\rho}} \right] \ln \left(\frac{\rho_o}{\bar{\rho}_r} \right) \qquad (3.1-6)$$

and

$$E_{TB} = \int_0^{V_{TB}} \bar{\rho}\,\bar{U}\; dV$$

$$= M_{TB}\left[\frac{\bar{U}_r - U_o}{\ln(\rho_o / \bar{\rho}_r)} + \frac{(\rho_o U_o - \bar{\rho}_r U_r)}{\rho_o - \bar{\rho}_r}\right] \qquad (3.1-7)$$

To determine the time derivatives of M_{TB} and E_{TB}, we need to specify the state variables. Both M_{TB} and E_{TB} depend only on the values of the fluid properties at the inlet and outlet of tube bundle. These properties can be uniquely determined with the state variables : the system pressure, p ; the subcooled liquid inlet internal energy, U_o ; and the vapor volume fraction at the tube bundle exit, $\langle\alpha_r'\rangle$. The total derivatives of M_{TB} and E_{TB} are :

$$\frac{d M_{TB}}{d t} = \left(\frac{\partial M_{TB}}{\partial U_o}\right)_{\langle\alpha_r\rangle,p} \frac{d U_o}{d t} + \left(\frac{\partial M_{TB}}{\partial \langle\alpha_r\rangle}\right)_{U_o,p} \frac{d\langle\alpha_r\rangle}{d t}$$

$$+ \left(\frac{\partial M_{TB}}{\partial p}\right)_{\langle\alpha_r\rangle,U_o} \frac{d p}{d t} \qquad (3.1-8)$$

and

$$\frac{d E_{TB}}{d t} = \left(\frac{\partial E_{TB}}{\partial U_o}\right)_{\langle\alpha_r\rangle,p} \frac{d U_o}{d t} + \left(\frac{\partial E_{TB}}{\partial \langle\alpha_r\rangle}\right)_{U_o,p} \frac{d\langle\alpha_r\rangle}{d t}$$

$$+ \left(\frac{\partial E_{TB}}{\partial p}\right)_{\langle\alpha_r\rangle,U_o} \frac{d p}{d t} \qquad (3.1-9)$$

The partial derivatives appearing in Eqs. (3.1-8) and (3.1-9) and associated property derivatives are shown in Tables 3.1-1 and 3.1-2. Plugging Eqs. (3.1-8) and (3.1-9) into Eq. (3.1-3), the resulting equation for the tube bundle region can be obtained :

$$B_1 \frac{d\,U_o}{d\,t} + B_2 \frac{d\,\langle\alpha_r\rangle}{d\,t} + B_3 \frac{d\,p}{d\,t} = W_o\,(H_o - H_r) + q_B \qquad (3.1\text{-}10)$$

where

$$B_1 = \left(\frac{\partial\,E_{TB}}{\partial\,U_o}\right)_{\langle\alpha_r\rangle,p} - H_r \left(\frac{\partial\,M_{TB}}{\partial\,U_o}\right)_{\langle\alpha_r\rangle,p}$$

$$B_2 = \left(\frac{\partial\,E_{TB}}{\partial\,\langle\alpha_r\rangle}\right)_{U_o,p} - H_r \left(\frac{\partial\,M_{TB}}{\partial\,\langle\alpha_r\rangle}\right)_{U_o,p}$$

$$B_3 = \left(\frac{\partial\,E_{TB}}{\partial\,p}\right)_{\langle\alpha_r\rangle,U_o} - H_r \left(\frac{\partial\,M_{TB}}{\partial\,p}\right)_{\langle\alpha_r\rangle,U_o}$$

3.1.2.2 Riser Region

As in the case of tube bundle, the mass and energy equations are :

$$\frac{d\,M_R}{d\,t} = W_r - W_n \qquad (3.1\text{-}11)$$

and

$$\frac{d\,E_R}{d\,t} = W_r\,H_r - W_n\,H_n \qquad (3.1\text{-}12)$$

By eliminating $\bar{W}_n$ with these two, the resulting equation is :

$$\frac{d\,E_R}{d\,t} - H_n \frac{d\,M_R}{d\,t} = W_r\,(H_r - H_n) \qquad (3.1\text{-}13)$$

The profiles of density and density product internal energy are :

$$\bar{\rho} = \rho_{\ell s} + <\alpha>\,(\rho_{vs} - \rho_{\ell s}) \qquad (3.1\text{-}14)$$

$$\bar{\rho}\,\bar{U} = \rho_{\ell s}\,U_{\ell s} + <\alpha>\,(\rho_{vs}\,U_{vs} - \rho_{\ell s}\,U_{\ell s}) \qquad (3.1\text{-}15)$$

where $<\alpha>$ is taken to be linear with respect to a volume coordinate between $<\alpha_r>$ and $<\alpha_n>$.

Thus

$$M_R = \int_{V_R} \bar{\rho}\,dV = \frac{V_R}{2}\,(\bar{\rho}_r + \bar{\rho}_n) \qquad (3.1\text{-}16)$$

and

$$E_R = \int_{V_R} \bar{\rho}\,\bar{U}\,dV = \frac{V_R}{2}\,(\bar{\rho}_r\,\bar{U}_r + \bar{\rho}_n\,\bar{U}_n) \qquad (3.1\text{-}17)$$

The following quantities are chosen as state variables for the riser region: the system pressure, p; inlet vapor volume fraction, $<\alpha_r>$; and exit vapor volume fraction, $<\alpha_n>$. The total derivatives of M_R and E_R can be written as,

$$\frac{d\,M_R}{d\,t} = \left(\frac{\partial\,M_R}{\partial\,\langle\alpha_r\rangle}\right)_{\langle\alpha_n\rangle,p} \frac{d\,\langle\alpha_r\rangle}{d\,t} + \left(\frac{\partial\,M_R}{\partial\,\langle\alpha_n\rangle}\right)_{\langle\alpha_r\rangle,p} \frac{d\,\langle\alpha_n\rangle}{d\,t}$$

$$+ \left(\frac{\partial\,M_R}{\partial\,p}\right)_{\langle\alpha_r\rangle,\langle\alpha_n\rangle} \frac{d\,p}{d\,t} \qquad (3.1\text{-}18)$$

and

$$\frac{d\,E_R}{d\,t} = \left(\frac{\partial\,E_R}{\partial\,\langle\alpha_r\rangle}\right)_{\langle\alpha_n\rangle,p} \frac{d\,\langle\alpha_r\rangle}{d\,t} + \left(\frac{\partial\,E_R}{\partial\,\langle\alpha_n\rangle}\right)_{\langle\alpha_r\rangle,p} \frac{d\,\langle\alpha_n\rangle}{d\,t}$$

$$+ \left(\frac{\partial\,E_R}{\partial\,p}\right)_{\langle\alpha_r\rangle,\langle\alpha_n\rangle} \frac{d\,p}{d\,t} \qquad (3.1\text{-}19)$$

The partial derivatives are given in Table 3.1-3. Plugging these equations into Eq. (3.1-13) , the resulting equation for the riser region is:

$$B_4 \frac{d\,\langle\alpha_r\rangle}{d\,t} + B_5 \frac{d\,\langle\alpha_n\rangle}{d\,t} + B_6 \frac{d\,p}{d\,t} = W_r\,(H_r - H_n) \qquad (3.1\text{-}20)$$

where

$$B_4 = \left(\frac{\partial\,E_R}{\partial\,\langle\alpha_r\rangle}\right)_{\langle\alpha_n\rangle,p} - H_n \left(\frac{\partial\,M_R}{\partial\,\langle\alpha_r\rangle}\right)_{\langle\alpha_n\rangle,p}$$

$$B_5 = \left(\frac{\partial E_R}{\partial \langle \alpha_n \rangle} \right)_{\langle \alpha_r \rangle, p} - H_n \left(\frac{\partial M_R}{\partial \langle \alpha_n \rangle} \right)_{\langle \alpha_r \rangle, p},$$

and

$$B_6 = \left(\frac{\partial E_R}{\partial p} \right)_{\langle \alpha_r \rangle, \langle \alpha_n \rangle} - H_n \left(\frac{\partial M_R}{\partial p} \right)_{\langle \alpha_r \rangle, \langle \alpha_n \rangle}$$

3.1.2.3 Steam Dome and Downcomer

The steam dome - downcomer region is divided into two control volumes : the saturated and subcooled volumes. For each volume, the conservation equations are applied. Two cases are considered. For Case 1, each control volume corresponds to the fixed physical region : the saturated volume to the steam dome and the subcooled volume to the downcomer. For Case 2, each control volume is not fixed but varies with time. The moving interface between these two control volumes is chosen as unknown.

The details and assumptions for each case are given in Ref. [S4]. Briefly, the case 1 is used for higher water levels. Some fixed level (e.g. the feed ring) is chosen to devide the saturated region from the subcooled region. For case 2, used for lower levels, it is assumed that some fixed volume of saturated liquid always exists. The switch from one case to another occurs when the saturation volumes for the two cases are equal.

[CASE 1]

For the saturated control volume (equivalent to the steam dome

region), the conservation equations are :

$$\frac{d\,M_{SAT}}{d\,t} = W_n - W_s - W_f \qquad (3.1\text{-}21)$$

$$\frac{d\,E_{SAT}}{d\,t} = W_n\,H_n - W_s\,H_{vs} - W_f\,H_{\ell s} \qquad (3.1\text{-}22)$$

Eliminating W_f , the resulting equation is ,

$$\frac{d\,E_{SAT}}{d\,t} - H_{\ell s}\frac{d\,M_{SAT}}{d\,t} = W_n\,(H_n - H_{\ell s}) - W_s\,(H_{vs} - H_{\ell s}) \qquad (3.1\text{-}23)$$

By definition,

$$M_{SAT} = \int_0^{V_{SD}} \rho\,dV + \int_0^{V_{STM}} \rho\,dV$$

$$= \rho_{\ell s} V_{SD} + (\rho_{vs} - \rho_{\ell s})\,V_V + \rho_{vs}\,V_{STM} \qquad (3.1\text{-}24)$$

$$E_{SAT} = \int_0^{V_{SD}} \rho\,U\,dV + \int_0^{V_{STM}} \rho\,U\,dV$$

$$= \rho_{1s}\,U_{\ell s}\,V_{SD} + (\rho_{vs}\,U_{VS} - \rho_{\ell s}\,U_{\ell s})\,V_V$$

$$+ \rho_{vs} U_{VS} V_{STM} \qquad (3.1\text{-}25)$$

where

V_{SD} : volume of steam dome;

V_V : volume of saturated steam in the steam dome ; and

V_{STM} : volume of main steam line

Next, for the subcooled control volume (equivalent to the downcomer region), the conservation equations are :

$$\frac{d M_{SUB}}{d t} = W_{fw} + W_f - W_o \qquad (3.1\text{-}26)$$

$$\frac{d E_{SUB}}{d t} = W_{fw} H_{fw} + W_f H_{\ell s} - W_o H_o \qquad (3.1\text{-}27)$$

Eliminating W_f , the resulting equation is :

$$\frac{d E_{SUB}}{d t} - H_{\ell s} \frac{d M_{SUB}}{d t} = W_{fw} (H_{fw} - H_{\ell s}) - W_o (H_o - H_{\ell s}) \qquad (3.1\text{-}28)$$

Approximately,

$$M_{SUB} = \int_0^{V_D} \rho \, dV = \rho_o V_D \qquad (3.1\text{-}29)$$

$$E_{SUB} = \int_0^{V_D} \rho\, U\, dV = \rho_o\, U_o\, V_D \qquad (3.1\text{-}30)$$

where V_D is the downcomer volume.

M_{SAT} and E_{SAT} are determined by pressure and vapor volume, which are chosen as the state variables. Note that vapor volume can be converted directly to water level (with the assumption that negligible mass of liquid is contained in the drain passages coming from the separators) Through the same procedures as the previous cases, the resulting equation yields:

$$B_7 \frac{d\,V_V}{d\,t} + B_8 \frac{d\,p}{d\,t} = W_n\,(H_n - H_{\ell s}) - W_s\,(H_{vs} - H_{\ell s}) \qquad (3.1\text{-}31)$$

where,

$$B_7 = \left(\frac{\partial\, E_{SAT}}{\partial\, V_V}\right)_p - H_{\ell s}\left(\frac{\partial\, M_{SAT}}{\partial\, V_V}\right)_p$$

and

$$B_8 = \left(\frac{\partial\, E_{SAT}}{\partial\, p}\right)_{V_V} - H_{\ell s}\left(\frac{\partial\, M_{SAT}}{\partial\, p}\right)_{V_V}$$

For M_{SUB} and E_{SUB}, the pressure and internal energy of the subcooled liquid are chosen as the state variables. The resulting

equation yields :

$$B_9 \frac{d U_o}{d t} + B_{10} \frac{d p}{d t} = W_{fw} (H_{fw} - H_{\ell s}) - W_o (H_o - H_{\ell s}) \qquad (3.1 -32)$$

where,

$$B_9 = \left(\frac{\partial E_{SUB}}{\partial U_o} \right)_p - H_{\ell s} \left(\frac{\partial M_{SUB}}{\partial U_o} \right)_p$$

and

$$B_{10} = \left(\frac{\partial E_{SUB}}{\partial p} \right)_{U_o} - H_{\ell s} \left(\frac{\partial M_{SUB}}{\partial p} \right)_{U_o}$$

all partial derivatives are given in Table 3.1-4.

[CASE 2]

The mass equation is applied to the saturated control volume :

$$\frac{d M_{SAT}}{d t} = W_n - W_s - \rho_{\ell s} (u_{\ell s} - u_i) A_i \qquad (3.1 -33)$$

where $u_{\ell s}$ and u_i are the velocities of saturated liquid and interface respectively (in the vicinity of the interface).
The quantity $\rho_{\ell s} u_{\ell s} A_i$ is equal to the flow rate across the interface if the interface is stationary, W_f and the quantity

$\rho_{\ell s}\ u_i\ A_i$ is a term due to the motion of the interface, which is equal to $\rho_{\ell s}\ (\ dV_v\ /\ dt\ )$. Thus Eq. (3.1-33) yields :

$$\frac{d\ M_{SAT}}{d\ t} - \rho_{\ell s}\ \frac{d\ V_V}{d\ t} = W_n - W_s - W_f \qquad (\ 3.1\ -34\ )$$

The energy equation for the saturated control volume is :

$$\frac{d\ E_{SAT}}{d\ t} = W_n\ H_n - W_s\ H_{\ell vs} - \rho_{\ell s}\ (\ u_{\ell s} - u_i\ )\ A_i\ H_k - p\ \frac{d\ V_V}{d\ t} \qquad (\ 3.1\ -35\ )$$

where,

$$H_k \begin{cases} = H_{ls} & \text{if } u_{\ell s} \geq u_i \\ = H_o & \text{if } u_{\ell s} < u_i \end{cases}$$

Last two terms in Eq. (3.1-35) are the convective term and work term. This equation can be rewritten as,

$$\frac{d\ E_{SAT}}{d\ t} - (\ \rho_{\ell s}\ H_k - p\ )\ \frac{d\ V_V}{d\ t} = W_n\ H_n - W_s\ H_{vs} - W_f\ H_k \qquad (\ 3.1\ -36\ )$$

Performing same procedures for the subcooled control volume, we can get :

$$\frac{d\,M_{SUB}}{d\,t} + \rho_{\ell s}\frac{d\,V_V}{d\,t} = W_{fw} - W_o + W_f \qquad (3.1\text{-}37)$$

$$\frac{d\,E_{SUB}}{d\,t} + (\rho_{\ell s}\,H_k - p)\frac{d\,V_V}{d\,t} = W_{fw}\,H_{fw} + W_f\,H_k - W_o\,H_o \qquad (3.1\text{-}38)$$

Eliminating W_f , the resulting equations for these control volumes are :

$$\frac{d\,E_{SAT}}{d\,t} - H_k\frac{d\,M_{SAT}}{d\,t} + p\frac{d\,V_V}{d\,t} = W_n\,(H_n - H_k) - W_s\,(H_{vs} - H_k) \qquad (3.1\text{-}39)$$

and

$$\frac{d\,E_{SUB}}{d\,t} - H_k\frac{d\,M_{SUB}}{d\,t} - p\frac{d\,V_V}{d\,t} = W_{fw}\,(H_{fw} - H_k) - W_o\,(H_o - H_k) \qquad (3.1\text{-}40)$$

M_{SAT} and E_{SAT} are given by,

$$M_{SAT} = V_{fo}\,\rho_{\ell s} + (V_V + V_{STM})\,\rho_{vs} \qquad (3.1\text{-}41)$$

and

$$E_{SAT} = V_{fo}\,\rho_{\ell s}\,u_{\ell s} + (V_V + V_{STM})\,\rho_{vs}\,u_{vs} \qquad (3.1\text{-}42)$$

For M_{SUB} and E_{SUB} ,

$$M_{SUB} = (V_{TOT} - V_V - V_{fo}) \rho_o \qquad (3.1 -43)$$

and

$$E_{SUB} = (V_{TOT} - V_V - V_{fo}) \rho_o U_o \qquad (3.1 -44)$$

where,

$V_{TOT} = V_{SD} + V_D$: volume of steam dome and downcomer, , and

V_{fo} : volume of saturated liquid

The state variables are the system pressure, p , and vapor volume, V_V for the saturated volume and additionally internal energy, U_o for the subcooled volume. Performing the same manupulation for Case 1 , Eqs. (3.1-39) and (3.1-40) yield respectively :

$$B_{11} \frac{d V_V}{d t} + B_{12} \frac{d p}{d t} = W_n (H_n - H_k) - W_s (H_{vs} - H_k) \qquad (3.1 -45)$$

and

$$B_{13} \frac{d U_o}{d t} + B_{14} \frac{d V_V}{d t} + B_{15} \frac{d p}{d t} = W_{fw} (H_{fw} - H_k) \qquad (3.1 -46)$$

where,

$$B_{11} = \left(\frac{\partial E_{SAT}}{\partial V_V} \right)_p - H_k \left(\frac{\partial M_{SAT}}{\partial V_V} \right)_p + p$$

$$B_{12} = \left(\frac{\partial E_{SAT}}{\partial p} \right)_{V_V} - H_k \left(\frac{\partial M_{SAT}}{\partial p} \right)_{V_V}$$

$$B_{13} = \left(\frac{\partial E_{SUB}}{\partial U_o} \right)_{V_V,p} - H_k \left(\frac{\partial M_{SUB}}{\partial U_o} \right)_{V_V,p}$$

$$B_{14} = \left(\frac{\partial E_{SUB}}{\partial V_V} \right)_{U_o,p} - H_k \left(\frac{\partial M_{SUB}}{\partial V_V} \right)_{U_o,p}$$

and

$$B_{15} = \left(\frac{\partial E_{SUB}}{\partial p} \right)_{U_o,V_V} - H_k \left(\frac{\partial M_{SUB}}{\partial p} \right)_{U_o,U_o}$$

All partial derivatives are given in Table 3.1-5.

3.1.2.4 Momentum Equation for the Recirculation Flow

A one-dimensional momentum equation is applied to the recirculating loop consisting of connected flow paths through the tube bundle, riser, steam dome and downcomer. The momentum equation for this loop is :

$$I \frac{d \bar{W}}{d t} = \Delta p - F \qquad (3.1\text{-}47)$$

where,

$$I = \oint \frac{ds}{A} \quad ;$$

$$\bar{W} = \oint \frac{W\, ds}{A} \Big/ I \quad ;$$

$$\Delta p = \oint \left(- \frac{\partial p}{\partial s} \right) ds = 0 \quad (\text{closed loop}) \quad ;$$

and

$$F = \oint \frac{1}{A} d \left(\frac{V' W^2}{A} \right) + \oint \frac{f W |W| ds}{2 \rho D_n A^2} + \oint \rho g \sin \theta \, ds$$

$$+ \sum_i \frac{K_i W_i^2}{2 \rho_i A_i^2}$$

All loop integrals are performed in a piecewise manner :

$$\oint = \sum_i \int_{R_i}$$

where, R_i is the i-th flow path of the loop , such as the tube bundle, riser, steam dome or dowmcomer region.

The tube bundle region is divided into two parts: a parallel flow portion in which is essentially parallel to the tube ; and a crossflow portion in which flow is predominantly transverse to the tube.

Geometrical notations for the momentum equation are given Fig. 3.1-4.

For the inertia I ,

$$I = \frac{L_P}{A_{TB}} + \frac{(L_{TB} - L_P)}{2}\left(\frac{1}{A_{TB}} + \frac{1}{A_{RI}}\right) + \frac{L_R}{2}\left(\frac{1}{A_{RI}} + \frac{1}{A_{RO}}\right)$$

$$+ \frac{(\ell_w - L_D)}{2}\left(\frac{1}{A_W} + \frac{1}{A_D}\right) + \frac{L_D}{A_D} \qquad (3.1\text{-}48)$$

And,

$$\bar{W} = \beta_1' W_o + \beta_2' W_p + \beta_3' W_r + \beta_4' W_n \qquad (3.1\text{-}49)$$

where,

$$I\,\beta_1' = \frac{(\ell_w - L_D)}{2}\left(\frac{1}{A_w} + \frac{1}{A_D}\right) + \left(\frac{L_D}{A_D} + \frac{L_D}{2\,A_{TB}}\right) ,$$

$$I\,\beta_2' = \frac{L_{TB}}{A_{TB}} ,$$

$$I\,\beta_3' = \frac{L_{TB} - L_P + L_R}{2\,A_{RI}} , \text{ and}$$

$$I\,\beta_4' = \frac{L_R}{2A_{RO}}$$

It is noted that $\sum_i^4 \beta_i' = 1$.

The last term of Eq. (3.1-46), F , consists of friction, acceleration, gravitation and other losses. That is :

$$F = F_f + F_a + F_g + F_o \qquad (3.1\text{-}50)$$

where,

$$F_f = \left(\frac{f_D L_D}{2 \rho_o D_{hD} A_D^2} + \frac{L_p f_o}{4 \rho_o D_{hTB} A_{TB}^2} \right) W_o |W_o| + \left(\frac{K_c}{2 \rho_{\ell s}} + \frac{L_p f_{\ell s,p}}{4 \rho_{\ell s} D_{hTB} A_{TB}^2} \right) W_p |W_p| \phi_{\ell o,p}^2 + \left(\frac{K_c}{2 \rho_{\ell s}} \right) W_r |W_r| \phi_{\ell o,r}^2$$

where

$\phi_{\ell o}^2$: two-phase multiplier

K_c : cross flow frictional loss coefficient

$$F_a = \left(\frac{1}{A_D^2} - \frac{1}{A_w^2} - \frac{2}{A_{TB}^2} \right) \frac{W_o^2}{2 \rho_o} + \left(\frac{1}{A_{TB}} - \frac{1}{A_{RI}} \right) \frac{V_p' W_p^2}{2 A_{TB}} + \left(\frac{1}{A_{TB}} - \frac{1}{A_{RO}} \right) \frac{V_r' W_r^2}{2 A_{RI}} + \left(\frac{1}{A_{RO}} + \frac{1}{A_{RI}} \right) \frac{V_n' W_n^2}{2 A_{RO}}$$

$$F_g = g L_{TB} \left(\frac{M_{TB}}{V_{TB}} \right) + g L_R \left(\frac{M_R}{V_R} \right) - \rho_{\ell s} \ell_{SAT} - \rho_o \ell_{SUB} ,$$

and,

$$F_o = K_{SEP} \frac{V' W_n^2}{2 A_{RO}^2} + K_D \frac{W_o^2}{2 \rho_o A_D^2}$$

where, K_{SEP} is the separator loss coefficient and K_D is the loss at the bottom of the downcomer.

3.1.2.5 Cross Flow Region

As an additional equation for matching the number of equations and unknowns, the mass conservation is applied to the cross flow region of the tube bundle.

$$\frac{d M_{TBC}}{d t} = W_p - W_r \qquad (3.1\text{-}51)$$

where,

$$M_{TBC} = \int_{V_P}^{V_{TB}} \bar{\rho} \, dV = \frac{V_{TB} \rho_o \bar{\rho}_r}{\rho_o - \bar{\rho}_r} \ln \left(\frac{\bar{\rho}_p}{\bar{\rho}_r} \right) \qquad (3.1\text{-}52)$$

The $\bar{\rho}_p$, the density at the parallel to cross flow transient in the tube bundle, is a known function of ρ_o and $\bar{\rho}_r$ with a linear specific volume approximation. The state variables for M_{TBC} are the system pressure p, inlet internal energy U_o, and outlet vapor volume fraction $\langle \alpha_r \rangle$. In the same manner in the previous subsections, the total derivative yields :

$$\frac{d M_{TB}}{d t} = \left(\frac{\partial M_{TBC}}{\partial U_o} \right)_{<\alpha_r>,p} \frac{d U_o}{d t} + \left(\frac{\partial M_{TBC}}{\partial <\alpha_r>} \right)_{U_o,p} \frac{d <\alpha_r>}{d t}$$

$$+ \left(\frac{\partial M_{TBC}}{\partial p} \right)_{<\alpha_r>,U_o} \frac{d p}{d t}$$

$$= W_p - W_r \qquad (3.1\text{-}53)$$

All partial derivatives are given in Table 3.1-6.

3.1.3 Primary Side Model

A schematic indicating the primary side regions and the variables of interest is shown in Fig. 3.1-5. Governing equations are obtained by applying conservation equations to each control volume. Also, equations are given to determine the heat transfer from the primary side to the secondary.

3.1.3.1 Plenum Model

The conservation equations for the inlet plenum are :

$$\frac{d M_1}{d t} = W_{IN} - W_1 \qquad (3.1\text{-}54)$$

$$\frac{d E_1}{d t} = W_{IN} H_{IN} - W_1 H_1 \qquad (3.1\text{-}55)$$

From these two equations,

$$\frac{d\,E_1}{d\,t} - \frac{(H_1 + H_{IN})}{2}\frac{d\,M_1}{d\,t} = \frac{(W_{IN} + W_1)}{2}(H_{IN} - H_1) \qquad (3.1\text{-}56)$$

where,

$$M_1 = \int_0^{V_{p1}} \rho\, dV = \rho_1 V_{p1}$$

$$E_1 = \int_0^{V_{p1}} \rho\, U_1\, dV = \rho_1 U_1 V_{p1}$$

Thus,

$$\frac{d\,M_1}{d\,t} = V_{p1}\left(\frac{d\rho_1}{dT_1}\right)_p \frac{dT_1}{dt}\,, \qquad (3.1\text{-}57)$$

and

$$\frac{d\,E_1}{d\,t} = V_{p1}\left[\rho_1\left(\frac{\partial\,U_1}{\partial\,T_1}\right)_p + U_1\left(\frac{\partial\,\rho_1}{\partial\,T_1}\right)\right]\frac{d\,T_1}{d\,t} \qquad (3.1\text{-}58)$$

Plugging these equations into Eq. (3.1-56) with the assumption that $W_{IN} = W_1$,

$$C_1\frac{d\,E_1}{d\,t} = W_{IN}(H_{IN} - H_1) \qquad (3.1\text{-}59)$$

where,

$$C_1 = V_{p1} \left[\rho_1 \left(\frac{\partial U_1}{\partial T_1} \right)_p + \left(U_1 - \frac{H_1 - H_{IN}}{2} \right) \left(\frac{\partial \rho_1}{\partial T_1} \right)_p \right]$$

In the same manner, an equation for the outlet plenum is found:

$$C_3 \frac{d T_3}{d t} = W_{IN} (H_2 - H_3) \qquad (3.1 -60)$$

where,

$$C_3 = V_{p2} \left[\rho_3 \left(\frac{\partial U_3}{\partial T_3} \right)_p + \left(U_3 - \frac{H_2 + H_3}{2} \right) \left(\frac{\partial \rho_3}{\partial T_3} \right)_p \right]$$

3.1.3.2 Tubeside Model

The conservation equations for the primary fluid within the tubes of the tube bundle are :

$$\frac{d M_2}{d t} = W_1 - W_2 \qquad (3.1 -61)$$

$$\frac{d E_2}{d t} = W_1 H_1 - W_2 H_2 - q_B \qquad (3.1 -62)$$

From these two equations ,

$$\frac{d E_2}{d t} - \frac{(H_1 + H_2)}{2} \frac{d M_2}{d t} = \frac{(W_1 + W_2)}{2} (H_1 - H_2) - q_B$$

(3.1 -63)

where,

$$M_2 = \int_0^{V_{TBP}} \rho \, dV = \rho_2 \, V_{TBP}$$

$$E_2 = \int_0^{V_{TBP}} \rho \, U \, dV = \rho_2 \, U_2 \, V_{TBP}$$

Thus,

$$\frac{d \, M_2}{d \, t} = V_{TBP} \left(\frac{d\rho_2}{dT_2} \right)_p \frac{dT_2}{dt} \qquad (3.1 -64)$$

,and

$$\frac{d \, E_2}{d \, t} = V_{TBP} \left[\rho_2 \left(\frac{\partial \, U_2}{\partial \, T_2} \right)_p + U_2 \left(\frac{\partial \, \rho_2}{\partial \, T_2} \right) \right] \frac{d \, T_2}{d \, t}$$

(3.1 -65)

Plugging these equations into Eq. (3.1-63) with the assumption that $W_{IN} = W_2$,

$$C_2 \frac{d \, E_2}{d \, t} = W_{IN} \, (H_1 - H_2) \, q_B \qquad (3.1 -66)$$

where,

$$C_2 = V_{TBP} \left[\rho_2 \left(\frac{\partial \, U_2}{\partial \, T_2} \right)_p + \left(U_2 - \frac{H_1 + H_2}{2} \right) \left(\frac{\partial \, \rho_2}{\partial \, T_2} \right)_p \right]$$

3.1.3.3 Heat Transfer Model

The overall heat transfer q_B, is calculated using the log-mean temperature difference and the overall heat transfer coefficient. That is:

$$q_B = U_{over} A_o \Delta T_{LM} \qquad (3.1\text{-}67)$$

where,

ΔT_{LM} = log-mean temperature difference

$$= \frac{T_1 - T_2}{\ln\left(\frac{T_1 - T_{SAT}}{T_2 - T_{SAT}}\right)} ,$$

A_o = total outside surface area of tubes , and

U_{over} = overall heat transfer coefficient based on outside surface area of tubes and a Thom representation for boiling heat transfer (see App.[C], Ref.[S4])

A special treatment of heat transfer is adopted when the cold leg temperature T_3 is near or below T_{SAT} (see Sect. 4.2.3, Ref.[S4]).

3.1.4 Numerical Solution

In this subsection, is presented the formulation of a numerical scheme for solving the model equations derived in previous subsections. The primary and secondary equations are decoupled by

calculating heat transfer rate explicitly.

3.1.4.1 Primary Side Equation

For the primary side, we have a set of three differential equations for three unknowns. In a compact matrix form :

$$\underline{C}\,\dot{\underline{T}} = \underline{g} \qquad (3.1\text{-}68)$$

where,

$\underline{C}$ = Diag [C_1 , C_2 , C_3] ;

$\underline{T}$ = Col [T_1 , T_2 , T_3] ; and,

$\underline{g}$ = Col [$W_{IN}\,(H_{IN} - H_1)$, $W_{IN}\,(H_1 - H_2) - q_B$, $W_{IN}\,(H_2 - H_3)$]

3.1.4.2 Secondary Side Equation

For the secondary side, we can sum up the conservation equations and momentum equation as follow :

$$\underline{A}\,\dot{\underline{x}} = \underline{f} \qquad (3.1\text{-}69)$$

or,

$$\underline{A}\,\frac{d}{dt}\begin{bmatrix} U_o \\ V_V \\ \langle\alpha_r\rangle \\ \langle\alpha_n\rangle \\ p \\ \bar{W} \end{bmatrix} = \begin{bmatrix} \bar{W}\,(H_o - H_r) + q_B \\ \bar{W}\,(H_r - H_n) \\ \bar{W}\,(H_n - H_k) - W_s\,(H_{vs} - H_k) \\ W_{fw}\,(H_{fw} - H_k) - \bar{W}\,(H_o - H_k) \\ W_{fw} - W_s \\ -F \end{bmatrix}$$

where,

$$H_k \begin{cases} = H_{\ell s} & V_V \leq V_{ref} \text{ or } u_i \leq u_f \\ = H_o & u_i > u_f \text{ and } V_V > V_{ref} \end{cases}$$

V_{ref} is the vapor volume at which we switch from a fixed control volume steam dome - downcomer to a variable volume steam dome - downcomer. The components of matrix $\underline{\underline{A}}$ are show in Table 3.1-7.

Other relations of W_o , W_p , W_r , and W_n with $\bar{W}$ are :

$$\bar{W} = W_o + E_1 \frac{d\,U_o}{d\,t} + E_2 \frac{d\langle\alpha_r\rangle}{d\,t} + E_3 \frac{d\langle\alpha_n\rangle}{d\,t} + E_4 \frac{d\,p}{d\,t} \qquad (3.1\text{-}70)$$

$$W_p = W_o - \frac{d\,M_{TB}}{d\,t} + \frac{dM_{TBC}}{d\,t} \qquad (3.1\text{-}71)$$

$$W_r = W_o - \frac{d\,M_{TB}}{d\,t} \qquad (3.1\text{-}72)$$

and,

$$W_n = W_o - \frac{d\,M_{TB}}{d\,t} - \frac{d\,M_R}{d\,t} \qquad (3.1\text{-}73)$$

where,

$$E_1 = \beta_2' \left(\frac{\partial\,M_{TBC}}{\partial\,U_o} \right)_{\langle\alpha_r\rangle,p} - (\beta_2' + \beta_3' + \beta_4') \left(\frac{\partial\,M_{TB}}{\partial\,U_o} \right)_{\langle\alpha_r\rangle,p}$$

$$E_2 = \beta_2' \left(\frac{\partial M_{TBC}}{\partial \langle \alpha_r \rangle} \right)_{U_o,p} - (\beta_2' + \beta_3' + \beta_4') \left(\frac{\partial M_{TB}}{\partial \langle \alpha_r \rangle} \right)_{U_o,p} - \beta_4' \left(\frac{\partial M_R}{\partial \langle \alpha_r \rangle} \right)_{U_o,p}$$

$$E_3 = -\beta_4' \left(\frac{\partial M_R}{\partial \langle \alpha_n \rangle} \right)_{\langle \alpha_r \rangle,p} \quad \text{, and}$$

$$E_4 = \beta_2' \left(\frac{\partial M_{TBC}}{\partial p} \right)_{\langle \alpha_r \rangle,U_o} - (\beta_2' + \beta_3' + \beta_4') \left(\frac{\partial M_{TB}}{\partial p} \right)_{\langle \alpha_r \rangle,U_o} - \beta_4' \left(\frac{\partial M_R}{\partial p} \right)_{\langle \alpha_r \rangle,\langle \alpha_n \rangle}$$

For W_f :

$$W_f = \frac{d M_{SUB}}{d t} - W_{fw} + W_o \qquad V_V \leq V_{ref} \qquad (3.1\text{-}74)$$

or,

$$W_f = \frac{d M_{SUB}}{d t} - W_{fw} - \rho_{\ell s} \frac{d V_V}{d t} + W_o \qquad V_V > V_{ref} \qquad (3.1\text{-}75)$$

For transient calculation , Eq. (3.1-69) updates 6 unknown state variables. Using Eqs. (3.1-70) through (3.1-75), we can determine recirculation flows at each region.

Table 3.1-1 (from [S4])

Partial Derivatives of M_{TB} and E_{TB}

Quantity	Expression
$\left(\frac{\partial M_{TB}}{\partial U_O}\right)_{\langle\alpha_r\rangle,p}$	$\frac{\bar{\rho}_r}{\rho_O - \bar{\rho}_r}\left(V_{TB} - \frac{M_{TB}}{\rho_O}\right)\left(\frac{\partial \rho_O}{\partial U_O}\right)_p$
$\left(\frac{\partial M_{TB}}{\partial \langle\alpha_r\rangle}\right)_{U_O,p}$	$\frac{\rho_O}{\rho_O - \bar{\rho}_r}\left(\frac{M_{TB}}{\bar{\rho}_r} - V_{TB}\right)\left(\frac{\partial \bar{\rho}_r}{\partial \langle\alpha_r\rangle}\right)_p$
$\left(\frac{\partial M_{TB}}{\partial p}\right)_{\langle\alpha_r\rangle,U_O}$	$\frac{\left(\frac{\partial M_{TB}}{\partial U_O}\right)_{\langle\alpha_r\rangle,p}\left(\frac{\partial \rho_O}{\partial p}\right)_{U_O}}{\left(\frac{\partial \rho_O}{\partial U_O}\right)_p} + \frac{\left(\frac{\partial M_{TB}}{\partial \langle\alpha_r\rangle}\right)_{U_O,p}\left(\frac{\partial \bar{\rho}_r}{\partial p}\right)_{\langle\alpha_r\rangle}}{\left(\frac{\partial \bar{\rho}_r}{\partial \langle\alpha_r\rangle}\right)_p}$

Table 3.1-1 (Continued)

Quantity	Expression
$\left(\frac{\partial E_{TB}}{\partial U_0}\right)_{\langle\alpha_r\rangle,p}$	$\frac{E_{TB}}{M_{TB}}\left(\frac{\partial M_{TB}}{\partial U_0}\right)_{\langle\alpha_r\rangle,p} + M_{TB}\left[\frac{\rho_0}{\rho_0 - \bar{\rho}_r} - \frac{1}{\ln(\rho_0/\bar{\rho}_r)}\right] + M_{TB}\left[\frac{U_0 - \bar{U}_r}{\rho_0 \ln^2(\rho_0/\bar{\rho}_r)}\right.$ $\left. - \frac{\bar{\rho}_r(U_0 - \bar{U}_r)}{(\rho_0 - \bar{\rho}_r)^2}\right]\left(\frac{\partial \rho_0}{\partial U_0}\right)_p$
$\left(\frac{\partial E_{TB}}{\partial \langle\alpha_r\rangle}\right)_{U_0,p}$	$\frac{E_{TB}}{M_{TB}}\left(\frac{\partial M_{TB}}{\partial U_0}\right)_{\langle\alpha_r\rangle,p} + M_{TB}\left[\frac{1}{\ln(\rho_0/\bar{\rho}_r)} - \frac{\bar{\rho}_r}{\rho_\ell - \bar{\rho}_r}\right]\left(\frac{\partial U_r}{\partial \langle\alpha_r\rangle}\right)_p$ $+ M_{TB}\left[\frac{\rho_0(U_0 - \bar{U}_r)}{(\rho_0 - \bar{\rho}_r)^2} - \frac{(U_0 - \bar{U}_r)}{\bar{\rho}_r \ln^2(\rho_0/\bar{\rho}_r)}\right]\left(\frac{\partial \bar{\rho}_r}{\partial \langle\alpha_r\rangle}\right)_p$

Table 3.1-1 (continued)

Quantity	Expression
$\left(\frac{\partial E_{TB}}{\partial p}\right)_{\langle\alpha_r\rangle, U_0}$	$\frac{E_{TB}}{M_{TB}}\left(\frac{\partial M_{TB}}{\partial p}\right)_{U_0,\langle\alpha_r\rangle} + M_{TB}\left[\frac{1}{\ln(\rho_0/\bar{\rho}_r)} - \frac{\bar{\rho}_r}{\rho_\ell - \bar{\rho}_r}\right]\left(\frac{\partial U_r}{\partial p}\right)_{\langle\alpha_r\rangle,\ \langle\alpha_n\rangle}$ $+ M_{TB}\left[\frac{(U_0 - \bar{U}_r)}{\bar{\rho}_r \ln^2(\rho_0/\bar{\rho}_r)} - \frac{\rho_0(U_0 - \bar{U}_r)}{(\rho_0 - \bar{\rho}_r)^2}\right]\left(\frac{\partial \bar{\rho}_0}{\partial p}\right)_{U_0,\langle\alpha_r\rangle}$ $+ M_{TB}\left[\frac{\rho_0(U_0 - \bar{U}_r)}{(\rho_0 - \bar{\rho}_r)^2} - \frac{(U_0 - \bar{U}_r)}{\bar{\rho}_r \ln^2(\rho_0/\bar{\rho}_r)}\right]\left(\frac{\partial \bar{\rho}_r}{\partial p}\right)_{\langle\alpha_r\rangle,\ \langle\alpha_n\rangle}$

Table 3.1-2 (from [S4])

Property Derivatives

Quantity	Expression
$\left(\frac{\partial \bar{\rho}}{\partial \langle \alpha \rangle}\right)_p$	$\rho_{vs} - \rho_{\ell s}$
$\left(\frac{\partial \bar{\rho}}{\partial p}\right)_{\langle \sigma \rangle}$	$\langle \alpha \rangle \frac{d\rho_{vs}}{dp} + (1 - \langle \alpha \rangle) \frac{d\rho_{\ell s}}{dp}$
$\left(\frac{\partial \bar{U}}{\partial \langle \alpha \rangle}\right)_p$	$\frac{\rho_{vs}U_{vs} - \rho_{\ell s}U_{\ell s}}{\bar{\rho}} - \frac{\bar{U}}{\bar{\rho}} \left(\frac{\partial \bar{\rho}}{\partial \langle \alpha \rangle}\right)_p$
$\left(\frac{\partial \bar{U}}{\partial p}\right)_{\langle \alpha \rangle}$	$\frac{\langle \alpha \rangle \frac{d}{dp} [U_{vs}\rho_{vs}] + (1 - \langle \alpha \rangle) \frac{d}{dp} [\rho_{\ell s}U_{\ell s}]}{\bar{\rho}} - \frac{\bar{U}}{\bar{\rho}} \left(\frac{\partial \bar{\rho}}{\partial p}\right)_{\langle \alpha \rangle}$

Table 3.1-3 (from [S4])

Partial Derivatives of M_R and E_R

Quantity	Expression
$\left(\frac{\partial M_R}{\partial \langle \alpha_r \rangle}\right)_{\langle \alpha_n \rangle, p}$	$\frac{V_R}{2}\left(\frac{\partial \bar{\rho}_r}{\partial \langle \alpha_r \rangle}\right)_p$
$\left(\frac{\partial M_R}{\partial \langle \alpha_n \rangle}\right)_{\langle \alpha_r \rangle, p}$	$\frac{V_R}{2}\left(\frac{\partial \bar{\rho}_n}{\partial \langle \alpha_n \rangle}\right)_p$
$\left(\frac{\partial M_R}{\partial p}\right)_{\langle \alpha_r \rangle, \langle \alpha_n \rangle}$	$\frac{V_R}{2}\left[\left(\frac{\partial \bar{\rho}_r}{\partial p}\right)_{\langle \alpha_r \rangle} + \left(\frac{\partial \bar{\rho}_n}{\partial p}\right)_{\langle \alpha_n \rangle}\right]$
$\left(\frac{\partial E_R}{\partial \langle \alpha_r \rangle}\right)_{\langle \alpha_n \rangle, p}$	$\frac{V_R}{2}\left[U_r \left(\frac{\partial \bar{\rho}_r}{\partial \langle \alpha_r \rangle}\right)_p + \bar{\rho}_r \left(\frac{\partial \bar{U}_r}{\partial \langle \alpha_r \rangle}\right)_p\right]$
$\left(\frac{\partial E_R}{\partial \langle \alpha_n \rangle}\right)_{\langle \alpha_r \rangle, p}$	$\frac{V_R}{2}\left[U_n \left(\frac{\partial \bar{\rho}_n}{\partial \langle \alpha_n \rangle}\right)_p + \bar{\rho}_n \left(\frac{\partial \bar{U}_n}{\partial \langle \alpha_n \rangle}\right)_p\right]$
$\left(\frac{\partial E_R}{\partial p}\right)_{\langle \alpha_r \rangle, \langle \alpha_n \rangle}$	$\frac{V_R}{2}\left[\bar{U}_r \left(\frac{\partial \bar{\rho}_r}{\partial p}\right)_{\langle \alpha_r \rangle} + \bar{\rho}_r \left(\frac{\partial \bar{U}_r}{\partial p}\right)_{\langle \alpha_r \rangle}\right]$ $+ \frac{V_R}{2}\left[\bar{U}_n \left(\frac{\partial \bar{\rho}_n}{\partial p}\right)_{\langle \alpha_n \rangle} + \bar{\rho}_n \left(\frac{\partial \bar{U}_n}{\partial p}\right)_{\langle \alpha_n \rangle}\right]$

Table 3.1-4 (from [S4])

Partial Derivatives for Eqs. 3.1-31 and 3.1-32

Quantity	Expression
$\left(\frac{\partial M_{SAT}}{\partial V_v}\right)_p$	$(\rho_{vs} - \rho_{\ell s})$
$\left(\frac{\partial M_{SAT}}{\partial p}\right)_{V_v}$	$\frac{d\rho_{\ell s}}{dp}(V_{SD} - V_v) + \frac{d\rho_{vs}}{dp}(V_v + V_{STM})$
$\left(\frac{\partial E_{SAT}}{\partial V_v}\right)_p$	$\rho_{vs}U_{vs} - \rho_{\ell s}U_{\ell s}$
$\left(\frac{\partial E_{SAT}}{\partial p}\right)_{V_v}$	$\left(\rho_{\ell s}\frac{dU_{\ell s}}{dp} + U_{\ell s}\frac{d\rho_{\ell s}}{dp}\right)(V_{SD} - V_v)$ + $\left(\rho_{vs}\frac{dU_{vs}}{dp} + U_{vs}\frac{d\rho_{vs}}{dp}\right)(V_v + V_{STM})$

Table 3.1-4 (continued)

$\left(\frac{\partial M_{SUB}}{\partial U_0}\right)_p$	$V_D \left(\frac{\partial \rho_0}{\partial U_0}\right)_p$
$\left(\frac{\partial M_{SUB}}{\partial p}\right)_{U_0}$	$V_D \left(\frac{\partial \rho_0}{\partial p}\right)_{U_0}$
$\left(\frac{\partial E_{SUB}}{\partial U_0}\right)_p$	$V_D \rho_0 + V_D U_0 \left(\frac{\partial \rho_0}{\partial U_0}\right)_p$
$\left(\frac{\partial E_{SUB}}{\partial p}\right)_{U_0}$	$V_D U_0 \left(\frac{\partial \rho_0}{\partial p}\right)_{U_0}$

Table 3.1-5 (from [S4])

Partial Derivatives for Eqs. 3.1-45 and 3.1-46

Quantity	Expansion
$\left(\frac{\partial M_{SAT}}{\partial V_v}\right)_p$	ρ_{vs}
$\left(\frac{\partial M_{SAT}}{\partial p}\right)_{V_v}$	$(V_v + V_{STM}) \frac{d\rho_{vs}}{dp} + V_{fo} \frac{d\rho_{\ell s}}{dp}$
$\left(\frac{\partial E_{SAT}}{\partial V_v}\right)_p$	$\rho_{vs} U_{vs}$
$\left(\frac{\partial E_{SAT}}{\partial p}\right)_{V_v}$	$(V_v + V_{STM})\left(U_{vs} \frac{d\rho_{vs}}{dp} + \rho_{vs} \frac{dU_{vs}}{dp}\right)$ $+ V_{fo}\left(U_{\ell s} \frac{d\rho_{\ell s}}{dp} + \rho_{\ell s} \frac{dU_{\ell s}}{dp}\right)$

Table 3.1-5 (continued)

Quantity	Expression
$(\frac{\partial M_{SUB}}{\partial U_0})_{V_0,p}$	$(V_{SD} - V_v - V_{fo})\ (\frac{\partial \rho_0}{\partial U_0})_p$
$(\frac{\partial M_{SUB}}{\partial V_v})_{U_0,p}$	$-\rho_0$
$(\frac{\partial M_{SUB}}{\partial p})_{U_0,V_v}$	$(V_{SD} - V_v - V_{fo})\ (\frac{\partial \rho_0}{\partial p})_{U_0}$
$(\frac{\partial E_{SUB}}{\partial U_0})_{V_v,p}$	$(V_{SD} - V_v - V_{fo})(\rho_0 + U_0\ (\frac{\partial \rho_0}{\partial U_0})_p)$
$(\frac{\partial E_{SUB}}{\partial V_v})_{U_0,p}$	$-\rho_0 U_0$
$(\frac{\partial E_{SUB}}{\partial p})_{U_0,V_v}$	$(V_{SD} - V_v - V_{fo})U_0\ (\frac{\partial \rho_0}{\partial p})_{U_0}$

Table 3.1-6 (from [S4])

Partial Derivatives of M_{TBC}

Quantity	Expression*
$\left(\frac{\partial M_{TBC}}{\partial U_0}\right)_{\langle\alpha_r\rangle,p}$	$\frac{V_{TB}\rho_r^2(1-\gamma)}{[(\rho_0-\bar{\rho}_r)[\gamma\rho_0+(1-\gamma)\bar{\rho}_r]} - \frac{M_{TBC}\bar{\rho}_r}{\rho_0(\rho_0-\bar{\rho}_r)} \left(\frac{\partial\rho_0}{\partial U_0}\right)_p$
$\left(\frac{\partial M_{TBL}}{\partial\langle\alpha_r\rangle}\right)_{U_0,p}$	$\frac{\rho_0}{\rho_0-\bar{\rho}_r}\left(\frac{M_{TBC}}{\bar{\rho}_r}-V_{TB}\right) + \frac{V_{TB}\rho_0^2\gamma}{(\rho_0-\bar{\rho}_r)[\gamma\rho_0+(1-\gamma)\bar{\rho}_r]}\left(\frac{\partial\rho_r}{\partial p}\right)_{\langle\alpha_\rho\rangle}$
$\left(\frac{\partial M_{TBC}}{\partial p}\right)_{\langle\alpha_r\rangle,U_0}$	$\frac{\left(\frac{\partial M_{TBC}}{\partial U_0}\right)_{\langle\alpha_r\rangle,p}\left(\frac{\partial\rho_0}{\partial p}\right)_{U_0}}{\left(\frac{\partial\rho_0}{\partial U_0}\right)_p} + \frac{\left(\frac{\partial M_{TBC}}{\partial\langle\alpha_r\rangle}\right)_{U_0,p}\left(\frac{\partial\bar{\rho}_r}{\partial p}\right)_{\langle\alpha_r\rangle}}{\left(\frac{\partial\bar{\rho}_r}{\partial\langle\alpha_r\rangle}\right)_p}$

*$\gamma = \frac{L_p}{L_{TB}}$

Table 3.1-7 (from [S4])

Components of Matrix $\underline{\underline{A}}$

Component	Expression
A_{11}	B_1 in Eq. (3.1-10) + $E_1 (H_o - H_r)$
A_{12}	0
A_{13}	B_2 in Eq. (3.1-10) + $E_2 (H_o - H_r)$
A_{14}	0
A_{15}	B_3 in Eq. (3.1-10) + $E_4 (H_o - H_r)$
A_{16}	0
A_{21}	$\left[\left(\frac{\partial M_{TB}}{\partial U_o} \right)_{\langle \alpha_r \rangle, p} + E_1 \right] (H_r - H_n)$
A_{22}	0
A_{23}	B_4 in Eq. (3.1-20) + $\left[\left(\frac{\partial M_{TB}}{\partial \langle \alpha_r \rangle} \right)_{U_o, p} + E_2 \right] (H_r - H_n)$
A_{24}	B_5 in Eq. (3.1-20) + $E_3 (H_r - H_n)$
A_{25}	B_6 in Eq. (3.1-20) + $\left[\left(\frac{\partial M_{TB}}{\partial p} \right)_{\langle \alpha_r \rangle, U_o} + E_4 \right] (H_r - H_n)$
A_{26}	0

Table 3.1-7 (continued)

A_{31}	$\left[\left(\frac{\partial M_{TB}}{\partial U_o} \right)_{<\alpha_r>,p} + E_1 \right] (H_n - H_k)$
A_{32}	B_7 or B_{11} in Eq. (3.1-31 or 45)
A_{33}	$\left[\left(\frac{\partial M_{TB}}{\partial <\alpha_r>} \right)_{U_o,p} + \left(\frac{\partial M_R}{\partial <\alpha_r>} \right)_{<\alpha_n>,p} + E_2 \right]$ $(H_n - H_k)$
A_{34}	$\left[\left(\frac{\partial M_R}{\partial <\alpha_n>} \right)_{<\alpha_r>,p} + E_3 \right] (H_n - H_k)$
A_{35}	B_8 or B_{12} in Eq. (3.1-31 or 45) + $\left[\left(\frac{\partial M_{TB}}{\partial p} \right)_{U_o,<\alpha_r>} + \left(\frac{\partial M_R}{\partial p} \right)_{<\alpha_r>,<\alpha_n>} + E_4 \right]$ $(H_n - H_k)$
A_{36}	0
A_{41}	B_9 or B_{13} in Eq. (3.1-32 or 46) $- E_1 (H_o - H_k)$
A_{42}	0 or B_{14} in Eq. (3.1-46)
A_{43}	$- E_2 (H_o - H_k)$
A_{44}	$- E_3 (H_o - H_k)$

Table 3.1-7 (continued)

A_{45} B_{10} or B_{15} in Eq. (3.1-32 or 46)

$- E_4 (H_o - H_k)$

A_{46} 0

A_{51} $\left(\frac{\partial M_{TB}}{\partial U_o} \right)_{<\alpha_r>,p} + \left(\frac{\partial M_{SUB}}{\partial U_o} \right)_{p \text{ or } p,\, V_V}$

A_{52} $\left(\frac{\partial M_{SAT}}{\partial V_V} \right)_{p} + \left(\frac{\partial M_{SUB}}{\partial V_V} \right)_{p,U_o}$

A_{53} $\left(\frac{\partial M_{TB}}{\partial <\alpha_r>} \right)_{U_o,p} + \left(\frac{\partial M_R}{\partial <\alpha_r>} \right)_{<\alpha_r>,p}$

A_{54} $\left(\frac{\partial M_R}{\partial <\alpha_n>} \right)_{<\alpha_r>,p}$

A_{55} $\left(\frac{\partial M_{TB}}{\partial p} \right)_{<\alpha_r>,U_o} + \left(\frac{\partial M_R}{\partial p} \right)_{<\alpha_r>,<\alpha_n>}$

$+ \left(\frac{\partial M_{SAT}}{\partial p} \right)_{V_V} + \left(\frac{\partial M_{SUB}}{\partial p} \right)_{U_o \text{ or } U_o,V_V}$

A_{56} 0

Table 3.1-7 (continued)

A_{61}, A_{62}	0	
A_{63}, A_{64}, A_{65}	0	
A_{66}	I	in Eq. (3.1-48)

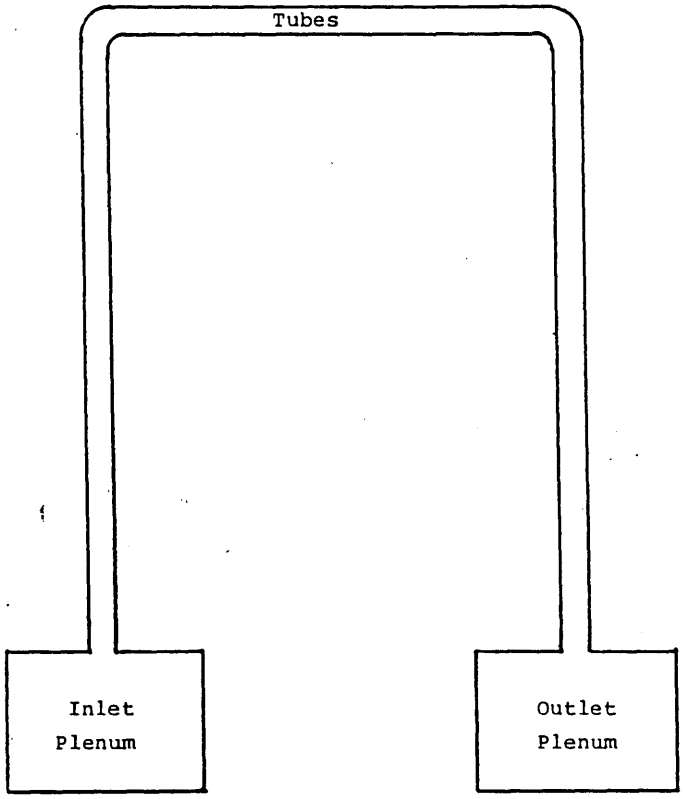

3.1-1 Primary side regions (from [S4])

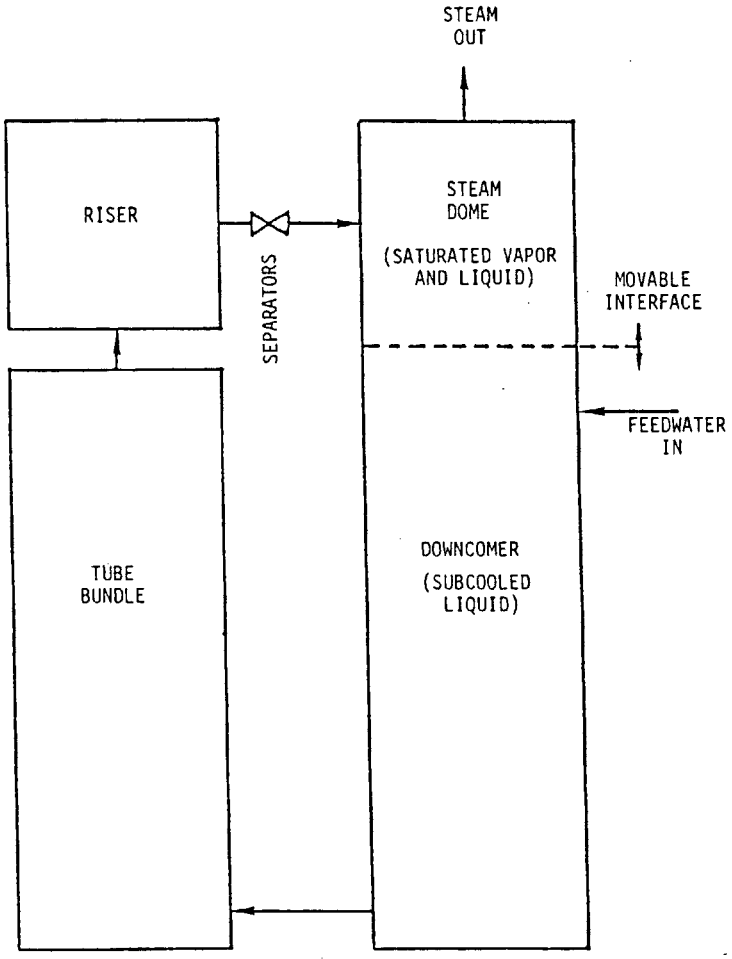

3.1-2 Secondary side regions (from [S4])

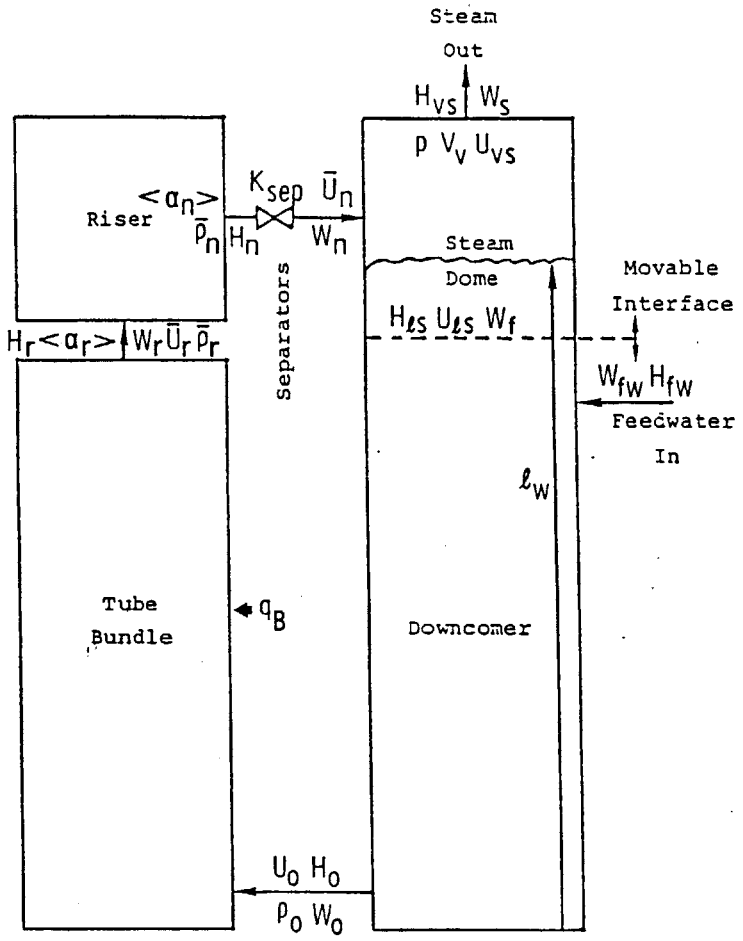

3.1-3 Secondary side nomenclature (from [S4])

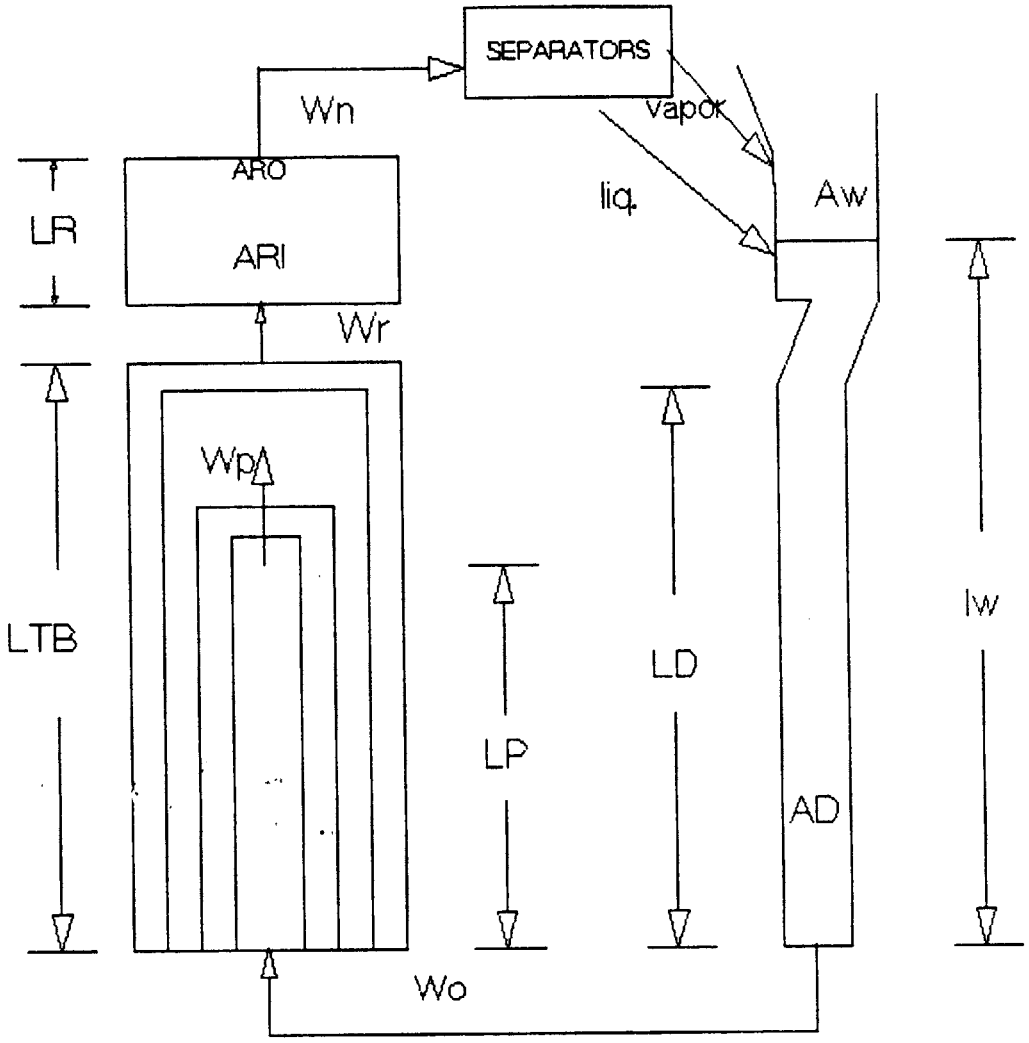

3.1-4 Notation for momentum equation

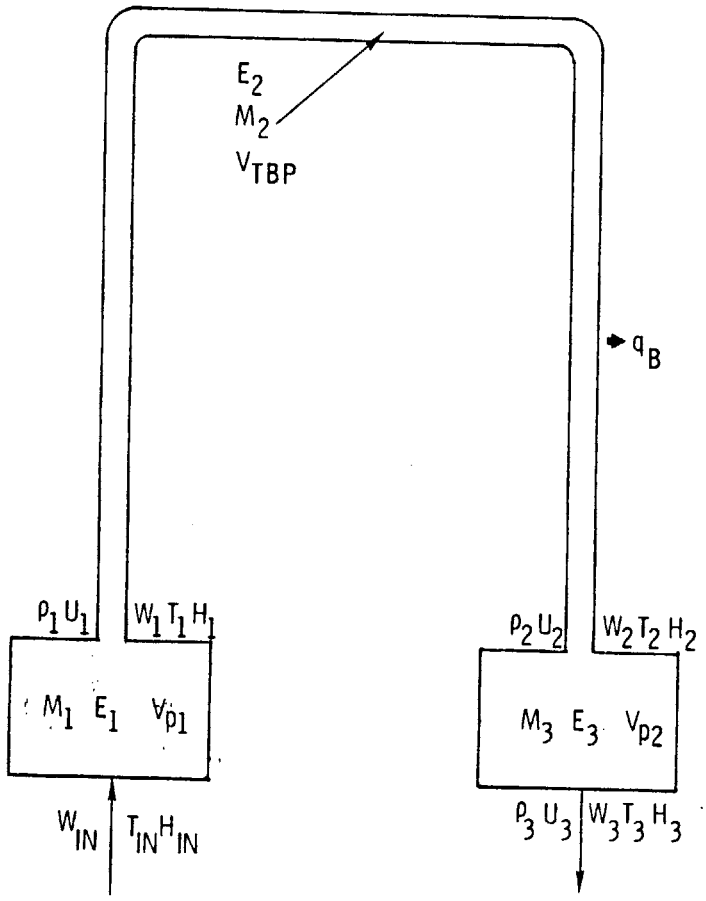

3.1-5 Primary side nomenclature (from [S4])

3.2 Model Modification

3.2.1 Motivation

The existing model has been evaluated over a wide range of conditions and the results of evaluation are encouraging in terms of computing speed and model accuracy.

A big challenge occurs when modeling the tube bundle region, the region for major heat transfer between the primary and secondary sides. Since the tube bundle region is treated as a single control volume, the solutions of governing equations can provide only a limited amount of information, such as inlet and outlet conditions. This limited information about state variables must be supplemented by "profiles" to obtain mass (M_{TB}) and energy (E_{TB}) integrals over the tube bundle volume. For integration with a one-dimensional approach, the axial property profiles are used, which may account for the thermodynamic phenomena inside the tube bundle region. During transients, however, determining the transient profiles is a time consuming task, which impairs the fast-running capability of the model. So the transient profiles are assumed to be similar to the steady-state profiles.

Since the steady-state profiles vary with the operating conditions, some additional variables should be introduced to account for this variation. To avoid the increase of the model order due to additional variables, fixed profiles over all operating conditions are used. Those profiles are based on the linear profiles of specific

volume ($\bar{v} = 1 / \bar{\rho}$) and internal energy ($\bar{U}$). Since the property profiles depend only upon the boundary values (state variables), the transient phenomena inside the tube bundle region are only approximately modeled. Neverthless, the evaluation shows that the model is appropriate to most transient cases except those that are very fast.

While being heated up through the tube bundle region, the fluid undergoes phase change, which is accompanied by the transitions in the flow and heat transfer patterns. These processes generate the transition points (about onset of boiling) of the property profiles, where changes in slope should occurs. Such a transition occurs for subcooled boiling at the point of bubble departure (onset of significant voids, OSV). The OSV point occurs near the inlet at rated power and near bulk boiling for low power (see Table 3.1-3, Ref.[S4]).

The bubble formation or collapse results in the change of the transition point in the property profile. As discussed in the previous chapter, the shrink and swell phenomena are attributed to the sudden bubble formation or collapse accompanying changes in steam or feedwater flow. So the shrink and swell phenomena may be more effectively simulated by considering the change of transition point in the property profiles.

However, the estimation of the transition point requires a detailed model with more control volumes and state variables. It is contrary to the purpose of the fast-running model. Therefore, the modification of the model is performed to solve those two complict

problems : better simulation of the shrink and swell phenomena ; and, computing time. The existing code (Ref. [S4]) uses an OSV point that is always at the inlet. Modification, described in the next section, adopts an OSV point that is always at bulk boiling.

3.2.2 Modification

To avoid the increase in computing time, no additional control volumes and state variables are introduced keeping the same order of the model.

The basic properties for the axial profile are the specific volume ($\bar{v} = 1 / \bar{\rho}$) and internal energy ($\bar{U}$) . In the existing model, both have the linear profile with the single slope along the whole tube bundle region. For better simulation of the shrink and swell effests, a motion of the OSV point is now adopted.

With a known transition point, the change of profile slope can be applied to both profiles for $\bar{v}$ and $\bar{U}$. Either of them, however, should be pre-specified to estimate the transition point without introducing additional state variables. The profile of $\bar{U}$ seems to be less influential on the shrink and swell effects than that of $\bar{v}$, because these effects are basically caused by the mass change in the tube bundle region. Therefore it is desirable to apply the change of slope to the profile of $\bar{v}$ at the transition point . For the estimation of the transition point , the profile of $\bar{U}$ is pre-specified by the linear approximation with the single slope along the whole tube bundle region in the same way as that of the existing

model. The transition point is estimated by the profile of $\bar{U}$ with an assumption that this point lies about the location of the onset of bulk boiling.

That is :

$$\frac{L_{TR}}{L_{TB}} \simeq \frac{L_B}{L_{TB}} = \frac{U_{\ell s} - U_o}{\bar{U}_r - U_o} \qquad (3.2-1)$$

where,

L_{TR} : axial location of transition point in profile

L_B : axial location of on-set of bulk boiling

From now on, the notation of L_{TR} "transition point", is replaced with L_B and called "boiling height".

Based on the boiling height L_B , the slope of linear profile for the specific volume is changed as shown in Fig. 3.2-1. The slope is $(v_{\ell s} - v_o) / L_B$ for the region below L_B and $(v_r - v_{\ell s}) / (L_{TB} - L_B)$ for the region above L_B . The first region is dominated by the subcooled single phase and the second by the saturated two phase.

3.2.3 Modified Equations

Based on the modified profile for the specific volume, the governing equations for the tube bundle region are correspondingly modified. The tube bundle region is divided into two regions : region

1 is the subcooled region (below L_B) ; and, region 2 is the saturated region (above L_B) as shown in Fig. 3.2-2 (a).

As the previous model, the conservation equations are applied to the whole tube bundle region rather than to each subregion. The resulting equations are the same as Eqs. (3.1-1) and (3.1-3) in the previous model. However, the profile of specific volume or density has been modified and the expressions for M_{TB} and E_{TB} (Eqs. 3.1-6 and 3.1-7) are replaced by:

$$M_{TB} = M_{TB1} + M_{TB2} \qquad (3.2-2)$$

and,

$$E_{TB} = E_{TB1} + E_{TB2} \qquad (3.2-3)$$

where

$$M_{TB1} = f\, V_{TB} \left(\frac{\rho_{\ell s}\, \rho_o}{\rho_o - \rho_{\ell s}} \ln \frac{\rho_o}{\rho_{\ell s}} \right) , \qquad (3.2-4)$$

$$M_{TB2} = (1 - f)\, V_{TB} \left(\frac{\bar{\rho}_r\, \rho_{\ell s}}{\rho_{\ell s} - \bar{\rho}_r} \ln \frac{\rho_{\ell s}}{\bar{\rho}_r} \right) , \qquad (3.2-5)$$

$$E_{TB1} = M_{TB1} \left(\frac{U_{\ell s} - U_o}{\ln (\rho_o / \rho_{\ell s})} + \frac{U_o\, \rho_o - U_{\ell s}\, \rho_{\ell s}}{\rho_o - \rho_{\ell s}} \right) , \qquad (3.2-6)$$

$$E_{TB2} = M_{TB2} \left(\frac{\bar{U}_r - U_{\ell s}}{\ln (\rho_{\ell s} / \bar{\rho}_r)} + \frac{U_{\ell s} \rho_{\ell s} - \bar{U}_r \bar{\rho}_r}{\rho_{\ell s} - \bar{\rho}_r} \right) , \qquad (3.2 - 7)$$

and

$$f = \frac{L_B}{L_{TB}} = \frac{U_{\ell s} - U_o}{\bar{U}_r - U_o}$$

The subscripts TB1 and TB2 denote subregions 1 and 2. The additional variable f in these expressions is uniquely specified by the existing state variables U_o , $<\alpha_r>$, and p . Therefore the addition of variable f does not increase the order of model.

Since the same state variables (U_o , $<\alpha_r>$, and p) are used, the total derivatives for M_{TB} and E_{TB} have the same expressions as Eqs. (3.1-8) and (3.1-9) in the previous model. But the partial derivative terms appearing in these equations are modified. The expressions for the partial derivative terms of the modifed model are given in Table 3.2-1 as the counterpart of Table 3.1-1 in the previous model.

The M_{TBC} , the mass of the cross flow region in the tube bundle is also modified, using the following two cases :

first: $f \leq \gamma$ (Fig. 3.2-2 (b)) ;

$$M_{TBC} = (1 - f) V_{TB} \left(\frac{\bar{\rho}_r \rho_{\ell s}}{\rho_{\ell s} - \bar{\rho}_r} \ln \frac{\bar{\rho}_p}{\bar{\rho}_r} \right) \qquad (3.2 - 8)$$

where,

$$\gamma = \frac{\bar{L}_P}{L_{TB}} \quad ,$$

L_P = axial location of the parallel to cross flow transition (geometrically fixed value) ,

and

$\bar{\rho}_P$ = density at L_P

or

$$\bar{\rho}_p = \left[\frac{1}{\bar{\rho}_r} - \frac{1 - \gamma}{1 - f} \left(\frac{1}{\bar{\rho}_r} - \frac{1}{\rho_{\ell s}} \right) \right]^{-1} \qquad (3.2 - 9)$$

second: $f > \gamma$ (Fig. 3.2-2 (c)) ;

$$M_{TBC} = M_{TB2} + f V_{TB} \left(\frac{\rho_{\ell s} \rho_o}{\rho_o - \rho_{\ell s}} \ln \frac{\bar{\rho}_p}{\rho_{\ell s}} \right) \qquad (3.2 -10)$$

where,

$$\bar{\rho}_P = \left[\frac{1}{\bar{\rho}_r} - \frac{1 - \gamma}{1 - f} \left(\frac{1}{\bar{\rho}_r} - \frac{1}{\rho_{\ell s}} \right) \right]^{-1} \qquad (3.2 -11)$$

The total derivative of M_{TBC} has also the same expression as Eq. (3.1-54) but the partial derivatives should be changed (we use the expression given in Table 4.1-6 with the modified M_{TBC}).

3.2.4 Modification Effects

Before discussing the modification effects, the shrink and swell phenomena observed in the downcomer are examined relating with the mass of tube bundle region, M_{TB} .

As mentioned in the previous chapter (2.3.1), the sudden change of steam or feedwater flow causes vapor volume formation or collapse in the tube bundle region. The resulting mass shift between the tube bundle region and downcomer causes the downcomer level to "shrink" or to "swell". Therefore, the tube bundle mass, which is varied with the mass shift, may be a good variable for estimating the shrink and swell effects.

There are four cases to be considered (see Fig. 2.3-1) :

1) swell due to steam flow increase ,
2) shrink due to steam flow decrease ,
3) shrink due to feedwater flow increase , and
4) swell due to feedwater flow decrease

As illustrative examples , only cases (1) and (3) are considered. Cases (2) and (4) show the same behavior as (1) and (3), respectively, except for the sign of changes.

First, in the case of steam flow increase, excessive steam removal results in a steam generator pressure decrease , which causes vapor volume formation. As a result, the volume taken up by the liquid/vapor mixture increases and liquid is displaced into the downcomer region. The resulting mass shift from tube bundle to downcomer causes the drop of interface between the liquid/vapor

mixture and subcooled liquid (modeled as the decrease of "boiling height" L_B in the modified model) in the tube bundle region as well as the "swell" of downcomer level.

During this transient, the tube bundle mass change is illustrated by looking at the specific volume profiles in tube bundle region (Fig. 3.2-3). In this plot , the quantitative values for specific volume (v_o , v_{ls} , and $\bar{v}$) are based on the steam flow step increase case shown in Fig. 3.2-4.

For the original model, (Fig. 3.2-3; solid line), the change of specific volume profile occurs only due to density changes at the inlet and outlet of tube bundle. The line $\overline{A\ B}$ represents the initial profile. During the transient, the point B (outlet specific volume, $\bar{v}_r$), moves to the point C ($\bar{v}_r'$), while point A (inlet specific volume, v_o), remains nearly unchanged. The area of triangle ABC represents indirectly the change of the tube bundle mass during the transient.

Meanwhile, for the modified model, (Fig. 3.2-3; dotted line), the slope of specific volume undergoes a transition at the boiling height L_B . Therefore, this model accounts for the change of specific volume profile due to the change of boiling height as well as due to the change of values in the inlet and outlet. In Fig. 3.2-3 (dotted line), the connected line $\overline{A\ D\ B}$ represents the initial profile. During the transient, the point B (outlet specific volume, $\bar{v}_r$), moves to the point C ($\bar{v}_r$), while point A (inlet, v_o), remains unchanged. In addition, the point D (saturated liquid specific volume, v_{ls}) at the

boiling height , shifts to the new point E (v_{ls}'). The area of polygon ADBCE represents indirectly the change of tube bundle mass in the modified model.

The modification effect on the tube bundle mass change can be considered by comparing the area of polygon ADBCE with that of triangle ABC . In this case (steam flow increase) , the modification effect is not significant; the change of outlet specific volume is so large that the overestimation of the original model (by the area of AFG which would be very small for the incompressible liquid) in the lower part of the tube bundle is comparable to the change due to the boiling height shift.

Next, in the case of a feedwater increase, the colder feedwater results in a decrease of the tube bundle inlet internal energy, which gives rise to bubble collapse. As a result, the volume taken by the liquid/vapor mixture decreases and the volume is replaced by subcooled liquid. The resulting mass shift from downcomer to tube bundle causes the elevation interface between the liquid/vapor mixture and subcooled liquid (modeled as the increase of " boiling height " L_B in the modified model) in the tube bundle region, as well as the "shrink" of downcomer level.

By the same way as in the previous case, the modification effects on the tube bundle mass change are illustrated using the specific volume profiles along the tube bundle region given in Fig 3.2-5 based on the illustrative simulation for the feedwater step increase (shown in Fig. 3.2-6)

For the original model (Fig. 3.2-5; solid line), the lines $\overline{A\ B}$ and $\overline{A'C}$ represent the initial and final profiles. Thus the area of polygon ABCA' represents indirectly the change of tube bundle mass. Meanwhile, for the modified model (Fig. 3.2-5; dotted line), the connected lines $\overline{A\ D\ B}$ and $\overline{A'E\ C}$ represent the initial and final profiles. The area of polygon ADBCEA' represents indirectly the change of tube bundle mass.

Comparing these two areas , the polygon ADBCEA' is greater than ABCA' by approximately the area of triangle D'EC ,which repesents the modification effect. Since the specific volume change in the outlet is not much greater than that in the inlet , the modification effect due to the change of boiling height is notable in this case (feedwater increase).

The above explanations are confirmed by the level responses to step increases in steam and feedwater flows from the simulated results given in Figs. 3.2-7 and 3.2-8. Detailed description of the steam generator used for the simulation will be given in the following subsection. One thing we note is an unexpected initial peak of the level response in the case of feedwater increase. This peak seems to be caused by a direct increase in the downcomer level when the increased feedwater is added but has not yet had time to travel to the downcomer region.

When combined with the level controller model, the modification effect may be crucial to the level dynamics related with the stability. As shown in Fig. 3.2-9, the modified model shows an

unstable level behavior due to the shrink and swell effects but the original one does not with the same controller. In this case, the "same" controller is not based on an actual controller; therefore it should not be inferred that the actual steam generator level would be unstable . This result, however, implies that the direction of modification (increasing the shrink and swell effects) is desirable to the design of the controller, of which the main purpose is to treat the shrink and swell effects. (The controller evaluated with the modified model will give the more practical conservatism than the original one).

Except for the simulation of the shrink and swell effects, the modified model is the essentially same as the original model, which was well validated over a wide range of operating conditions. Furthermore, the modification does not impair the fast-running capability. Therefore, we have no hesitation to adopt the modified model for this research. From now on, "our steam generator model" means the modified model.

3.2.5 Model Validation

For evaluating the applicability, our steam generator model is tested against actual plant data. The plant adopted for testing is a typical Westinghouse plant (4-loop , 1150 MWe). Each steam generator is a Westinghouse Model F type, a recirculating U-tube steam generator. For simulating this steam generator, the geometric modeling is given in Appendix [C]. The modeling includes the

downcomer geometric representation for the water level calculation.

In Fig. 3.2-10, the calculated levels by our steam generator model (designated "Simulation") are compared with plant level measurements (designated "Plant Data"). The reactor is operating at a nearly constant power level of 12 % for two hours. Input to the model includes : measured values of feedwater flow rate (as a function of time); primary variables such as hot-leg temperature, pressure and flow rate (as a function of time); a measured value of feedwater temperature taken to be constant ; and two piecewise constant values for steam flow rate chosen to give the right long term water level behavior.

The comparision shows a good simulation in the amplitude and phase of the level swings, although it seems that the amplitude of the level swings are slightly larger in the plant data than in the simulation. It is worthwhile noting the phase relation between the level in Fig. 3.2-10 and the feedflow rate shown in Fig. 3.2-11. Both simulation and plant data indicate that these variables are almost perfectly out of phase ; as the flow increases, the level decreases. We view this similarity of phase behavior as providing excellent support for model adequacy.

In Fig. 3.2-12, a similar comparision is shown for core operation at a nearly constant power level of 30 % . The input feed flow rate is shown in Fig. 3.2-13. The conclusions are similar to those for 12%.

There may be a big difference between these two power levels of 12 % and 30 % at which the comparision are made. At 12 % power level,

the feedwater temperature is relatively lower, because the feedwater heaters are not operating (the turbine comes on-line approximately 15% power). At this condition, the automatic level control suffers from unstable dynamics due to the shrink and swell effects. We see clearly these control problems in Fig. 3.2-10. It is noted that the stable level behavior shown in the middle part of the plot is attributed to manual control. Meanwhile, at 30 % power level, the feedwater temperature is relatively much higher because of the operating feedwater heater (the turbine is on-line). At this condition, the control problems due to the shrink and swell effects have disappeared.These simulation results imply that our steam generator model is applicable to either operating conditions (whether the shrink and swell effects are significant or not).

When our steam generator model is loaded on an IBM-XT or its compatible (640K RAM), it is found that simulated time-to-execution time ratios range from 2 to 1.5 with integration time step size of 0.25 to 5 seconds. This result implies that this model is eventually applicable for incorporation in an on-line controller.

3.3 A Chapter Summary

To obtain physical ideas about steam generator dynamics, to develop a new control algorithm, and to substitute for actual plant testing, an existing model was adopted and modified in its simulation capability at low power conditions.

First the existing model was described. Then, associated with

steam generator low power dynamics, the modification of the model was described. The model for the tube bundle region was modified for the better simulation of the reverse dynamics due to the shrink and swell effects at low power conditions. To avoid extra computing time due to the modification, the model order remains the same by introducing an algebraic equation for the new boiling height variable.

The modification effects were discussed with the physical interpretations which were confirmed with transient simulations. It was found that the modification effects for the shrink and swell might be crucial to the system stability in conjunction with the automatic controller. We also saw that the modification went in a desirable direction for the purpose of a new controller design.

Calculations of our steam generator model were compared to plant data. The results showed a good agreement.

Table 3.2-1

Partial Derivatives for M_{TB} and E_{TB} in the modified model

Quantity	Expression
$\left(\frac{\partial M_{TB}}{\partial U_o} \right)_{\langle \alpha_r \rangle, p}$	$\left(\frac{\partial M_{TB1}}{\partial U_o} \right)_{\langle \alpha_r \rangle, p} + \left(\frac{\partial M_{TB2}}{\partial U_o} \right)_{\langle \alpha_r \rangle, p}$
$\left(\frac{\partial M_{TB1}}{\partial U_o} \right)_{\langle \alpha_r \rangle, p}$	$\frac{M_{TB1}}{\bar{U}_r - U_o} - \frac{M_{TB1}}{U_{\ell s} - U_o} + \frac{\rho_{1s}}{\rho_o - \rho_{\ell s}} \left(f V_{TB} - \frac{M_{TB1}}{\rho_o} \right) \left(\frac{\partial \rho_o'}{\partial U_o} \right)_p$
$\left(\frac{\partial M_{TB2}}{\partial U_o} \right)_{\langle \alpha_r \rangle, p}$	$\frac{M_{TB2}}{\bar{U}_r - U_o}$
$\left(\frac{\partial M_{TB}}{\partial \langle \alpha_r \rangle} \right)_{U_o, p}$	$\left(\frac{\partial M_{TB1}}{\partial \langle \alpha_r \rangle} \right)_{U_o, p} + \left(\frac{\partial M_{TB2}}{\partial \langle \alpha_r \rangle} \right)_{U_o, p}$

Table 3.2-1 (continued)

$\left(\frac{\partial M_{TB1}}{\partial \langle\alpha_r\rangle}\right)_{U_o,p}$	$\frac{M_{TB1}}{U_o - \bar{U}_r}\left(\frac{\partial \bar{U}_r}{\partial \langle\alpha_r\rangle}\right)_p$
$\left(\frac{\partial M_{TB2}}{\partial \langle\alpha_r\rangle}\right)_{U_o,p}$	$\frac{M_{TB2}}{U_o - \bar{U}_r}\left(\frac{\partial \bar{U}_r}{\partial \langle\alpha_r\rangle}\right)_p + \frac{M_{TB2}}{\bar{U}_r - U_{\ell s}}\left(\frac{\partial \bar{U}_r}{\partial \langle\alpha_r\rangle}\right)_p + \frac{\rho_{\ell s}}{\rho_{\ell s} - \bar{\rho}_r}\left((1-f)\,V_{TB} - \frac{M_{TB2}}{\bar{\rho}_r}\right)\left(\frac{\partial \bar{\rho}_r}{\partial \langle\alpha_r\rangle}\right)_p$
$\left(\frac{\partial M_{TB}}{\partial p}\right)_{\langle\alpha_r\rangle,U_o}$	$\left(\frac{\partial M_{TB1}}{\partial p}\right)_{\langle\alpha_r\rangle,U_o} + \left(\frac{\partial M_{TB2}}{\partial p}\right)_{\langle\alpha_r\rangle,U_o}$
$\left(\frac{\partial M_{TB1}}{\partial p}\right)_{\langle\alpha_r\rangle,U_o}$	$\left[\frac{(\bar{U}_r - U_o)\left(\frac{\partial U_{\ell s}}{\partial p}\right) - (U_{\ell s} - U_o)\left(\frac{\partial \bar{U}_r}{\partial p}\right)_{\langle\alpha_r\rangle}}{(\bar{U}_r - U_o)\,(U_{\ell s} - U_o)}\right]_{M_{TB1}} + \frac{\rho_{\ell s}}{\rho_o - \rho_{\ell s}}\left(f\,V_{TB} - \frac{M_{TB1}}{\rho_o}\right)\left(\frac{\partial \rho_o}{\partial p}\right)_{U_o} - \frac{\rho_o}{\rho_o - \rho_{\ell s}}\left(f\,V_{TB} - \frac{M_{TB1}}{\rho_{\ell s}}\right)\left(\frac{\partial \rho_{\ell s}}{\partial p}\right)$

Table 3.2-1 (continued)

$\left(\frac{\partial M_{TB2}}{\partial p}\right)_{\langle\alpha_r\rangle,U_o}$	$\left[\frac{(U_{\ell s}-U_o)\left(\frac{\partial \bar{U}_r}{\partial p}\right)_{\langle\alpha_r\rangle} - (\bar{U}_r - U_o)\left(\frac{\partial U_{\ell s}}{\partial p}\right)}{(\bar{U}_r - U_o)(U_{\ell s} - U_o)}\right]M_{TB2}$ $- \frac{\rho_{\ell s}}{\rho_{\ell s} - \bar{\rho}_r}\left((1-f)V_{TB} - \frac{M_{TB2}}{\bar{\rho}_r}\right)\left(\frac{\partial \bar{\rho}_r}{\partial p}\right)_{\langle\alpha_r\rangle}$ $+ \frac{\bar{\rho}_r}{\rho_{\ell s} - \bar{\rho}_r}\left((1-f)V_{TB} - \frac{M_{TB2}}{\rho_{\ell s}}\right)\left(\frac{\partial \rho_{\ell s}}{\partial p}\right)$
$\left(\frac{\partial E_{TB}}{\partial U_o}\right)_{\langle\alpha_r\rangle,p}$	$\frac{E_{TB1}}{M_{TB1}}\left(\frac{\partial M_{TB1}}{\partial U_o}\right)_{\langle\alpha_r\rangle,p} + \frac{E_{TB2}}{M_{TB2}}\left(\frac{\partial M_{TB2}}{\partial U_o}\right)_{\langle\alpha_r\rangle,p}$ $+ M_{TB1}\left(\frac{\rho_o}{\rho_o - \rho_{\ell s}} - 1/\ln\left(\frac{\rho_o}{\rho_{\ell s}}\right)\right)$ $+ M_{TB1}\left(\frac{U_o - U_{\ell s}}{\rho_o \ln^2(\rho_o/\rho_{\ell s})} - \frac{\rho_{\ell s}(U_o - U_{\ell s})}{(\rho_o - \rho_{\ell s})^2}\right)\left(\frac{\partial \rho_o}{\partial U_o}\right)_p$

Table (3.2-1) (continued)

$$\left(\frac{\partial E_{TB}}{\partial U_o} \right)_{\langle \alpha_r \rangle, p}$$

$$\frac{E_{TB1}}{M_{TB1}} \left(\frac{\partial M_{TB1}}{\partial \langle \alpha_r \rangle} \right)_{U_o, p} + \frac{E_{TB2}}{M_{TB2}} \left(\frac{\partial M_{TB2}}{\partial \langle \alpha_r \rangle} \right)_{U_o, p}$$

$$- M_{TB2} \left(\frac{\bar{\rho}_r}{\rho_{\ell s} - \bar{\rho}_r} - 1/\ln\left(\frac{\rho_{\ell s}}{\bar{\rho}_r}\right) \right) \left(\frac{\partial \bar{U}_r}{\partial \langle \alpha_r \rangle} \right)_p$$

$$- M_{TB2} \left(\frac{U_{\ell s} - \bar{U}_r}{\bar{\rho}_r \ln^2(\rho_{\ell s}/\bar{\rho}_r)} - \frac{\rho_{\ell s} (U_{\ell s} - \bar{U}_r)}{(\rho_{\ell s} - \bar{\rho}_r)^2} \right) \left(\frac{\partial \bar{\rho}_r}{\partial \langle \alpha_r \rangle} \right)_p$$

$$\left(\frac{\partial E_{TB}}{\partial p} \right)_{\langle \alpha_r \rangle, U_o}$$

$$\frac{E_{TB1}}{M_{TB1}} \left(\frac{\partial M_{TB1}}{\partial p} \right)_{\langle \alpha_r \rangle, U_o} +$$

$$- M_{TB1} \left(\frac{\rho_{\ell s}}{\rho_o - \rho_{\ell s}} - 1/\ln\left(\frac{\rho_o}{\rho_{\ell s}}\right) \right) \left(\frac{\partial U_{\ell s}}{\partial p} \right)$$

$$+ M_{TB1} \left(\frac{U_o - U_{\ell s}}{\rho_o \ln^2(\rho_o/\rho_{\ell s})} - \frac{\rho_{ls} (U_o - U_{\ell s})}{(\rho_o - \rho_{\ell s})^2} \right) \left(\frac{\partial \rho_o}{\partial p} \right)_{U_o}$$

$$- M_{TB1} \left(\frac{U_o - U_{\ell s}}{\rho_{\ell s} \ln^2(\rho_o/\rho_{\ell s})} - \frac{\rho_o (U_o - U_{\ell s})}{(\rho_o - \rho_{\ell s})^2} \right) \left(\frac{\partial \rho_{\ell s}}{\partial p} \right)$$

Table 3.2-1 (continued)

$$+ \frac{E_{TB2}}{M_{TB2}} \left(\frac{\partial M_{TB2}}{\partial p} \right)_{U_o, \langle \alpha_r \rangle}$$

$$+ M_{TB2} \left(\frac{\rho_{\ell s}}{\rho_{\ell s} - \bar{\rho}_r} - 1/\ln\left(\frac{\rho_{\ell s}}{\bar{\rho}_r}\right) \right) \left(\frac{\partial U_{\ell s}}{\partial p} \right)$$

$$+ M_{TB2} \left(\frac{U_{\ell s} - \bar{U}_r}{\rho_{\ell s} \ln^2(\rho_{\ell s} / \bar{\rho}_r)} - \frac{\bar{\rho}_r (U_{\ell s} - \bar{U}_r)}{(\rho_{\ell s} - \bar{\rho}_r)^2} \right) \left(\frac{\partial \rho_{\ell s}}{\partial p} \right)$$

$$- M_{TB2} \left(\frac{U_{\ell s} - \bar{U}_r}{\bar{\rho}_r \ln^2(\rho_{\ell s} / \bar{\rho}_r)} - \frac{\rho_{ls} (U_{\ell s} - \bar{U}_r)}{(\rho_{\ell s} - \bar{\rho}_r)^2} \right) \left(\frac{\partial \bar{\rho}_r}{\partial p} \right)_{\langle \alpha_r \rangle}$$

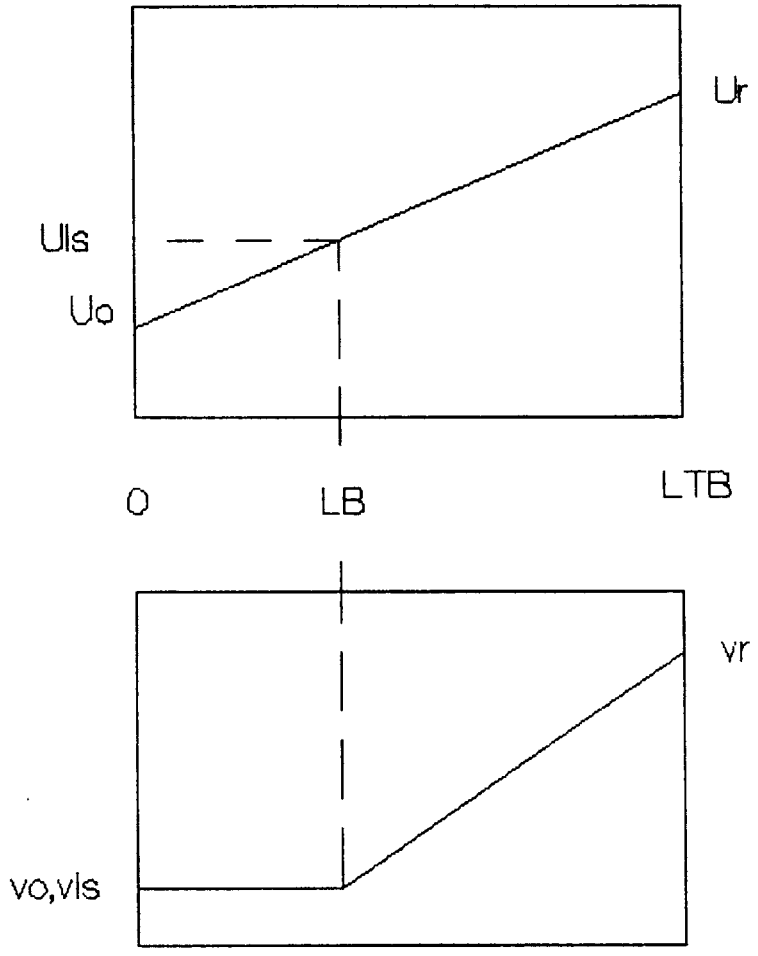

3.2-1 Specific volume profile in the modified model

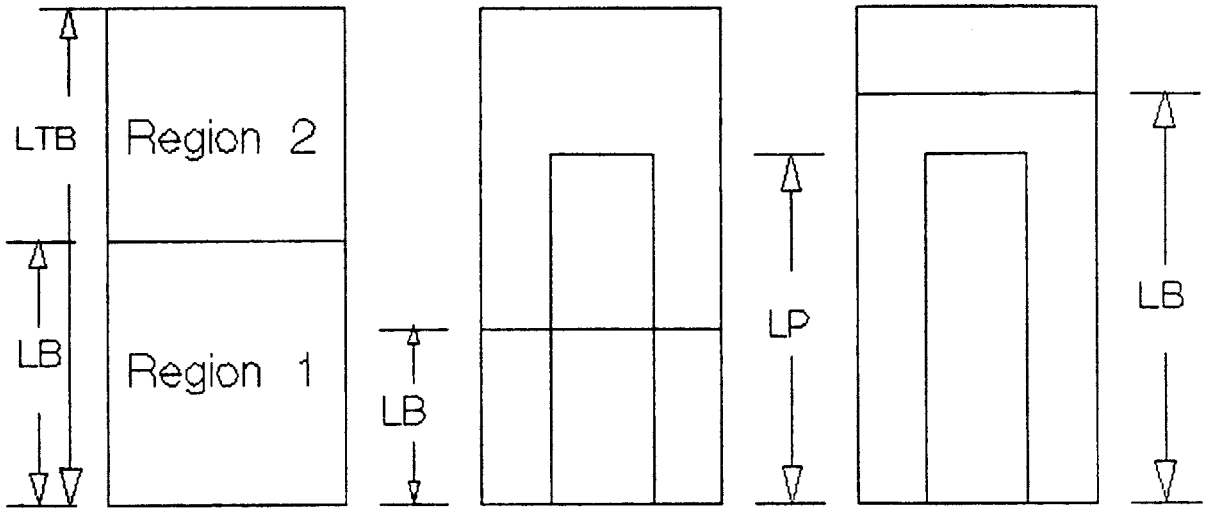

3.2-2 Tube bundle regions in the modified model (a),(b),(c)

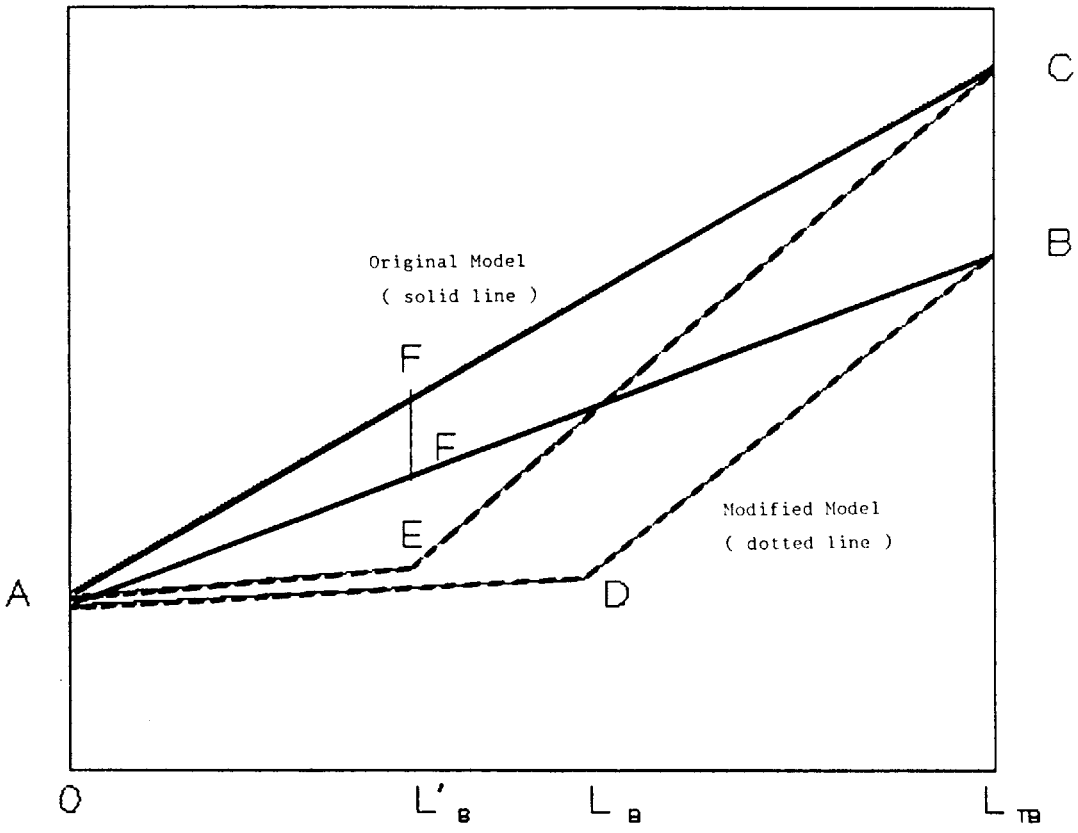

3.2-3 Specific volume proflie change due to the steam flow step-up

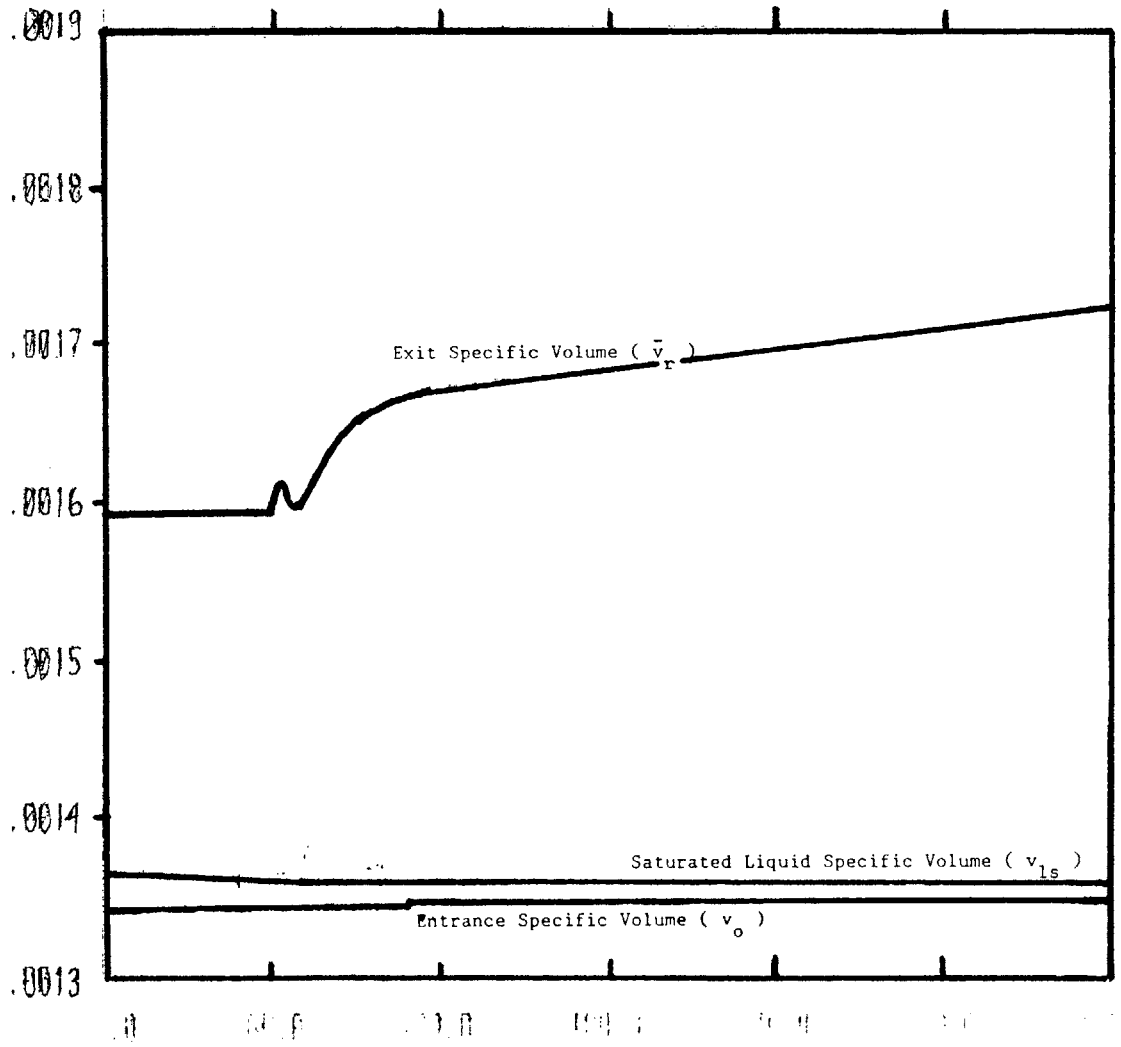

3.2-4 Transient response of specific volumes to the steam flow step-up

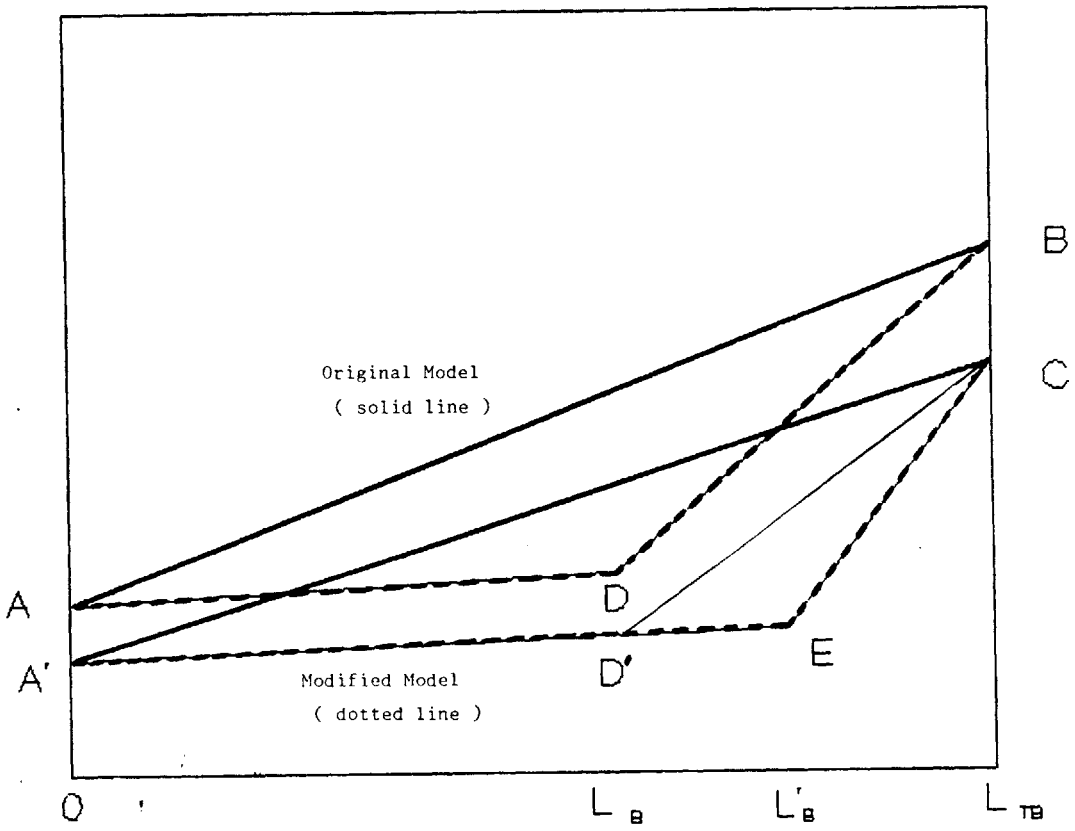

3.2-5 Specific volume profile change due to the feed flow step-up

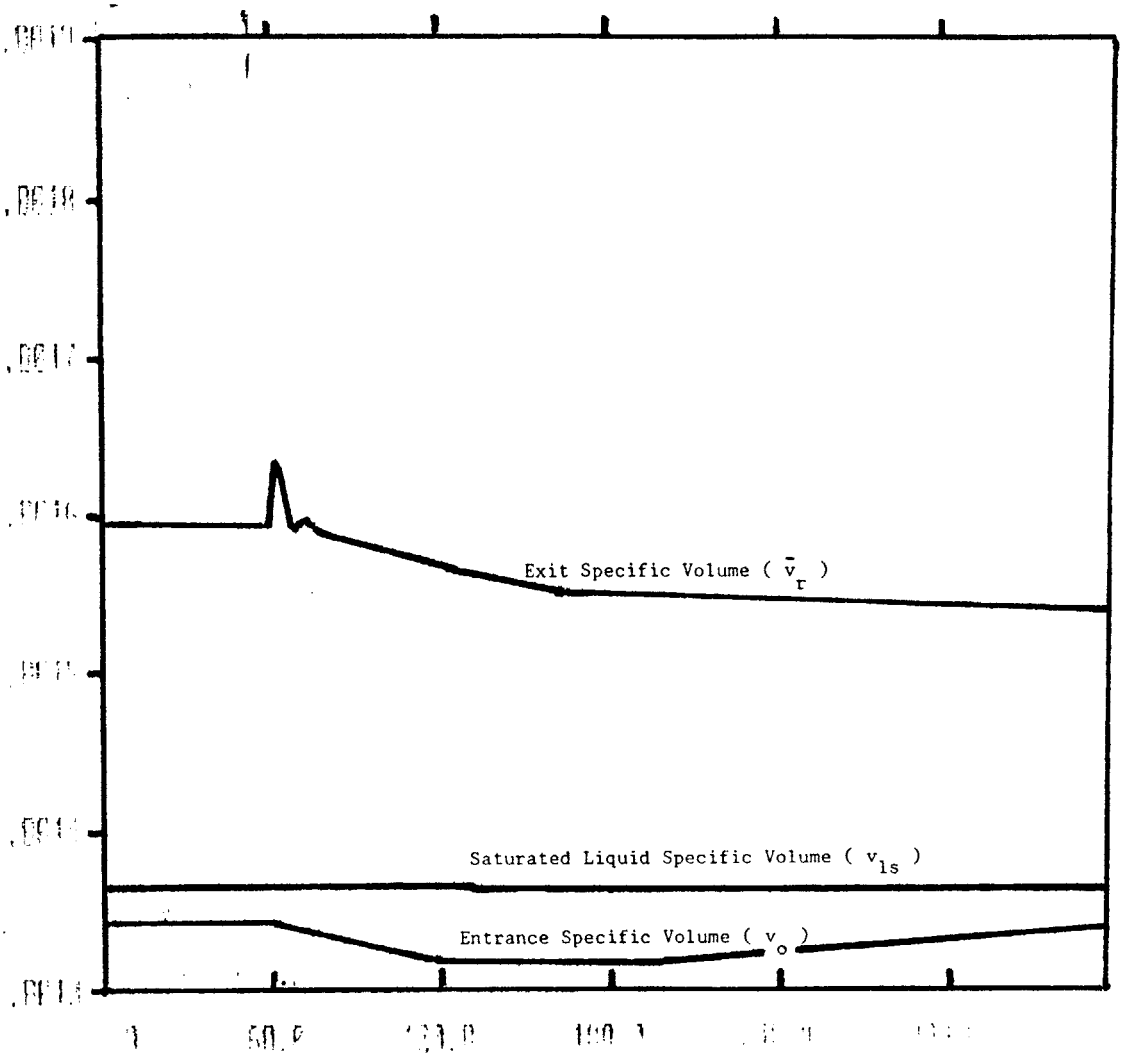

3.2-6 Transient response of specific volumes to the feed flow step-up

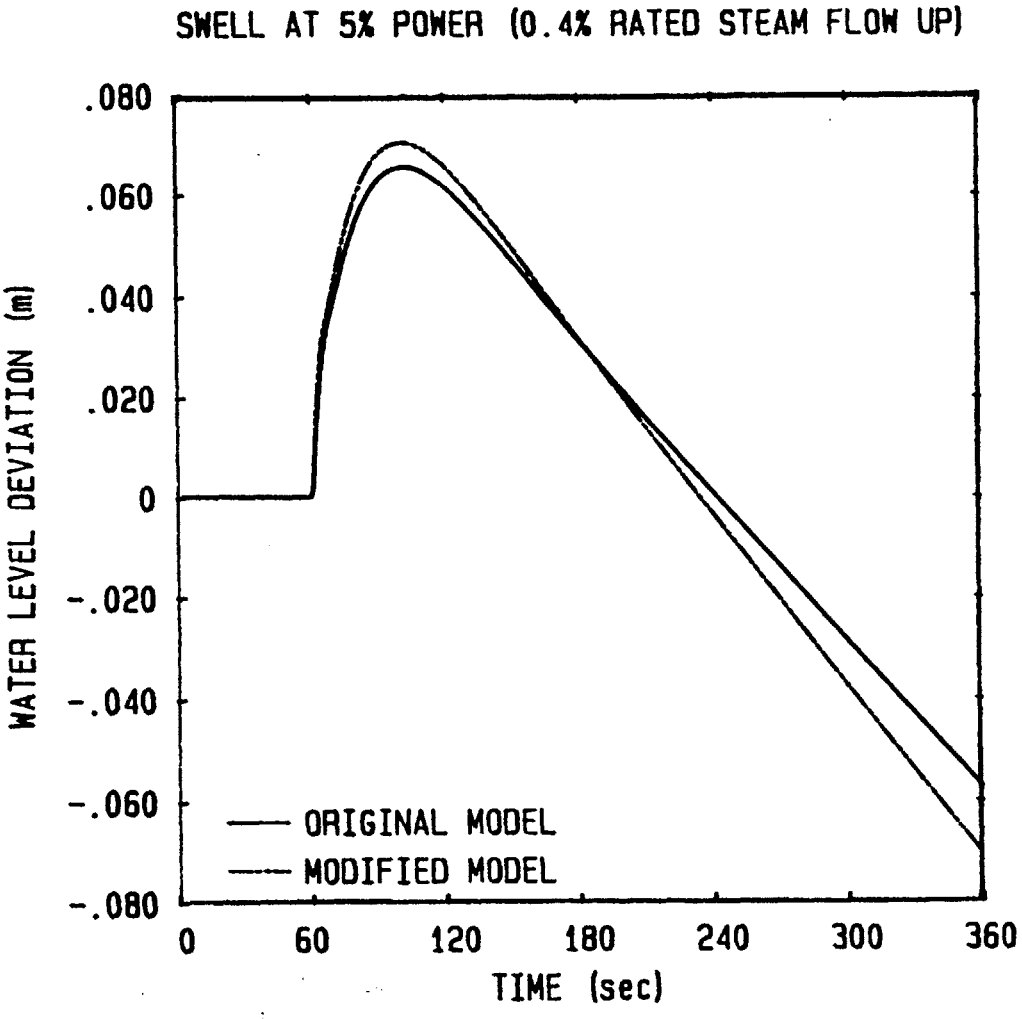

3.2-7 Modification effect in the level response to the steam flow step-up

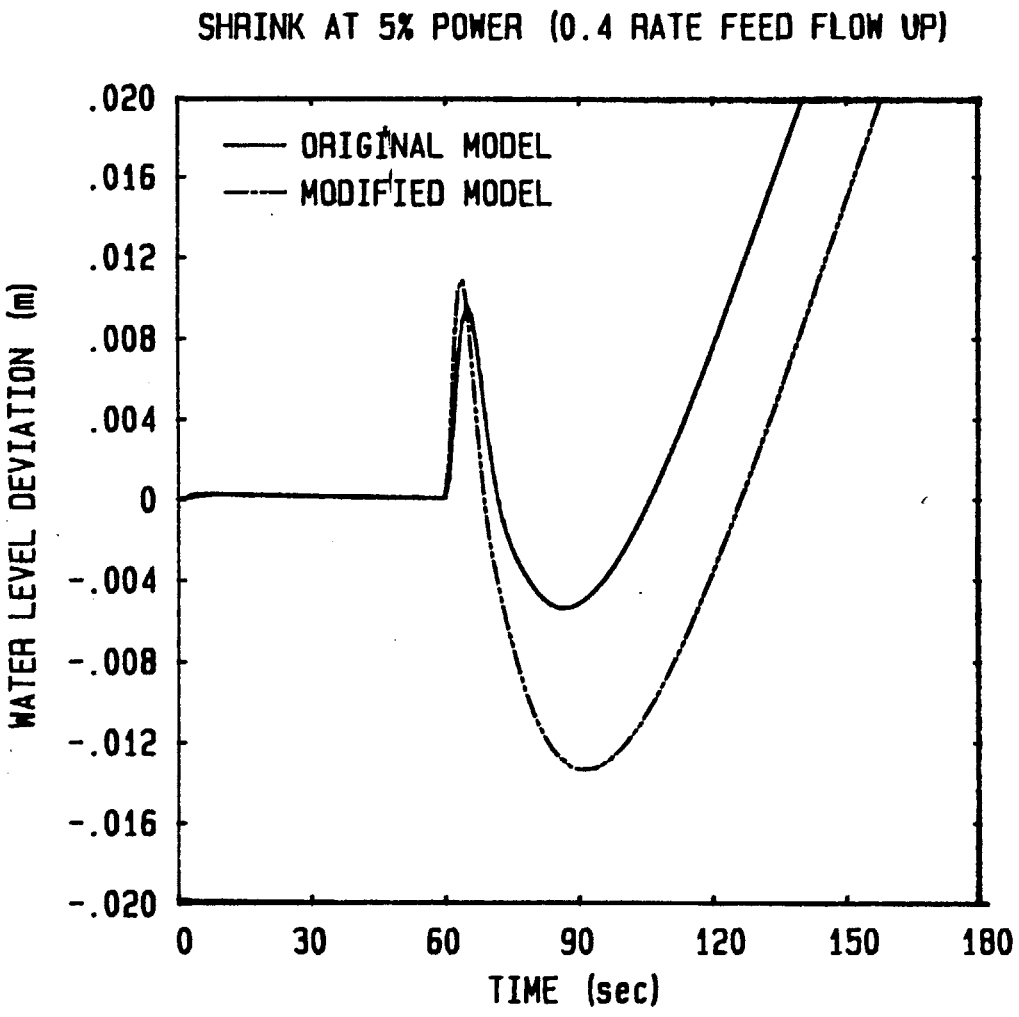

3.2-8 Modifiaction effect in the level response to the feed flow step-up

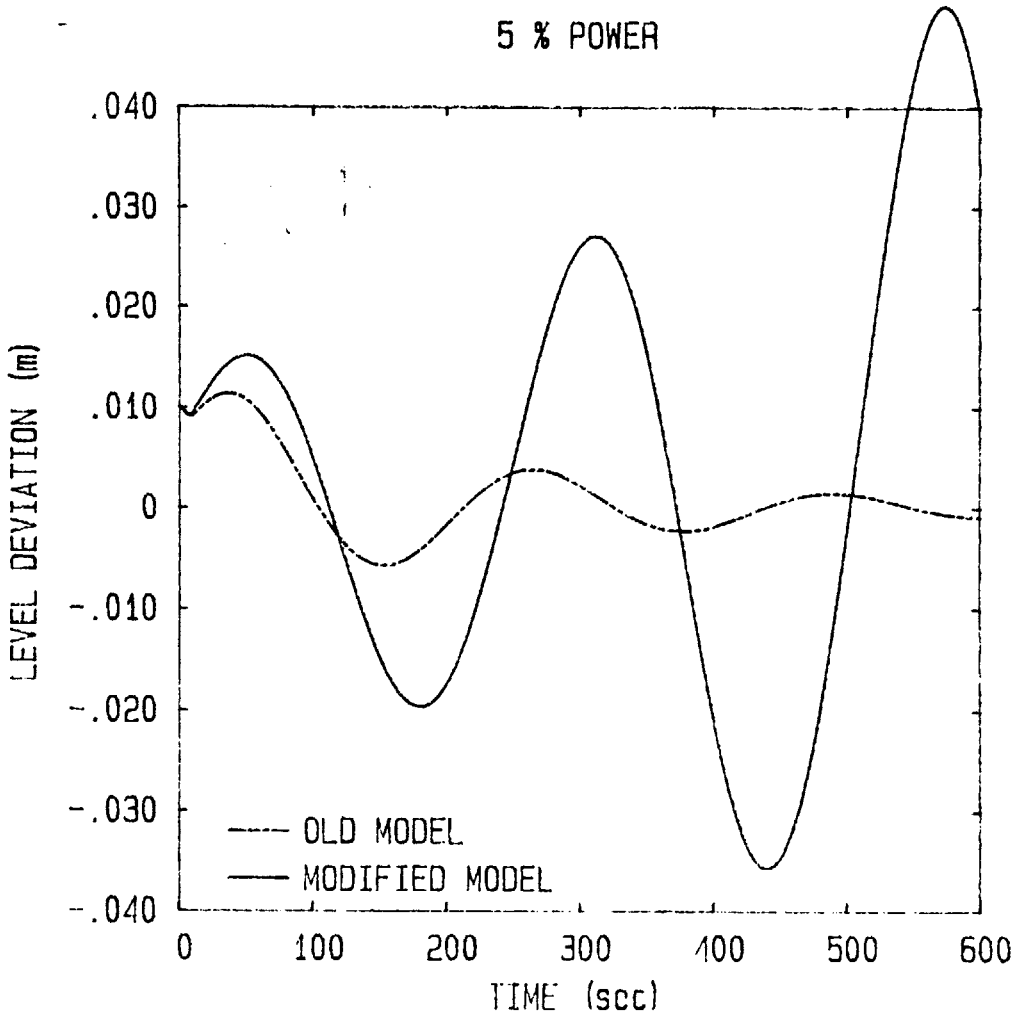

3.2-9 Modification effect in the controlled level response

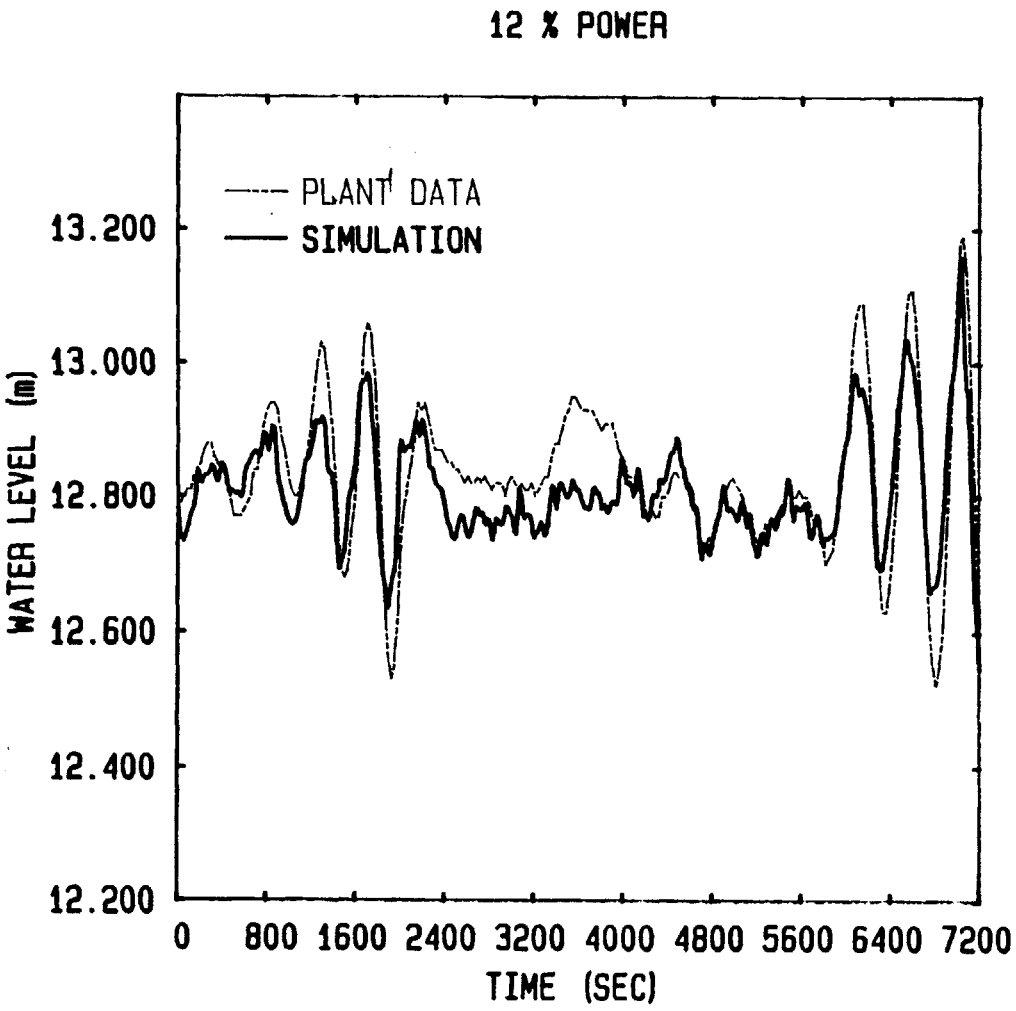

3.2-10 Calculated water level with plant data at 12 % power

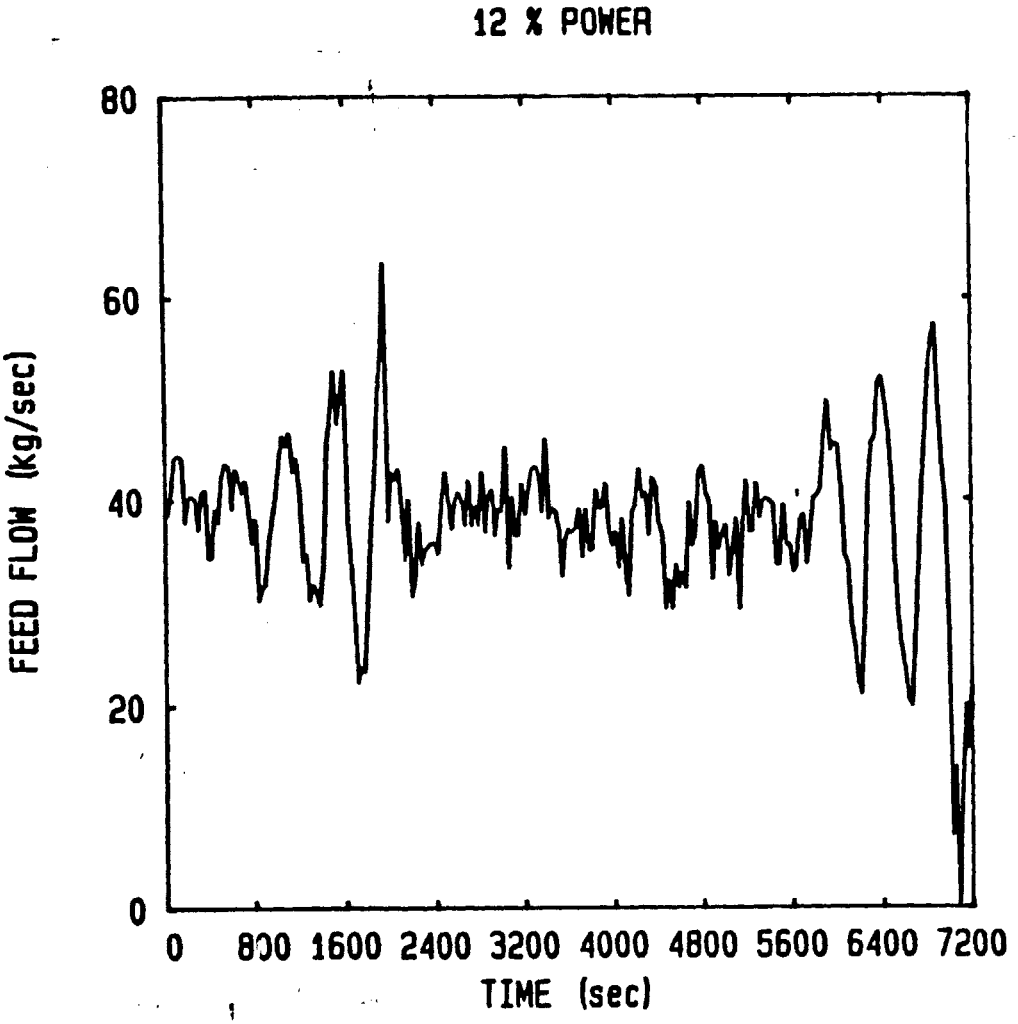

3.2-11 Feedwater flow input at 12 % power

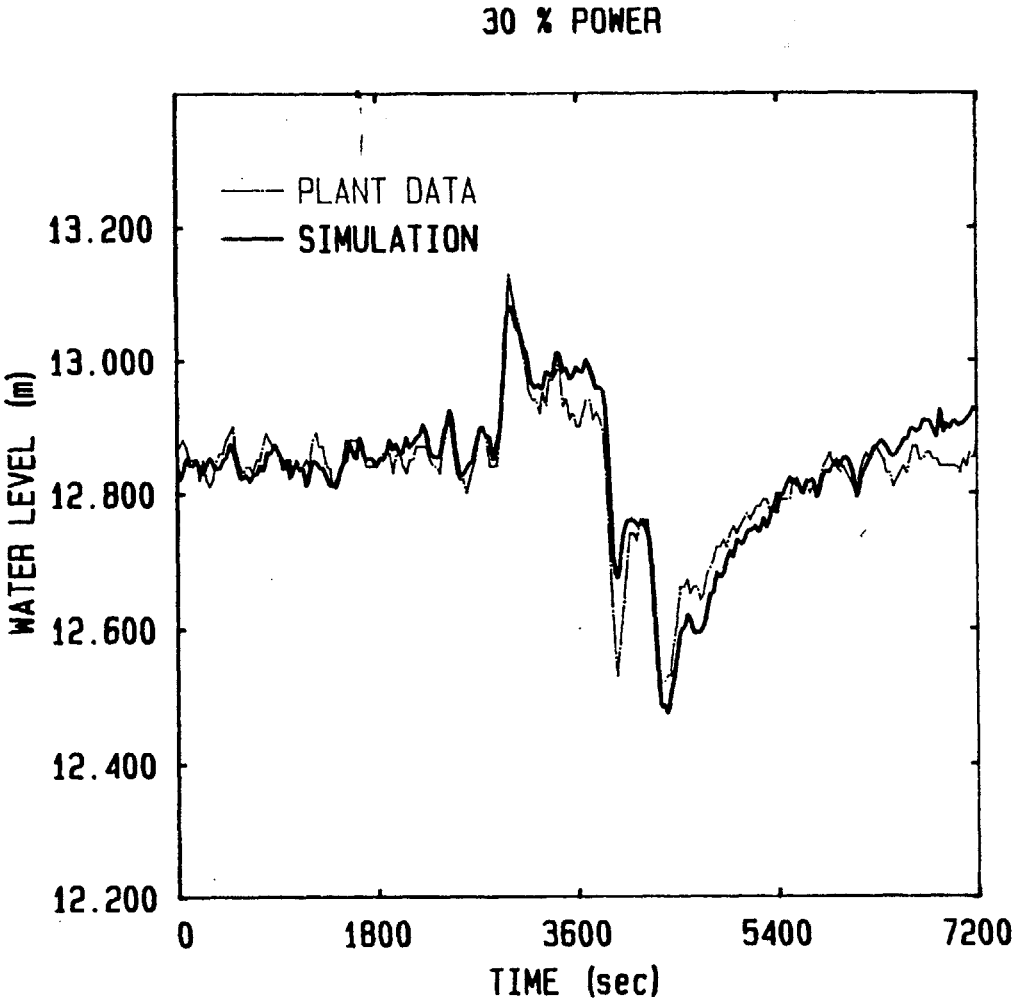

3.2-12 Calculated water level with plant data at 30 % power

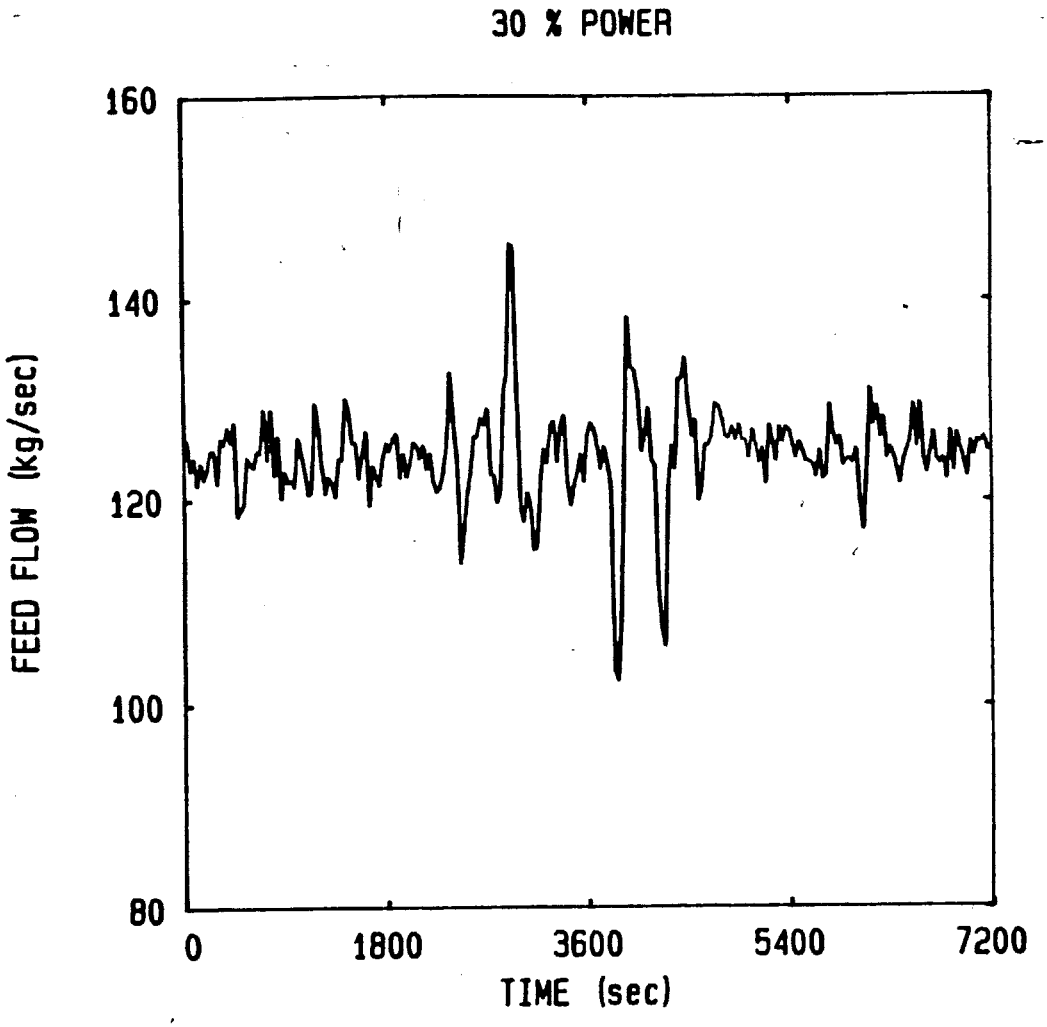

3.2-13 Feedwater flow input at 30 % power

Chapter 4

CONTROLLER DESIGN

In Chapter 2, a detailed description has been given for the controller of the steam generator water level in a PWR plant and for existing associated problems. In this chapter, a description is given of efforts to combine a controller simulation action with the steam generator dynamic model.

In the first part of this chapter, a conventional controller is discussed along with a calculational description of existing problems. In the second part, a new controller is proposed along with its solutions to the existing control problems.

The evaluation of the proposed controller will be given in the next chapter.

4.1 Conventional Controller

4.1.1 Description of a "Conventional Controller"

A simplified controller is modeled for representing the steam generator water level control system in a PWR plant.

This controller is of a three-element proportional-plus-integral (P.I) type. It represents the basic control scheme of the existing installed units at high power (at low power, steam flow and feed flow inputs are either eliminated or are replaced by well-behaved estimates).

The control action of a three-element proportional-plus-integral controller is described by the following equation in terms of the primary control variables : feedwater flowrate W_{fw} ; steam flowrate W_s ; and downcomer water level L_w ;

$$\frac{d\,W_{fw}}{d\,t} = K_{pw}\left(\frac{d\,\epsilon_W}{d\,t} + \frac{1}{T_{iw}}\,\epsilon_W\right) + K_p\left(\frac{d\,\epsilon_L}{d\,t} + \frac{1}{T_i}\,\epsilon_L\right) \quad (4.1 - 1)$$

where

t = time (s) ;

K_{pw} = proportional flow gain ;

$\epsilon_W = (W_s - W_{fw})$, flow error (kg/s) ;

T_{iw} = flow integral time (fixed at 200 s) ;

K_p = proportional level gain (kg/m-s) ;

T_i = integral time (s) ($1/T_i$ = reset rate) ;

$\epsilon_L = (L_{Ref} - L_w)$, level error (m) ; and

L_{Ref} = reference (programmed) water level (m)

The schematic for this controller is given in Fig. 4.1-1.

A typical installed controller (Chapter 2) is different in detail but uses the same three variables (W_{fw}, W_s, and L_w) to calculate a control error . Adjustment of feedwater flow is performed in a more indirect and non-linear manner by combining with the pump speed controller and by using more complex control logic with the cascaded proportional-plus-integral (P.I) controllers.

In spite of the simplification adopted in Eq.4.1-1, this simplified representation of the controller has most of the characteristics of the existing installed units. Futhermore, its simplicity permits the effects of parameter changes on control characteristics to be made clear.

From now on, the simpified model given in Eq. (4.1-1) is used to represent the "conventional controller" for the steam generator water level in a PWR plant.

4.1.2 Existing Control Problems

To examine the nature of existing control difficulties, performance of the conventional controller is discussed by presenting the simulated level responses that combine Eq. 4.1-1 with our steam generator model (Chapter3).

The important parameters to be considered are two gains (level gain, K_p and flow gain, K_{pw}), the integral time, T_i and the operating power level. While the gains and integral time define the characteristics of the controller, the power level is associated with the steam generator dynamics.

In Fig. 4.1-2, water level behavior is shown in its response to a power increase from 10% to 15%. The power increase is performed over a one minute span (5%/minute) by ramping steam flow and hotleg temperature. Several findings from these results are :

1) As the level gain K_p increases from 100 to 200 (level error (ϵ_L) effect increases), the level control system becomes unstable (Fig.

4.1-2 (a)).

2) A similar result is obtained by decreasing the integral time (T_i) from 50 s to 25 s (Fig. 4.1-2 (b)).

3) As the flow gain K_{pw} decreases from 1.0 to 0.1 (flow error (ϵ_W) effect decreases), the system becomes unstable (Fig. 4.1-2 (c)).

4) Fig. 4.1-3 shows the responses of level to similar transients initiated at higher power levels (30 % and 95 %). Using control parameters that make the system unstable at low power (10 %), the system is stable at higher powers. A finding is that the system becomes more stable as power goes up.

To summarize these findings, it appears that the ratio of ϵ_W/ϵ_L effects and power level are the crucial factors to determine the system stability : As the ratio of ϵ_W/ϵ_L or power level decreases, the system becomes unstable.

This stability problem is attributed to non-minimum phase properties (described in the following subsection) of the steam generator level dynamics due to the shrink and swell effects. As described in the previous chapters , the shrink and swell effects sensed within the downcomer give a reverse level indication that complicates the choice of proper control action. If these reverse effects combined with a high level feedback gain, the result may be large enough to make the system unstable. On the other hand , the flow error signals always give the right indication for the control action. The unstable dynamics can be avoid by a high flow gain , which compensates for the reverse effects. Thus the system stability

increases as the ratio ϵ_W/ϵ_L increases.

The shrink and swell effects become accentuated as the power level decreases because of following reasons :

1) A given increment in steam or feed flowrate is a relatively larger fraction of the existing flow at a low power condition.

2) Cold feedwater exists at a low power condition and is much colder than saturated recirculating liquid. Thus tube bundle vapor content is very sensitive to changes in the ratio of feedwater flow to recirculating liquid flow.

Results of these effects are well shown in Fig. 4.1-4 (a) and (b). Fig. 4.1-4 (a) shows the level response to a step increase of feedwater flow with steam flow held constant. And Fig. 4.1-4 (b) shows the level response to a step increase of steam flow with feedwater flow held constant. Thus the steam generator "reverse challenge" also implies that system stability increases with the power level as well as with the ratio ϵ_W/ϵ_L . These results confirm features of earlier studies (Ref.[I1], figs.2 and 3).

Once the turbine is on-line and feedwater heaters start to operate, the feedwater becomes hot enough to weaken the shrink and swell effects. After that, the feedback gains can be set to the values for the optimized performance of the controller without being subject to stringent constraints due to stability problems. Therefore our study of control problems is focused on low power conditions prior to the turbine on-line (typically below 15 %).

In this regime, the profound reverse dynamics due to the shrink and swell effects require a high ratio of ϵ_W/ϵ_L to satisfy the stability requirements. One simple solution is to increase the flow gain , K_{pw} . However, a second problem exists at low power conditions. It is the large uncertainty of the flow sensors at low flowrate, low power conditions. Since the flow error in the controller is subject to significant uncertainty and may mislead the control action. Actually, as shown in the plant data (Fig. 4.1-5), the steam and feedwater flow measurements are quite erratic. Other detectors connected to the same flow elements show equally erratic behavior but show no correlation with those plotted. Therefore existing detectors are too uncertain to use for the control input. Thus the high flow gain implies that the flow error term is relatively more important than the level error term. Therefore, the controller response depends to a large extent on unreliable input signals. This adverse condition leads to the decrease in controller robustness with respect to flow measurements. We use the term "robustness to flow measurements" to designate the controller attribute of a response which remains effective despite flow measurements uncertainty.

The other way to satisfy the stability requirements is to decrease the level error ϵ_L by decreasing the proportional gain K_p or increasing the integral time T_i. These approaches lead to a poor controller capability; the level response to the imposed transient becomes sluggish (Fig. 4.1-6). We use the term "capability" to designate the controller attribute of a fast effective response in

counteracting imposed disturbances. The stability and capability are usually the conflicting controller attributes that must be subjected to a trade-off for a good controller design.

At low power conditions, a different scheme is often used in existing plants. In this case, the uncertain flow error term is replaced by a term proportional to the reactor power from neutron detectors. Also, in order to satisfy the stability requirements, the level gain of the controller is set to a relatively small value. Great care is exerted to avoid rapid changes while in automatic control. It is often found that manual control is adopted to avoid trips caused by automatic control.

In conclusion, the control schemes provided conventionally do not permit satisfactory automatic level control at low power conditions. Now we seek a controller that has both robustness to flow measurements and good capability. This is achieved by increasing the level feedback without incurring a stability penalty.

Before proposing the new controller, the nature of the stability problem of the conventional controller is verified by using a simplified linear steam generator level model in the following subsection.

4.1.3 Simplified Steam Generator Level Model

Since our steam generator model is still a nineth order non-linear system, it is not easy to apply analytic control concepts to evaluate performance. Special techniques for the non-linear system

analysis (e.g. Ref. [G2], [H3]). These techniques are not practical to use for the analysis of our system.

For this reason, a low-order linear model for the steam generator level dynamics (designated a "simplified model") is adopted to gave an approximate representation of our steam generator model. The simplified model is deduced through system identification (Ref. [A1], [D1]) from the transient responses of our steam generator model to the step input. The approach follows (but is somewhat simpler than) the approach of Irving and Bihoreaux (Ref. [I1]). With this simplified linear model, we can evaluate controller performance analytically, especially in relation to stability.

The simplified model is given as a Laplace transfer function with the inputs feedwater flowrate and steam flowrate; and the output downcomer water level, as follow :

$$L_w(s) = \left(\frac{G_1}{s} - \frac{G_2}{1 + \tau_2 s} \right) W_{fw}(s) + M(s) W_{fw}(s)$$

$$- \left(\frac{G_1}{s} - \frac{G_2'}{1 + \tau_2' s} \right) W_s(s) \qquad (4.1-2)$$

where, s is the Laplace variable ; $L_w(s)$, $W_{fw}(s)$, and $W_s(s)$ are the Laplace transforms, respectively, of $(L_w(t) - L_w(0))$, $(W_{fw}(t) - W_{fw}(0))$, and $(W_s(t) - W_s(0))$

Each term of Eq. 4.1-2 can be interpreted as follow :

1) G_1 / s is the mass capacity effect of the steam generator (designated "mass capacity term"). G_1 is a positive constant and independent of the power level.

2) $- G_2 / (1 + \tau_2 s)$ and $- G_2' / (1 + \tau_2' s)$ are the reverse effects due to the shrink and swell from the step change of feedwater flow and steam flow respectively (designated "reverse dynamics term"). G_2 and G_2' are positive and found to decrease with the power level increase. τ_2 and τ_2' are time constants for reverse dynamics and are also found to decrease with the power level increase.

3) M (s) is a "mechanical oscillation" term due to the direct addition of the feedwater to the downcomer column. Therefore this term appears only in the response to feedwater change. As shown in Fig. (4.1-4), an initial level peak exists that is attributed to this term. It is found that this term quickly damps out. In further analysis, this term is neglected.

Many of the characteristics of the "simplified model" can be examined by considering behavior with steam flow maintained at a constant value. In this case, the transfer function can be written as:

$$T(s) = \frac{L_w(s)}{W_{fw}(s)} = \left(\frac{G_1}{s} - \frac{G_2}{1 + \tau_2 s} \right) \qquad (4.1 - 3)$$

or

$$= \left(\frac{G_1 - (G_2 - G_1 \tau_2) s}{s (1 + \tau_2 s)} \right) \qquad (4.1 - 4)$$

This transfer function is characterized by two poles and one zero :

$$p_1 = 0 \; ; \; p_2 = - 1 / \tau_2 \qquad (\text{poles}) \qquad (4.1 - 5)$$

and

$$z_1 = G_1 / (G_2 - G_1 \tau_2) \qquad (\text{zero}) \qquad (4.1 - 6)$$

For the numerical values of some of these parameters as a function power level, a system identification was performed in Appendix [D] from the transient responses to step increases in feedwater using full nonlinear steam generator model. Results are given in Table 4.1-1. It is noted that z_1 is always positive and increasing with the power level increase.

Since the zero lies in the right half s-plane, the system is of a non-minimum phase (Ref. [O1],[H2],[S5]). When combined the controller, the non-minimum phase system encounters the stability problems at a high feedback. Consider the closed loop transfer function for system controlled by a single element P.I controller (shown in Fig.4.1-7). That is, consider the "conventional controller" of Eq.4.1-1 with a proportional gain K_p ,an integral time T_i, and $K_{pw} = 0$ to obtain the following closed loop transfer function:

$$T_{CL}(s) = \frac{K_p (1 + 1 / T_i s) \quad T (s)}{1 + K_p (1 + 1 / T_i s) T (s)} \qquad (4.1 - 7)$$

From this closed loop transfer function, we obtain two zeros and three poles:

$z_1 = G_1 / (G_2 - G_1 \tau_2)$, and $z_2 = - 1 / T_i$ (zeros) ;

and

p_1^c , p_2^c , and p_3^c (poles) ; roots of the following characteristic equation ,

$$(T_i \tau_2) s^3 + T_i \left(1 - \frac{K_p G_1}{z_1} \right) s^2 + K_p G_1 \left(T_i - \frac{1}{z_1} \right) s$$

$$+ K_p G_1 = 0 \qquad (4.1 - 8)$$

For stability, all poles should lie in the left half s-plane. By applying Routh stability criterion (Ref. [02]) to Eq. (4.1-8), we can obtain the stability requirements as follow :

$$[1 - K_p (G_2 - G_1 \tau_2)] > 0 \ ; \qquad (4.1\text{-}9\ (a))$$

$$[T_i - (G_2 - G_1 \tau_2) / G_1] > 0 \ ; \qquad (4.1\text{-}9\ (b))$$

and

$$K_p < \frac{1}{G_2 - G_1 \tau_2} \left(1 - \frac{\tau_2}{T_i - (G_2 - G_1 \tau_2) / G_1} \right)$$

(4.1-9 (c))

The detailed stability analysis is given in Appendix [E].

From the results of this stability analysis, we can make following remarks :

1) The steam generator level dynamics (open loop) is of a non-minimum phase ,which is attributed to the shrink and swell effects (positive value of (G_2 - G_1 τ_2)), and the controlled (closed loop) system is subject to a corresponding feedback gain constraint to maintain stability.

2) As the power level goes down, the stability constraint becomes more stringent with a larger value of (G_2 - G_1 τ_2). Therefore, a high feedback gain may cause an instability at low power condition. Such analytically obtained knowledge is found to be useful in the design of a new controller in the next section.

4.2 Proposed Controller

In this part of the chapter, a new physically-based control algorithm (designated a "proposed controller") is suggested to solve the problems encountered by the "conventional controller" described in the previous section.

The proposed approach to the design of a new controller is based on an assumption that the current analog control loop has been replaced with digital computer control (Ref. [E1]). This premise greatly expands the range of possible approaches. The digitizing

effects of the controller (Ref. [A1],[F1]) are not considered in the design of a new controller. They are discussed as one of the practical features in Appendix [F].

4.2.1 Physically-Based Design Approach

A proposed controller is aimed at both good capability and good robustness to flow measurements. Level gain is increased without incurring the stability penalty. The challenge is to make the controller with a high level gain survive the reverse dynamics due to the shrink and swell effects at low power conditions. It starts with extracting physical ideas by observing the downcomer level behavior associated with the shrink and swell effects.

Returning to the simplified model for the downcomer level dynamics given in Eq. (4.1-3) , we consider the response of the level to a unit step increase of the feedwater flow :

$$L_w(s) = \left(\frac{G_1}{s} - \frac{G_2}{1 + \tau_2 s} \right) \frac{1}{s} \qquad (4.2-1)$$

Taking the inverse Laplace transform of this equation , we obtain the time response of the level :

$$L_w(t) - L_w(0) = G_1 t - G_2 (1 - e^{-t/\tau_2}) \qquad (4.2-2)$$

or

$$\delta L_w(t) = \delta L_{w1}(t) + \delta L_{w2}(t) \qquad (4.2-3)$$

where,

$\delta L_w(t) = L_w(t) - L_w(0)$; $L_w(0)$ = initial level ;

$\delta L_{w1}(t) = G_1 t$: mass capacity term ;

$\delta L_{w2}(t) = - G_2 (1 - e^{- t/\tau_2})$: reverse dynamics term

In Figs. 4.2-1 and 4.2-2, the level response $\delta L_w(t)$ by the nonlinear model is shown with its decomposed ingredients $\delta L_{w1}(t)$ and $\delta L_{w2}(t)$. We see that Eq. (4.2-2) is a good linear approximation.

In Fig. 4.2-2 , we see the reverse dynamics term δL_{w2} , the portion of level response contributed by the shrink effect to the feedwater flow step increase, is temporarily reverse to the actual mass behavior and then saturated to a constant term. The parameter, G_2 represents the magnitude of the shrink and swell effects and τ_2 is its time constant for saturation. It is found that the values of G_2 and τ_2 increase as the power level decreases. It implies that the shrink and swell effects become more pronounced and act more slowly at low power conditions. It means that it becomes more difficult to treat the reverse dynamics of shrink and swell at low power conditions either by the automatic or by the manual control.

As the reverse dynamics increases, the value of $(G_2 - G_1 \tau_2)$ becomes more positive. Concerning the stability of the controlled system, the more positive value of $(G_2 - G_1 \tau_2)$ imposes the more restrictive constraint on the level feedback gain as given in Eq. (4.1-9).

The above discussion leads to the consideration of another control variable, which is less susceptible to the reverse dynamics than the actual level and allows the controller to have a higher feedback gain. This other variable is one related to the steam generator mass content. It is obtained by compensating the actual level for the reverse dynamics of shrink and swell. This variable is designated a "compensated level" to distinguish it from the "actual level".

For a better explanation, consider the simplified model of Eqs. (4.2-2) and (4.2-3). We introduce a compensation term $\delta L^c_{w2}(t)$ for the reverse dynamics term $\delta L_{w2}(t)$ as follows :

$$\delta L^c_{w2}(t) = + G^c_2 \left(1 - e^{- t/\tau_2} \right) \qquad (4.2-4)$$

Then, the compensated level $\delta L^c_w(t)$ is :

$$\delta L^c_w(t) = \delta L_w(t) + \delta L^c_{w2}(t)$$

$$= \delta L_{w1}(t) + \left(\delta L_{w2}(t) + \delta L^c_{w2}(t) \right)$$

$$= G_1 t - \left(G_2 - G^c_2 \right) \left(1 - e^{- t/\tau_2} \right) \qquad (4.2-5)$$

Performing a stability analysis similar to that done previously (Eq. 4.1-9), the feedback terms (K_p and T_i) for the compensated level are subject to the following modified constraints :

$$[\ 1\ -\ K_p\ (\ (\ G_2\ -\ G_2^c\ )\ -\ G_1\ \tau_2\ )\ ]\ >\ 0\ ; \qquad (4.2\text{-}6\ (a))$$

$$[\ T_i\ -\ (\ (\ G_2\ -\ G_2^c\ )\ -\ G_1\ \tau_2\ )\ /\ G_1\ ]\ >\ 0\ ; \qquad (4.2\text{-}6\ (b))$$

and

$$K_p\ <\ \frac{1}{(\ G_2\ -\ G_2^c\ )\ -\ G_1\ \tau_2}\left[\ 1\ -\ \frac{\tau_2}{T_i\ -\ ((G_2-\ G_2^c)\ -\ G_1\ \tau_2\ )\ /\ G_1}\ \right]$$

(4.2-6 (c))

Provided that $G_2^c > 0$, then the stability constraints on K_p and T_i are mitigated. To be completely free of these constraints, the condition is :

$$(\ G_2\ -\ G_2^c\ )\ -\ G_1\ \tau_2\ \leq\ 0$$

or

$$G_2^c\ \geq\ (\ G_2\ -\ G_1\ \tau_2\ ) \qquad (\ 4.2\ -\ 7\ )$$

If G_2^c is equal to G_2 :

$$G_2^c\ =\ G_2\ , \qquad (\ 4.2\ -\ 8\ )$$

then obviously Eq. (4.2-7) is satisfied by the margin of $G_1\ \tau_2$. In this case, the reverse dynamics term $\delta L_{w2}\ (t)$ is exactly eliminated and then the compensated level $\delta L_w^c\ (t)$ becomes equal to the mass capacity term $\delta L_{w1}\ (t)$. Therefore the compensated level

always gives a proper indication of the mass inventory change. This condition can be considered a target condition for calculating the compensation term.

Then, how we can get the compensation term δL^c_{w2} (t) , which has been suggested in the form of G^c_2 (1 - $e^{- t/\tau_2}$) to compensate the reverse dynamics term of $-G_2$ (1 - $e^{- t/\tau_2}$) ?

If the reverse dynamics term δL_{w2} (t) were measured directly , it would be used as an optimal compensation term δL^c_{w2} (t) simply by changing the sign. However, there is no physical sensor for this term.

If the mass capacity term δL_{w1} (t) is available (or its equivalent, a sensor that measures mass contents), it could be directly used as a compensated level δL^c_w (t) . The term δL_{w1} (t) is, in principle, obtainable indirectly from by the flow mismatch using the feedwater and steam flow measurements. However, as mentioned before, the flow measurements are too uncertain to use at low power.

Now, we try to find another variable for the compensation term δL^c_w (t) . This variable should have a time variation with the form of G (1 - $e^{- t/\tau_2}$) in response to a change of a feedwater flow. That is, the variable should exponentially saturate to a certain value G with the time constant τ_2. As a good candidate, the calculated mass of the tube bundle region M_{TB} is considered. As described in Chapter 2 , the shrink and swell effects are mainly attributed to the tube bundle mass change. Thus the tube bundle mass change may be a good measure of the downcomer level change contributed by the shrink

and swell effects.

To support this suggestion, a physical explanation is given that is based on the simplified model. For a better physical understanding, the response of the downcomer level L_w (t) is replaced by that of the downcomer mass M_{DC} (t) with the following relationship :

$$\delta M_{DC}\ (t) = \rho_{\ell s}\ A_{DC}\ \delta L_w\ (t) \qquad (4.2 - 9)$$

where

$\rho_{\ell s}$ = saturated liquid density (assumed constant) ,

A_{DC} = the area of the downcomer at the location of level measurement , and

$\delta M_{DC}\ (t) = M_{DC}\ (t) - M_{DC}\ (0)$;

$M_{DC}\ (0)$ = initial downcomer mass

This term M_{DC} (t) is measurable because there is a physical sensor for L_w (t) . The term can be also decomposed into two terms :

$$\delta M_{DC}\ (t) = \delta M_{DC1}\ (t) + \delta M_{DC2}\ (t) \qquad (4.2 - 10)$$

where

$$\delta M_{DC1}\ (t) = \rho_{\ell s}\ A_{DC}\ \delta L_{w1}\ (t)$$

and

$$\delta M_{DC2}\ (t) = \rho_{\ell s}\ A_{DC}\ \delta L_{w2}\ (t)$$

The subscripts 1 and 2 denote the contributions due to the mass capacity term and the reverse dynamics term respectively. Neither

δM_{DC1} (t) nor δM_{DC2} (t) is measurable.

Compare Eq. (4.2-10) to Eqs. (4.2-2) and (4.2-3) of the simplified model. At times that are long compared to τ_2: the first term (δM_{DC1}) on the right hand side of Eq. (4.2-10) shows a linear increase: the second term (δM_{DC2}) is constant. The offset between them depends on the steam generator dynamics. Note that this interpretation is based on a constant value of A_{DC} (characteristic of the Westinghouse Type F steam generator and corrected with minor changes in interpretation for other cases).

Now consider the simulation results shown in Fig.4.2-3. Calculated masses are given in response to a step increase in feedwater flow (using our non-linear steam generator model). At long times, the tube bundle mass (δM_{TB}) is virtually constant. The riser mass (δM_R) and the downcomer mass (δM_{DC}) are varying in a linear manner.

The following relationships apply for interrelating the mass variables of interest:

From a total mass balance,

$$\delta M_{TOT} = \delta M_{DC} + \delta M_R + \delta M_{TB}; \qquad (4.2\text{-}11)$$

or equivalently,

$$\delta M_{DC} = (\delta M_{TOT} - \delta M_R) - \delta M_{TB} \qquad (4.2\text{-}12)$$

By comparing this result with Eq. (4.2-10), we see that the term in parentheses on the right hand side has a linear behavior analogous to δM_{DC1} and that the tube bundle mass term ($-\delta M_{TB}$) has a constant behavior analogous to δM_{DC2}. We therefore intend to use an approximate

calculation for the tube bundle mass (multiplied by a constant specified parameter) to approximate the reverse dynamics term (δM_{DC2}). Since there are many approximations involved in the plausibility argument just presented, and since our model only approximates actual behavior, the suitability of this choice must be confirmed by test calculations and, eventually, by applications in experimental situations. (For additional support for this choice, a set of calculation have been performed for a step increase in steam flow (Fig. 4.2-4). The behavior of tube bundle mass change parallels that of Fig. 4.2-3, from which we may infer satisfactory behavior.)

The next problem is how to estimate the tube bundle mass. The tube bundle mass is not a measurable variable because it has no physical sensor. However, this variable is found to be observable (Ref. [G3],[H2]). This means that the variable can be estimated from measurable ones. The model to estimate the unmeasurable variable from available measurements is called an "observer". For estimating the tube bundle mass , a fourth-order non-linear observer is developed based on our steam generator model. It is described in some detail in the next subsection.

4.2.2 Design for an Observer for Tube Bundle Mass

The tube bundle mass M_{TB} can be calculated by our steam generator model described in chapter 3. Eqs. (3.2-2) , (3.2-4) , and (3.2-5) give the explicit form of M_{TB} :

$$M_{TB} = f\, V_{TB}\left(\frac{\rho_{\ell s}\, \rho_o}{\rho_o - \rho_{\ell s}} \ln \frac{\rho_o}{\rho_{\ell s}} \right)$$

$$+ (1 - f)\, V_{TB} \left(\frac{\bar{\rho}_r\, \rho_{\ell s}}{\rho_{\ell s} - \bar{\rho}_r} \ln \frac{\rho_{\ell s}}{\bar{\rho}_r} \right) \qquad (4.2\text{-}13)$$

where,

$$f = \frac{U_{\ell s} - U_o}{\bar{U}_r - U_o}$$

All quantities in this equation can be specified by the state variables (the internal energy U_o at the tube bundle inlet, average void fraction $<\alpha_r>$ at the tube bundle exit and the saturated pressure p of the steam generator). Only the pressure p is measurable with existing physical sensors. The others, U_o and $<\alpha_r>$, are not measurable but may be observable. We can see the observability of these variables, U_o and $<\alpha_r>$ as follow : We know that our steam generator model makes it possible to estimate these variables. If all input variables of our model are measurable, it is obvious that these variables are observable and our model may be directly used as an observer.

The input variables of our model are the steam flow W_s, feedwater flow W_{fw}, and feedwater temperature T_{fw} for the secondary side and the reactor coolant system pressure p_{pr}, flowrate W_{pr}, and hot leg temperature T_H for the primary side. All these variables have physical sensors and are measurable. Practically,

however, as we have shown, the steam and feedwater flow measurements are too uncertain to be used at low power conditions of interest. We intend to exclude these uncertain measurements in the design of a new controller if possible. Therefore, our model can not be used directly as an appropriate observer.

Now, we note that our model calculates two measurable variables as outputs: the saturated pressure of the steam generator p, and the downcomer water level, L_w. It seems possible to eliminate the uncertain steam and feedwater flow measurements from the input variables and to replace them with measured values of p and L_w. Then the state variables U_o and $<\alpha_r>$ can be observable from the practically reliable measurements even at low power conditions. This modification was also addressed in Ref. [S4] with a different motivation (estimating W_s and W_{fw}) but that attempt was unsuccessful.

In order to input p and L_w instead of W_s and W_{fw}, our model requires modification of the secondary transient scheme as given in Eq. (3.1-69). In the modified version of this equation, the derivatives of the pressure p, and the steam dome-downcomer vapor volume V_V are obtained from the successive values of measurements for p and L_w as follow :

$$\dot{p}^n = \frac{p^{n+1} - p^n}{t^{n+1} - t^n} \qquad (4.2\text{-}14)$$

and

$$\dot{V}_V^{\,n} = \frac{V_V^{\,n+1}[\,L_w^{\,n+1}\,] - V_V^{\,n}[\,L_w^{\,n}\,]}{t^{n+1} - t^{n}} \qquad (4.2\text{-}15)$$

where,

p , L_w : pressure and level measurements ,

$V_V[\,L_w\,]$: saturated vapor volume corresponding to level the measurement L_w (obtained using known geometry) , and

superscripts n and $n+1$ denote the old time and new time.

Thus the equation can be reduced to fourth order differential equations by eliminating W_s and W_{fw} . The momentum equation for $\bar{W}$ is solved independantly of the other equations as in Chapter 3. Then the equations in the matrix expression are :

$$\begin{bmatrix} A_{11} & A_{13} & A_{14} \\ A_{21} & A_{23} & A_{24} \\ A^*_{31} & A^*_{33} & A^*_{34} \end{bmatrix} \frac{d}{dt} \begin{bmatrix} x_1 \\ x_2 \\ x_3 \end{bmatrix} = \begin{bmatrix} s_1 \\ s_2 \\ s_3 \end{bmatrix} \qquad (4.2\text{-}16)$$

where,

$$A^*_{31} = A_{51} - \frac{A_{31}}{H_{vs} - H_k} - \frac{A_{41}}{H_{fw} - H_k} ,$$

$$A^*_{33} = A_{53} - \frac{A_{33}}{H_{vs} - H_k} - \frac{A_{43}}{H_{fw} - H_k} ,$$

$$A^*_{34} = A_{54} - \frac{A_{34}}{H_{vs} - H_k} - \frac{A_{44}}{H_{fw} - H_k} \quad , \text{ and}$$

$$A^*_{35} = A_{55} - \frac{A_{35}}{H_{vs} - H_k} - \frac{A_{45}}{H_{fw} - H_k} \quad ;$$

$$x_1 = U_o \quad , \quad x_2 = \langle \alpha_r \rangle \quad , \text{ and } \quad x_3 = \langle \alpha_n \rangle \quad ;$$

$$s_1 = \bar{W} (H_o - H_r) + q_B - A_{15} \quad ,$$

$$s_2 = \bar{W} (H_r - H_n) - A_{25} \dot{p} \quad , \text{ and}$$

$$s_3 = \bar{W} \left(\frac{H_o - H_k}{H_{fw} - H_k} - \frac{H_n - H_k}{H_{vs} - H_k} \right) - A^*_{32} \dot{V}_V - A^*_{35} \dot{p}$$

Notation is the same as defined in Chapter 3. We retain the same features of the model in Chapter 3 for all other parts such as the steady-state, primary side transient and heat transfer model.

The model with this modification can be used as an observer for the tube bundle mass. We see that the steam and feedwater flow measurements are no longer needed for observing the tube bundle mass. All measurements used are always practically available with physical sensors.

For the validation of the observer, the variables U_o and $\bar{U}_r$ (representing $\langle \alpha_r \rangle$),which specify the tube bundle mass when combined

with the pressure measurement p, are calculated by the observer during the transients (step increase in feedwater or steam flow). These results are compared with those by our model (our model has exact information about the steam and feedwater flow as input) in Fig. 4.2-5 (a) and (b). We see no difference between them. It implies that the observer is validated so far as our model is validated and so far as pressure and level measurements are accurate. Also, execution speed of the observer is fast enough to be used in real time, as we expect, because it is based on our fast running model.

By estimating the tube bundle mass with the observer, we can calculate the compensated level. Its responses are compared with those of the actual level on the step increase in feedwater or in steam flow in Fig. 4.2-6 or 4.2-7. In these figures, we see that the compensated levels suffer less from the shrink and swell effects than the actual level and represent well the actual steam generator mass change. This compensated level is to be used as a primary control variable in a new controller, which is proposed in the following subsection.

4.2.3 Description of a " Proposed Controller "

In this subsection, we develop a new controller (designated a " proposed controller ") which permits a solution to the problems encountered by the conventional controller. As mentioned before, most problems occur at low power (mainly because of the reverse dynamics of shrink and swell and because of uncertain flow measurements).

In order to compare the proposed controller with the conventional one, we use a similar control equation (three-element proportional-plus-integral type) as that used for the conventional controller in Eq. (4.1-1):

$$\frac{d\,W_{fw}}{d\,t} = K_{pw}\left(\frac{d\,\epsilon_W}{d\,t} + \frac{1}{T_{iw}}\,\epsilon_W\right) + K_p\left(\frac{d\,\epsilon_Y}{d\,t} + \frac{1}{T_i}\,\epsilon_Y\right) \qquad (4.2\text{-}17)$$

where,

$$Y_w = L_w - \alpha\,(\delta L_r - \delta L_i)\ , \qquad (4.2\text{-}18)$$

$$\delta L_i = \beta\,(\delta L_i)_{Ref}\ , \qquad (4.2\text{-}19)$$

and,

$$Y_{Ref} = L_{Ref} + \delta L_a \qquad (4.2\text{-}20)$$

with the following description for each term :

ϵ_W = flow error (kg/s) = $W_s - W_{fw}$,

ϵ_Y = compensated level error (m) = $Y_{Ref} - Y_W$,

Y_w = compensated level (m),

δL_r = reverse level change (m); described below

δL_i = inherent level change (m); described below

$(\delta L_i)_{Ref}$ = reference inherent level change (m),

α , β : (off-line) adaptive parameters ,

Y_{Ref} = reference compensated level (m), and

δL_a = (on-line) adaptive adjustment (m); described below

A schematic for the proposed controller is given in Fig. 4.2-8.

Before giving a detailed description of each term, it is worthwhile making the following remarks about Eq. (4.2-17) for the proposed controller compared with Eq. (4.2-1) for the conventional one:

1) The level error part of the proposed controller uses the compensated level Y_w as a control variable instead of the actual level L_w.

2) Since Y_w is compensated for the reverse dynamics due to the shrink and swell effects, its feedback terms (K_p and T_i) may be free of the stability constraint even at low power.

3) Furthermore when using Y_w, we may decrease the flow gain K_{pw} without incurring a stability penalty. Thus it is possible to exclude the dependence on the uncertain flow measurements by setting $K_{pw} = 0$. That means a perfect robustness relative to the flow measurement error.

4) Above remarks indicate the possibility that the proposed controller may solve the major low power control problems attributed to reverse dynamics and uncertain flow measurements.

Now we look into the relation between the compensated level and actual level given in Eq. (4.2-18), and we discuss individual term.

The first correction term, δL_r, designated a "reverse level change", represents the portion of downcomer level change due to short

term variations in the tube bundle mass. In equation form, the time response of the reverse level change, δL_r (t) , is related to that of the tube bundle mass change, δM_{TB} (t) , during the transient as follows:

$$\delta L_r \text{ (t)} = - \delta M_{TB} \text{ (t)} / (\rho_{\ell s} A_{DC}) \qquad (4.2 \text{ -21 })$$

where

$\rho_{\ell s}$ = saturated liquid density (assumed constant)

A_{DC} = the area of the downcomer at the location of level measurement, and

$\delta M_{TB} \text{ (t)} = M_{TB} \text{ (t)} - M_{TB} \text{ (0)}$;

$M_{TB} \text{ (0)}$ = initial tube bundle mass

The tube bundle mass change, δM_{TB} , is calculated by using the observer developed in the previous subsection. During a short term transient, the reverse level change compensates the downcomer level measurement for the reverse dynamics effect.

If the steady-state operating variables, such as power level, change during the transient, then the steady-state tube bundle mass (designated an "inherent tube bundle mass" with the denotation M_{TBi}) is changed, too (Fig. 4.2-9). When reaching a new steady-state condition at time t_{ss} , the actual downcomer level L_w suffers from a steady-state error e_{ss} caused by operation of the reverse level change:

$$e_{ss} = L_{Ref} - L_w = -\delta L_r (t_{ss}) \qquad (4.2\text{-}22)$$

or

$$e_{ss} = -\left(M_{TB}(t_{ss}) - M_{TB}(0) \right) / \left(\rho_{\ell s} A_{DC} \right) \qquad (4.2\text{-}23)$$

This steady-state error can also be expressed in terms of the difference between the inherent tube bundle mass at the initial and final steady-state conditions :

$$e_{ss} = -\left(M_{TBi}[Q_f] - M_{TBi}[Q_i] \right) / \left(\rho_{\ell s} A_{DC} \right) \qquad (4.2\text{-}24)$$

where

$M_{TBi}[Q_i]$ = inherent tube bundle mass corresponding to the initial steady-state power Q_i

and

$M_{TBi}[Q_f]$ = inherent tube bundle mass corresponding to the final steady-state power Q_f

In order to compensate for this steady-state error, a second correction term δL_i (designated an "inherent level change") is introduced into the compensated level. The exact expression of δL_i is :

$$\delta L_i = -e_{ss} = \left(M_{TBi}[Q_f] - M_{TBi}[Q_i] \right) / \left(\rho_{\ell s} A_{DC} \right) \qquad (4.2\text{-}25)$$

The inherent level change (δL_i) can be estimated on an on-line basis during the transient. The transient change of measured input variables, which imply a change of steady-state power, may be used for this estimation of δL_i. In our case, the change of the primary hot-leg temperature is used for this purpose. In Fig. 4.2-10, the inherent tube bundle mass M_{TBi} is given as a function of the hot-leg temperature (T_H) taken from calculations. Using this plot, we can obtain a relation between the inherent tube bundle mass and the corresponding hot leg temperature such as :

$$M_{TBi} / (\rho_{\ell s} A_{DC}) = F (T_H) \qquad (4.2 -26)$$

where F is a piece-wise linear function

By adopting such a pre-defined relation, we can incorporate the inherent level change term in the compensated level as follow:

$$Y_w (t) = L_w (t) - (\delta L_r (t) - \delta L_i (t)) \qquad (4.2 -27)$$

where

$$\delta L_i (t) = F [T_H(t)] - F [T_H(0)] \qquad (4.2 -28)$$

Note that the insertion of $\delta L_i (t)$ does not affect the stability of Y_w since it is based on a pre-determined function (F) of an external input variable (T_H) and is independent of the controlling

variable W_{fw} .

If both the relation F and the observer calculations are exact one, then:

$$F[\ T_H(t_{ss})\ ] = M_{TB}\ (t_{ss}) \quad \text{and}$$

$$F[\ T_H(0)\ ] = M_{TB}\ (0)$$

Thus the steady-state error would be compensated completely. Since they cannot be exact, an adaptive parameter β is introduced for possible improved compensation as follow :

$$\delta L_i = \beta\ (\ \delta L_i\ )_{Ref} \qquad (\ 4.2\ -29\ )$$

where

$$(\ \delta L_i\ )_{Ref} = F\ [\ T_H(t)\ ]\ -\ F\ [\ T_H(0)\ ] \qquad (\ 4.2\ -30)$$

By changing β in the adaptive manner , we can adjust δL_i to the value which minimizes the existing steady-state error. The "adaptive manner" means to change the parameter based on the evaluation of the performance. In our case, this parameter is given as an input, which is determined adaptively on an off-line basis. The development of methods for on-line adaptation of the parameter β is left for future study.

Now our compensated level may be written as :

$$Y_w = L_w - (\delta L_r - \beta (\delta L_i)_{Ref}) \qquad (4.2 -31)$$

As discussed in subsection (4.2-1), the amount of compensation by using the tube bundle mass change is smaller than the actual reverse dynamics term because of omitting the contribution of the riser mass change. Thus there should be a provision for increasing the compensation term in Eq. (4.2 -31) in an attempt to obtain the complete compensation. This provision is incorporated by introducing a proportionality constant α as follows:

$$Y_w = L_w - \alpha (\delta L_r - \beta (\delta L_i)_{Ref}) \qquad (4.2 -32)$$

Considering α_t as a design target value, with which we can best compensate the total reverse dynamics term, we make following remarks:

1) $\alpha = 0$: no compensation (conventional controller)

2) $\alpha < \alpha_t$: under-compensation

   $\alpha = \alpha_t$: exact-compensation

   $\alpha > \alpha_t$: over-compensation

It was found that it is desirable to put the parameter α within the range around α_t , which always ensures the satisfactory performance of the controller. This range seems to be large enough to cover fairly large deviations between the estimated and the actual value of α_t .

It is also expected to be large enough to override the shift of α_t due to the changes of operating condition. These remarks will be confirmed in a preliminary way in the next chapter with an analytic evaluation and an actual simulation.

The parameter α may be changed in the adaptive manner for better performance of the controller. Like the parameter β , α is now given as an input and thus the adaptation is on an off-line basis. The on-line adaptive scheme for α is left for future work.

One final adaptation is now incorporated. In Eq. (4.2-32), the modeled correction $- \alpha (\delta L_r - \beta (\delta L_i)_{Ref})$ is intended to be zero when the system is approaching the steady-state condition. However, this term is expected to reach a non-zero value because of model imperfections. Using the compensated level (Y_w) as a control variable, we need reset its reference value (Y_{Ref}) by the magnitude of the error ($L_{Ref} - L_w$) observed when Y_w has settled down to its reference value Y_{Ref} .

This model error compensation is performed in an on-line adaptive manner by introducing the third and final correction term δL_a , designated an "adaptive adjustment" as follow :

1) Initially, $\delta L_a = 0$.

2) Measure the rate of level change, we check whether the system has reached a steady-state condition or not as follow :

$$\left(\frac{\Delta L_w}{\Delta t} \right) \leq \epsilon \quad \text{then} \quad \text{steady-state}$$

where

ϵ = a pre-set value for a steady-state decision criterion;

$\Delta t \gg T_{noise}$ (a time interval long enough to avoid noise problems and to be sure that the steady condition is being maintained); and

ΔL_w = the level change over the latest Δt interval.

3) Measure the level error at this steady-state condition, $(L_{Ref} - L_w)_{ss}$.

4) If $(L_{Ref} - L_w)_{ss}$ is larger than some specified value, change the adaptive adjustment, δL_a :

$$\delta L_a^{new} = \delta L_a^{old} + (L_{Ref} - L_w)_{ss} \qquad (4.2\text{-}53)$$

5) Change the reference compensated level Y_{Ref} by using the new value of δL_a :

$$Y_{Ref} = L_{Ref} + \delta L_a^{new} \qquad (4.2\text{-}54)$$

6) This new value of Y_{Ref} is maintained until the system approaches another steady-state condition.

In summary, the first two correction terms (the reverse level

change δL_r and the inherent level change δL_i) provide a physically based proposed controller which offers a solution to the difficulties encounted by the conventional controller. This solution is expected to be an excellent one if based upon perfect models ; the third correction term (the adaptive adjustment δL_a) improves the proposed controller by minimizing the adverse influences of model imperfections.

4.3 A Chapter Summary

The proposed approach to the design of a new controller was described in detail.

A mathematical equation was used to represent the control action of a "conventional controller". In conjunction with our steam generator model (non-linear), the problems encountered by the conventional controller were simulated and correlated with the actual problems of existing controllers mentioned in Chapter 2.

To clarify the physical ideas about the nature of problems, a simplified model (linear), which represents the steam generator level dynamics, was used. Based on those physical ideas, possible solutions were proposed and incorporated in a new control equation, the "proposed controller".

Two physically-based correction terms were developed to provide a solution to the problems. These terms were based on the mass in the tube bundle region. It was found that the tube bundle mass was not measurable but was observable using practically available physical

sensors. For this on-line estimation of the tube bundle mass, an observer based on the fourth order non-linear model was developed. The observer was validated in its practical applicability. An on-line adaptive adjustment scheme was incorporated in the proposed controller to minimize the adverse influence of model imperfections.

The improvements expected for the proposed controller have been indicated in an analytic manner using the simplified model. In the next chapter, our non-linear steam generator model will be subjected to plausible transients and the proposed controller will be more completely evaluated.

Table 4.1.1 Simplified Model Parameters

Percent Power	G_1 ($\times 10^{-3}$)	G_2 ($\times 10^{-3}$)	τ_2	$G_1/(G_2-G_1\tau_2)$
5 %	0.1154	9.01	35 sec	0.0232
10 %	0.1154	6.61	20 sec	0.0268
30 %	0.1154	3.00	15 sec	0.0900
50 %	0.1154	1.68	9 sec	0.1791
95 %	0.1154	0.600	5 sec	4.982

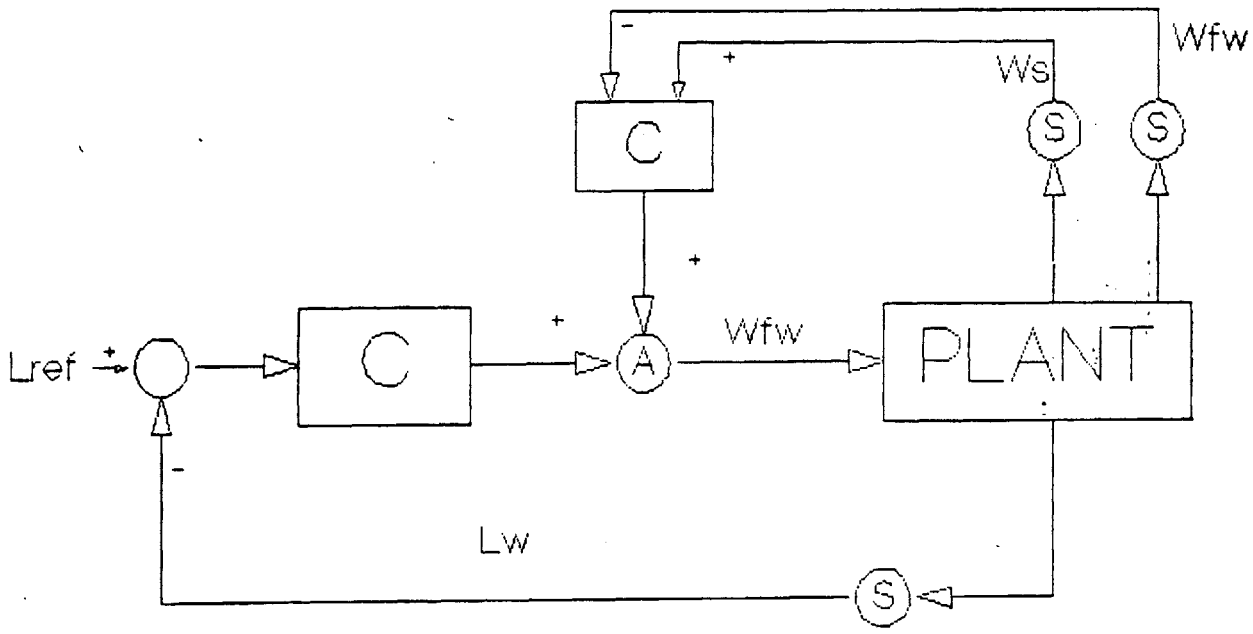

C : Controller
A : Actuator
S : Sensor

(Conventional Control Structure)

4.1-1 Schematic of the conventional controller

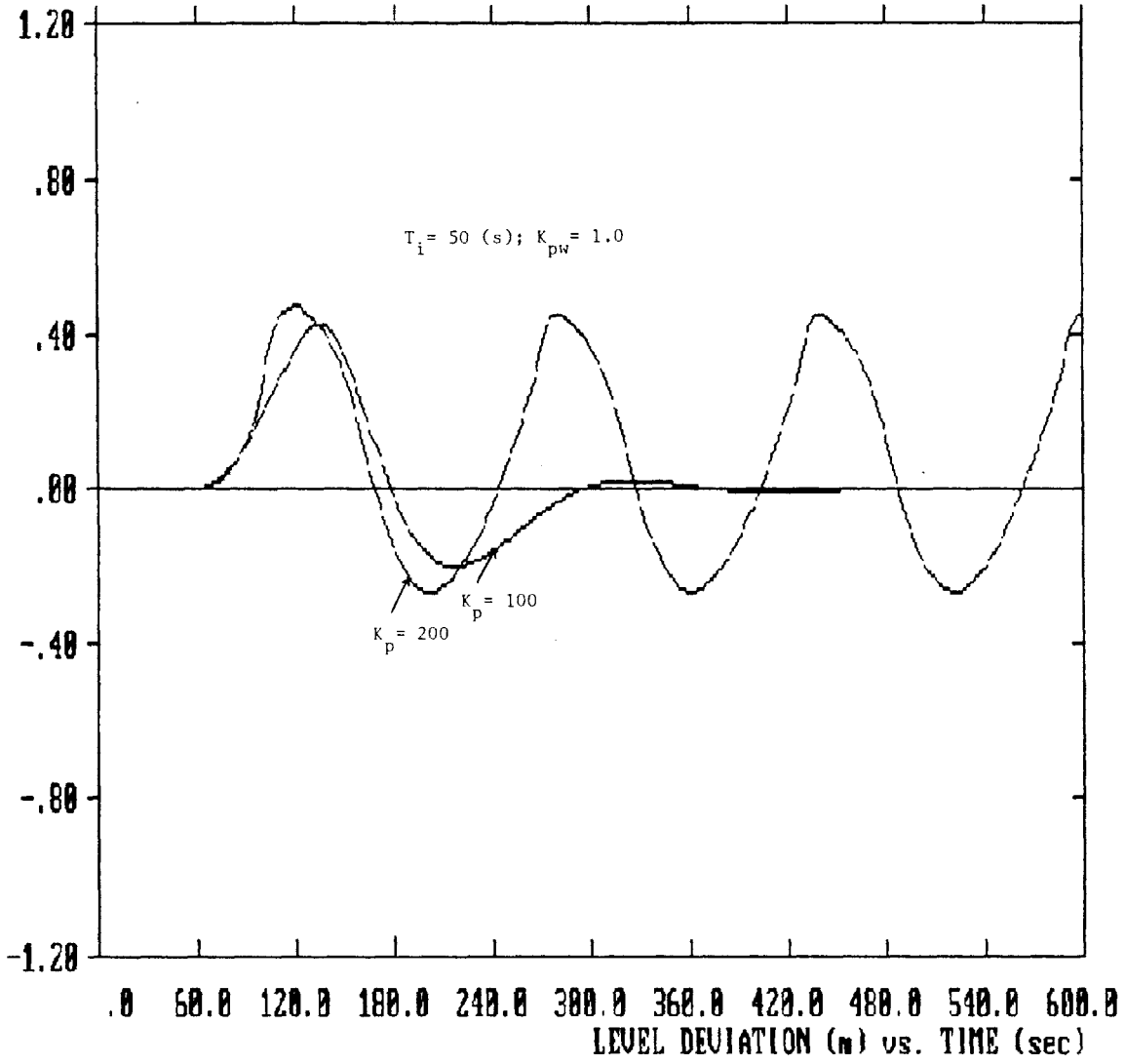

4.1-2 Transient level responses to the power increase (10%→15%)

(a) With variation of level gain

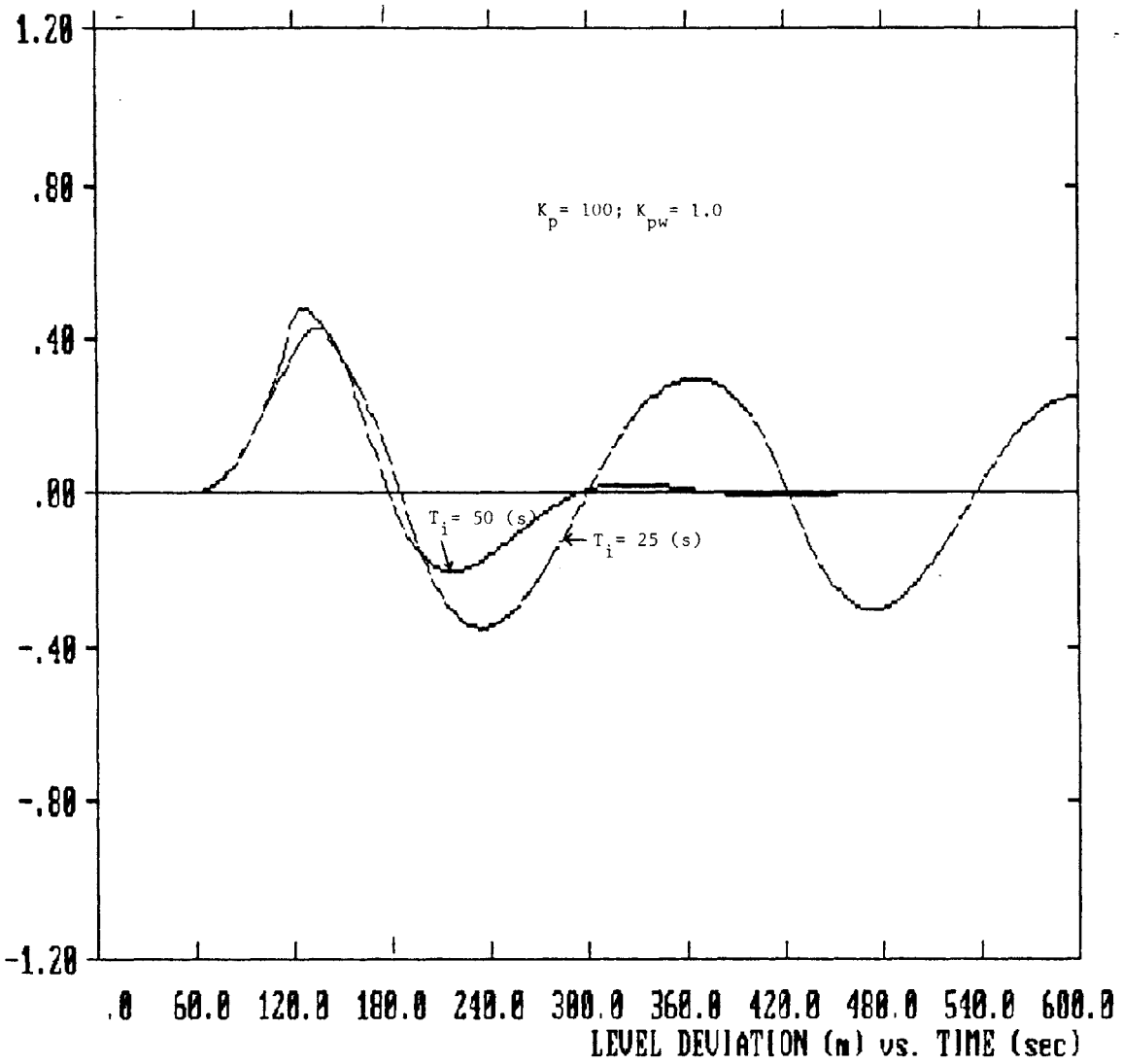

(b) With variation of integral reset time

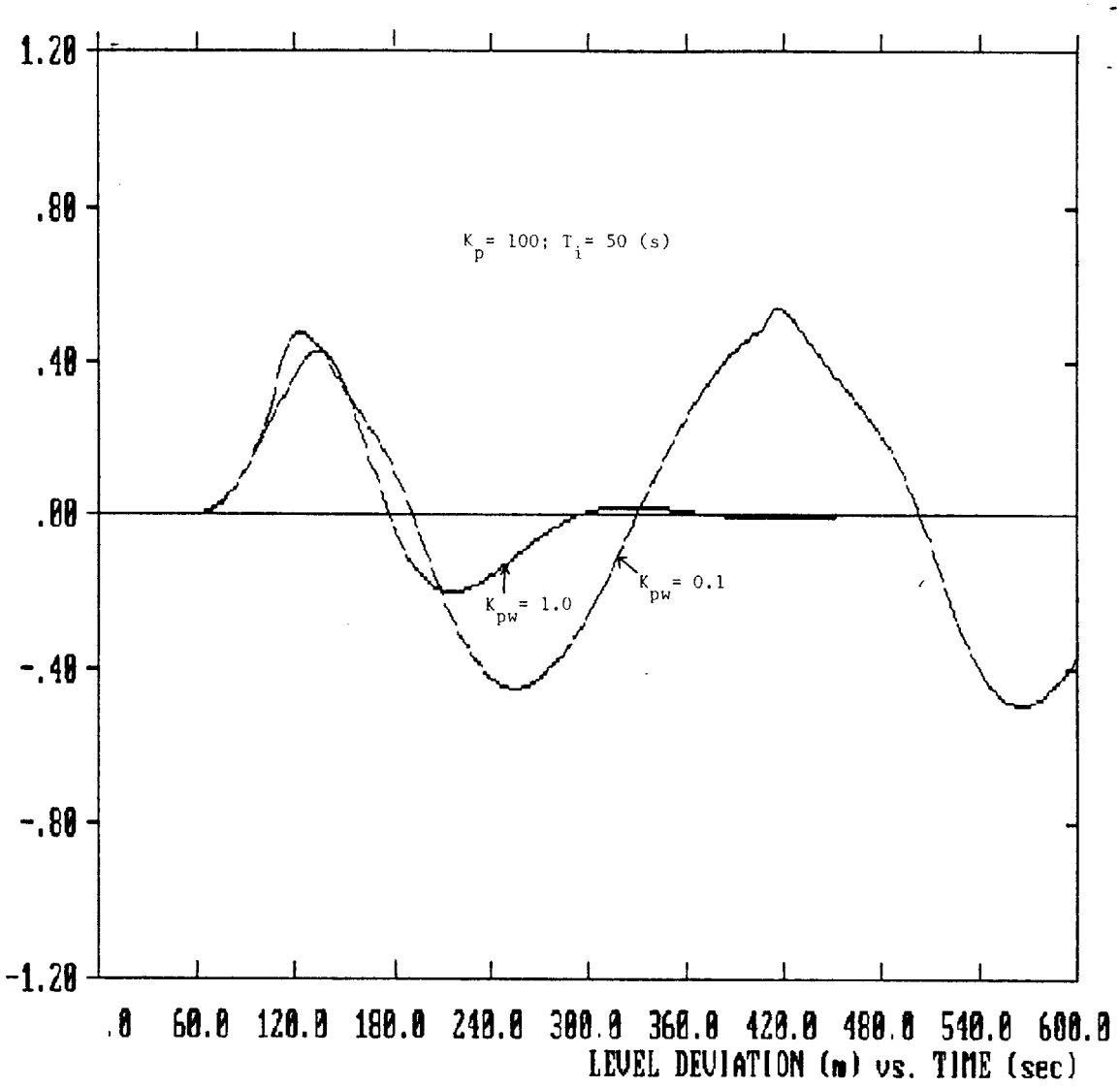

(c) With variation of flow gain

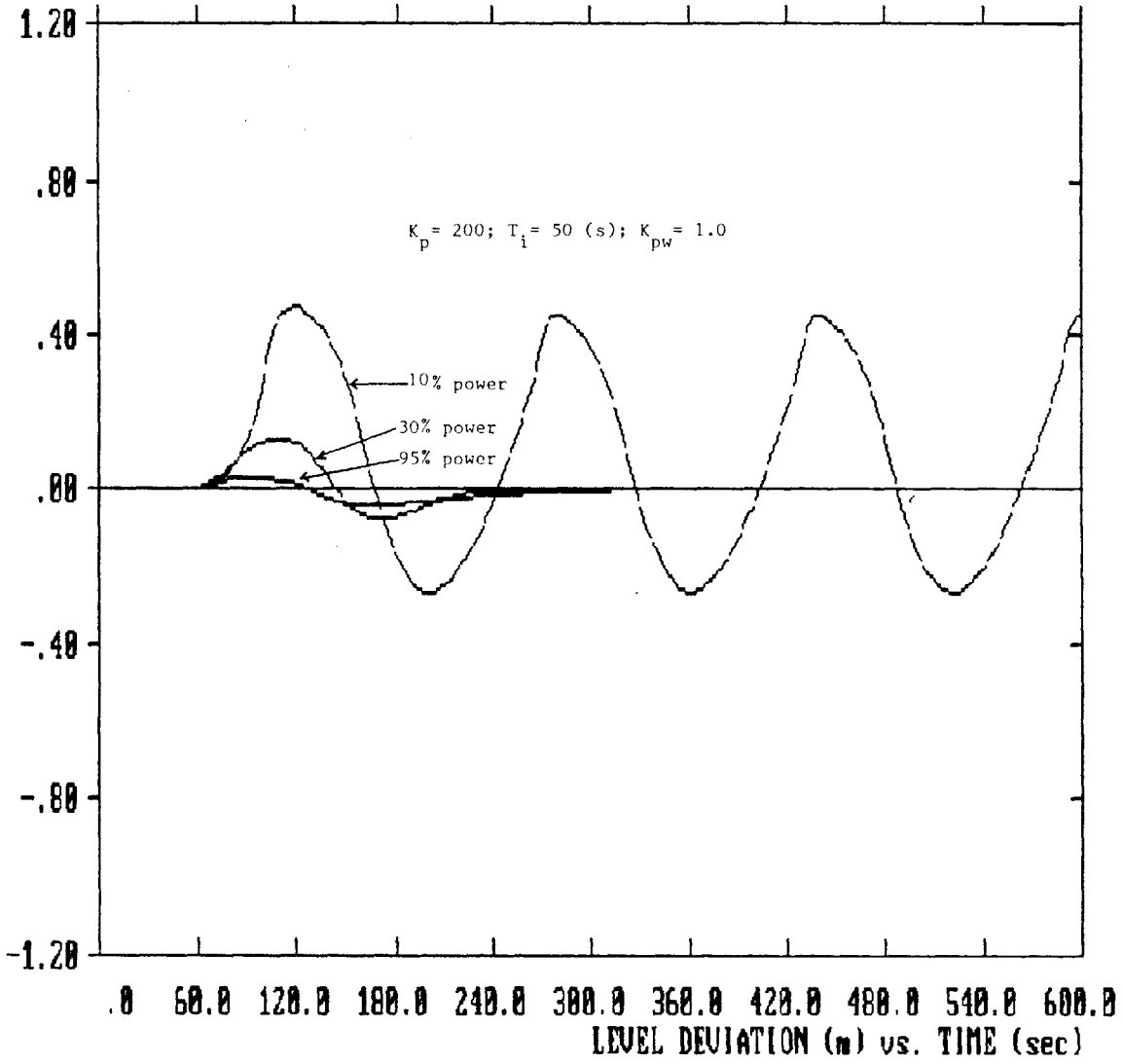

4.1-3 Transient level responses to the power increase at the various power levels

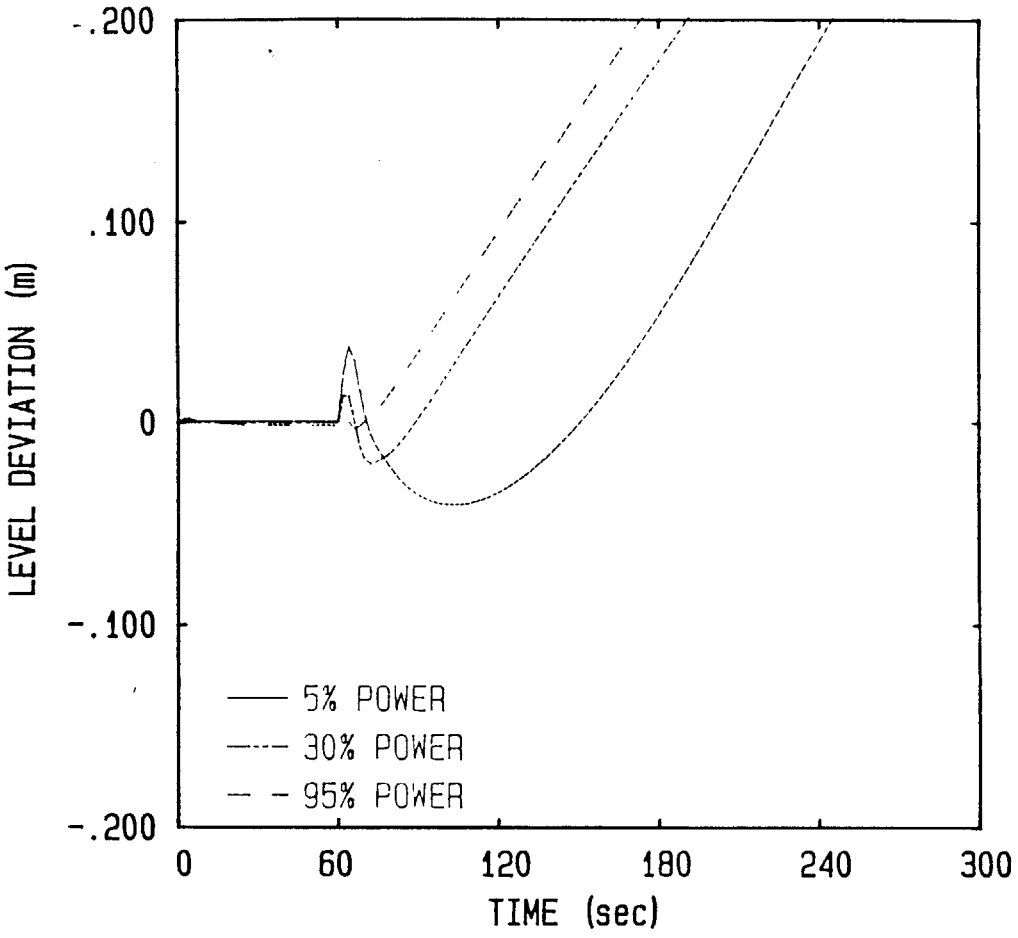

4.1-4 Transient level responses at the various power levels

(a) To the feed flow step-up

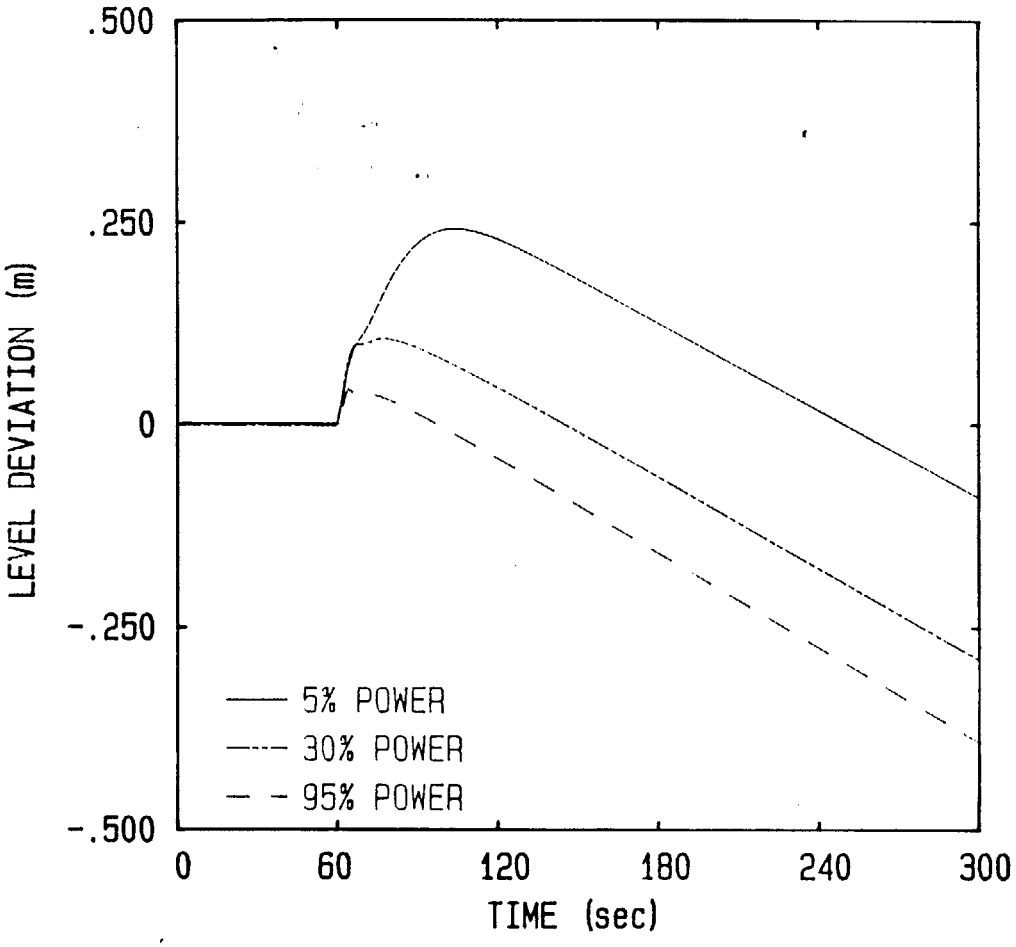

(b) To the steam flow step-up

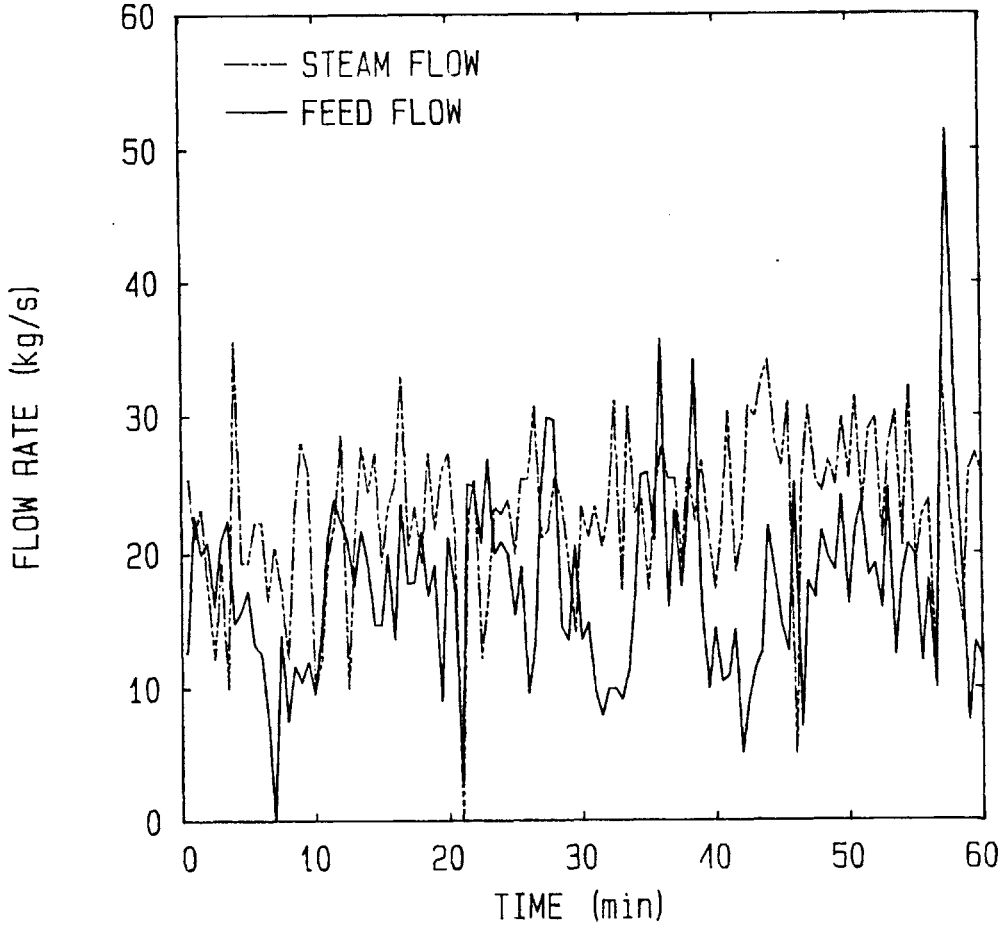

4.1-5 Plant data for the feedwater and steam flow measurements

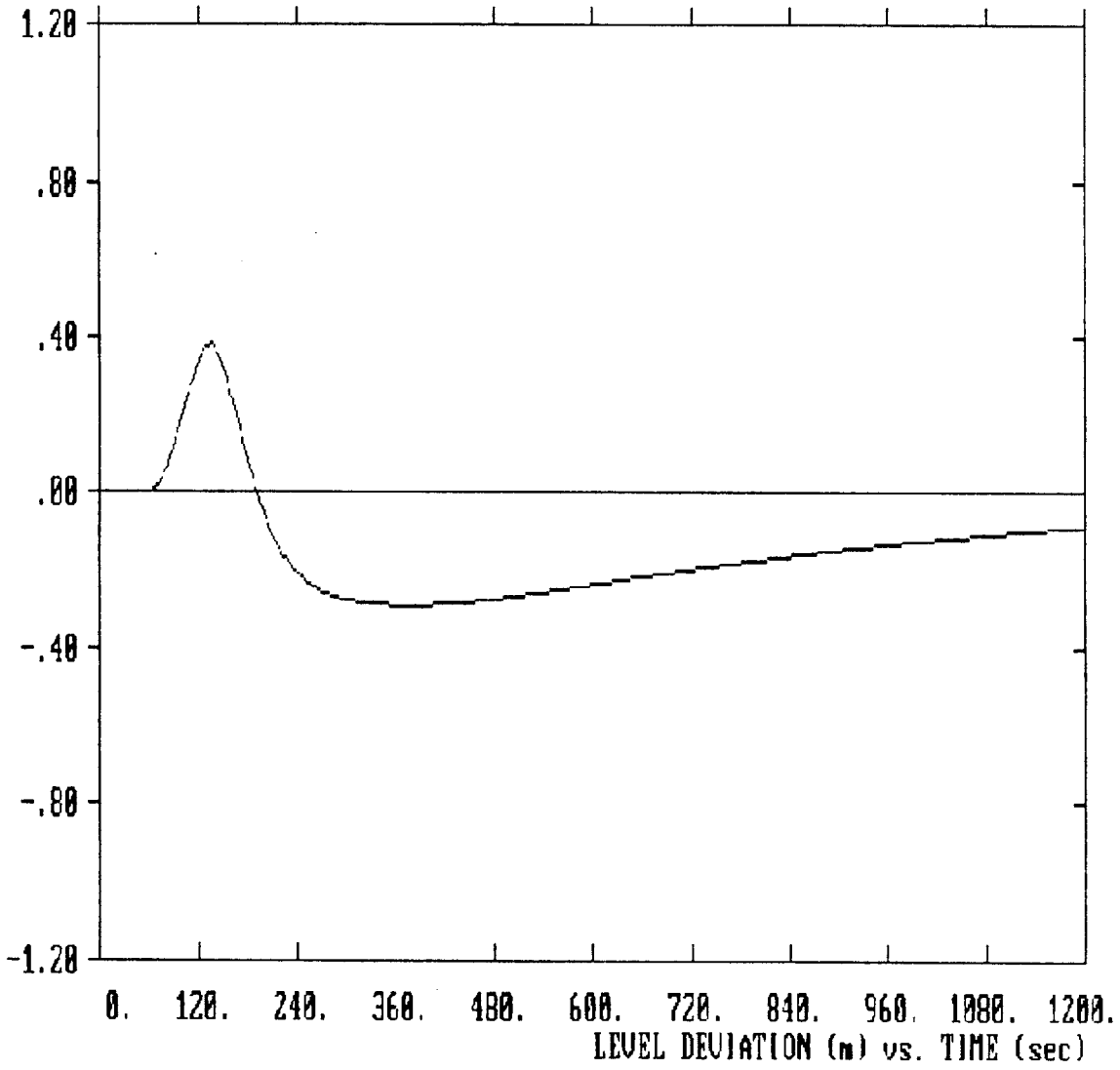

4.1-6 Level response to the power increase (10%→15%) with a small gain and long integral time (K_p=65; and T_i=750 s)

Fig. 4.1-7 Block Diagram for Level Control System (P.I)

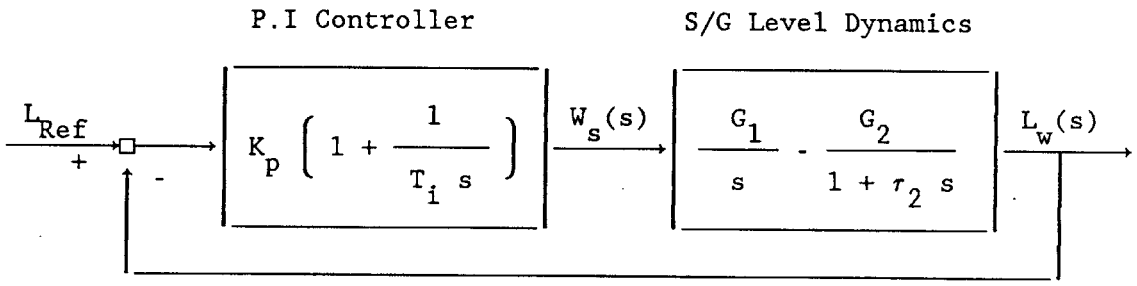

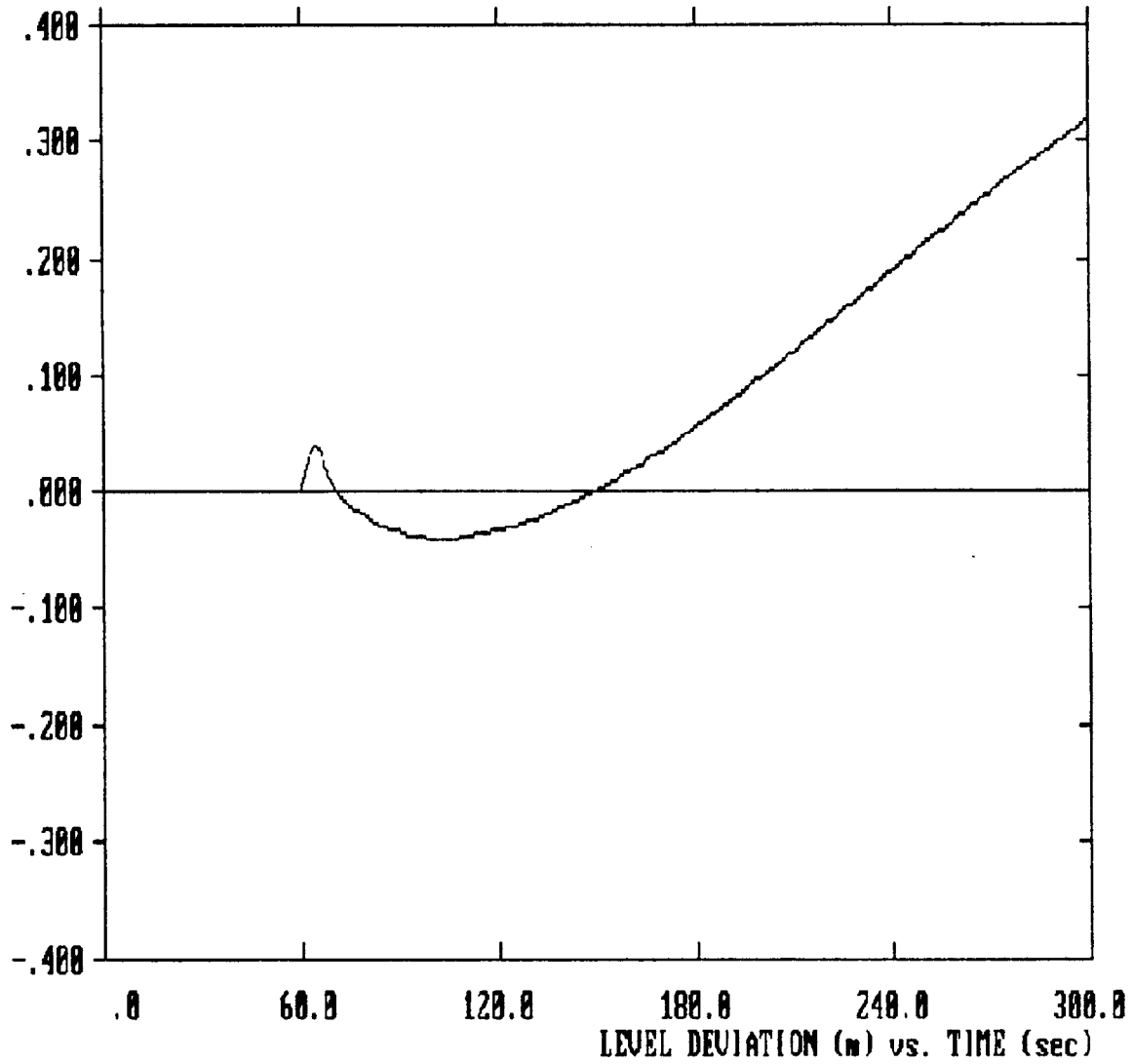

4.2-1 Level response to the feed flow step-up at 5% power

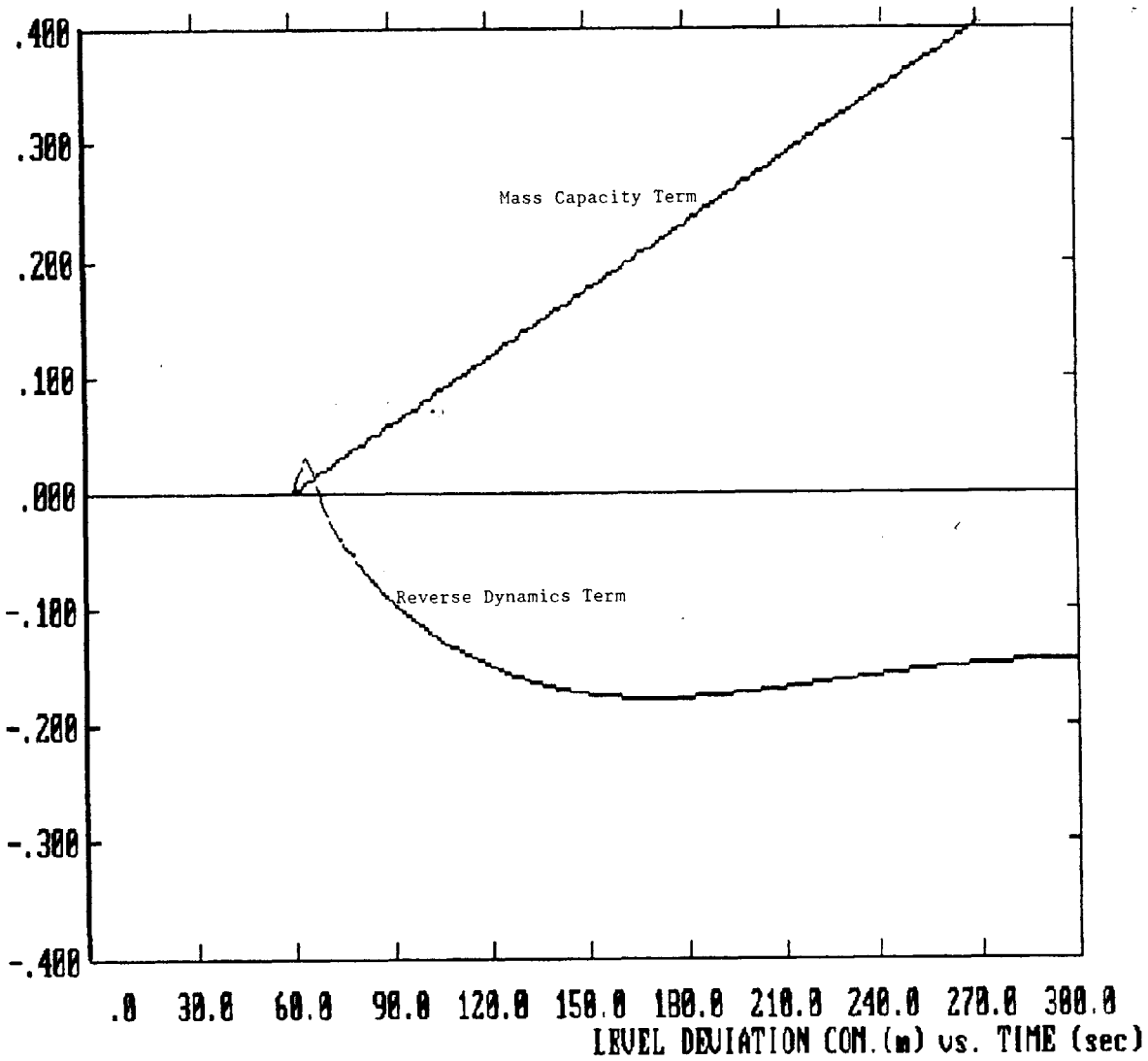

4.2-2 Decomposed ingredients of level response to the feed flow step-up at 5% power

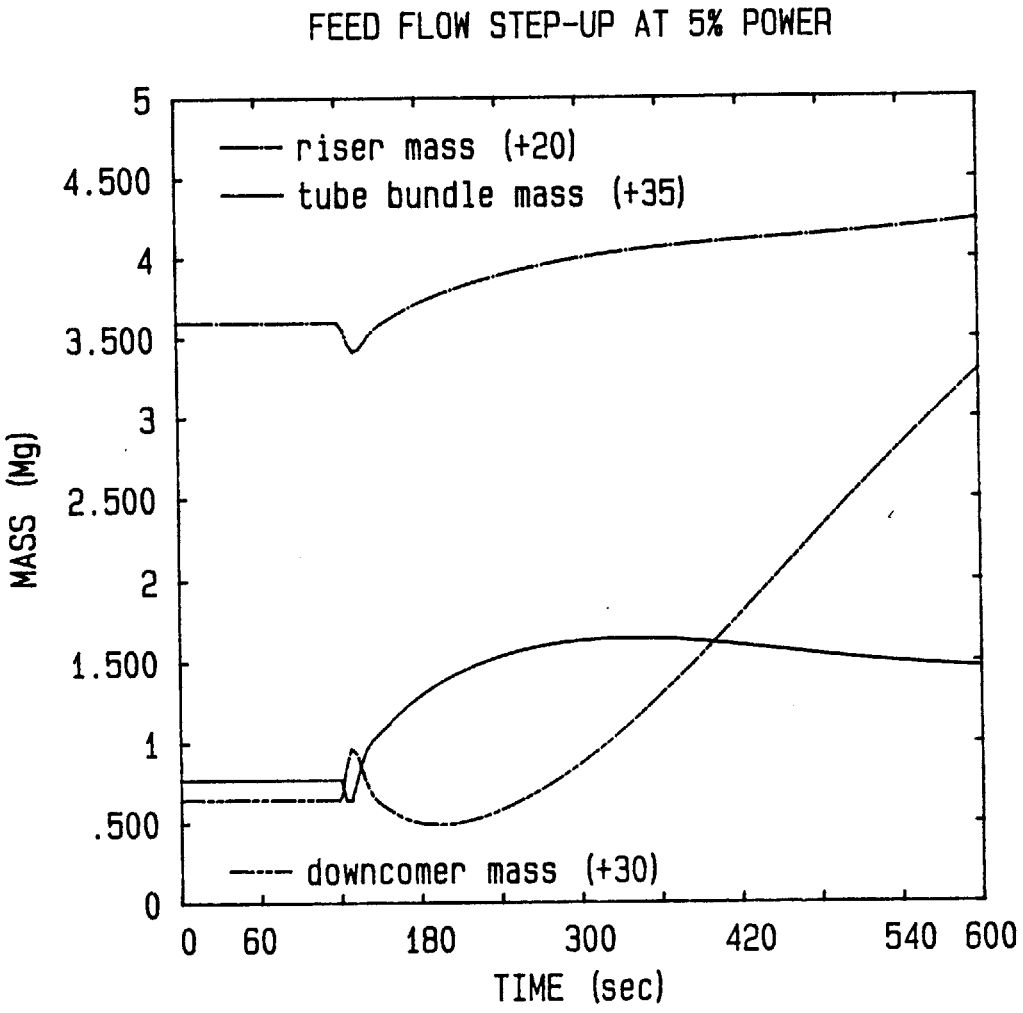

4.2-3 Mass responses to the feed flow step-up at 5% power

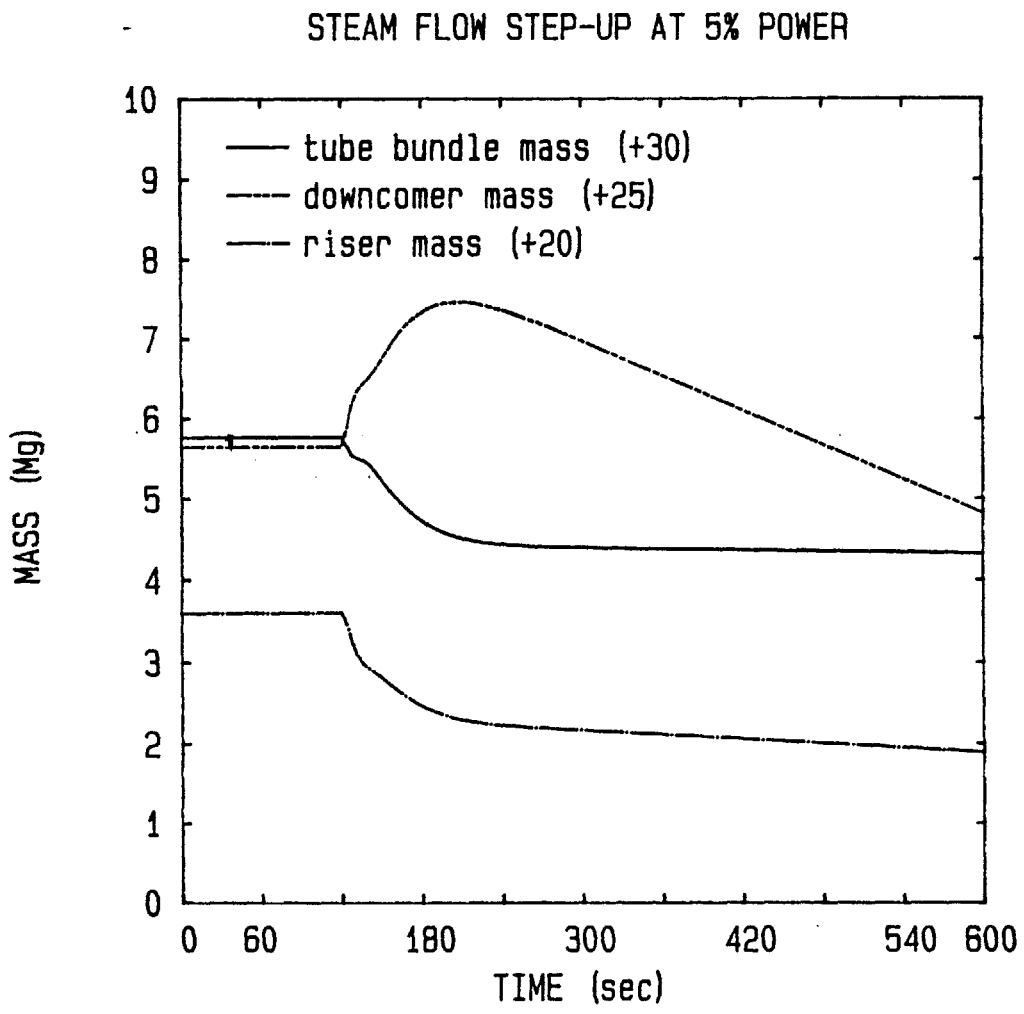

4.2-4 Mass response to the steam flow step-up at 5% power

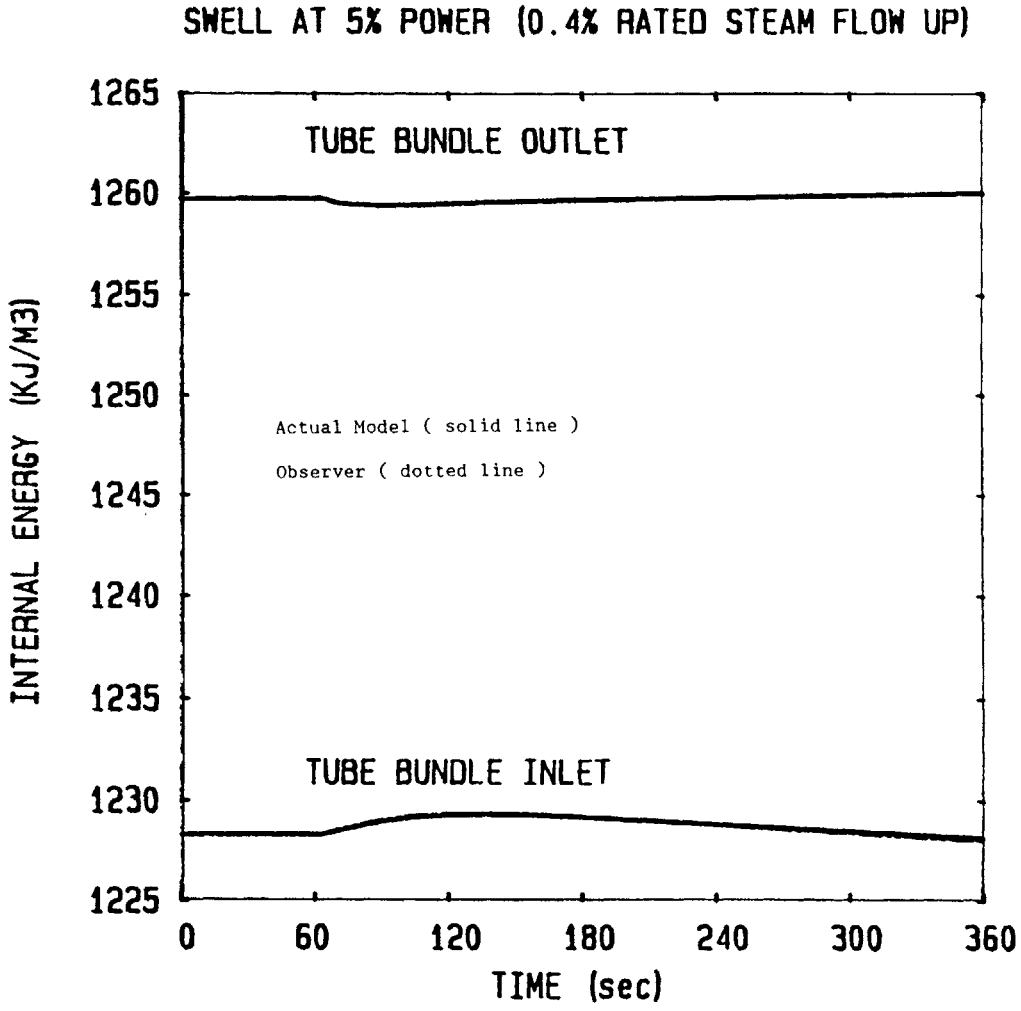

4.2-5 (a) Internal energy responses to the feed flow step-up at 5% power

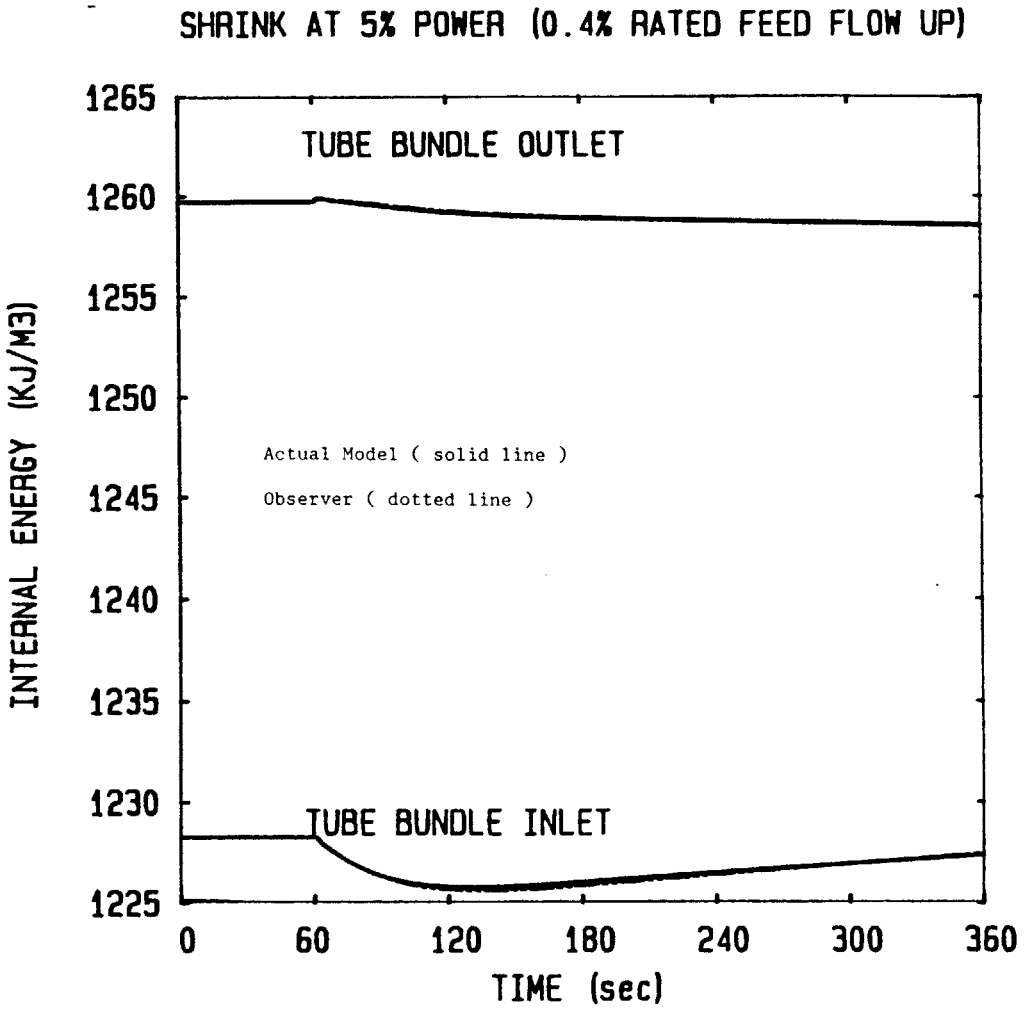

4.2-5 (b) Internal energy responses to the steam flow step-up at 5% power

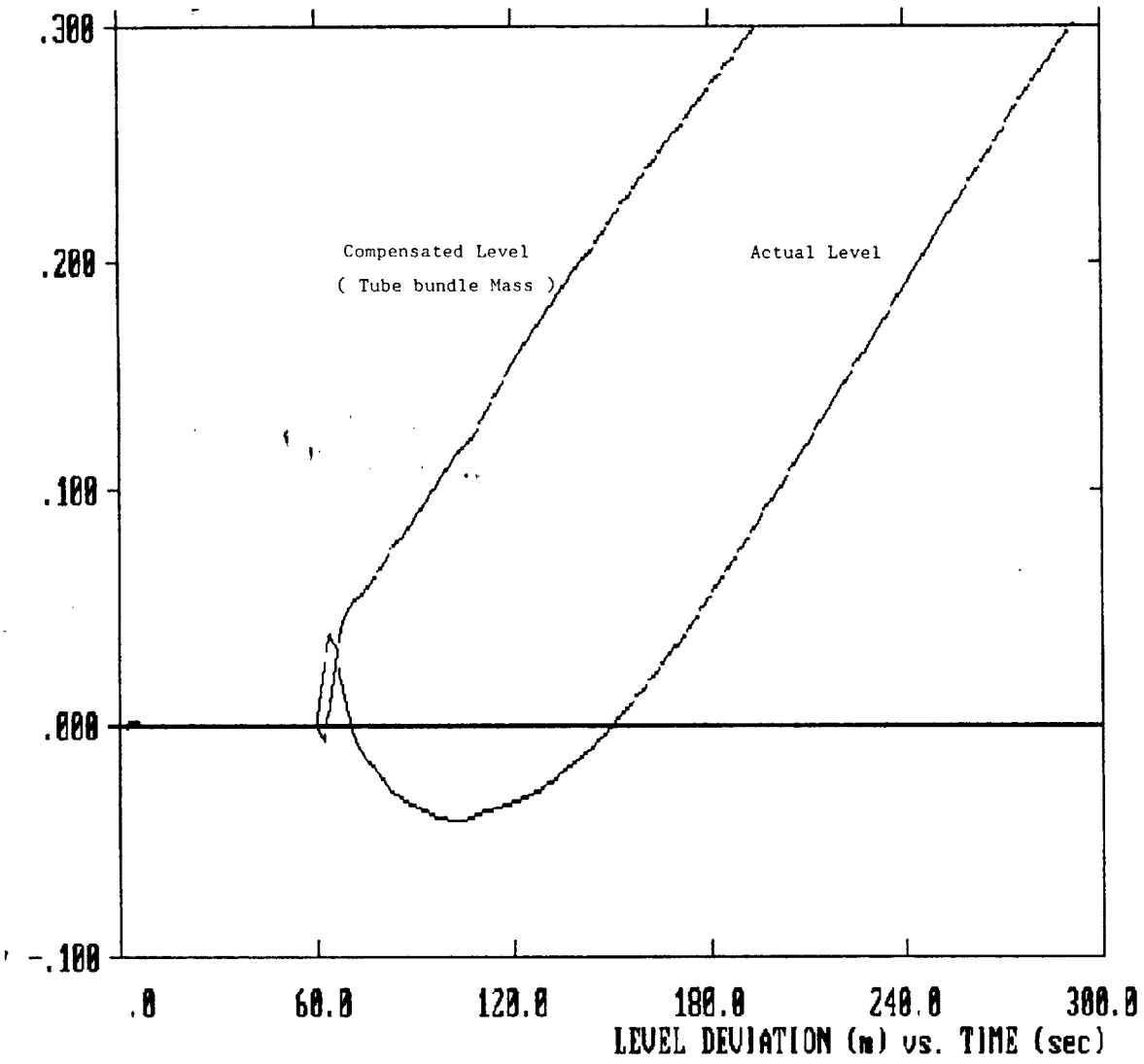

4.2-6 Compensated level response by the tube bundle mass to the feed flow step-up at 5% power

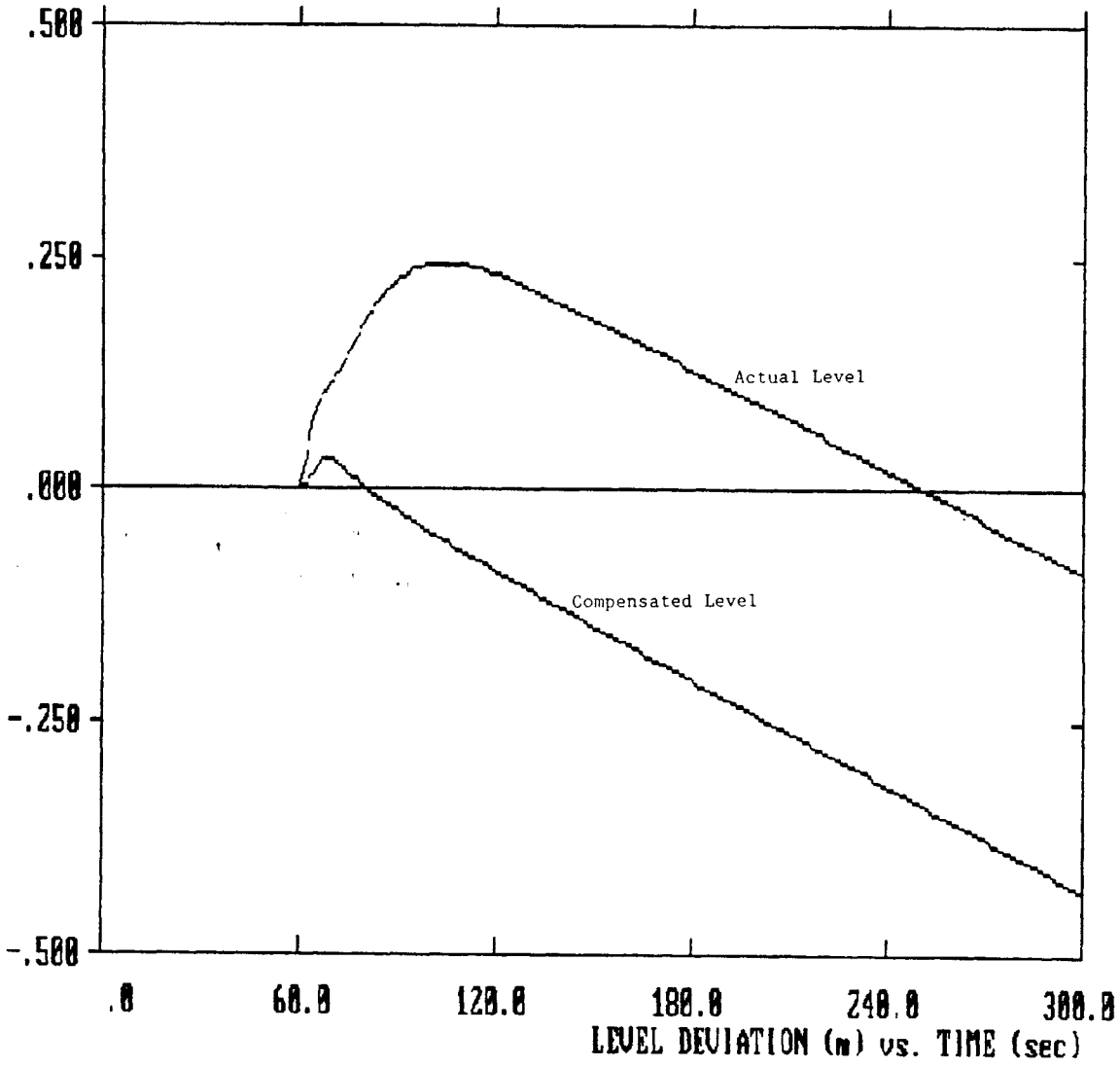

4.2-7 Compensated level response by the tube bundle mass to the steam flow step-up

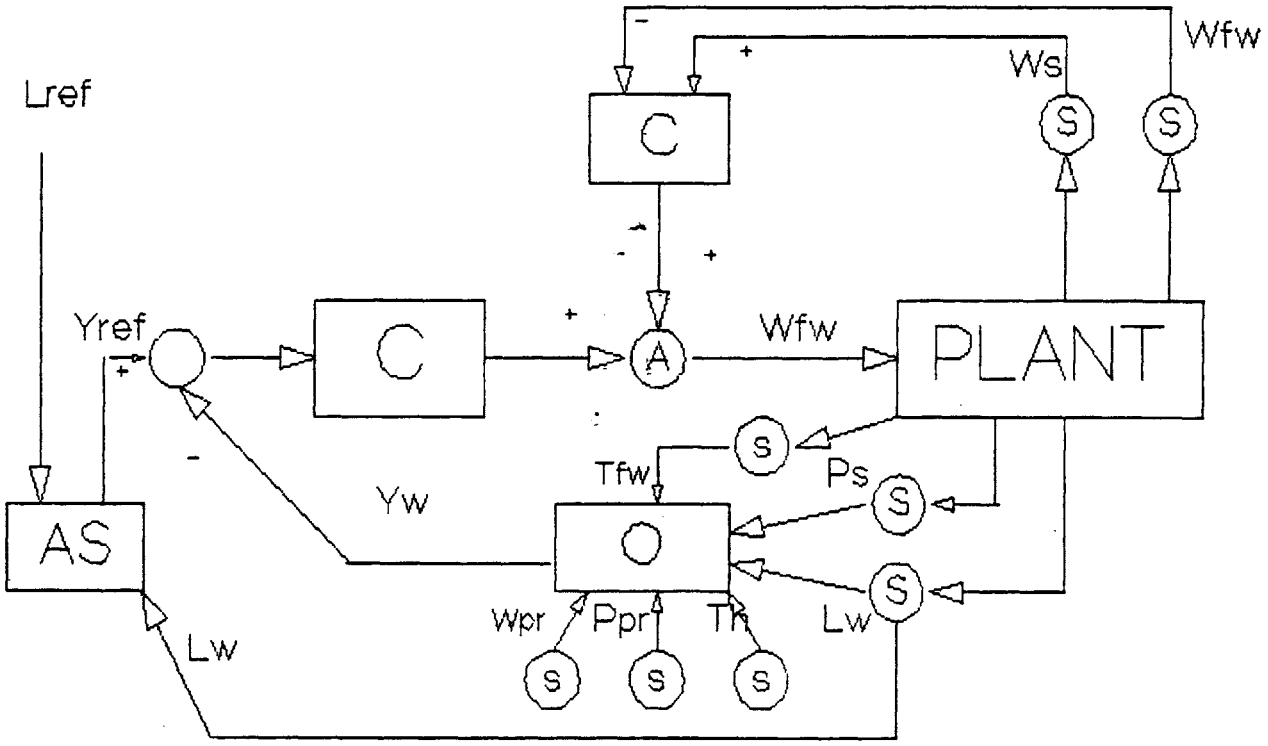

C : Controller O : Observer
A : Actuator AS : Adaptive Scheme
S : Sensor

⟨ Proposed Control Structure ⟩

4.2-8 Schematic of the proposed controller

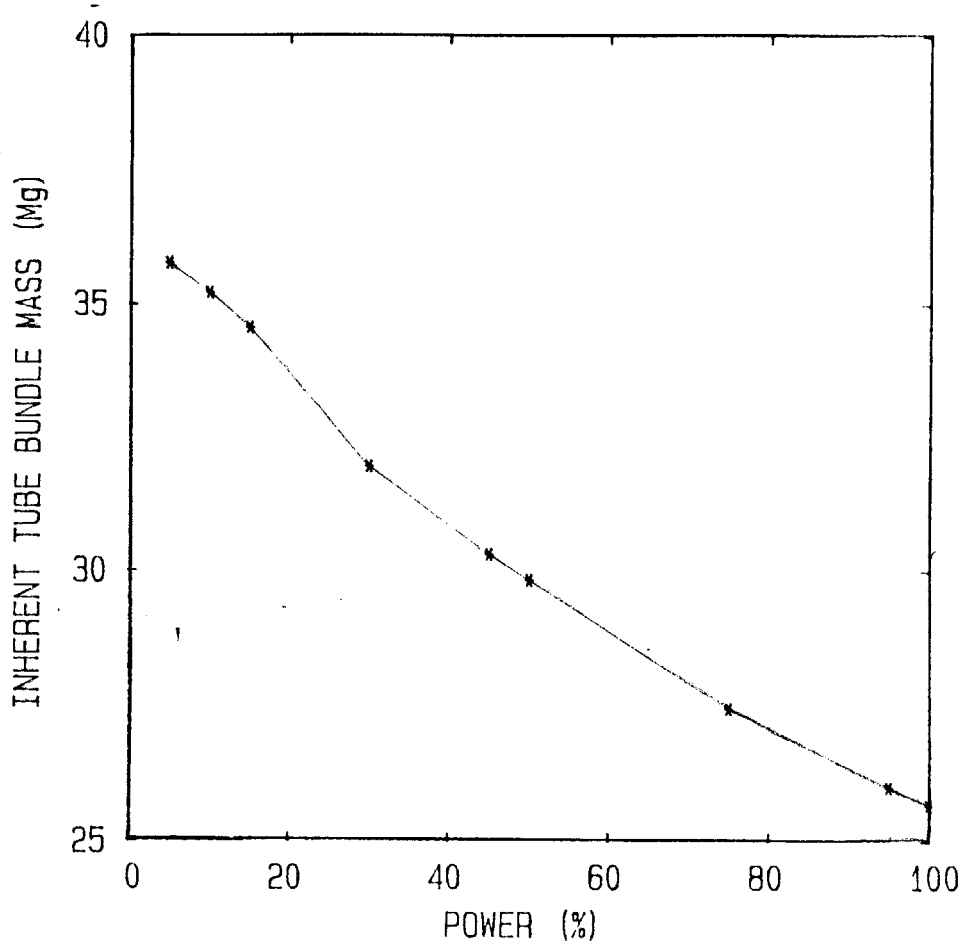

4.2-9 Inherent tube bundle mass versus power

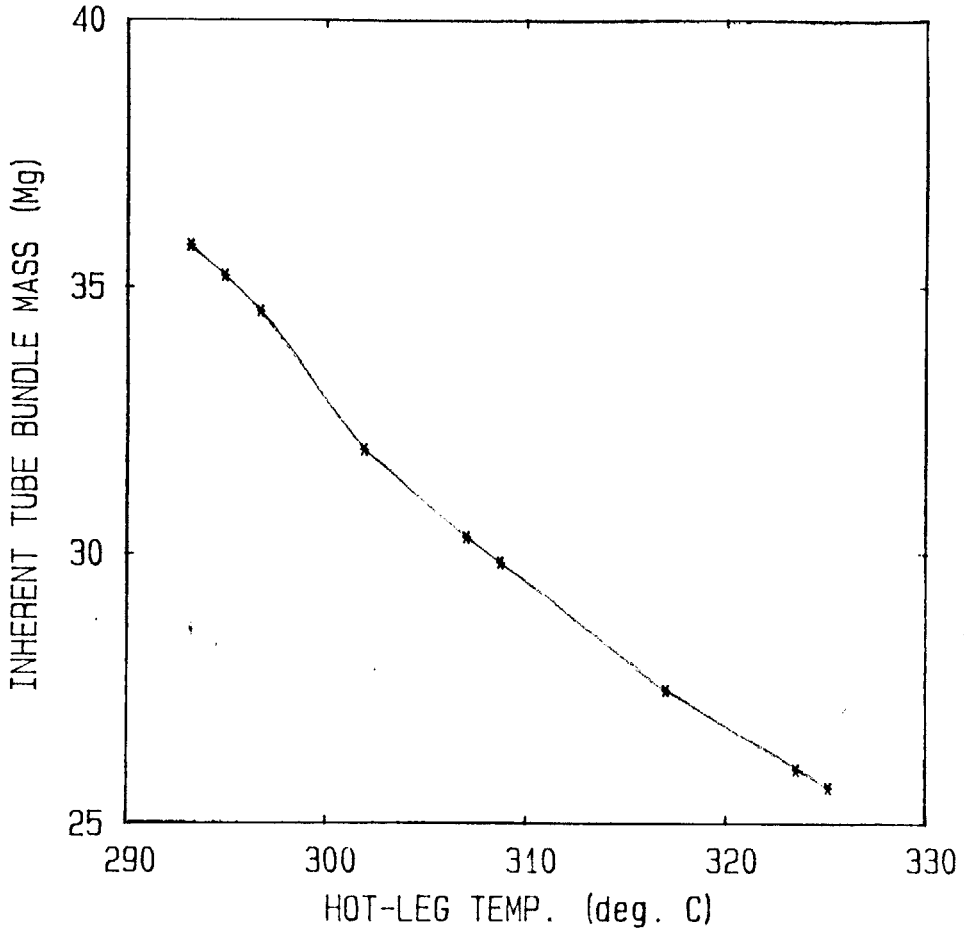

4.2-10 Inherent tube bundle mass versus primary hot-leg temperature

Chapter 5

EVALUATION OF PROPOSED CONTROLLER

In this chapter, substitutes are provided for actual plant test for evaluation of the proposed controller. Transient simulations are performed for this purpose with our steam generator model. The modeled steam generator is the Westinghouse Type F used in Chapter 3 (Geometric details are given in Appendix [C]).

First, the physical ideas which lead to the proposed controller are validated by studing the behavior of the steam generator state variables during transients. Second, by using a sensitivity study of the proposed correction terms, the effectiveness on the controller performance is analytically evaluated and then confirmed with actual simulations. Finally, by applying the proposed controller to a wide spectrum of operating conditions, performances of the controller are evaluated from a practical point of view.

5.1 Validation of Physical Ideas

5.1.1 Steam Generator Variables during Steady Operation

As a background information, some variables are presented in Fig 5.1-1 for steady state operation at various power levels. The plant is operated so that the primary cold-leg temperature ("T_C") is approximately the same (291^o C) at all power levels, and the primary hot-leg temperature ("T_H") increase approximately linearly from 291^o C

at zero power to 325° C at full power. The other important external temperature is that of the feedwater being supplied to the secondary side of the steam generator. This temperature ("T_{fw}") is very low (approximately 45° C) at power levels below about 15% . Since at these levels the turbine bypass is in operation, the steam flow goes directly to the condenser, and there is no feedwater heating. Above a power level of about 15%, however, the main turbine and the electrical generator are in operation, and there is feedwater heating. At even higher power levels, the temperature T_{fw} increases from about 150° C at 15% power to 227° C at full power. These values are based on actual plant data. The T_H and T_{fw} variables are input to our steam generator model. Heat transfer calculations for the steam generator indicate that the exit steam temperature ("T_s") decreases from 291° C at zero power to 285° C at full power. The temperature variables are displayed in Fig. 5.1-1 (a).

The steam generator internal pressure is the saturation pressure that corresponds to the calculated value of T_s ; it is displayed in Fig. 5.1-1 (b).

Based on T_s and T_{fw} , the steady steam flowrate W_s corresponding to its percent power is calculated and shown in Fig. 5.1-1 (c). Of course it is the same as the feedwater flowrate W_{fw}.

Fig. 5.1-1 (d) shows the mass contents for three regions on the secondary side of the steam generator. The mass content variables are displayed for: the downcomer region M_{DC} (also includes vapor mass in the steam dome); the tube bundle region M_{TB} ; and the riser region

M_R. Since the reference water level L_{Ref} is programmed to be the same at all powers for this plant, the downcomer mass M_{DC} is virtually constant. The other two mass contents decrease, however, as power increases. This decrease is a direct result of an increasing vapor content at higher power levels.

Finally, using the steady-state loop momentum equation, the downcomer flow rate W_o is calculated and shown in Fig. 5.1-1 (e).

5.1.2 Steam Generator Variables during Transient Operation

The behavior of the steam generator variables are calculated and displayed for a transient. To show the transient response more clearly, a fast transient is considered as an illustrative example. In this example, the steam generator is operating in a nearly steady manner at 12% power prior to a time (t) of 150 s . At t = 150 s, a linear ramp increase in steam flow is initiated. The ramp terminates at t = 180 s at a steam flow corresponding to 36% power. The steam flow is then maintained to be constant at this "36%" value for $t > 180$ s. Additional input variables must be specified as a function of time to complete the definition of the illustrative transient. The variables (T_H and T_{fw}) were taken to have their steady value corresponding to 12% power for $t \leq 165$ s ; to have their steady value corresponding to 36% power for $t \geq 195$ s ; and to undergo linear ramp in T_H and two piecewise linear ramps in T_{fw} (based on Fig. 5.1-1 (a)) for $165 \text{ s} < t < 195$ s. The remaining input variables (primary flow and primary pressure) were held constant. All input variables are

shown in Fig. 5.1-2.

We employ the proposed controller to operate in response to this transient. In this case, we do not give any credit to the flow measurements ("W_s" and "W_{fw}") as inputs to the controller. This is based on the practical assumption that they are too uncertain to use at low power conditions.

With the control equation of the proposed controller given as Eq. (4.2-32) in Chapter 4 , we set the control parameters as : K_{pw}=0 ; K_p=200 ; T_i = 50 s ; α=1.8 ; and β=1.0 (Variations of each parameter will be discussed in the following subsections). With such a proposed controller, the calculated steam generator responses are shown Fig. 5.1-3.

First, in Fig. 5.1-3 (a), the calculated heat transfer rate implies that the transient inputs shown in Fig. 5.1-2 result in the expected long term result (power change from 12% to 36%). The increase in steam flow (see Fig. 5.1-2) causes a sharp drop in steam generator pressure (Fig. 5.1-3 (b)). The drop in pressure in turn causes an increase in the vapor content in the tube bundle with M_{TB} correspondingly down as shown in Fig. 5.1-3 (c). However, not enough time has elapsed to remove this extra mass from the steam generator. Therefore, the mass shifts to the downcomer region with M_{DC} correspondingly up as shown in Fig. 5.1-3 (c). The final response of interest is the increase in downcomer water level shown in Fig. 5.1-3 (d) where the level deviation (L_w - L_{Ref}) has the same behavior as L_w since L_{Ref} is constant. This increase in level, called a

"swell", is a good representation of of M_{DC} behavior but, as expected, a very bad representation of the total mass content of the steam generator M_{TOT} . As shown in Fig. 5.1-3 (e), the feed flow W_{fw} is less than the steam flow W_s during most of the transient. This implies that the total mass M_{TOT} is decreasing while the level swell gives the reverse indication.

If a conventional controller were used, the increase in level would cause a large decrease in feedwater flow. The decrease in feedwater flow causes a further level swell. In such a manner, the system can become unstable as described in the first section of Chapter 4.

Meanwhile, using the proposed controller, the compensated level Y_w in the form of Eq. (4.2-33) is used for controller input. The behavior of Y_w is displayed with L_w in Fig. 5.1-3 (d). The compensated level Y_w is used to generate the error for control action. As shown in this figure, the variable Y_w does not suffer as drastically from the swell occurrence and it gives a stable behavior settling down to its reference value Y_{Ref} . The control error based on $(Y_{Ref} - Y_w)$ actuates the feedwater flow W_{fw} in a stable manner and then the actual level L_w is stablized, too.

The simulation results validate the physical idea that the behavior of tube bundle mass is a good measure of the shrink and swell effects. That is, the level compensation by use of δL_r based on the tube bundle mass always gives an appropriate indication for use in taking control action.

After the transient, all the variables are approaching their steady-state values corresponding to the existing power level (36%). We see that the steady-state tube bundle mass (the so-called "inherent tube bundle mass") is decreased by 4 Mg (from 35 Mg to 31 Mg) from its pre-transient value (see Fig. 5.1-3 (c)). This inherent tube bundle mass change is compensated for during this transient by using the compensation term δL_i. The final steady-state condition is adjusted by using the relation between the inherent tube bundle mass and T_H based on a steady-state calulation (see again Fig. 4.2-10). Such a physical idea is confirmed the fact that the actual level L_w is returned nearly to its reference value L_{Ref} with a very small steady-state error (see again Fig. 5.1-3 (d)). The remaining steady-state error due to the model imperfection can be treated by the adaptive adjustment δL_a, an adjustment not needed for the present example.

5.1.3 Sensitivity Study of Correction Terms

By using the parameters such as α and β, the correction terms can be adjusted to achieve better control performance. Now through a sensitivity study for these parameters, the effectiveness of the correction terms is evaluated.

For the sensitivity study, a milder transient is adopted as an example for the wide range of parameter variation (Very fast transients sometimes are beyond the simulation capability of our model and certainly are beyond plant needs). This present transient

undergoes the power increase from 10% to 15% in one minutue. In other respects, the transient is similar to the previous example.

First, through a sensitivity study of the parameter α , we want to see the effects of the reverse level change (δL_r) compensation on the system performance as related to stability. These effects are to be illustrated analytically by using the root-locus method (Ref. [O1], [H2], [S5] and Appendix [E]). And then with an actual simulation, we want to see if such illustrations are confirmed by the non-linear model. Based on the simplified model, the transfer function for the compensated level dynamics can be expressed as follows:

$$T(s) = \frac{G_1 (1 - s / z_1)}{(s - p_1) (s - p_2)} \qquad (5.1 - 1)$$

where

$$p_1 = - 1 / \tau_2 \quad ; \quad p_2 = 0 \quad (\text{poles})$$

and

$$z_1 = \frac{G_1}{G_2 (1 - \alpha / \alpha_t) - G_1 \tau_2} \qquad (5.1 - 2)$$

where α_t is the design target value of α.

Combined with the proportional-plus-integral controller, the open loop transfer function is :

$$T_{OL}(s) = \left(\frac{s + 1 / T_i}{s} \right) T(s) \qquad (5.1 - 3)$$

Thus the open loop poles and zeros are :

$$p_1 = -1 / \tau_2 \; ; \quad p_{2,3} = 0 \text{ (double poles)} \; ;$$

and

$$z_1 \text{ (Eq. 5.1-2)} \; ; \quad z_2 = -1 / T_i$$

The closed loop transfer function of the controlled system with the proportional gain K_p is :

$$T_{CL}(s) = \frac{K_p T_{OL}}{1 + K_p T_{OL}} \qquad (5.1 - 4)$$

The zeros are the same as those of the open loop transfer function and the closed loop poles are the roots of the characteristic equation :

$$1 + K_p T_{OL}(s) = 0$$

or

$$(T_i \tau_2) s^3 + T_i \left(1 - \frac{K_p G_1}{z_1} \right) s^2 + K_p G_1 \left(T_i - \frac{1}{z_1} \right) s$$

$$+ K_p G_1 = 0 \qquad (5.1 - 5)$$

The closed loop pole and zero configuration determines the performance

of the controlled system. The root-locus method enables us to find the closed loop poles from the open loop poles and zeros with the feedback proportional gain K_p as a parameter in the complex s-plane (With increasing K_p from zero to the infinity, the closed loop poles move from the open loop poles to the zeros). As shown in Eq. (5.1-2) and (5.1-5), the variation of the parameter α results in a change of the zero placement, which changes the location of the closed loop poles.

In Figs. 5.1-4 to 5.1-14, the closed loop responses are shown for the proposed controller using the illustrative transient and varying the parameter α . In the part (a) of each figure, the root-locus plot is given based on the simplified linear model. The motion of the closed loop poles with increasing K_p from 0 to 1000 is shown by arrows. At every increase by 50 in K_p , the corresponding closed loop pole placements are marked with " X " and the placements for the plant design value of K_p (428.9) are marked with rectangles. In part (b), the simulated level behavior of the proposed controller is shown to confirm the analytic illustration of part (a). For the parameters of the simplified model, we use the numerical values in Table 4.1-1. The integral time T_i is based on the actual design value (200 s) and no credit is given for flow measurements ($K_{pw} = 0$). From the results, valuable findings include:

1) The parameter $\alpha = 0$ (Fig. 5.1-4) represents a conventional controller. Since the controlled system has a non-minimum phase due to the shrink and swell effects (the zero z_1 lies on the right half

s-plane), it is subject to the stability constraint on the proportional gain K_p as given in Eq. (4.1-9). The root-locus plot for this case (Fig. 5.1-4 (a)) shows that the system becomes unstable with K_p greater than 200 (the closed loop poles lie on the right hand s-plane). For the value of $K_p = 428.9$ (the design value for the main feedwater controller of an actual unit), we obtain two complex poles and one real pole (three roots of the cubic characteristic equation Eq. 5.1-5) as follow :

$$p_1^c \, , \, p_2^c \simeq 0.02 \pm 0.04 \, j$$

and

$$p_3^c \simeq - 0.005$$

Obviously p_1^c and p_2^c are the dominant poles, which determine the transient behavior of the system (p_3^c lies very near a zero z_2 and thus its effects is negligible) (Ref. [D1],[O1]). Thus we expect the transient level behavior in the dominant mode of $e^{(0.02 \pm 0.04j)t}$, which gives an unstable oscillatory behavior. From this, we can estimate the exponential blow-up time constant (τ_b) and oscillation period (T_o) of the dominant mode :

$$\tau_b = 1 \, / \, (0.02) = 50 \text{ s} \quad ; \text{ and}$$
$$T_o = 2\pi \, / \, (0.04) = 157 \text{ s}$$

The corresponding transient response by the actual simulation also

shows the unstable oscillatory behavior (Fig. 5.1-4 (b)). We can see a good agreement in the oscillation period. Because the actuation by the feedwater valve is limited to positive flows ($W_{fw} \geq 0$), the amplitude does not exponentially increase but oscillates within the limited valves. It is noted that the average level slowly increases.

Meanwhile, for the very small value of $K_p = 65$ (the design value for the low power feed water controller of an actual unit), we have the following closed loop poles :

$$p_1^c , p_2^c \simeq - 0.001 \pm 0.005 j \quad ; \text{ and}$$
$$p_3^c \simeq - 0.025$$

p_1^c and p_2^c are still dominant poles (the mode contributed by p_3^c decays relatively quickly). The transient response is expected to be stable but is very sluggish because of the long damping time constant ($\tau_d = 1/0.001 = 1000$ s). The period is also very long ($T_o = 2\pi/(0.005) = 1200$ s). The simulation results support this analytic expectation.

2) From the results of 1), it is found that the conventional controller does not provide satisfactory control at low power, where the stable range of K_p is too narrow. Even with the value of K_p in the stable range, the stability margin is so small (the closed poles lie very near the imaginary axis) that the design uncertainty or drift of dynamics may cause the system to be unstable. As the power increases, the stable range of K_p for the conventional controller is greatly expanded. This analytic finding is illustrated in Fig.

5.1-5 and 5.1-6 in a manner similar to that in 1).

3) By introducing a positive value of α, a major design parameter in the proposed controller, we can obtain a significant wider stable range of K_p . Repeat Eq. 5.1-2 for the zero z_1:

$$z_1 = \frac{G_1}{G_2 \left(1 - \alpha / \alpha_t \right) - G_1 r_2}$$

where α_t = the design target value of α with which we can compensate the reverse dynamics completely

As α is increased and passes through the value for which the denominator of z_1 is equal to zero, z_1 jumps to negative infinity from positive infinity and the system becomes minimum phase. This value is designated a marginal value denoted by "α_m". It is obvious that $0 < \alpha_m < \alpha_t$. For the sensitivity study , it is found that $\alpha_m \simeq 1.2$ and $\alpha_t \simeq 1.8$.

4) With $\alpha = 1.0$ (Fig. 5.1-7), the controlled system still exhibits a non-minimum phase ($\alpha < \alpha_m$). As shown in the root-locus plot (Fig. 5.1-7 (a)), however, the stable range of K_p is wide enough to select a value of K_p that permits a satisfactory controller performance. For the design value of $K_p = 428.9$, the dominant closed loop poles are :

$$p_1^c , p_2^c = - 0.013 \pm 0.04 j$$

with the damping time constant τ_d = 77 s and the oscillation period T_o = 157 s. This indicates that the level would be damped to less than 1 % (4 mm) within 360 seconds (about $2T_o$). In the corresponding simulation results (Fig. 5.1-7(b)), we see a good agreement of the level behavior with the analytic expectation.

For the value of K_p = 1000, the system becomes marginally stable with the dominant closed loop poles on the imaginary axis ($0 \pm 0.065j$). The level is expected to oscillate in a limited cycle with a period $T_o \simeq 100$ s. The simulation result shows this expected behavior (It is noted that the average level does not increase in this case). These results imply that there is still a system stability constraint on K_p ; however, this constraint is much less restrictive than that of the conventional case.

5) By increasing the value of α over α_m , the system is of the minimum phase and is no longer subject to the constraints for the stability. Fig. 5.1-8 and Fig 5.1-9 show the change of the locus of closed loop poles as α passes the marginal value α_m. As shown these plots, the closed loop poles are on the left hand s-plane and the system is always stable.

6) With α = 1.5 (Fig. 5-10), chosen as an example value in this range ($\alpha_m < \alpha < \alpha_t$), the system is one of minimum phase. For the design value of K_p = 428.9, the dominant closed loop poles, in Fig. 5.1-10 (a), are :

$$p_1^c \ , \ p_2^c \ = \ - \ 0.04 \ \pm \ 0.0015 \ j$$

with $\tau_d = 25$ s ; and oscillation period $T_o = 420$ s.
Thus the amplitude is damped to a negligible value within one period. No visible oscillation would be expected. The simulated result is also at a good agreement (Fig. 5.1-10 (b)). Even for the high value of $K_p = 1000$, the system is stable and well damped as expected. The transient behaviors of these two cases ($K_p = 428.9$ and $K_p = 1000$) are very similar and satisfactory. It implies that the proposed controller is very tolerant to the design uncertainty of choosing a proportional gain.

7) With $\alpha = \alpha_t$ (the target value $\alpha_t \simeq 1.8$), a complete compensation is achieved. The pole and zero cancellation occurs and the system is reduced to second order (two closed loop poles exist). As shown in the root-locus plot in Fig. 5.1-11 (a), the dominant pole is : $p_1^c = -0.04$ (the other pole p_2^c is very near the zero position and thus its effect is small)

The simulated level response, as expected analytically, is shown in Fig. 5.1-11 (b) with a superior behavior (non-oscillatory and quickly damping).

8) For further increases of α above α_t , the system is still stable but has some undesirable features in the transient response. With $\alpha = 3.5$ as an example, in Fig. 5.1-12 (b) we see a slowly damped overall oscillation with long period $T_o \simeq 1500$ s. A small amplitude oscillation also occurs with very short period.

The first one is analytically explained by the root-locus plot (Fig. 5.1-12(a)). For $K_p = 428.9$, three closed-loop poles are obtained as follow :

$$p_1^c \, , \, p_2^c = - 0.01 \pm (4 \times 10^{-3}) \, j \quad ; \text{ and}$$
$$p_3^c = -0.17$$

The mode due to p_3^c decays quickly. The dominant poles are p_1^c and p_2^c . From these poles, the damping time constant is $\tau_d = 100$ s and the oscillation period is $T_o = 2\pi / (4 \times 10^{-3}) = 1507$ s. This analytic result gives a good interpretation for the first undesirable feature (a sluggish approach to the new steady state).

The second (local) oscillation results from high order terms in the tube bundle mass model and can not be treated in the simplified linear version. These terms usually have a negligible amplitude and short period. But in the case of excessive overcompensation, they grow to the magnitude shown in the transient response.

These problems give an upper bound to the choice of the controller design parameter α .

In conclusion, it is worthwhile adding following remarks about these findings:

1) The root-locus plots for the closed loop poles, as based on the simplified linear model, are generally consistent with the transient system responses from our non-linear model.

2) In choosing the design parameter α for the proposed controller, it is desirable to set the value of α around α_t. The value of α_t cannot be known precisely. It varies with operating conditions, and subject to modeling uncertainties. However, the range of the value α, for satisfactory performance, is wide enough to cover the uncertainty in the estimation of α_t and the drift of α_t due to the change in operating conditions. As shown in Fig. 5.1-13, for the current simulations, the transient behaviors are satisfactory over a wide range (α between 1.0 to 2.0). This finding implies that the proposed controller has a large tolerance for design uncertainty in choosing the parameter α. In addition, the effects of design uncertainties can be further reduced by adjusting α in an adaptive manner.

3) Once the value of α is greater han α_m ($\simeq 1.2$), the system is no longer subject to a constraint on T_i in addition to that on K_p (For example, use of the very small value $T_i = 10$ s , combined with $\alpha = 1.5$ gives the satisfactory performance shown in Fig. 5.1-14 (a) and (b)). Therfore, we can set these feedback terms to the values for the best performance without being concerned for stability.

The discussion on selection of controller parameter α is now complete. Selection of controller parameter β is also required. We want see the effects of the inherent level change (δL_i) compensation for the steady-state error. A family of transient level response curves with various values of β is shown in Fig.(5.1-15). From the results, the findings are :

1) The value of β does not affect the stability of the system but it contributes to the steady-state error in the first stabilized condition.

2) In this case, the terminal value of (δL_i) is obtained from a steady-state calculation using the same nonlinear model as used in the simulaion. Therefore, $\beta = 1$, gives perfect compensation for the steady-state error. Practically, however, (δL_i) is in error due to model imperfections. The error causes the steady-state level to be different than desired after settling to a new steady condition. As shown in the figure for $\beta = 0.0$ and $\beta = 2.0$, the on-line adaptive adjustment (δL_a) performs a perfect compensation for the remained error. However, to minimize the transient effect accompanying an on-line adaptive adjustment due to (δL_a), initial good information about (δL_i) is highly desirable. An off-line adaptive adjustment of (δL_i) or β can be employed for this purpose.

5.2 Application of the Proposed Controller

In this part of the chapter, the proposed controller is applied to control for a wide spectrum of operating conditions. The resulting calculated performances of the controller are evaluated from a practical point of view.

5.2.1 Change in Power

The transient of power increase from start-up to full power is

imposed on the proposed controller to illustrate its achievement to a satisfactory automatic control over a full power range. The power level is increased over a total range from 5% (the model does not work near 0%) to 100% through many ramps for a total time of about three hours. In each ramp, the power level is increased by five percent for one minute; the new power level is maintained at a constant value for nine minutes; then a new ramp is started. The inputs for the transient simulation are given in a similar manner to those for the previous illustrative examples. The transient inputs are shown in Fig. 5.2-1.

We employ the proposed controller with following parameters :

$K_{pw} = 0$ (no credit to the flow measurements) ;

$K_p = 428.9$; $T_i = 20$; $\alpha = 1.8$; and $\beta = 1.0$

The results are shown in Fig. 5.2-2. From these results, findings are :

1) The calculated percent power or heat transfer rate (Fig. 5.2-2 (a)) implies that the transient inputs shown in Fig 5.2-1 result in the specified transient.

2) The transient response of the water level (Fig. 5.2-2 (b)) indicates that the proposed controller shows good performance for the entire range of power. The level always settles down within 3 minutes after a single power increase without any stability problem. Even at very low power, the maximum overshoot of water level was less than 10% (0.366 m) of the narrow range which corresponds to values achieved by a good manual control during somewhat milder plant maneuvers (see Fig.

5.2-3).

3) The transient response of the control variable W_{fw} (Fig.5.2-2 (c)) shows a good match to the input steam flow in spite of the lack of flow measurements.

4) The transient responses of other variables (Figs. 5.2-2 (d) through (g)) show expected behavior. From the response of pressure (Fig. 5.2-2 (d)), we see that the swelling effect is diminishing as the power increases.

5) The reference level is programmed to be constant at 50% over full range of power. Other types of steam generators employ a 33% to 44% level program, with which the steam generator level is programmed from 33% level at zero power to 44% level at twenty percent power and maintained at 44% level up to full power. With such a programmed level, the proposed controller also shows good performance (Figs. 5.2-4)

6) In our simulation, the power increase rate (average = 0.5%/min and maximum = 5%/min) is faster than actual plant cases (As shown in Fig. 5.2-3, average = 3%/hr and maximum = 0.25%/min). This implies that there is a performance margin in evaluating the controller.

5.2.2 Change in Reference Level

By step increasing the reference level, the capability of the proposed controller can be evaluated at various power levels. Consider reference level increase of 100 mm (≈ 3% of narrow range) in a step

manner at t = 30 s. We employ the proposed controller with the same parameters as in the previous case.

The response of water level for this transient is shown in Fig. 5.2-5 for 10%, 50%, and 95% power level respectively. From the results, it can be seen that the behavior of the variable is sufficiently damped to the acceptable range within three minutes without any stability problem. And we can see that the performance of the controller are good over whole range of power.

5.3 A Chapter Summary

The proposed controller has been evaluated in various ways in conjunction with our non-linear steam generator model representing an actual unit. First, the physical ideas, on which the proposed controller is based, were validated by looking into the transient response. Through a sensitivity study, the effectiveness of the proposed correction terms are evaluated both analytically and also by using transient simulations. The transient results by the non-linear model shows good consistency with the analytic expectations from the linear model. With those studies, the improved performance of the "proposed controller", with respect to the "conventional controller", were confirmed.

Next, by applying the proposed controller to a wide spectrum of operating conditions, the performances of the controller were evaluated from a practical point of view. Against a long term calculated power increase from low power to full power. The proposed

controller showed the good performance for the entire range of power. Water level was settled down within 3 minutes following each 5% power ramp (one minute duration). There were no stability problems. The maximum overshoot in water level occured at low power and was an acceptable magnitude (10% of narrow range $\approx$ 0.366 m). By artificially imposing step changes in reference level, further demonstration of good controller capability was achieved.

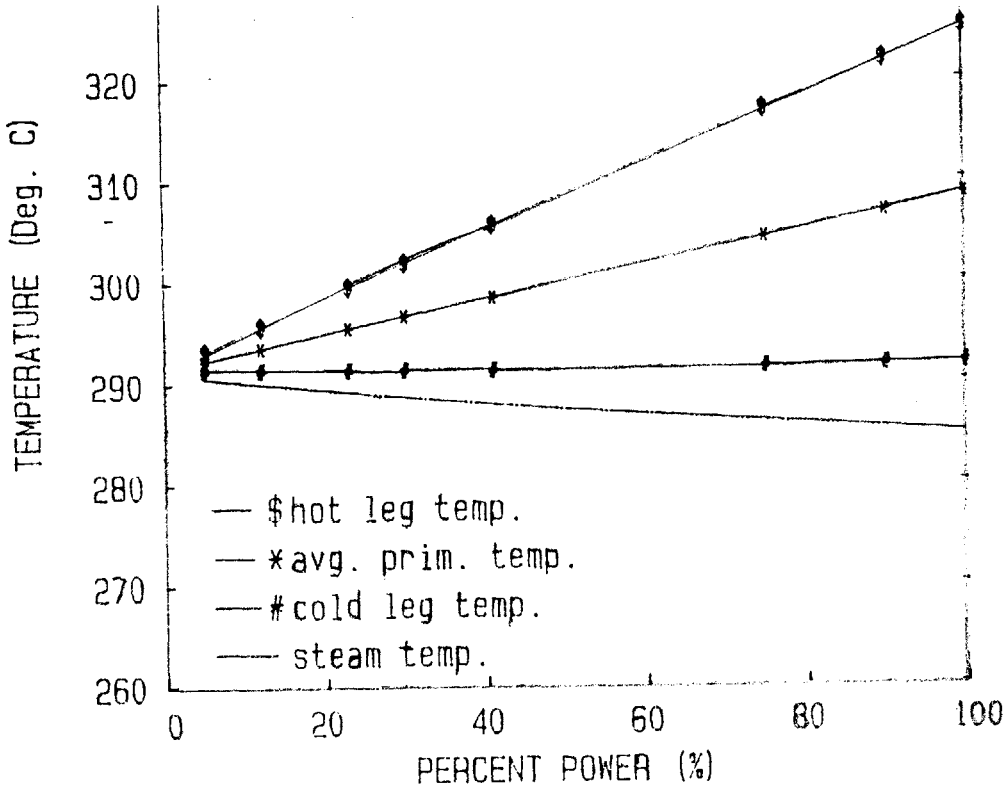

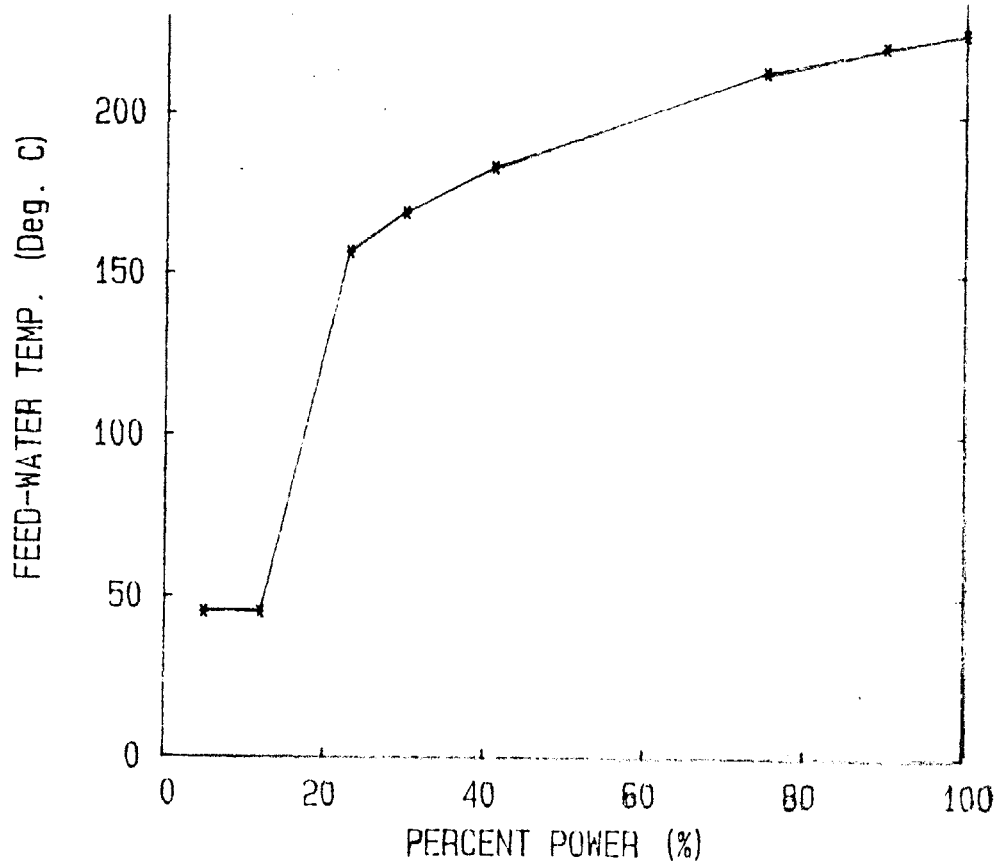

5.1-1 Steady-state variables

(a) Primary, steam , and feedwater temperatures

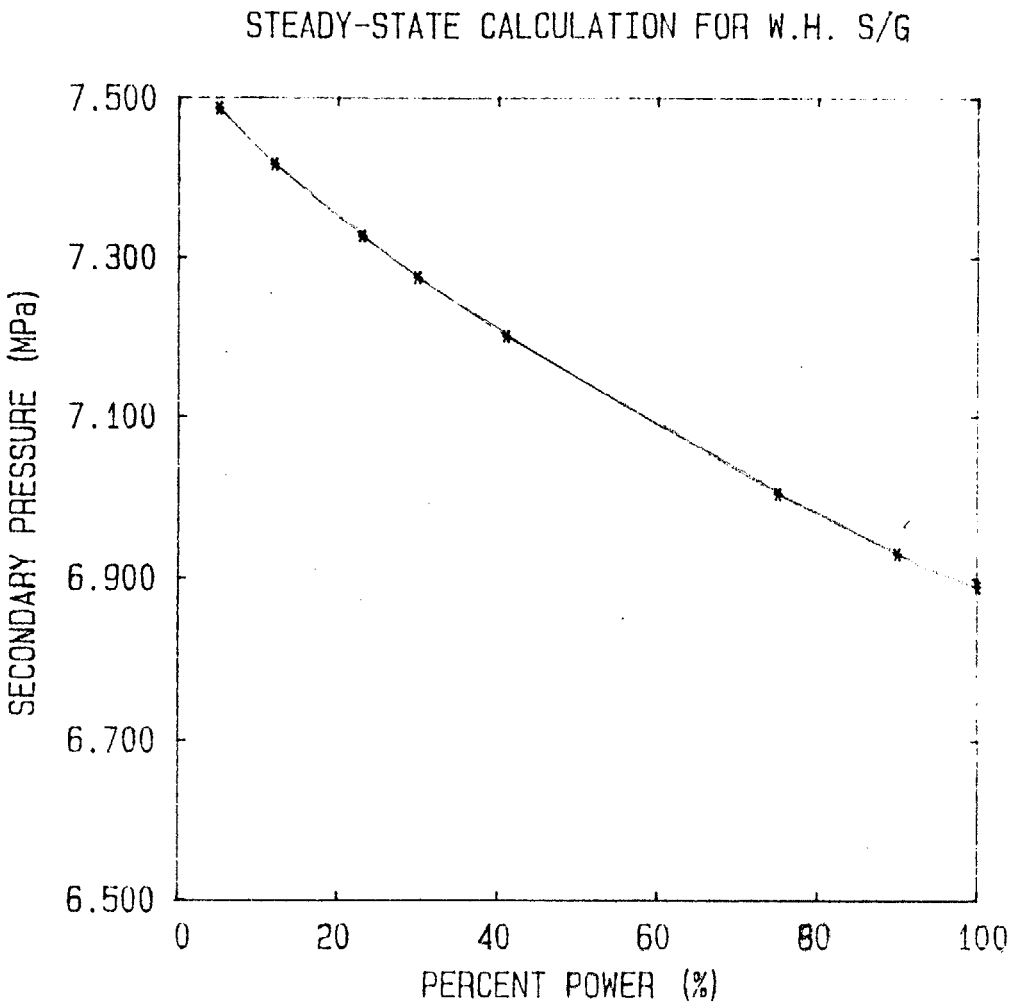

(b) Steam pressure

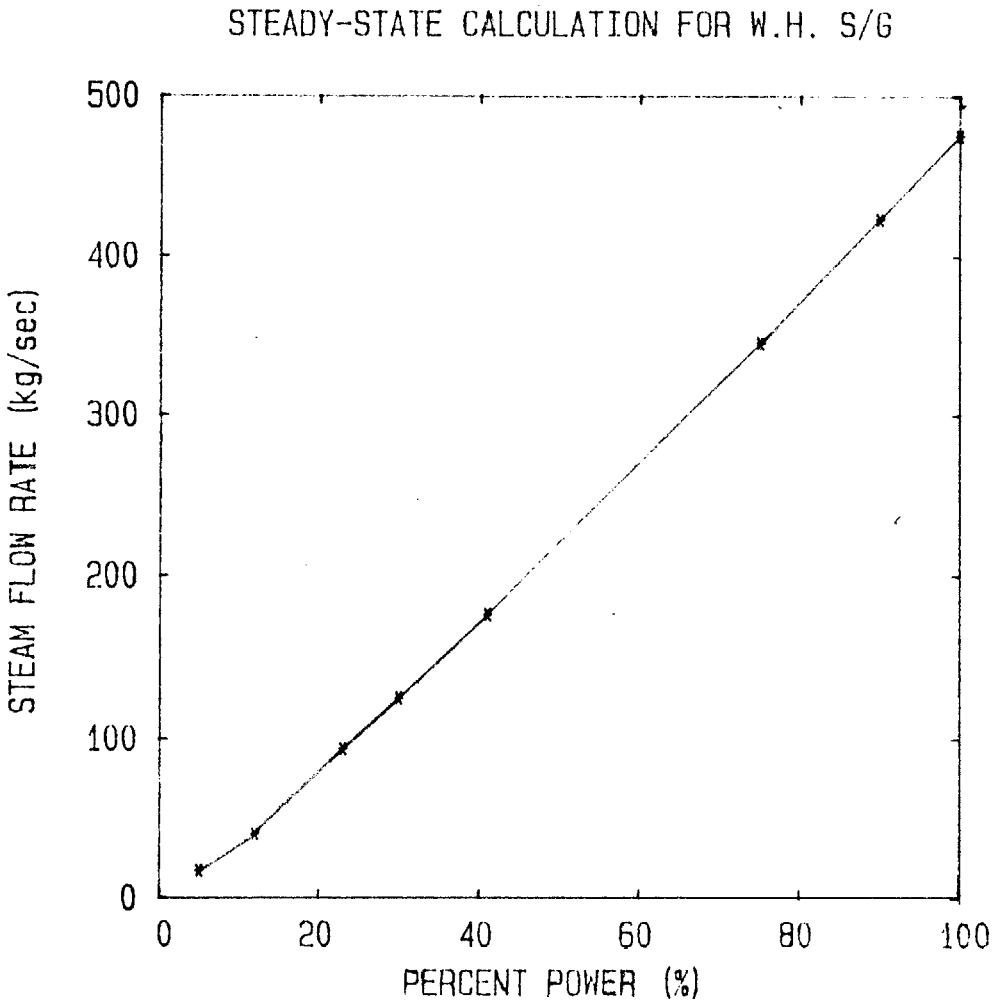

(c) Steam flow rate

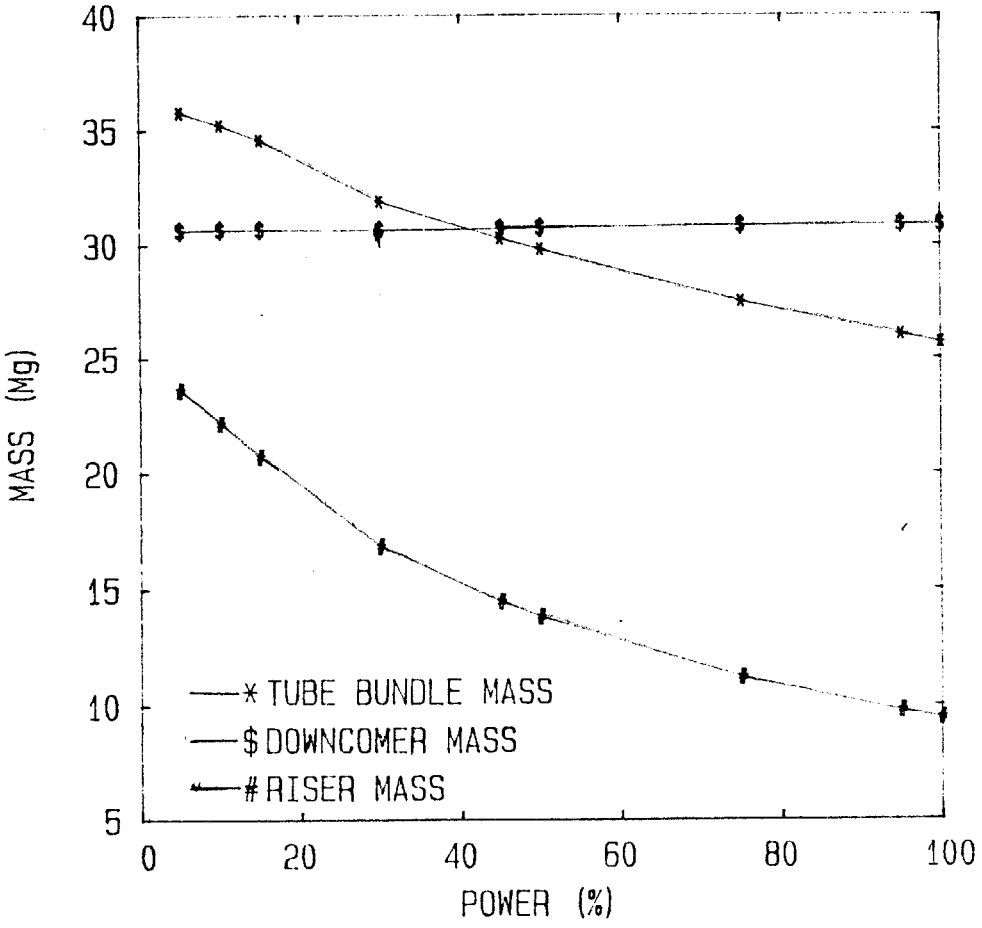

(d) Tube bundle, riser, and downcomer mass

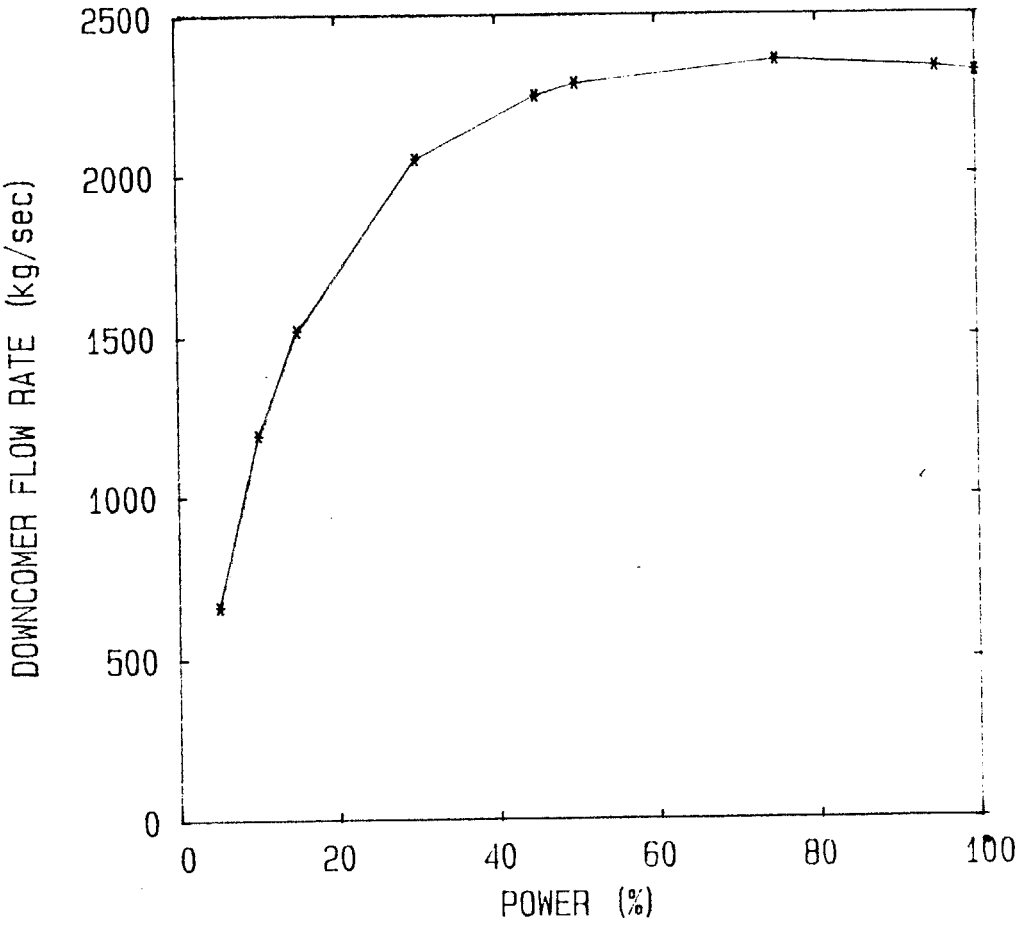

(e) Downcomer flow rate

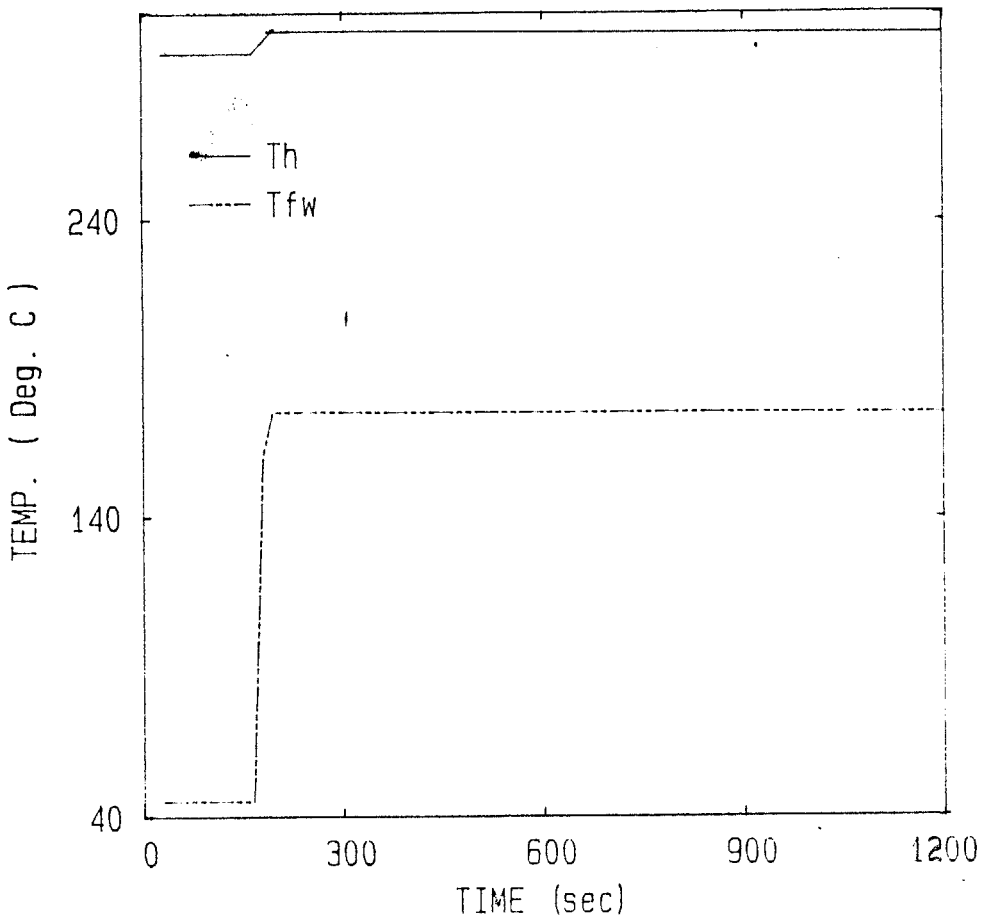

5.1-2 Transient (12%→36%) input for the primary hot-leg temperature, feedwater temperature and steam flow

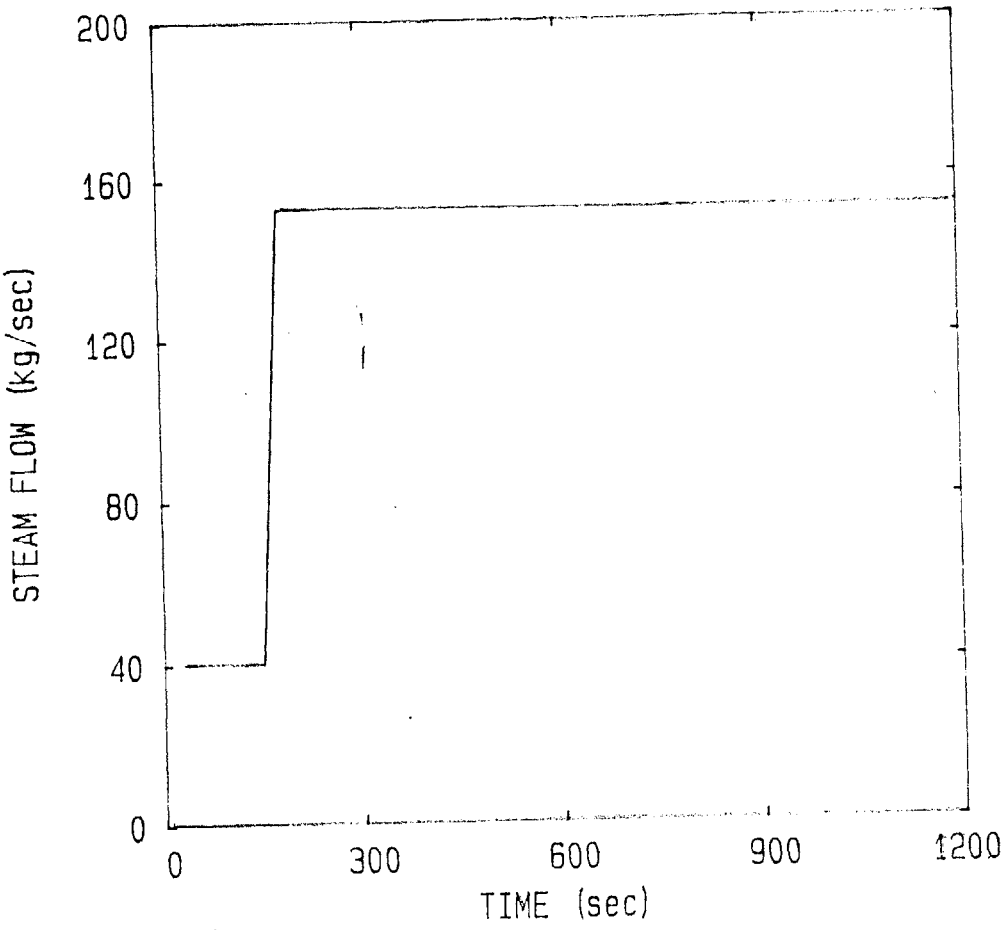

5.1-2 (continued)

Transient (12%→36%) input for the primary hot-leg temperature, feedwater temperature and steam flow

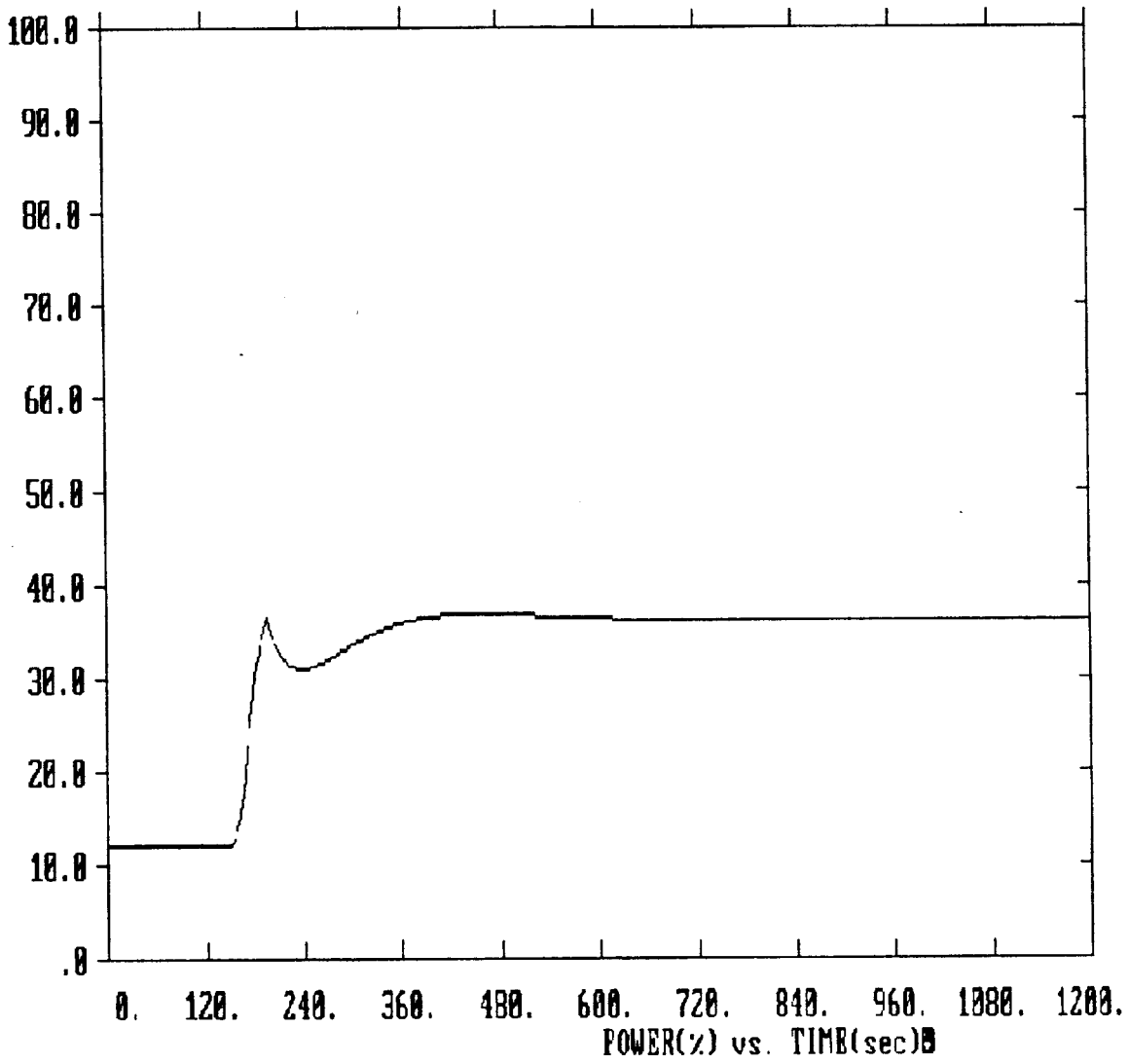

5.1-3 Transient (12%→36%) responses with the proposed controller

(a) Calculated power

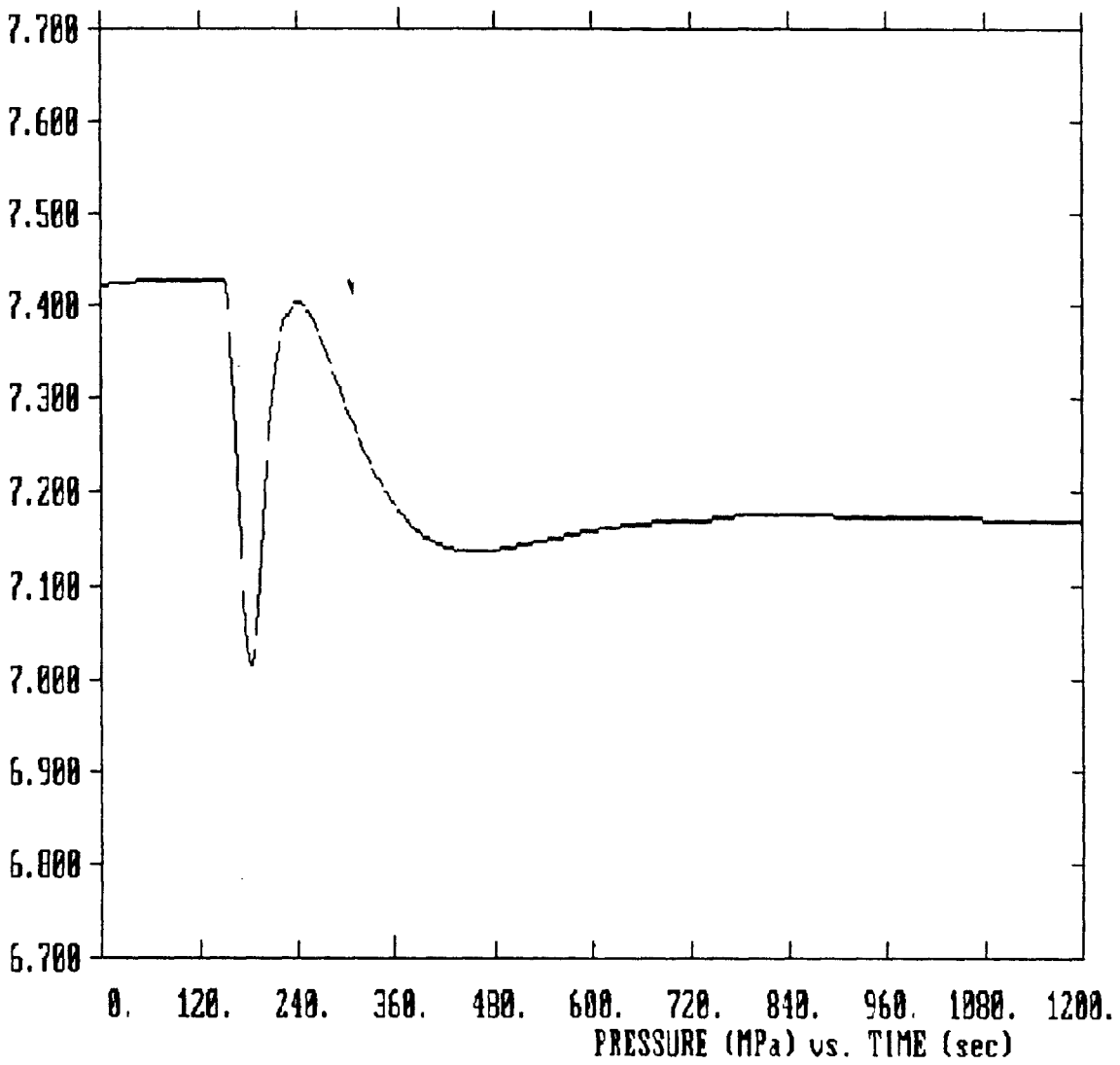

(b) Steam pressure

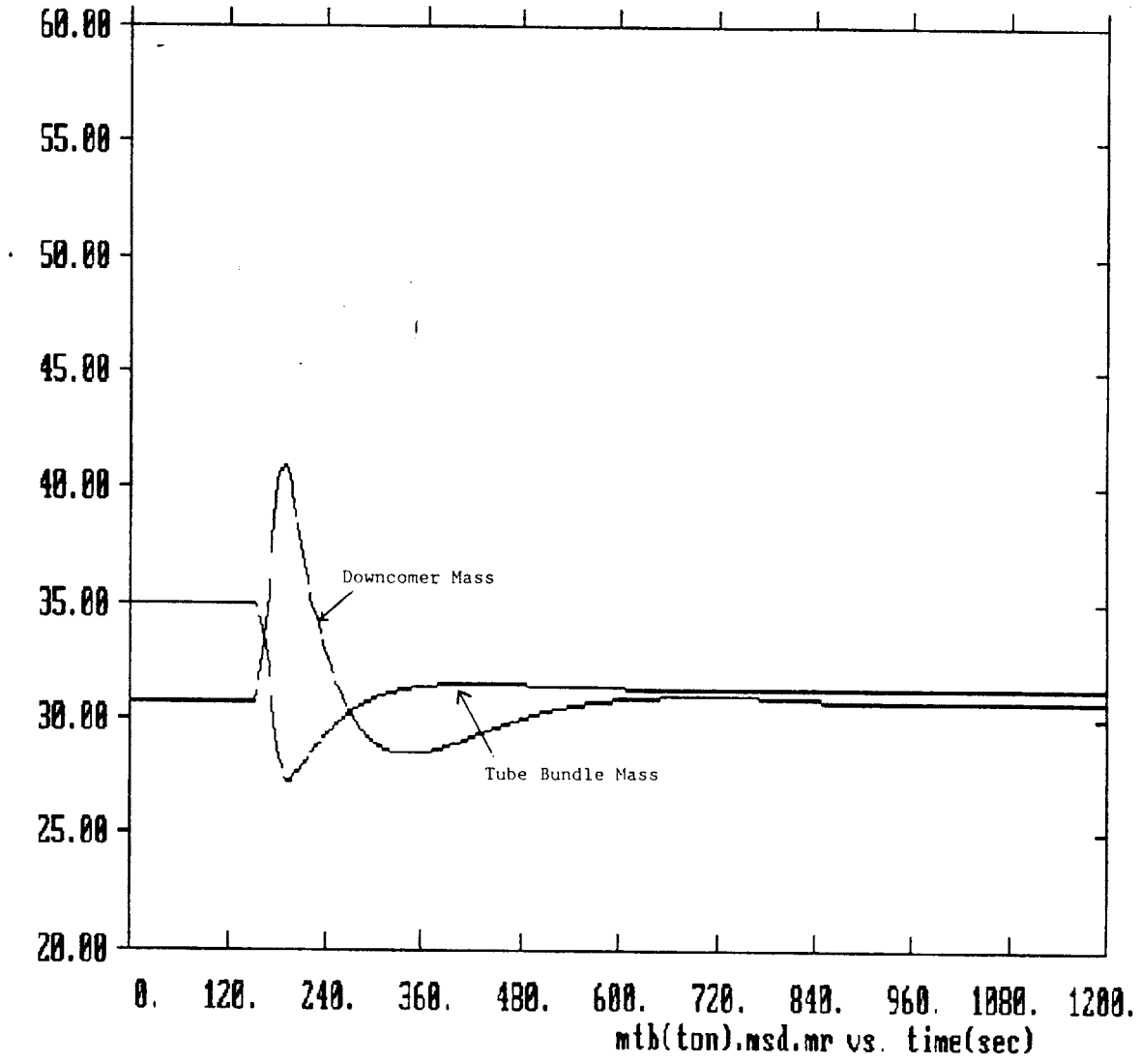

(c) Tube bundle mass and downcomer mass

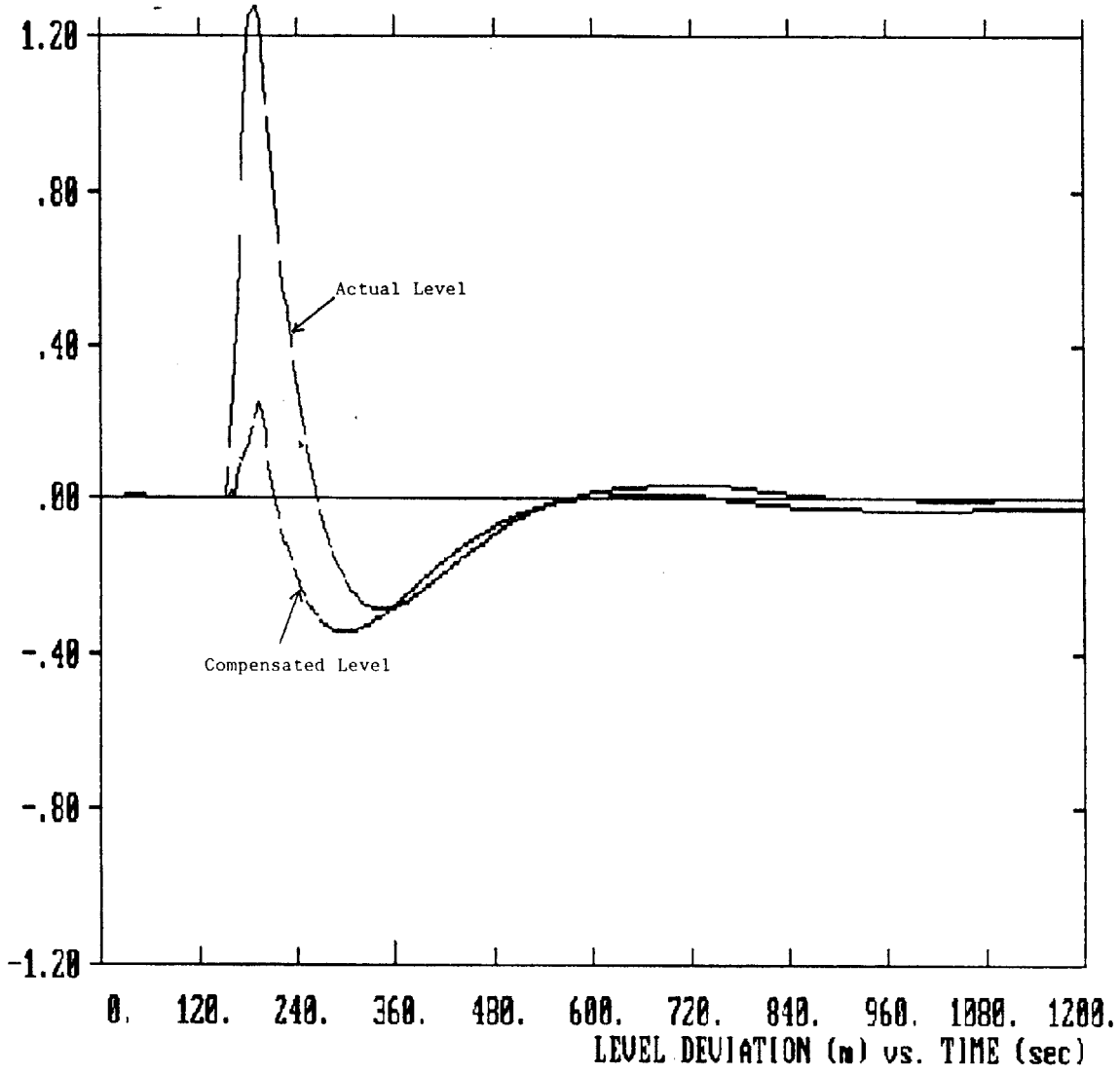

(d) Actual level and compensated level

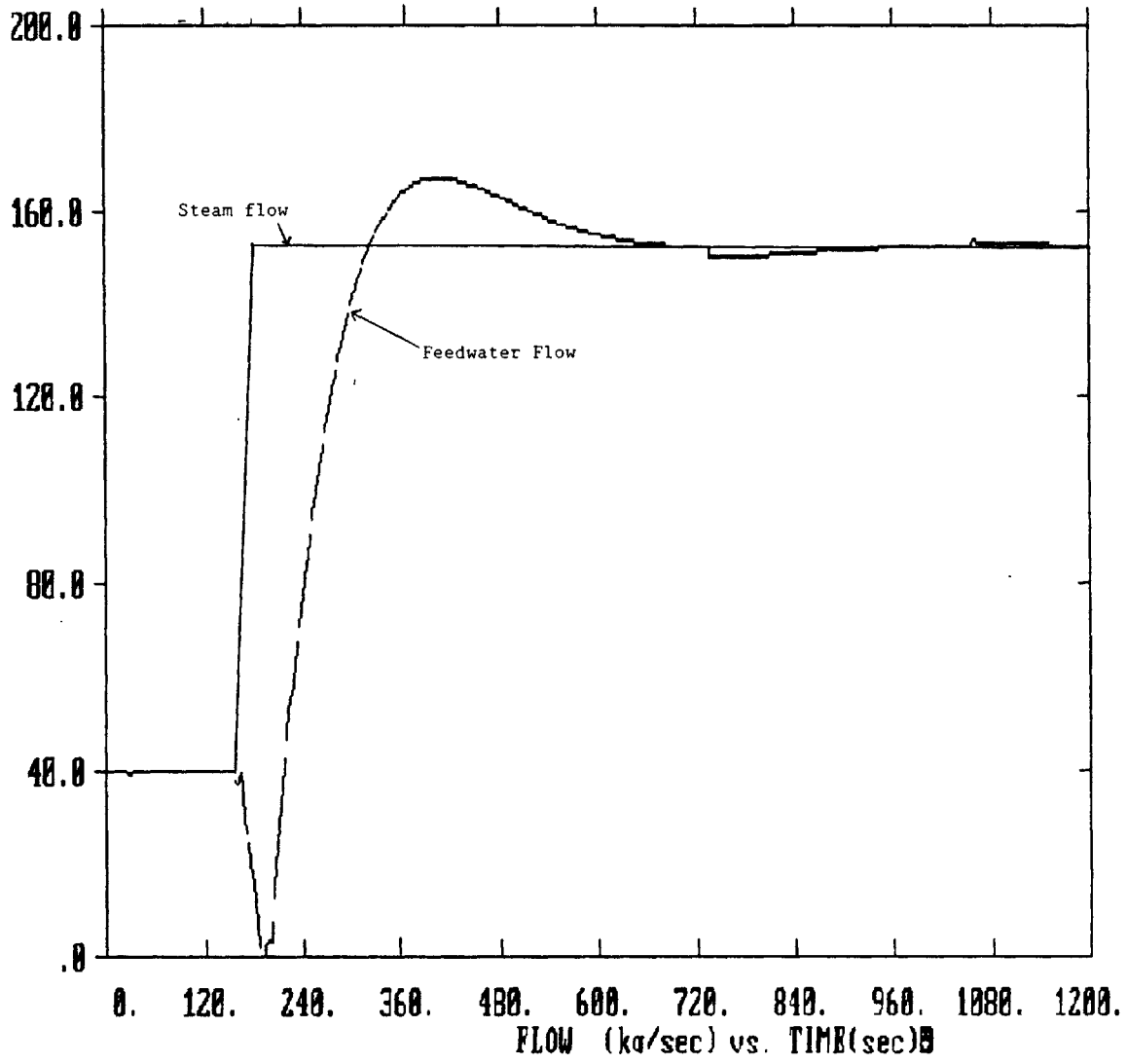

(e) Feedwater and steam flows

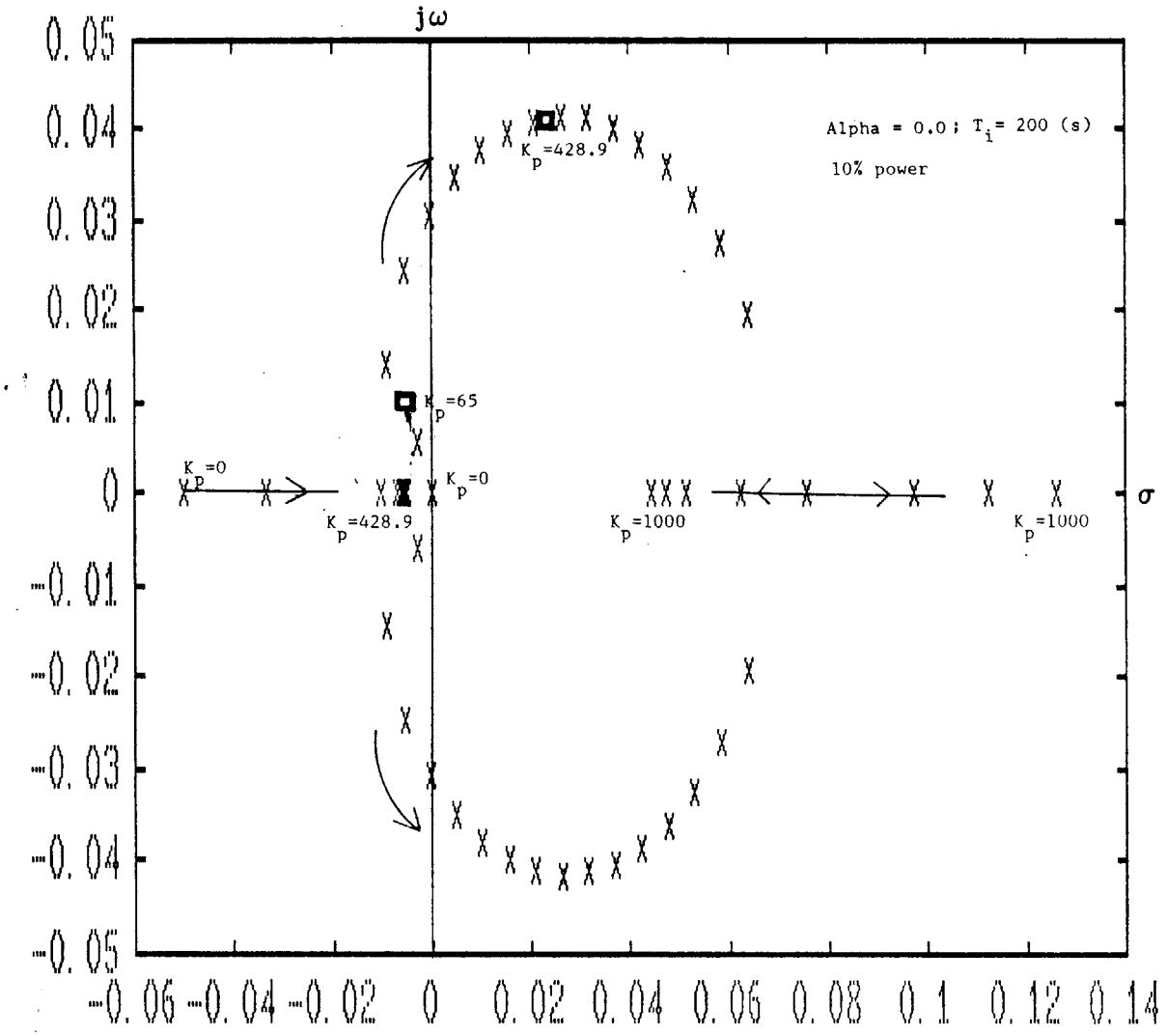

5.1-4 (a) Root-Locus plot for α=0.0 (T_i=200 s; 10% power)

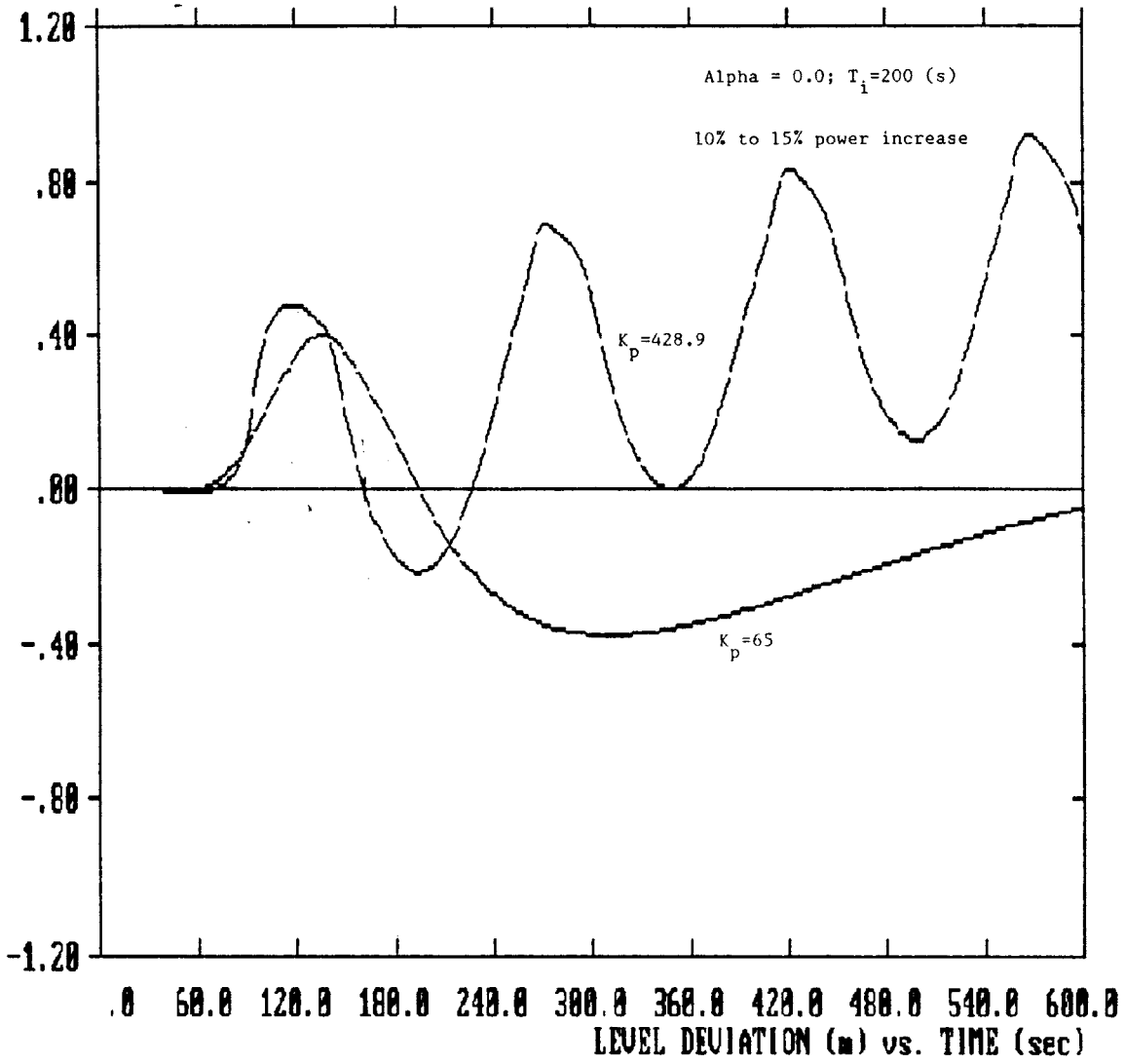

5.1-4 (b) Transient level response to the power increase (10%→15%) for α= 0.0 with K_p=428.9 and K_p=65 (T_i=200 s)

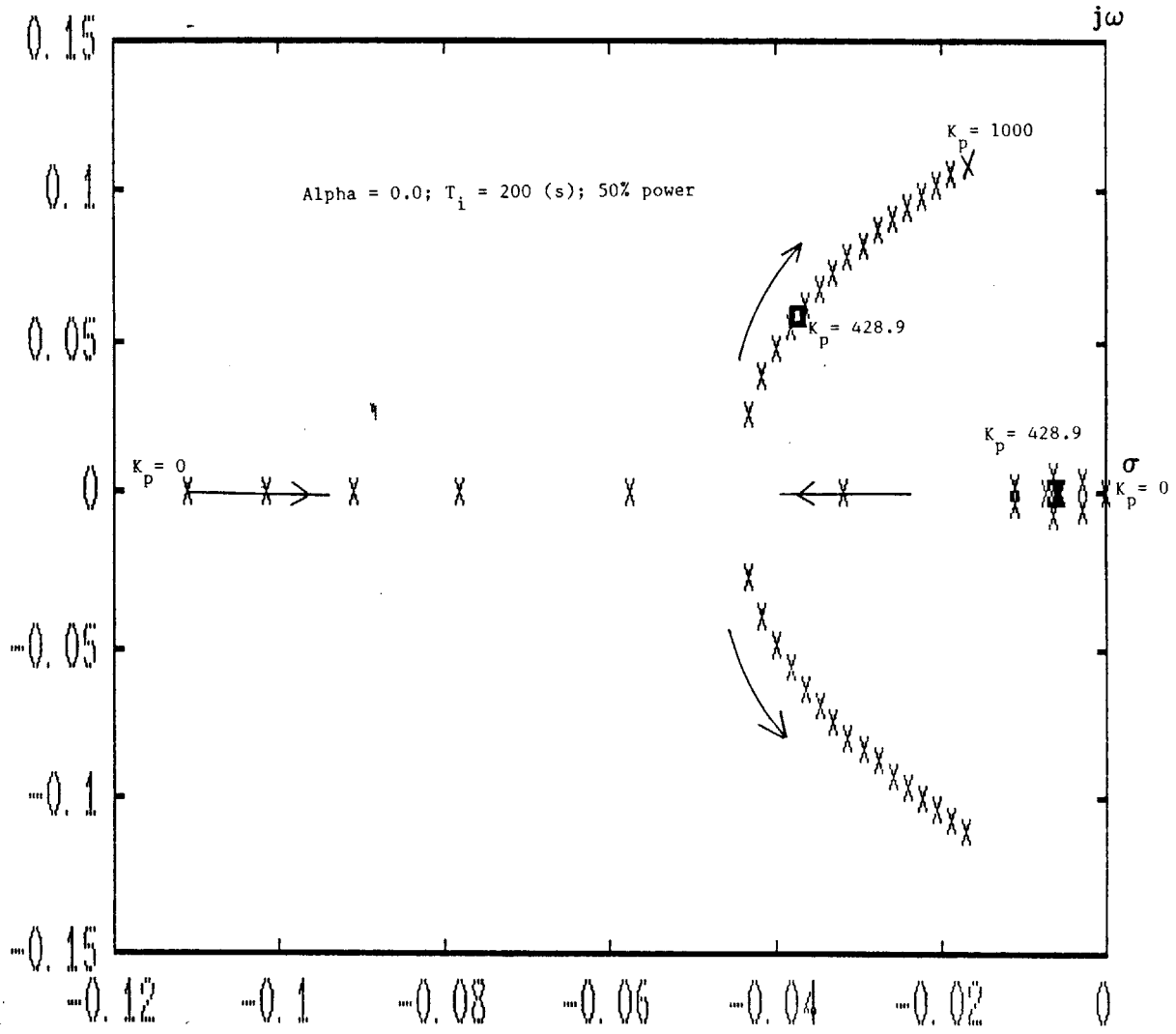

5.1-5 (a) Root-Locus plot for α=0.0 (T_i=200 s; 50% power)

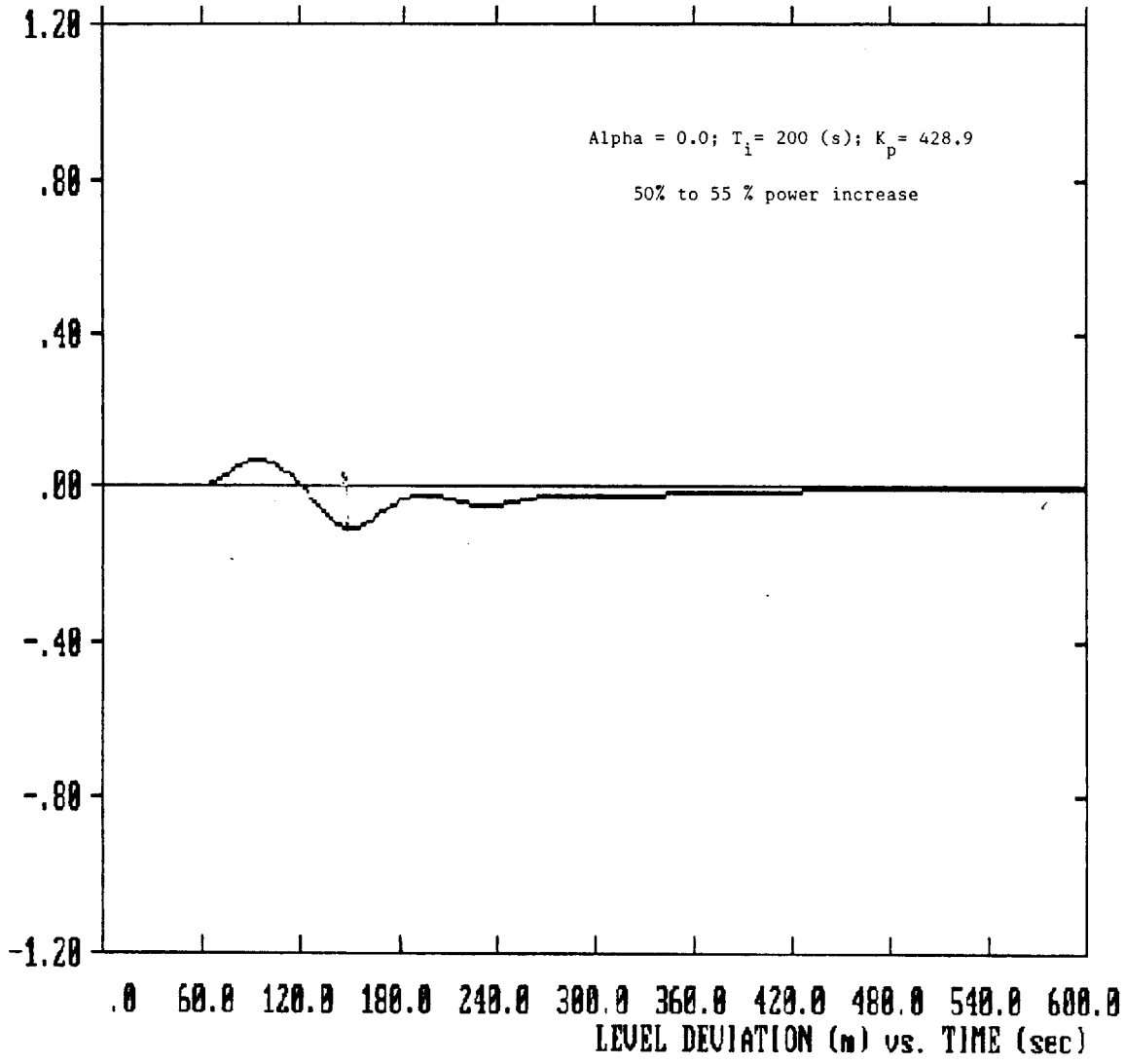

5.1-5 (b) Transient level response to the power increase (50%→55%) for α=0.0 with K_p=428.9 (T_i=200 s)

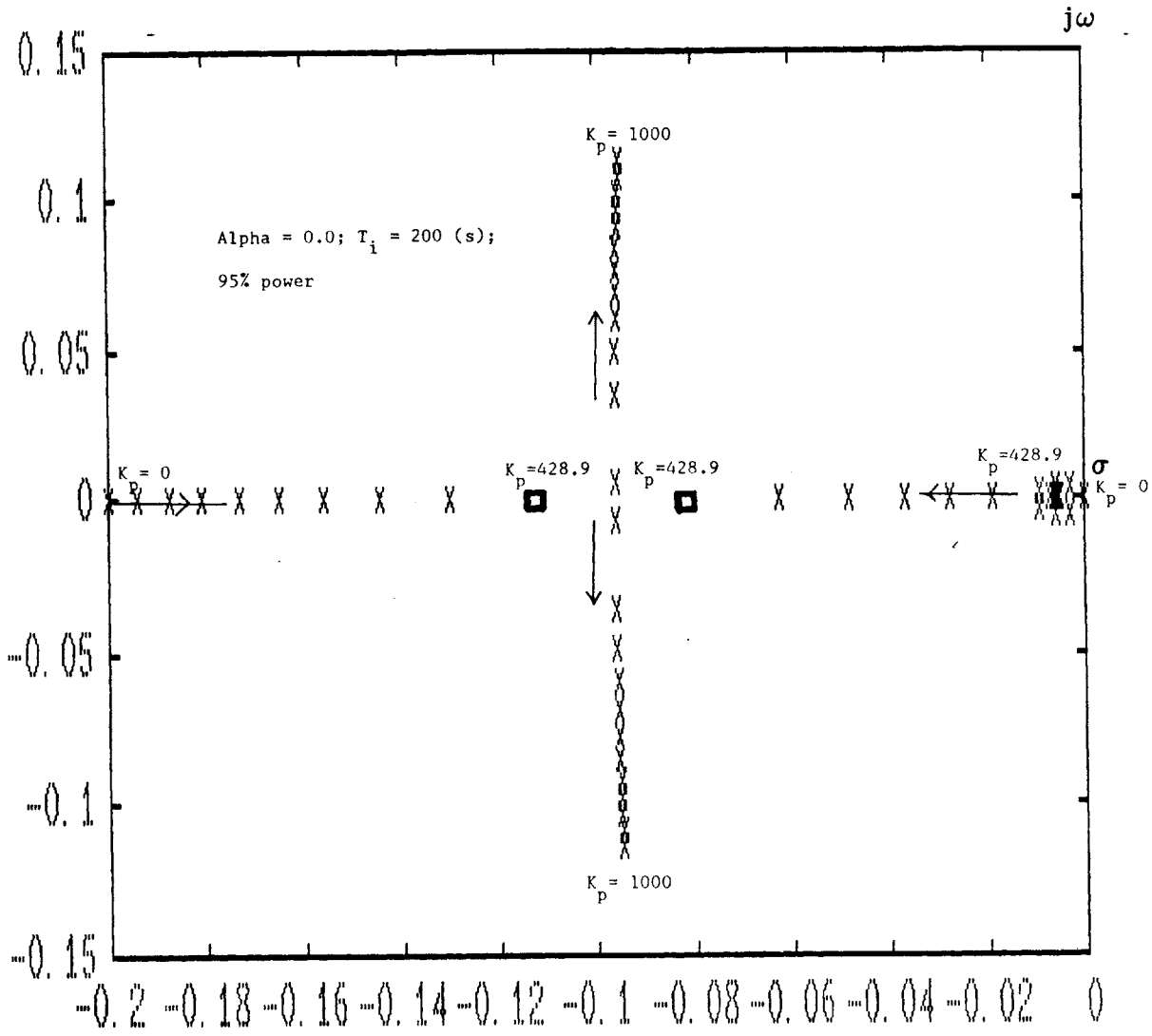

5.1-6 (a) Root-Locus plot for α=0.0 (T_i=200 s; 95% power)

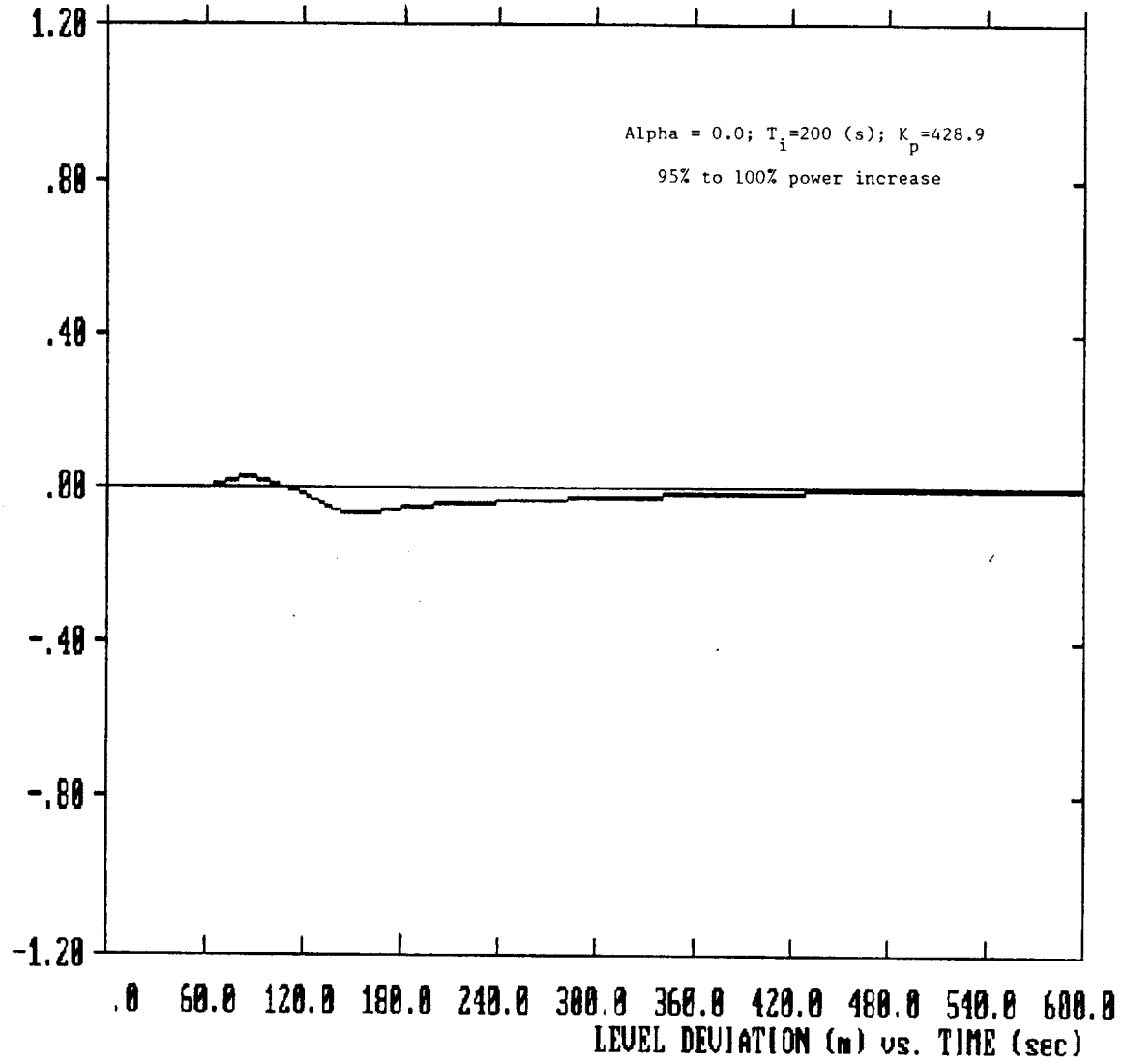

5.1-6 (b) Transient level response to the power increase (95%→100%) for α=0.0 with K_p=428.9 (T_i=200 s)

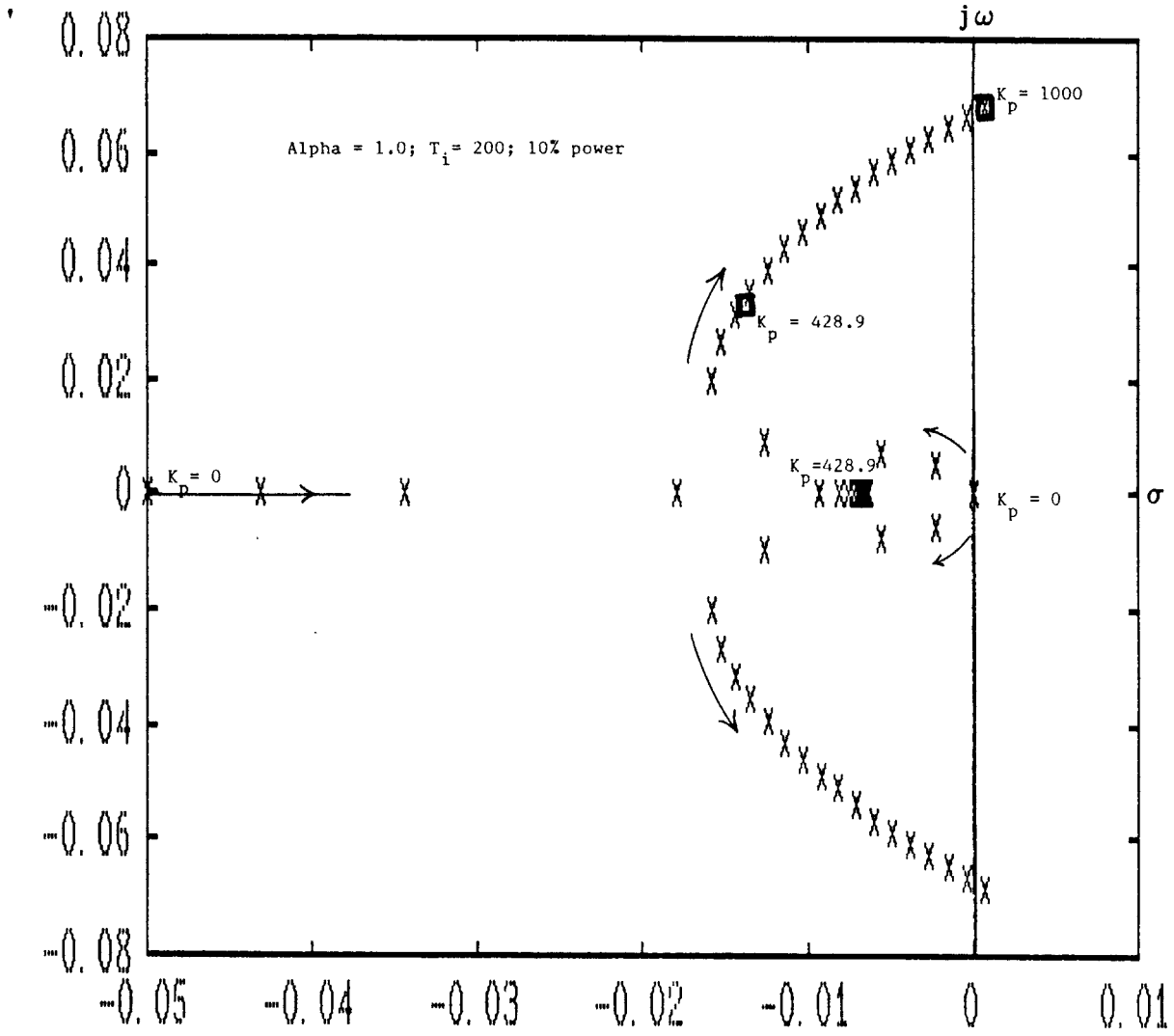

5.1-7 (a) Root-Locus plot for α=1.0 (T_i=200 s; 10% power)

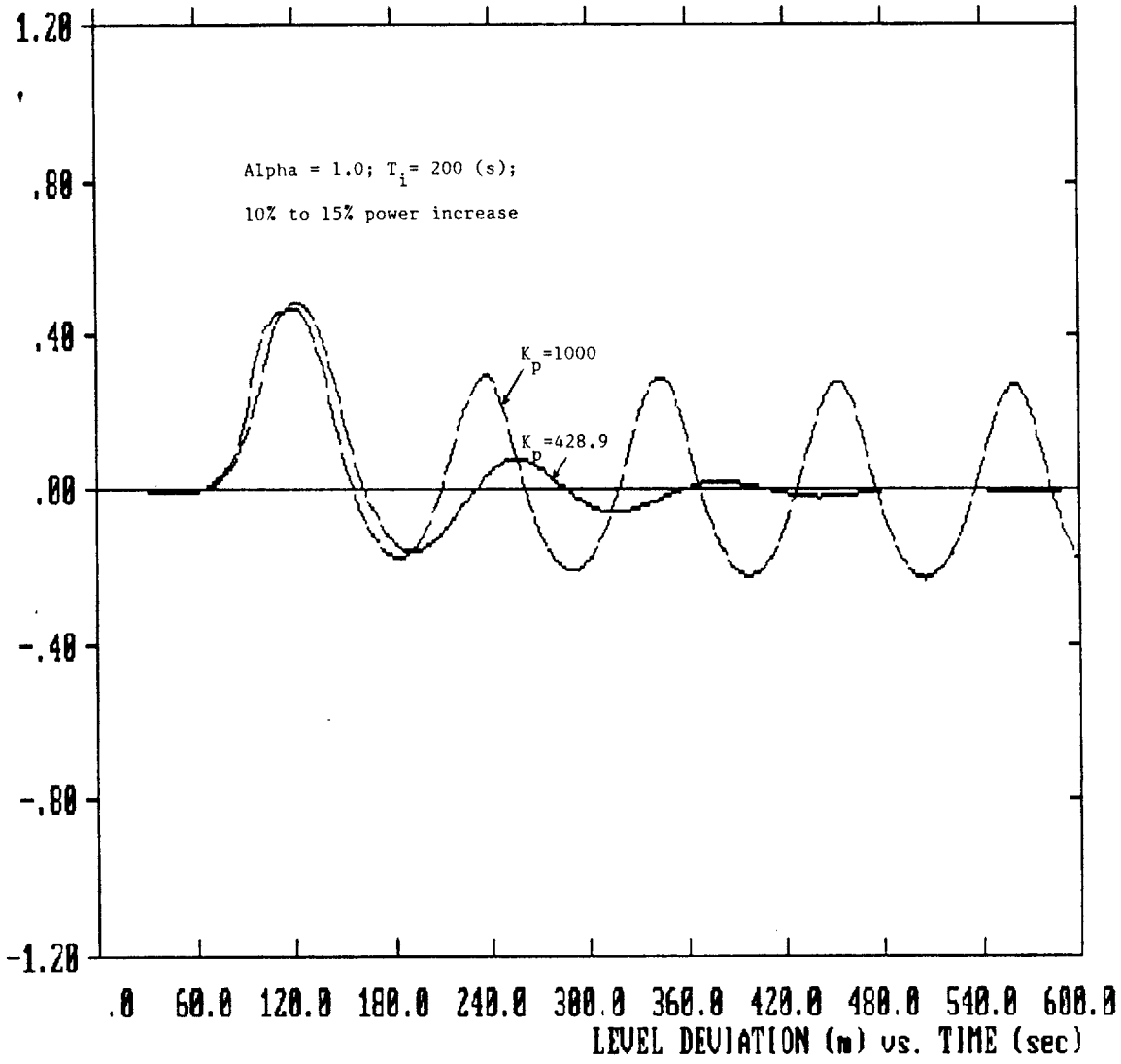

5.1-7 (b) Transient level response to the power increase (10%→15%) for α=1.0 with K_p=428.9 and K_p=1000 (T_i=200 s)

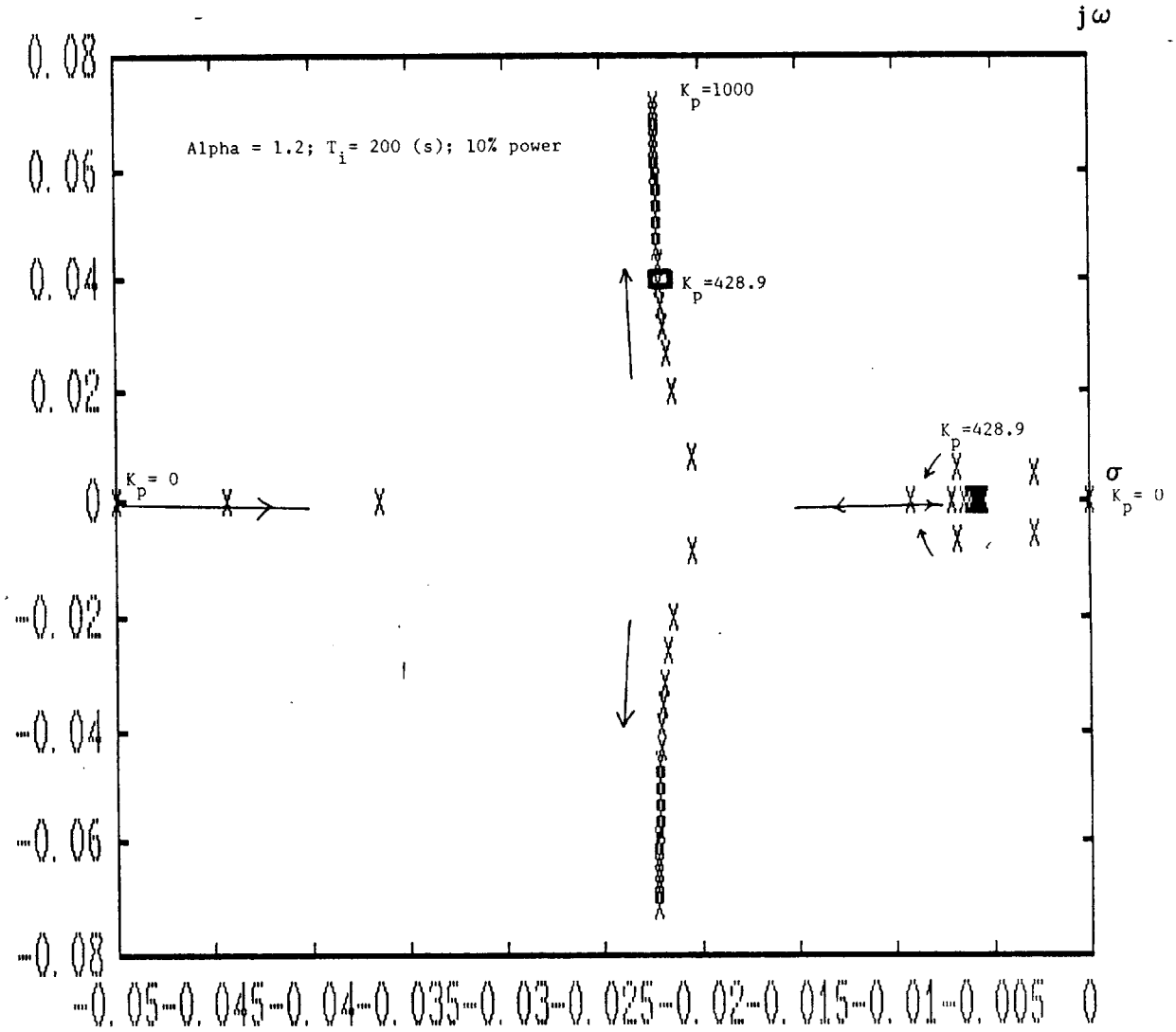

5.1-8 Root-Locus plot for α=1.2 (α_m) (T_i=200 s; 10% power)

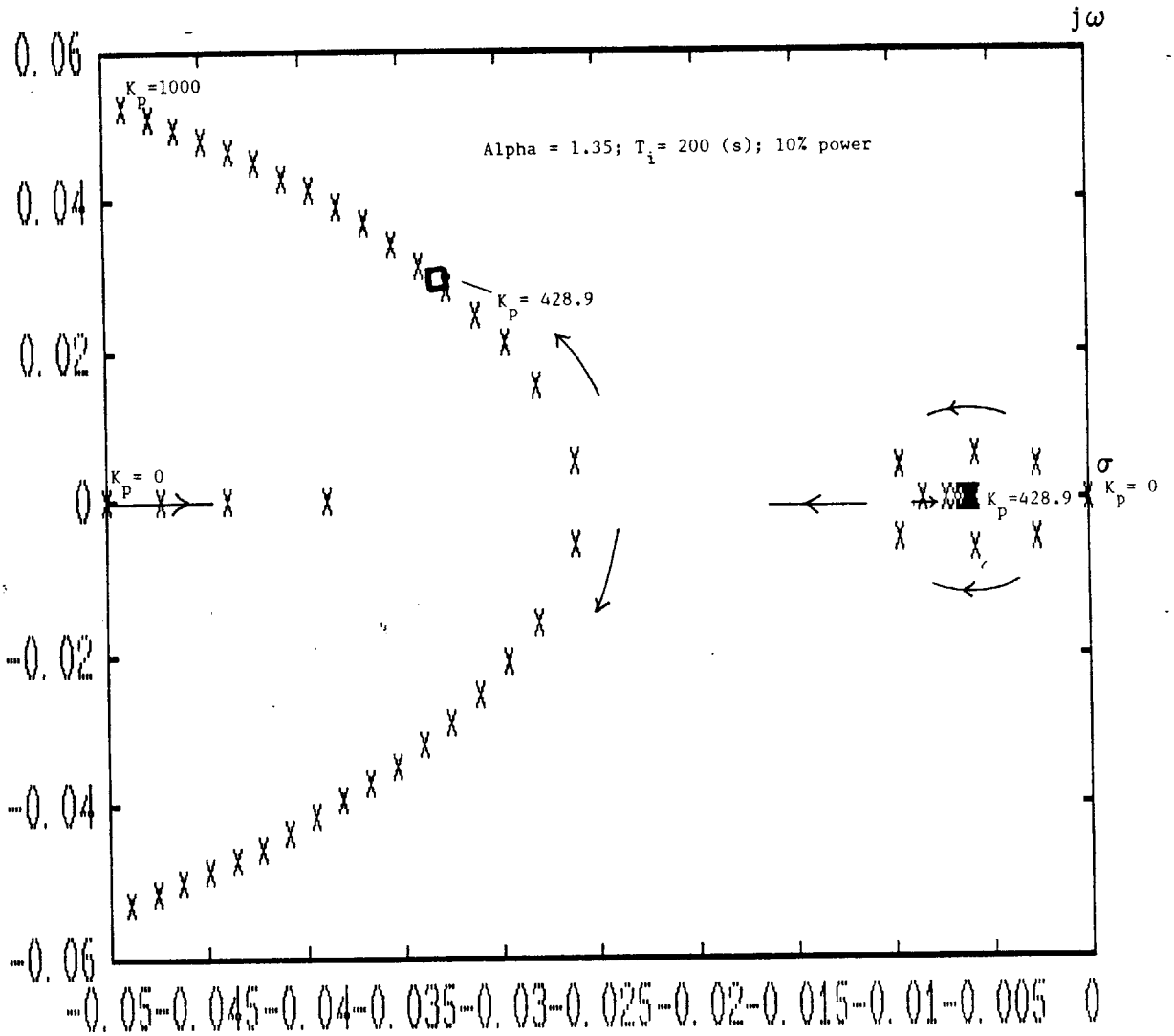

5.1-9 Root-Locus plot for α=1.35 (T_i=200 s; 10% power)

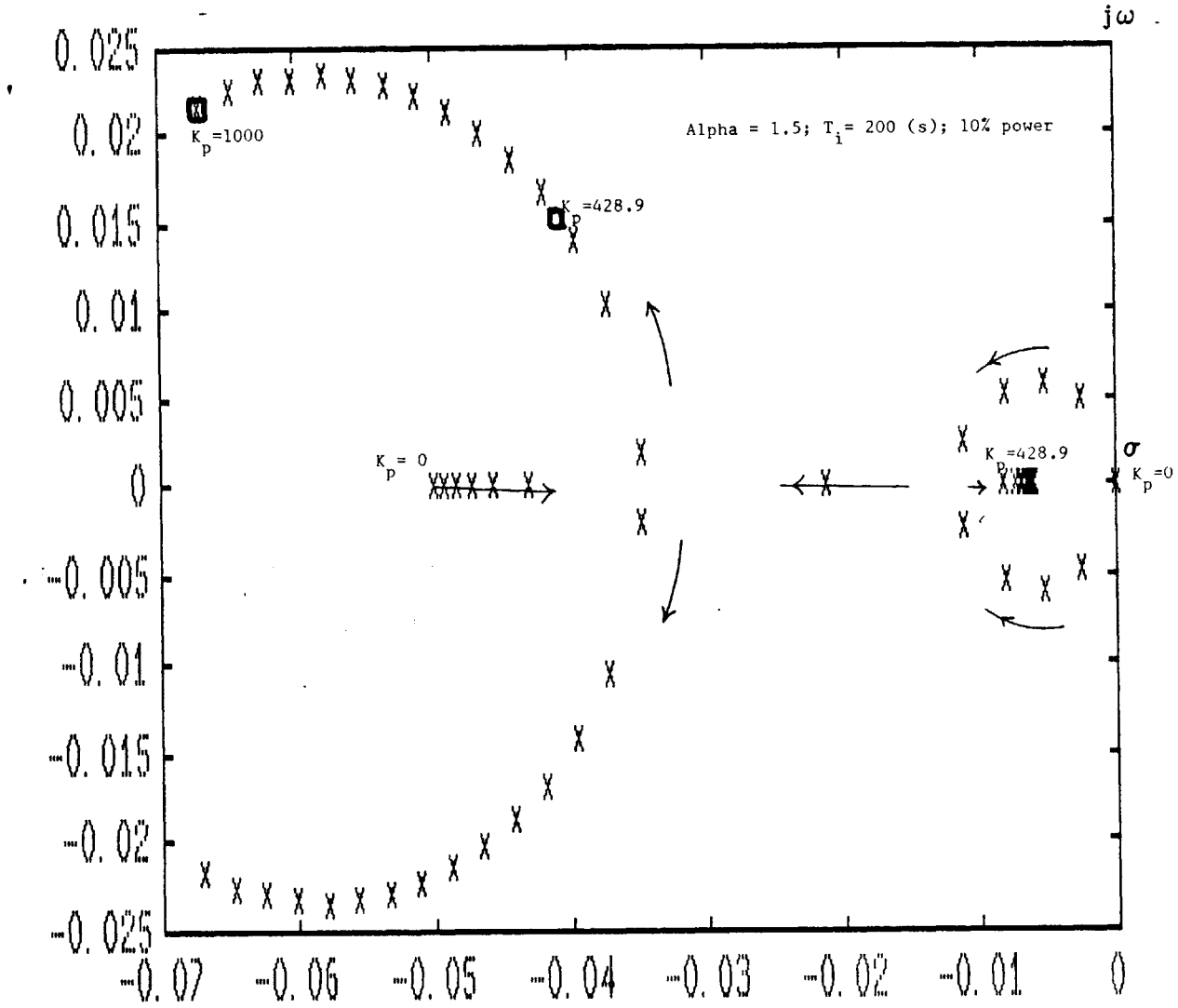

5.1-10 (a) Root-Locus plot for α=1.5 (T_i=200 s; 10% power)

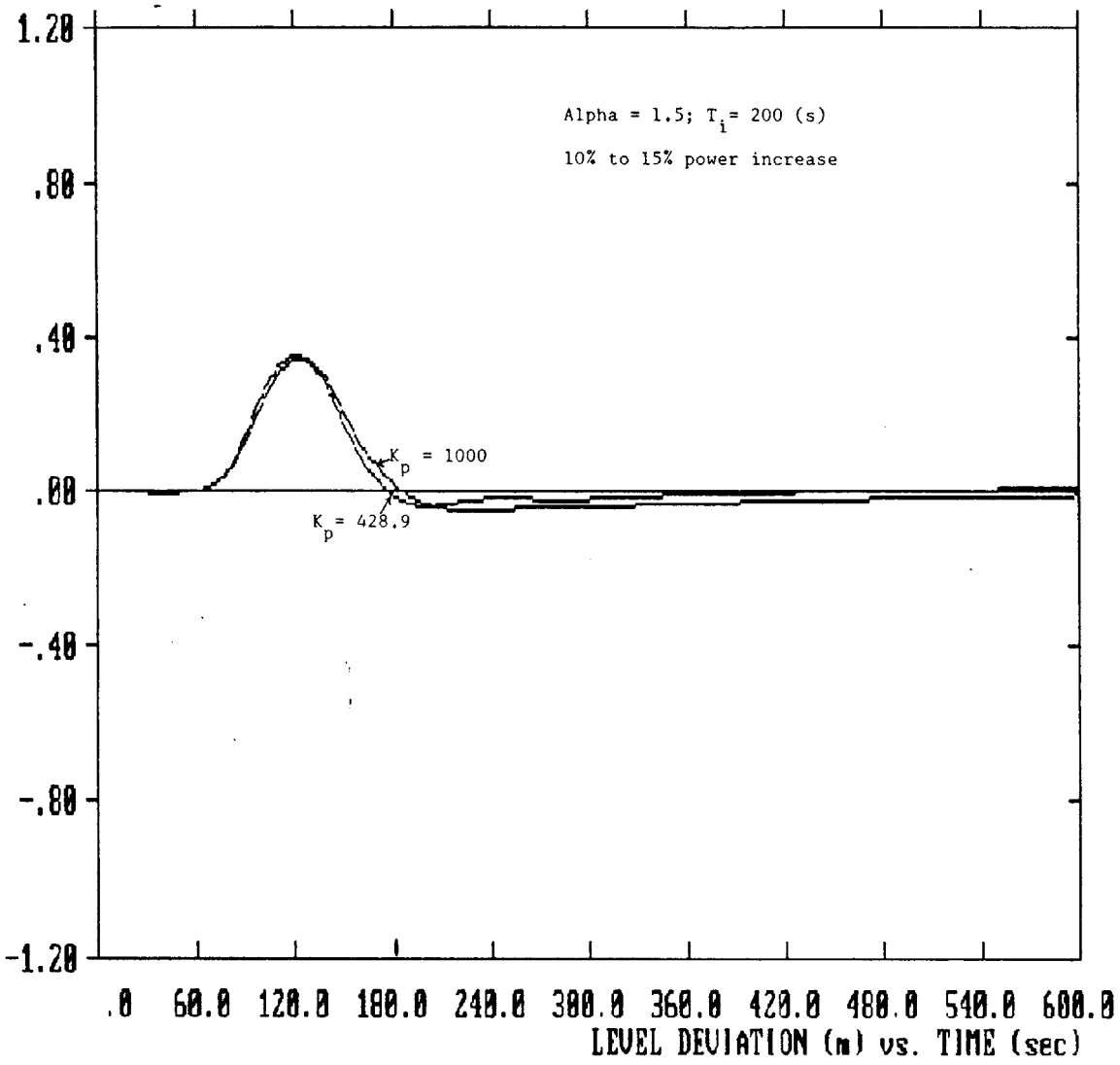

5.1-10 (b) Transient level response to the power increase

(10%→15%) for α=1.5 with K_p=428.9 and K_p=1000

(T_i=200 s)

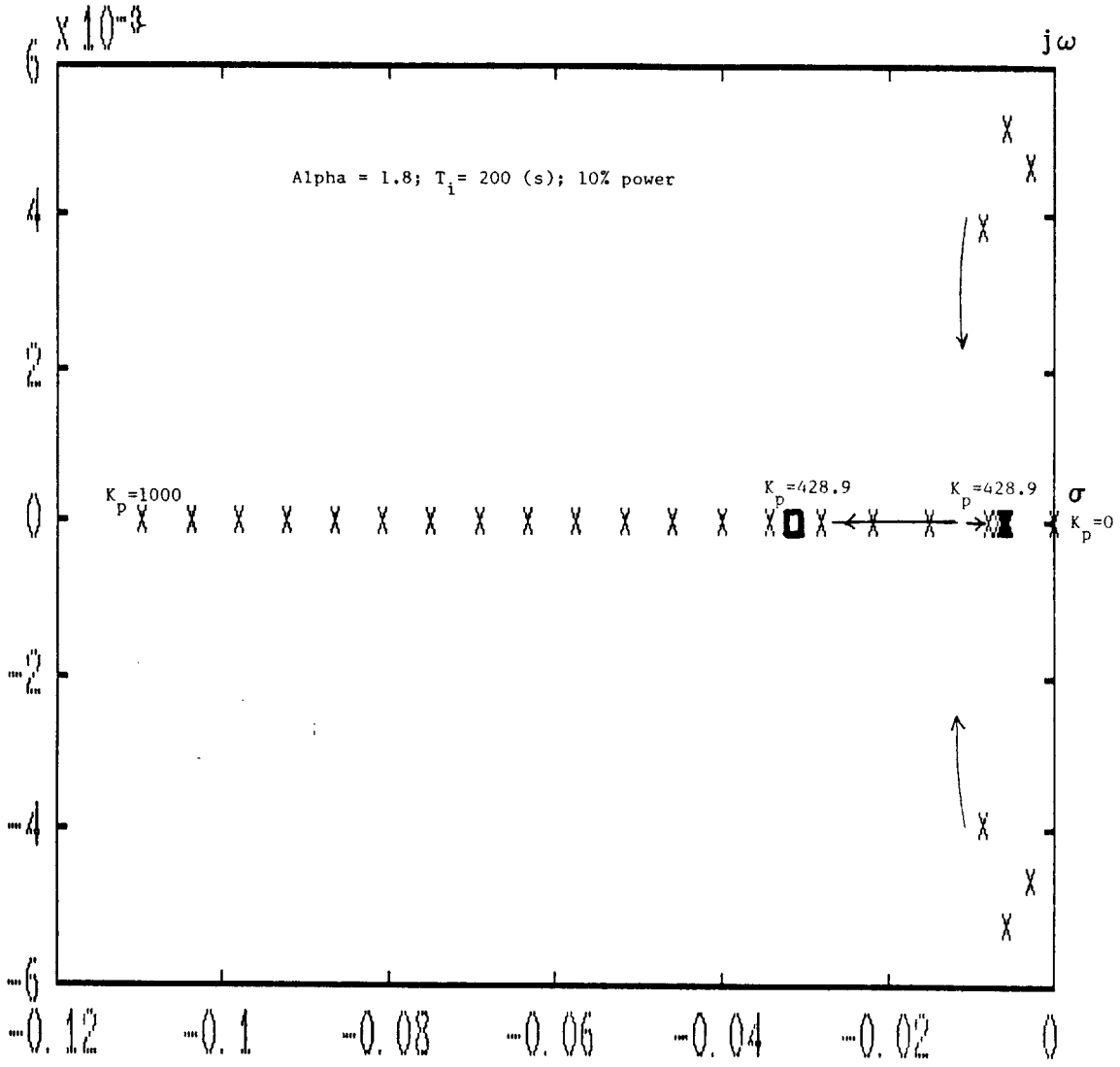

5.1-11 (a) Root-Locus plot for α=1.8 (α_t) (T_i=200 s; 10% power)

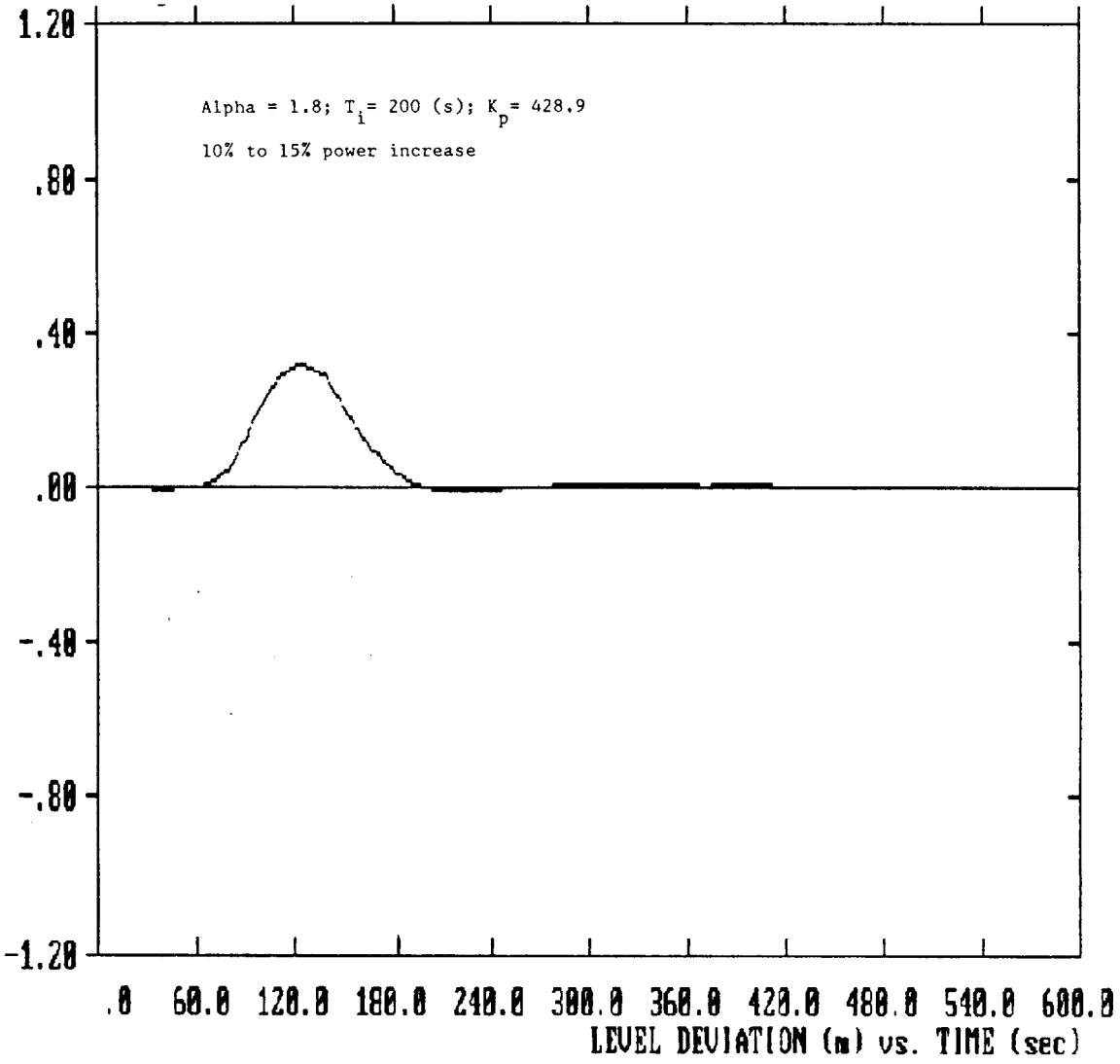

5.1-11 (b) Transient level response to the power increase (10%→15%) for α=1.8 (α_t) with K_p=428.9 (T_i=200 s)

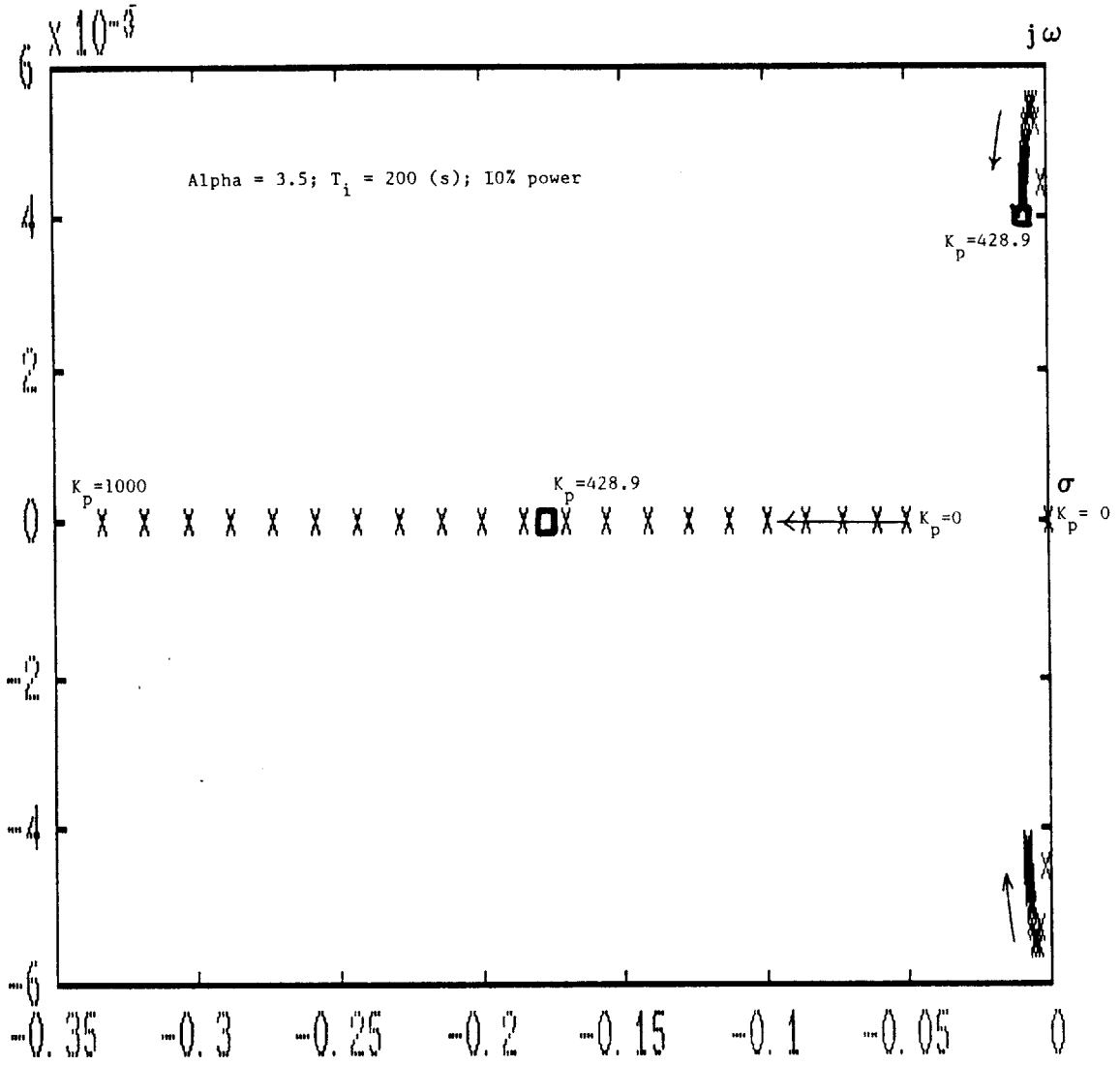

5.1-12 (a) Root-Locus plot for α=3.5 (T_i=200 s;10% power)

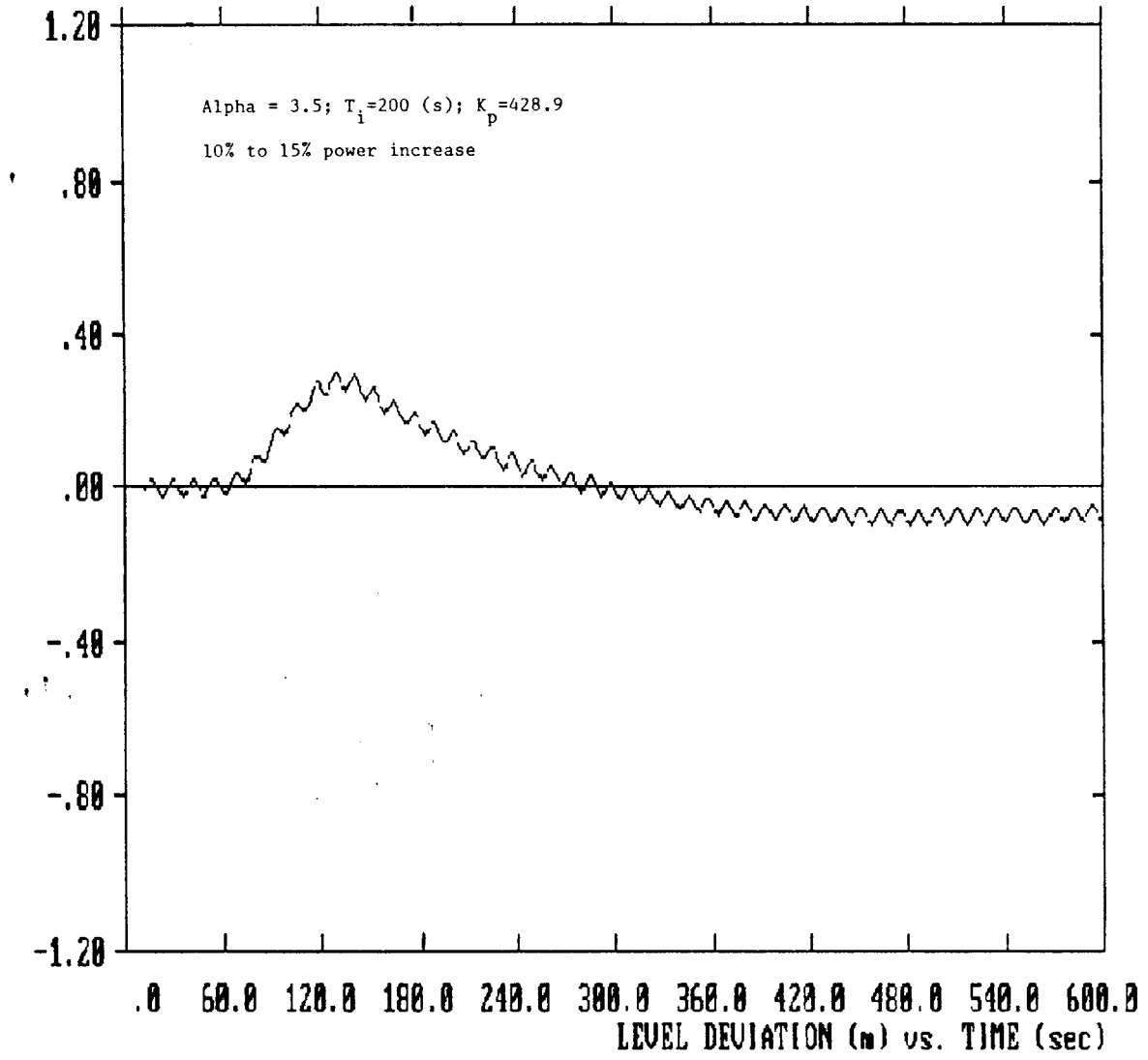

5.1-12 (b) Transient level response to the power increase (10%→15%) for α=3.5 with K_p=428.9 (T_i=200 s)

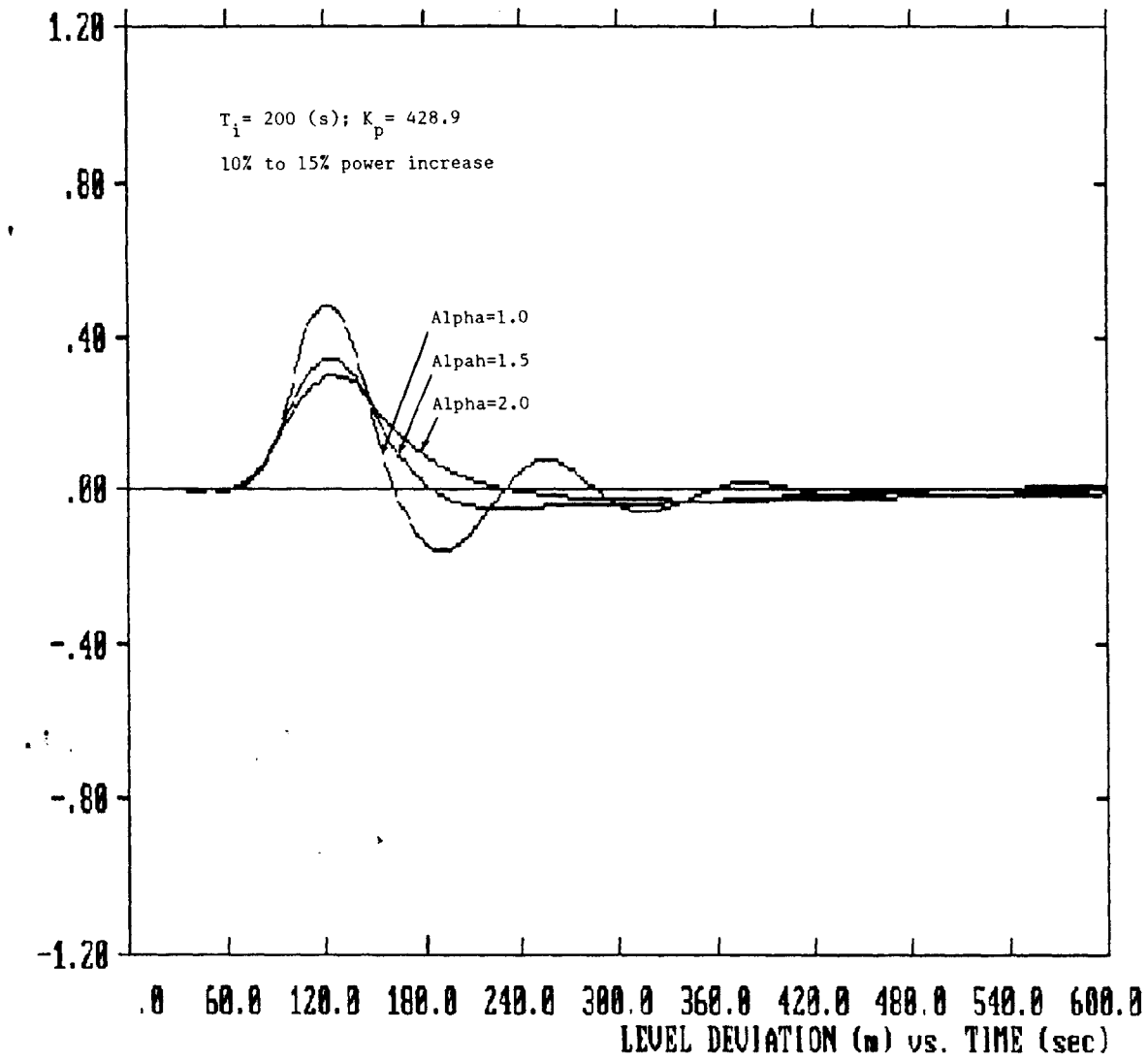

5.1-13 Transient level responses to the power increase (10%→15%) with K_p=428.9 for $1.0 \leq \alpha \leq 2.0$ (T_i=200 s)

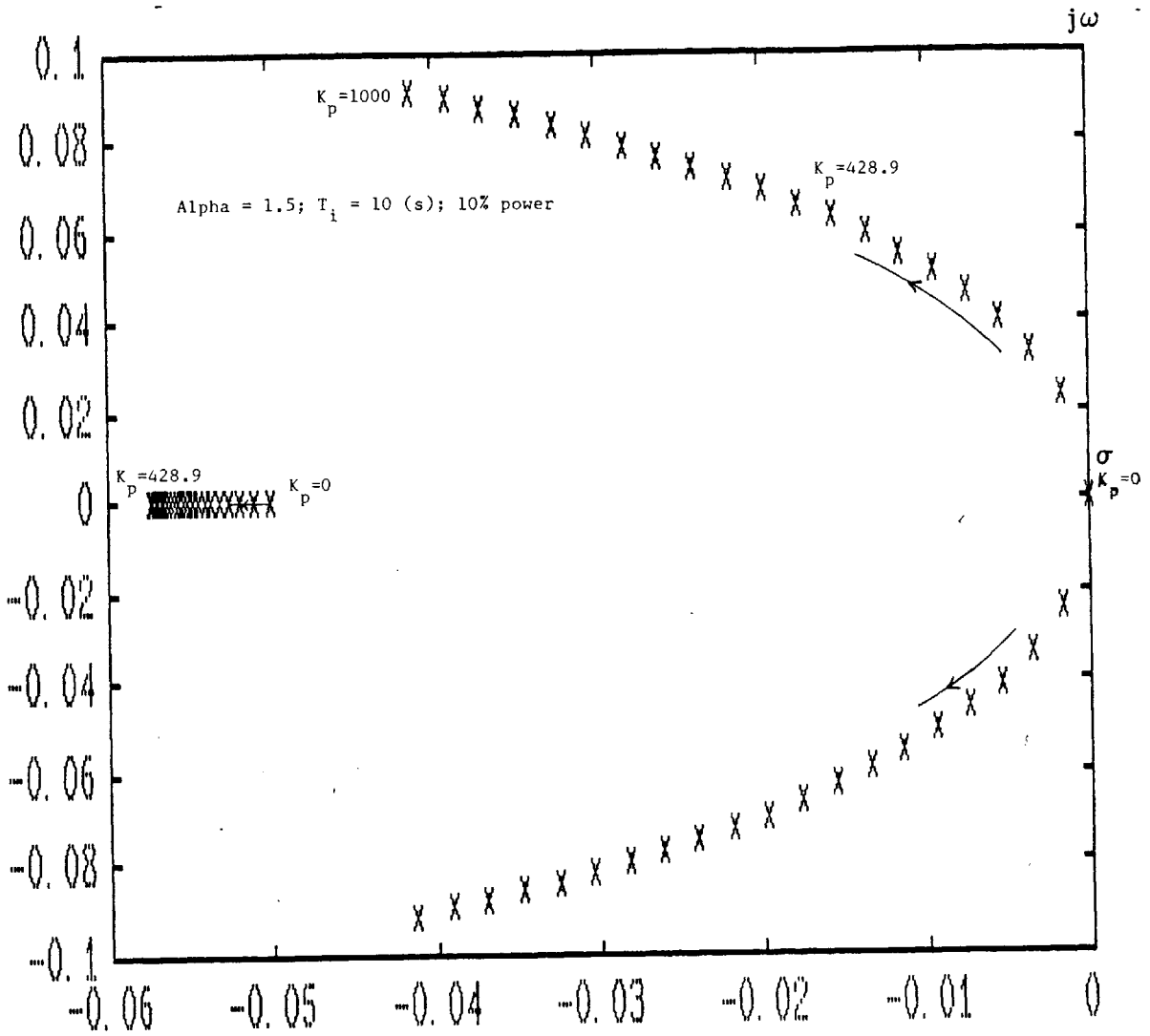

5.1-14 (a) Root-Locus plot for α=1.5 with T_i=10 s (10% power)

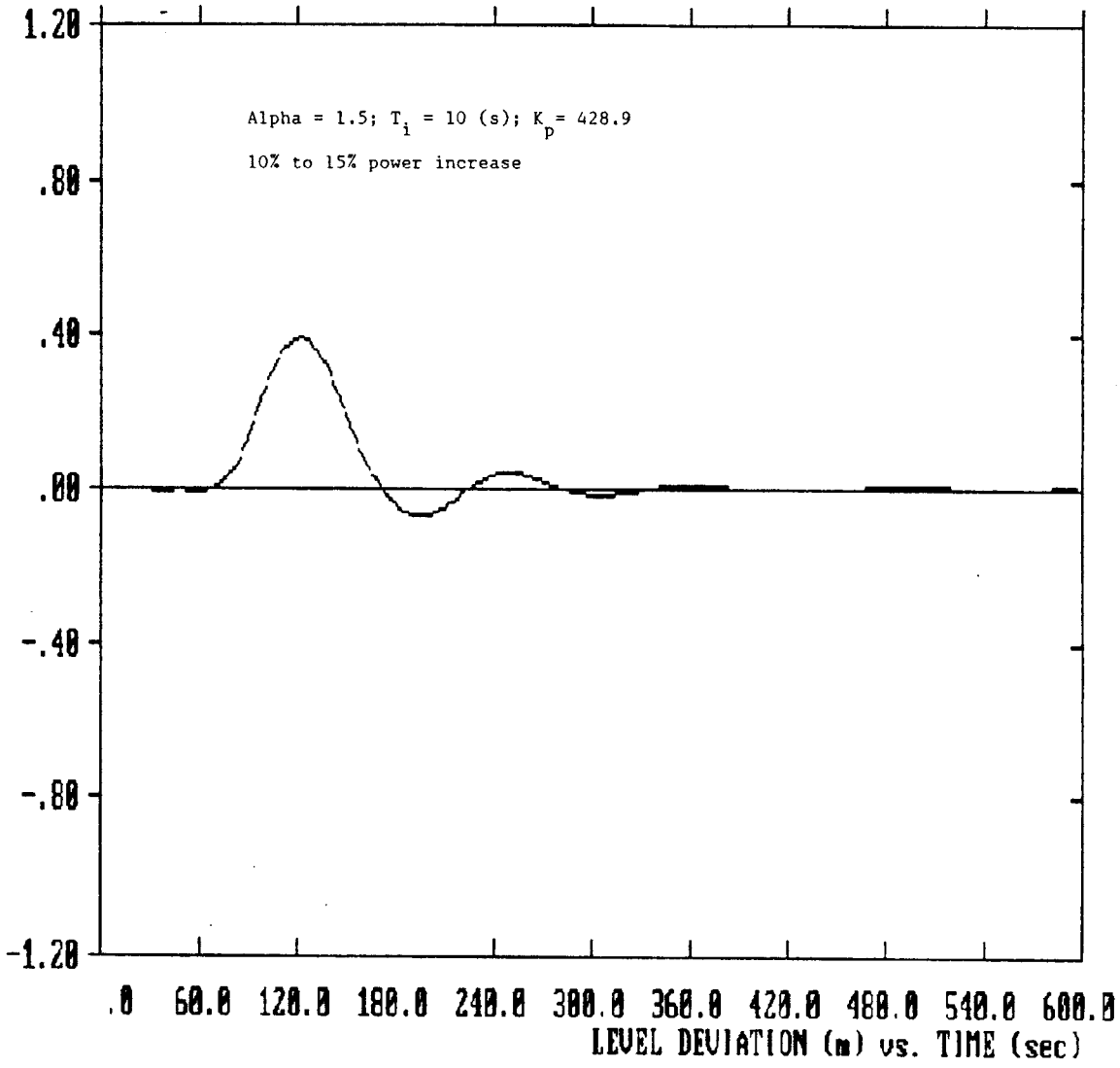

5.1-14 (b) Transient level response to the power increase (10%→15%) for α=1.5 with K_p=428.9 and T_i= 10 s

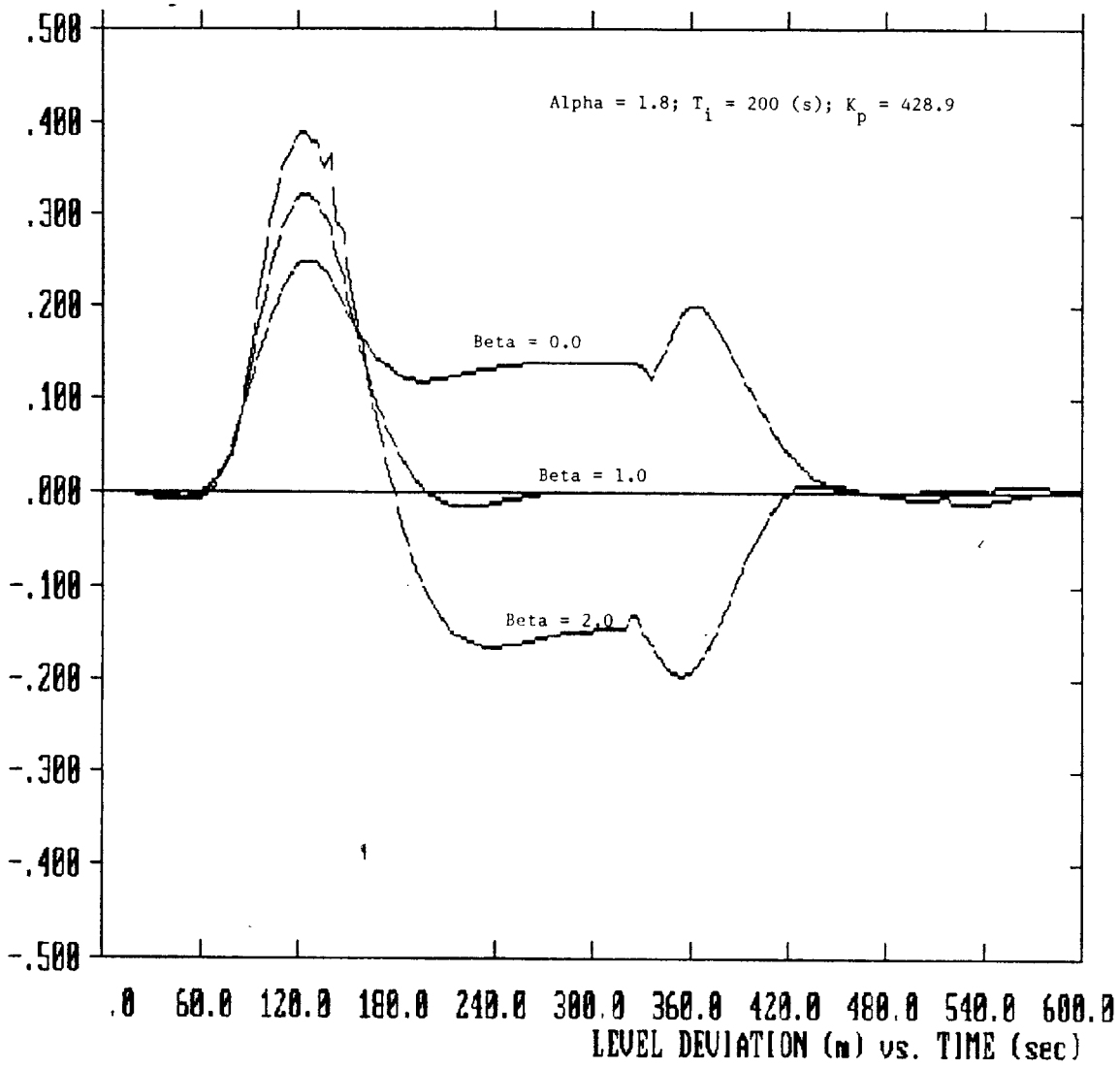

5.1-15 Transient level response to the power increase (10%→15%) for $0.0 \leq \beta \leq 2.0$ (α=1.8; K_p=428.9; T_i=200 s)

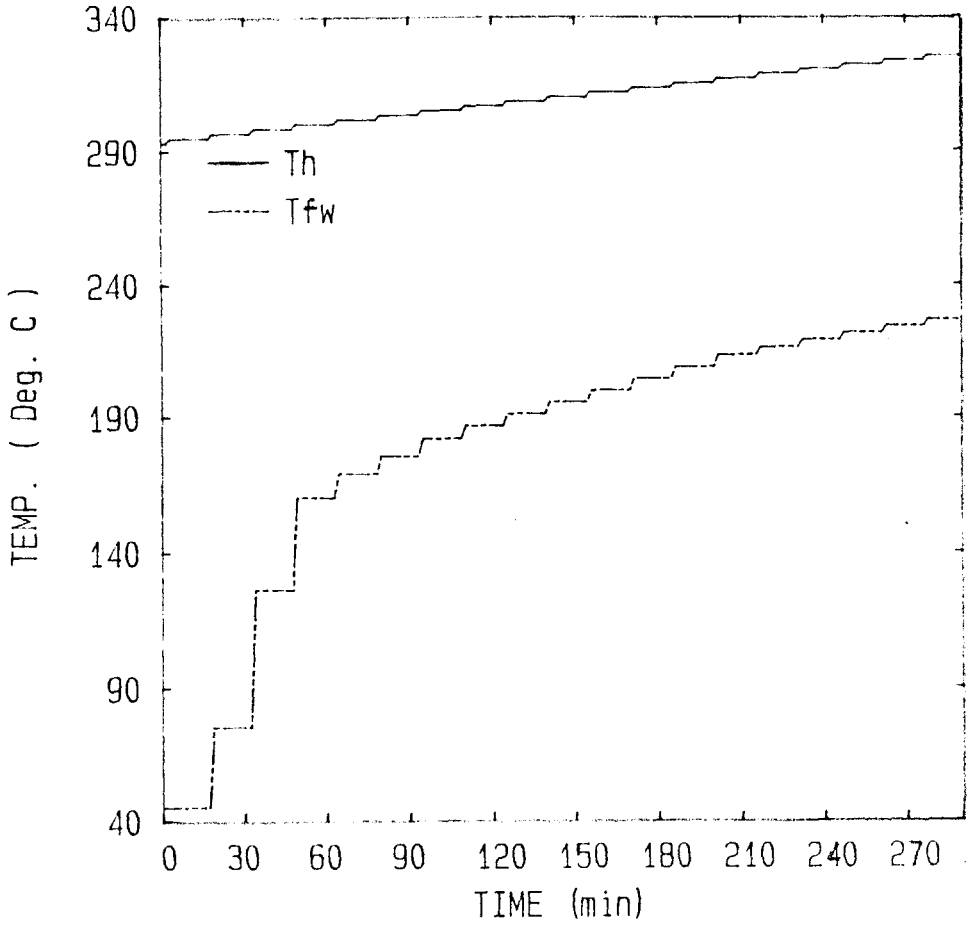

5.2-1 Transient (5%→100%) input for the primary hot-leg temperature, feedwater temperature and steam flow

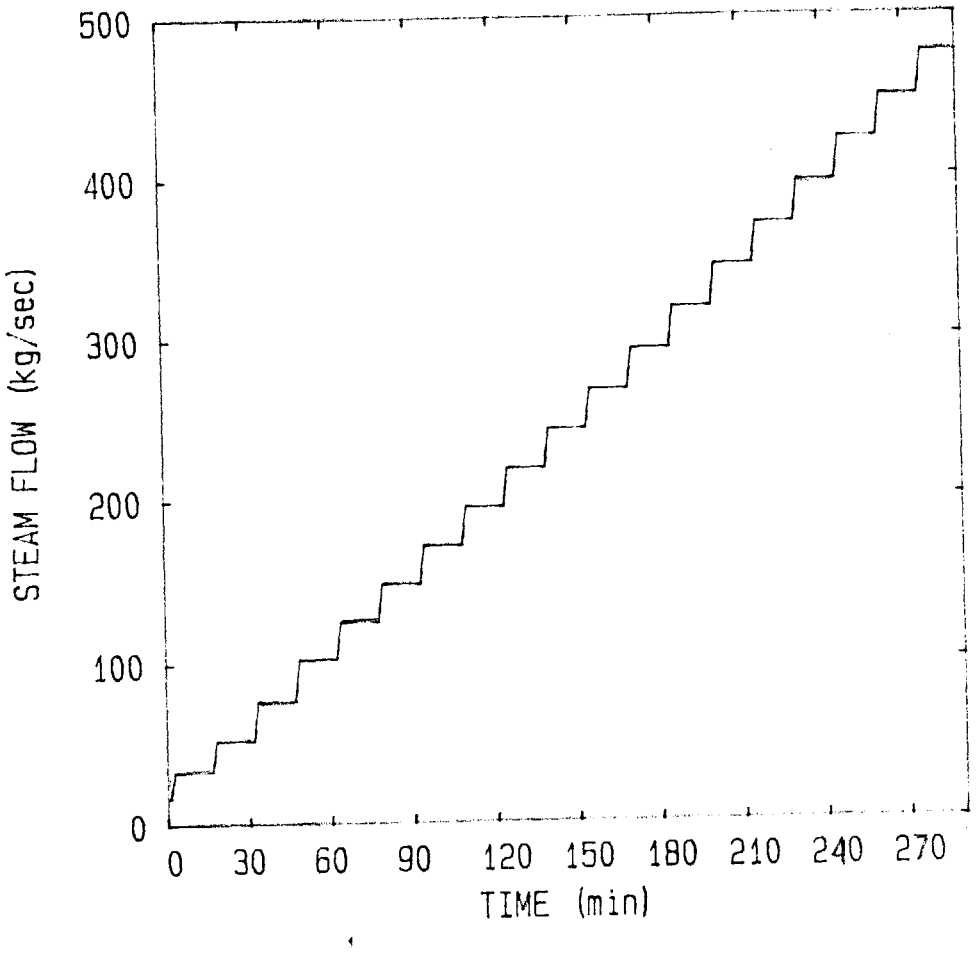

5.2-1 (continued)

Transient (5%→100%) input for the primary hot-leg temperature, feedwater temperature and steam flow

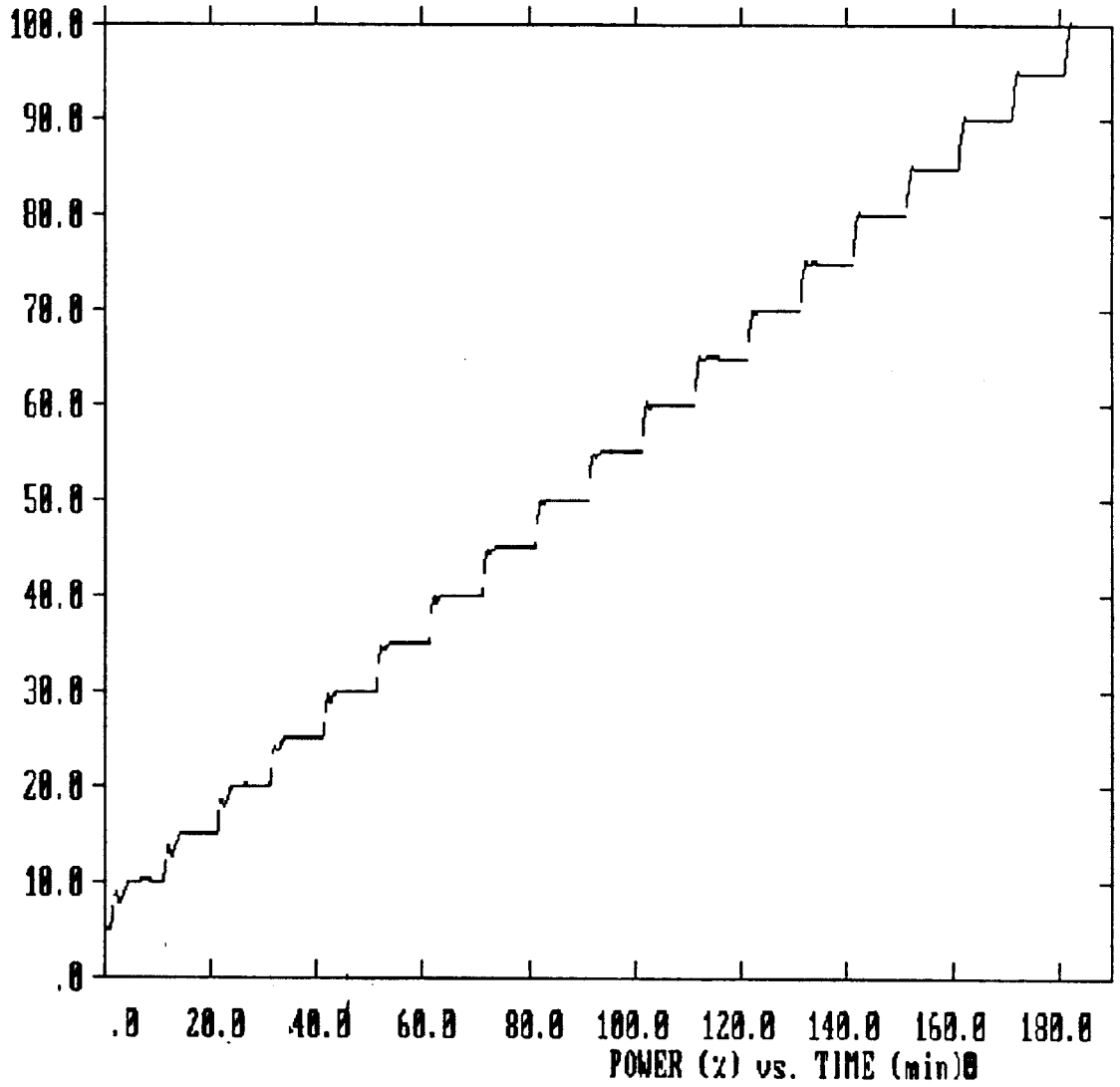

5.2-2 Transient (5%→100%) responses with the proposed controller

(a) calculated power

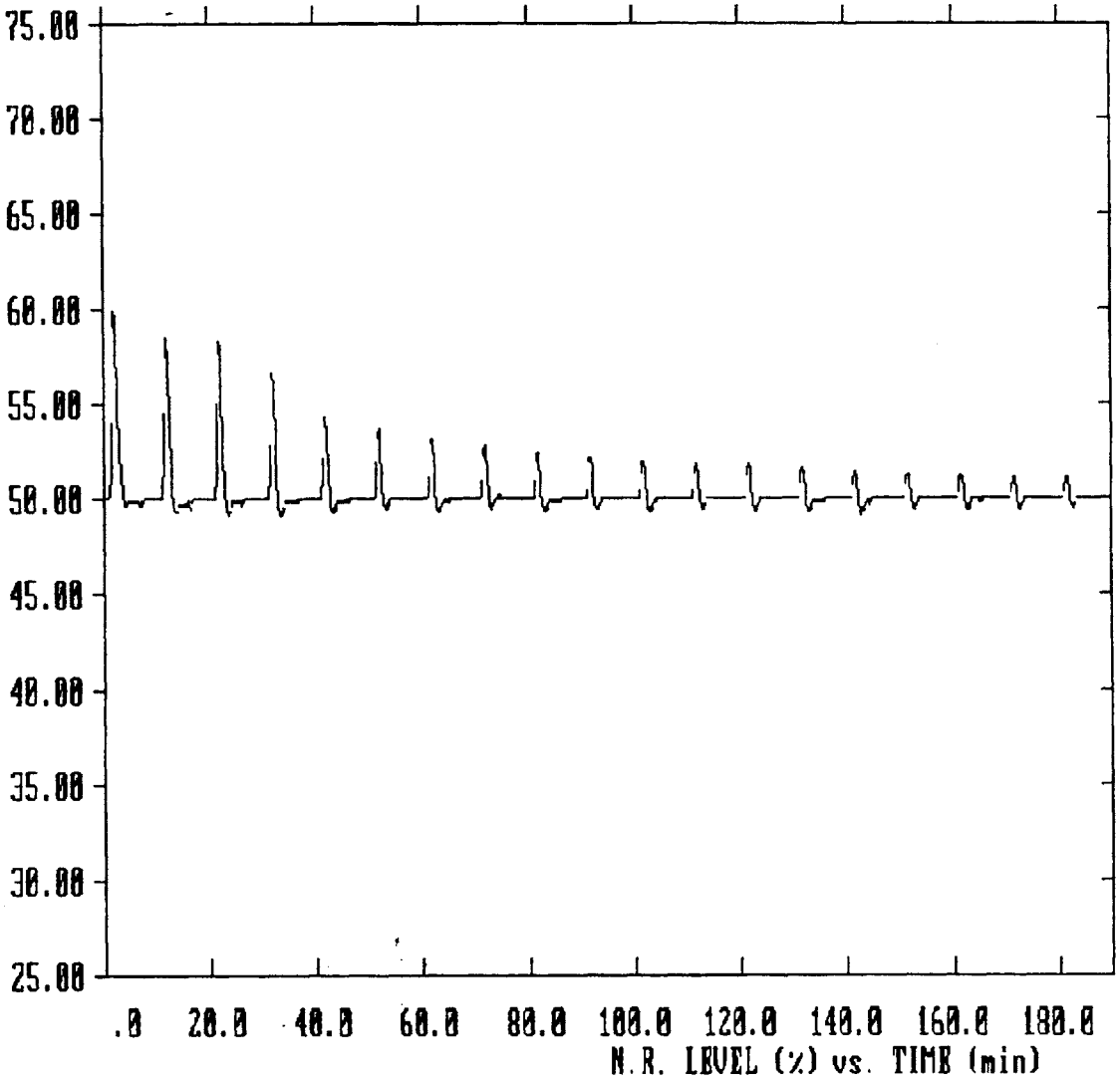

(b) narrow range water level

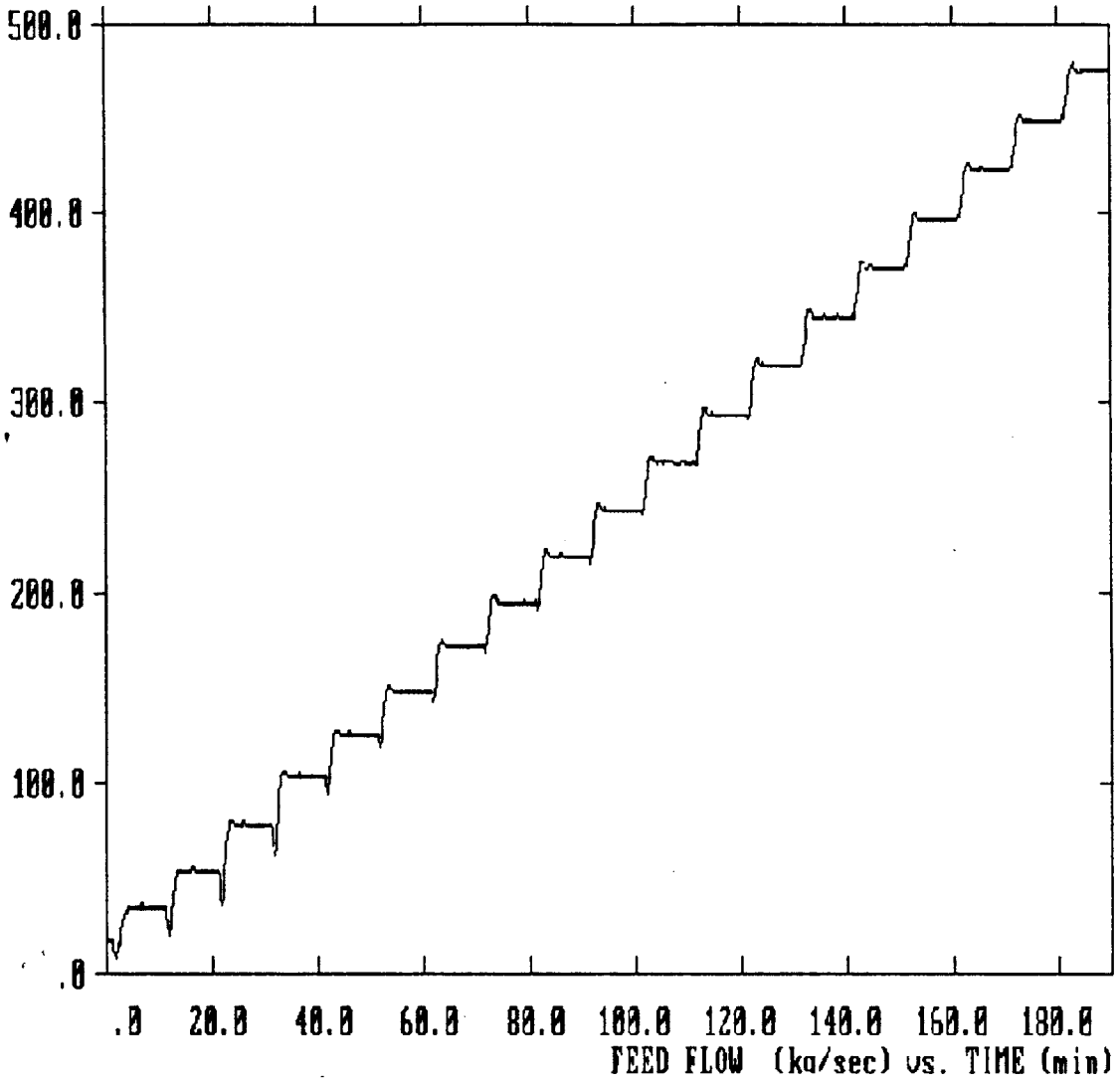

(c) feedwater flow rate

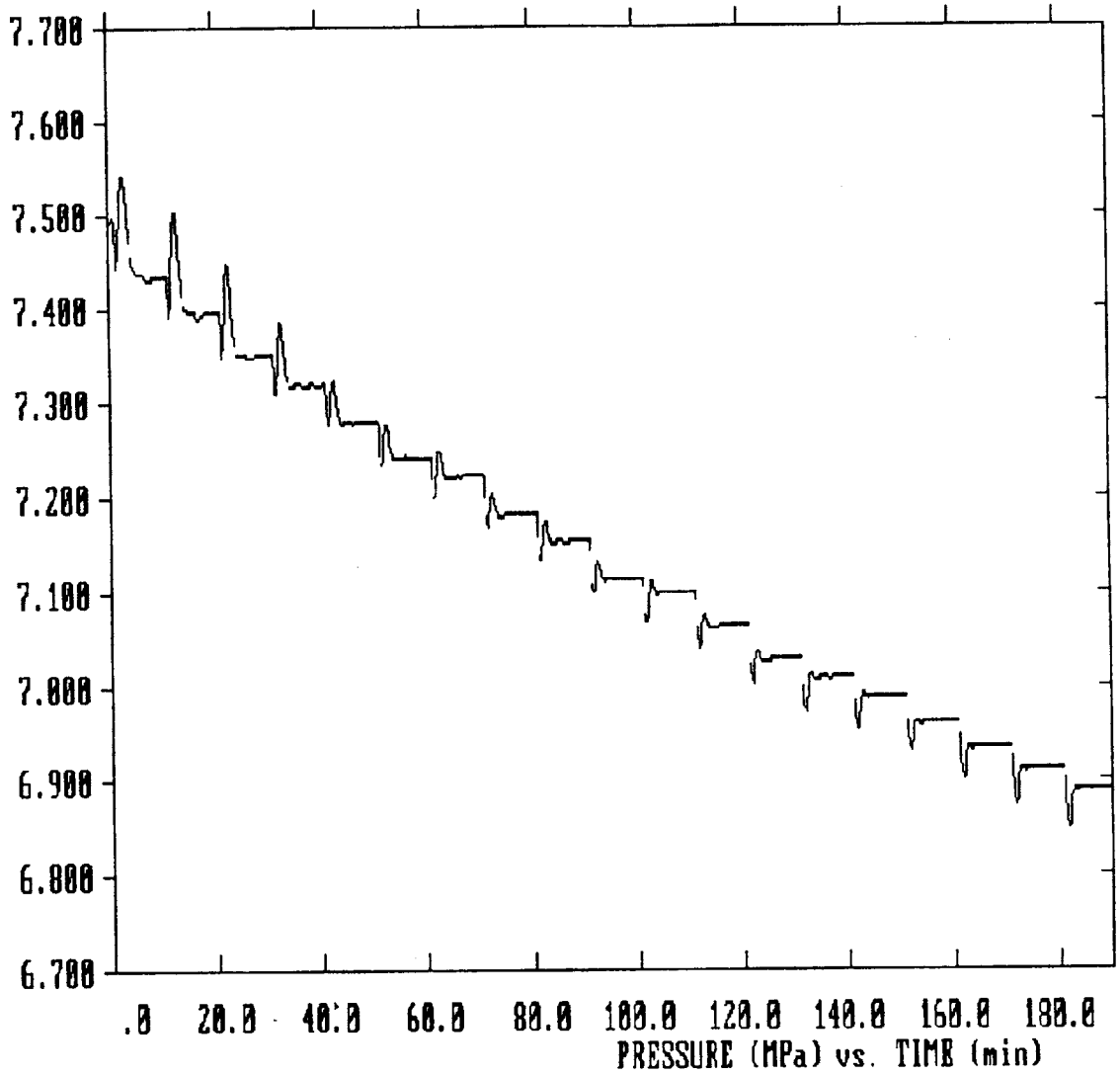

(d) steam pressure

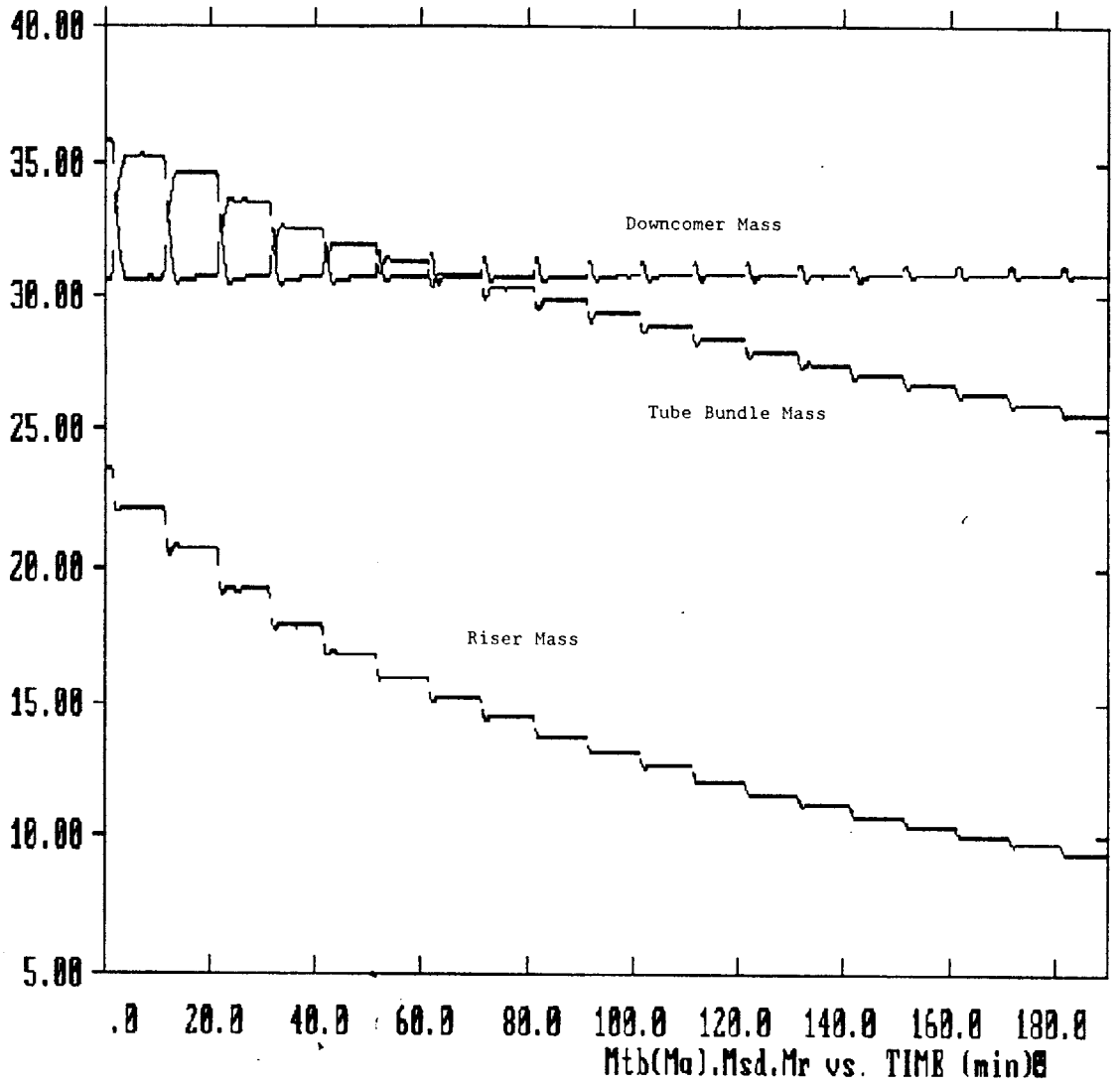

(e) tube bundle, riser, and downcomer mass

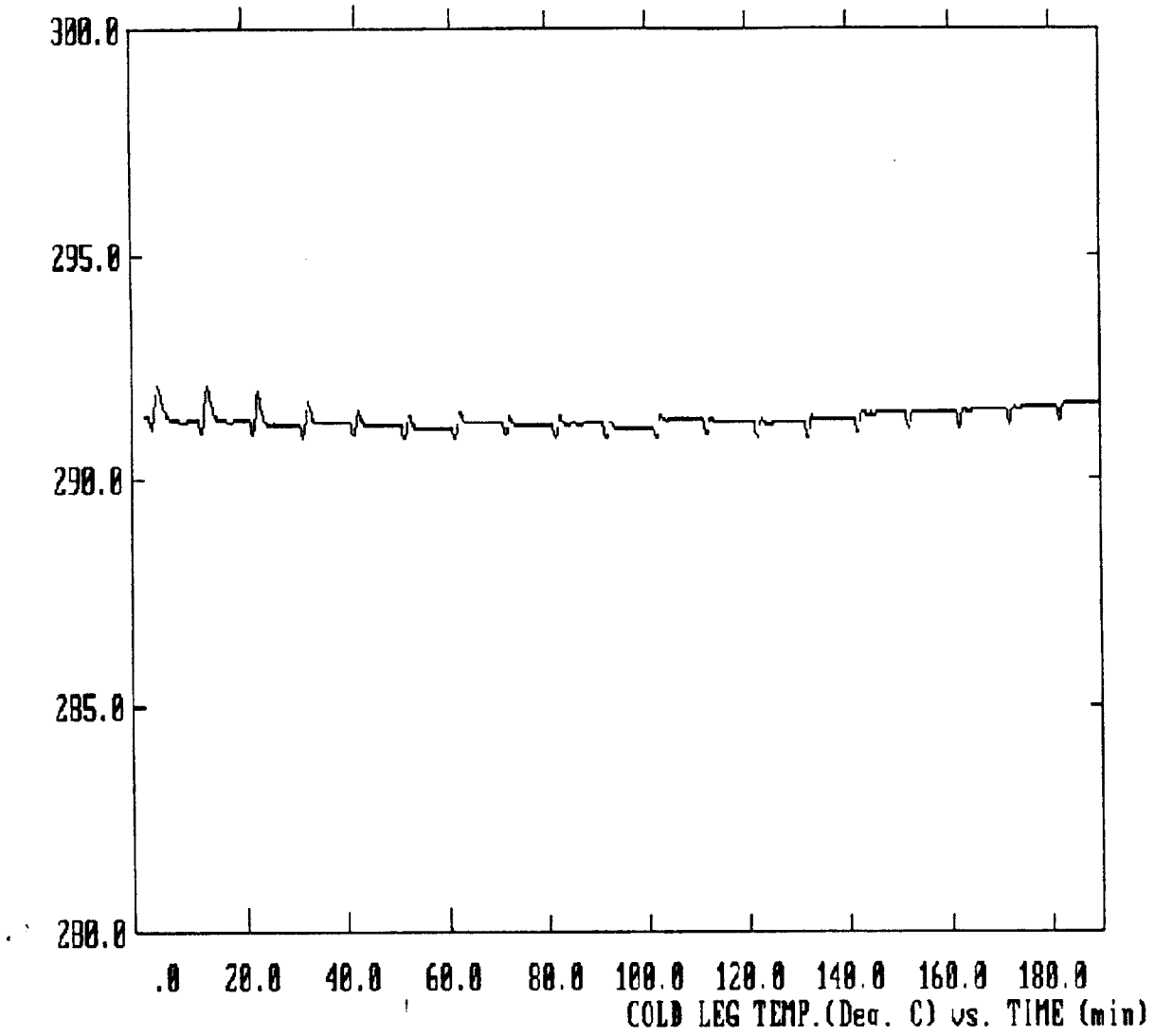

(f) primary cold-leg temperature

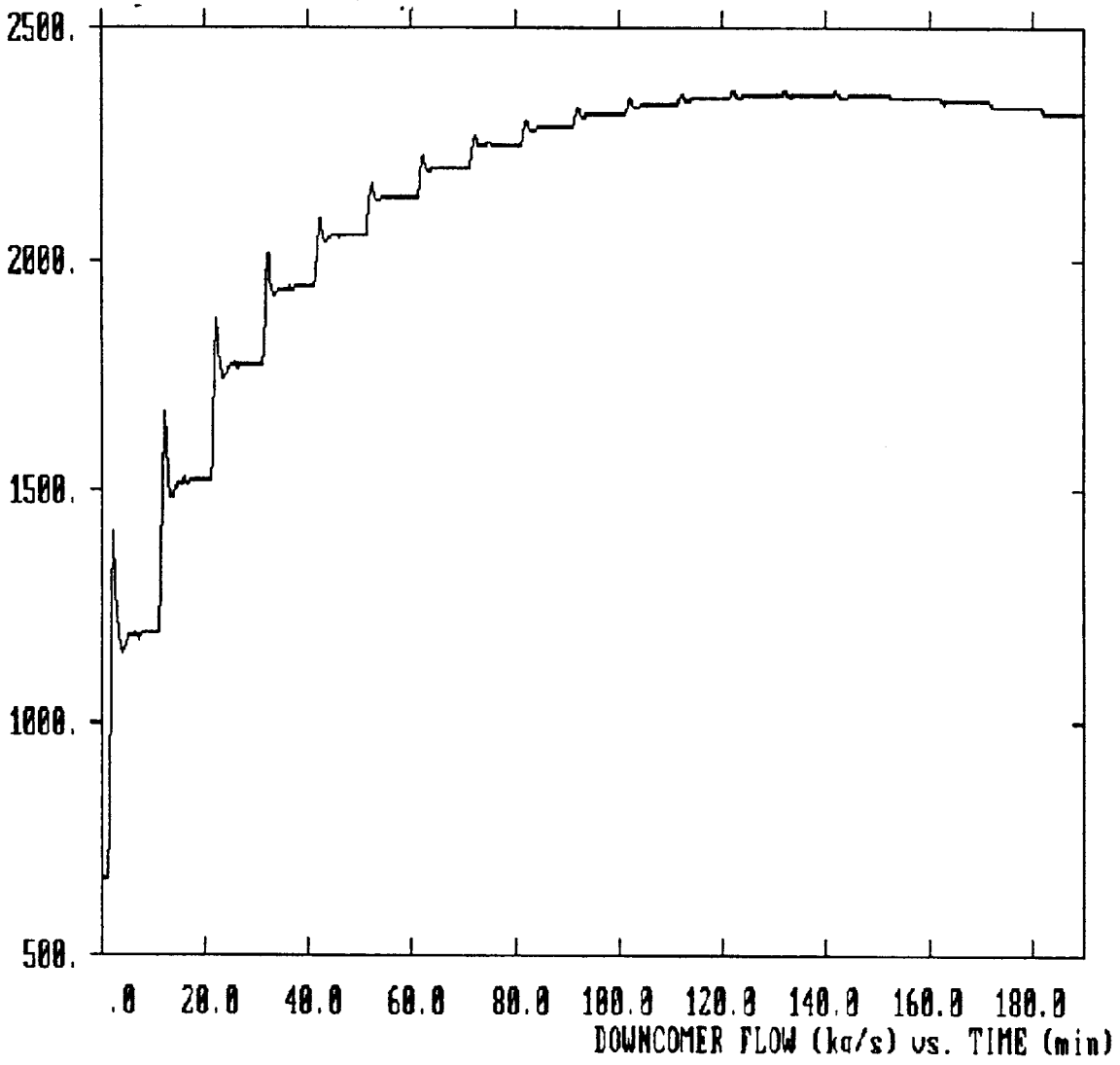

(g) downcomer flow rate

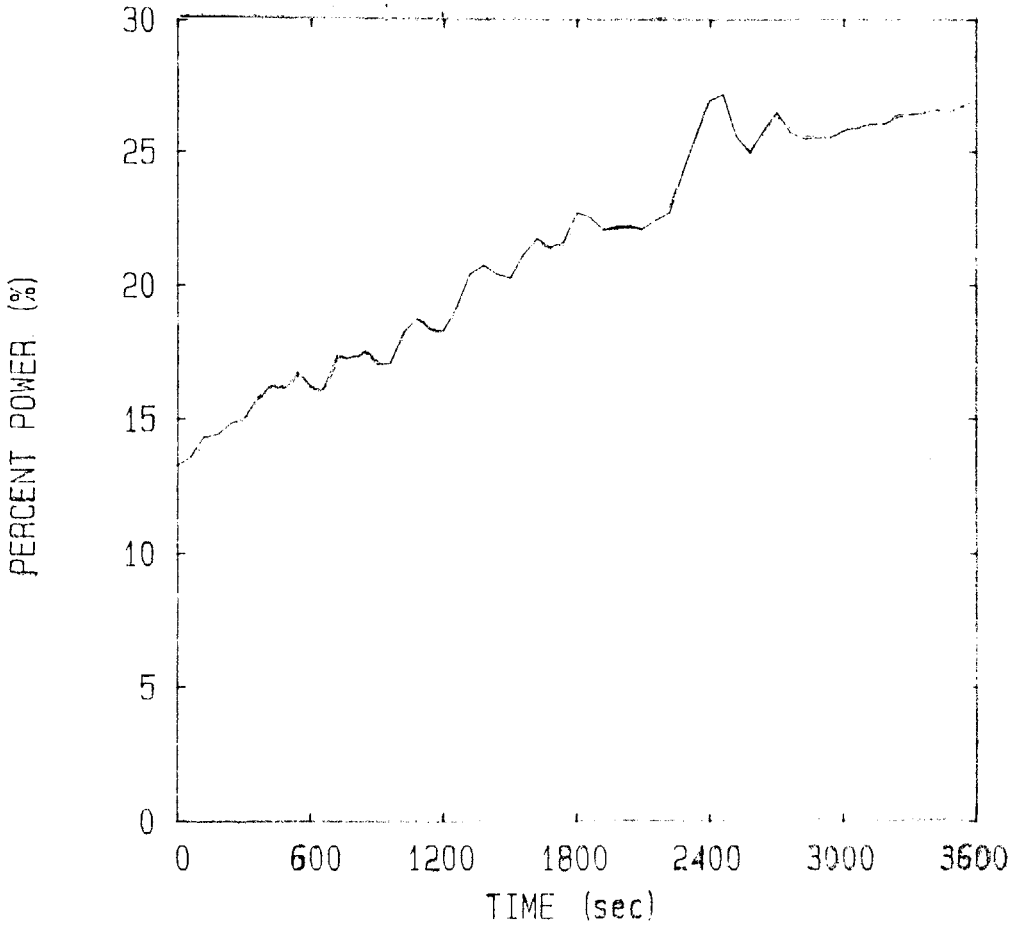

5.2-3 Plant data

(a) percent power

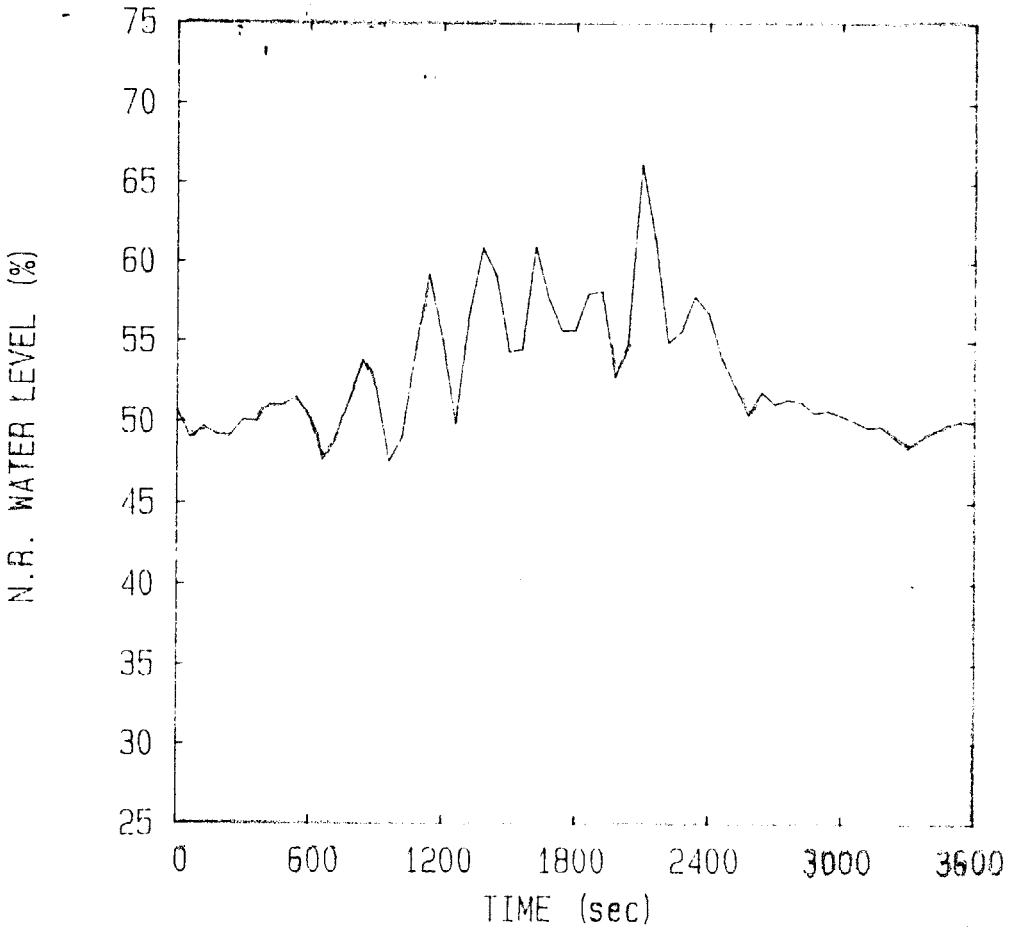

(b) narrow range water level

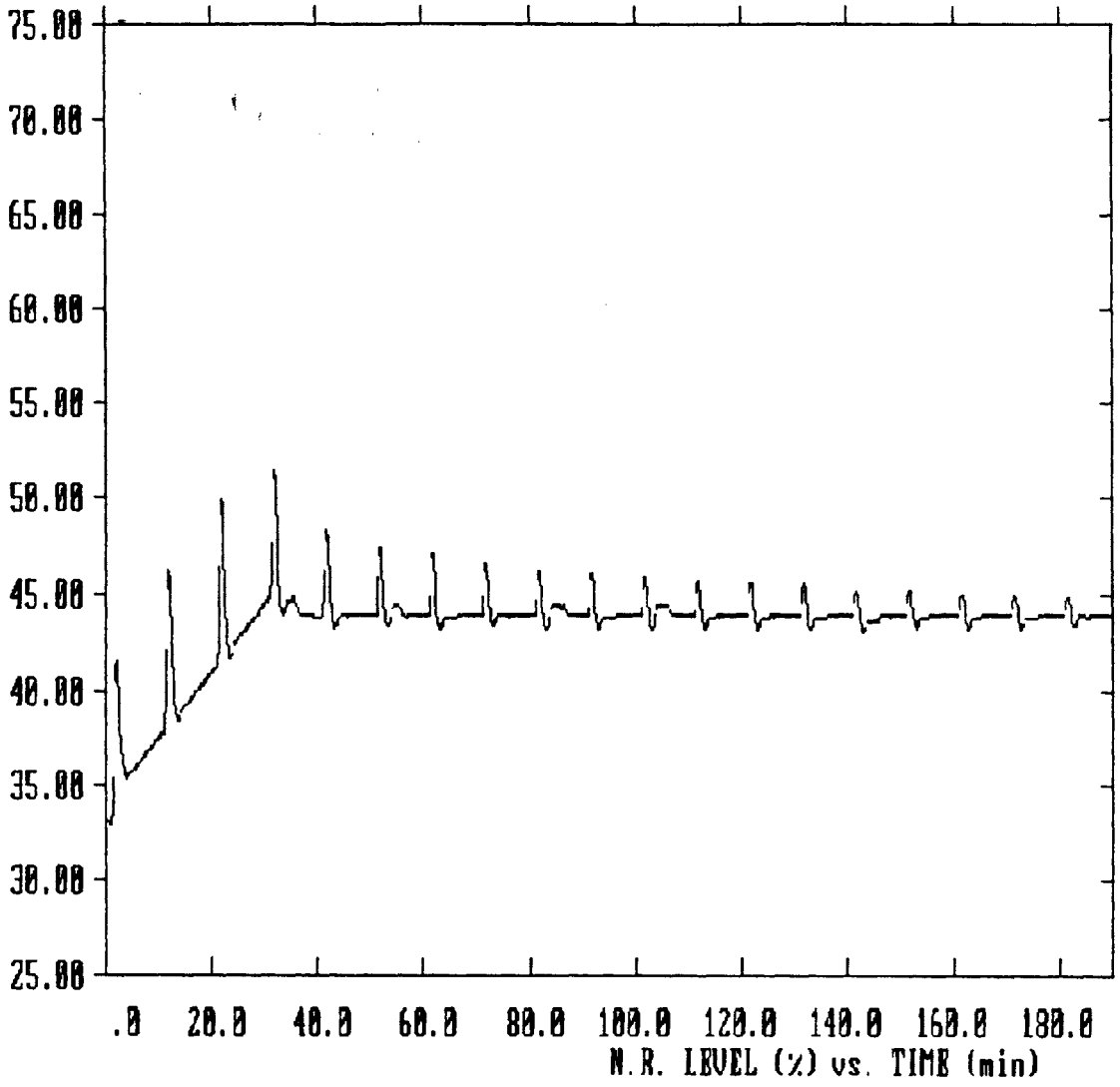

5.2-4 Transient responses with the 33% to 44% level program

(a) narrow range water level

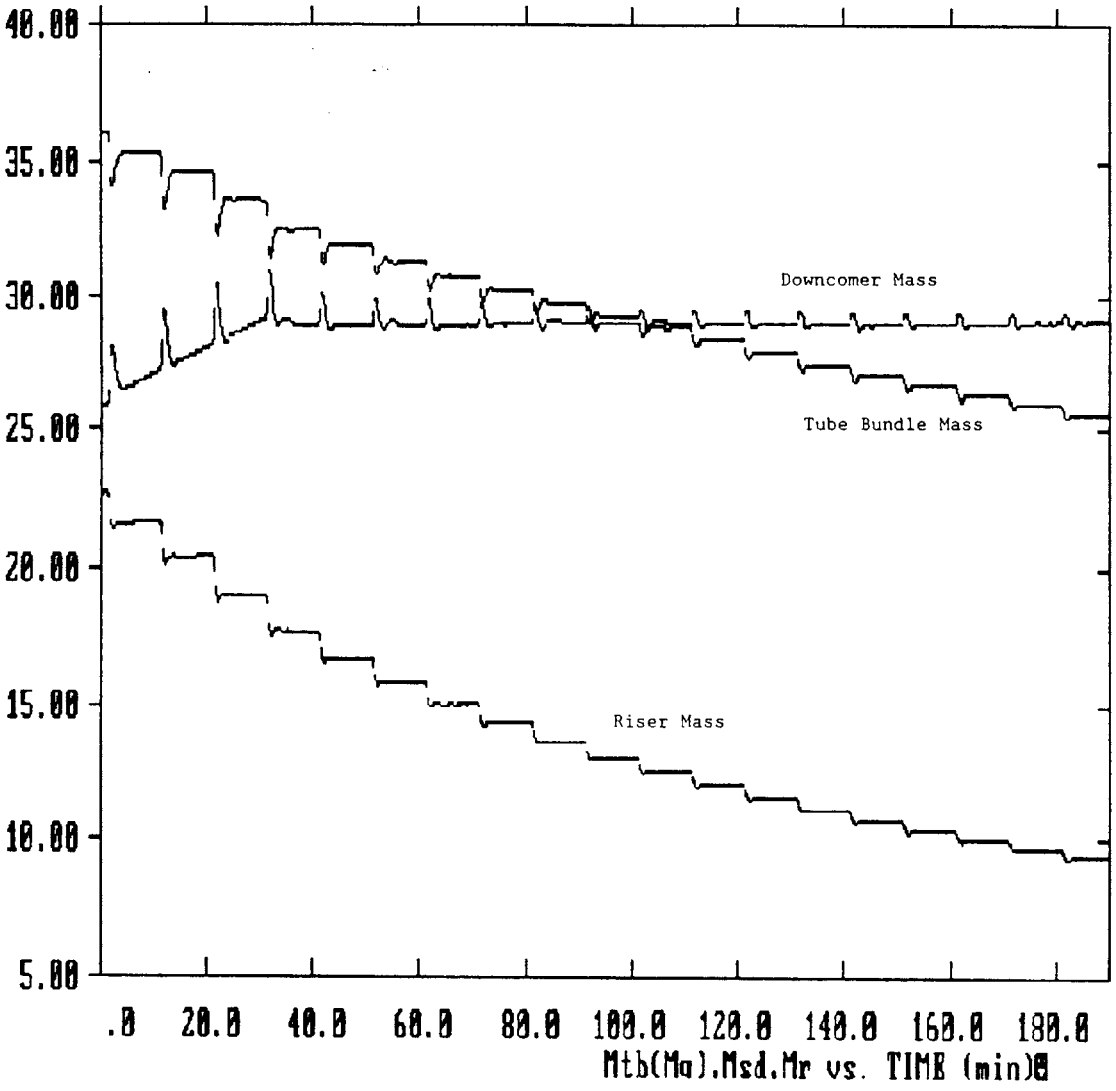

(b) tube bundle, riser, and downcomer mass

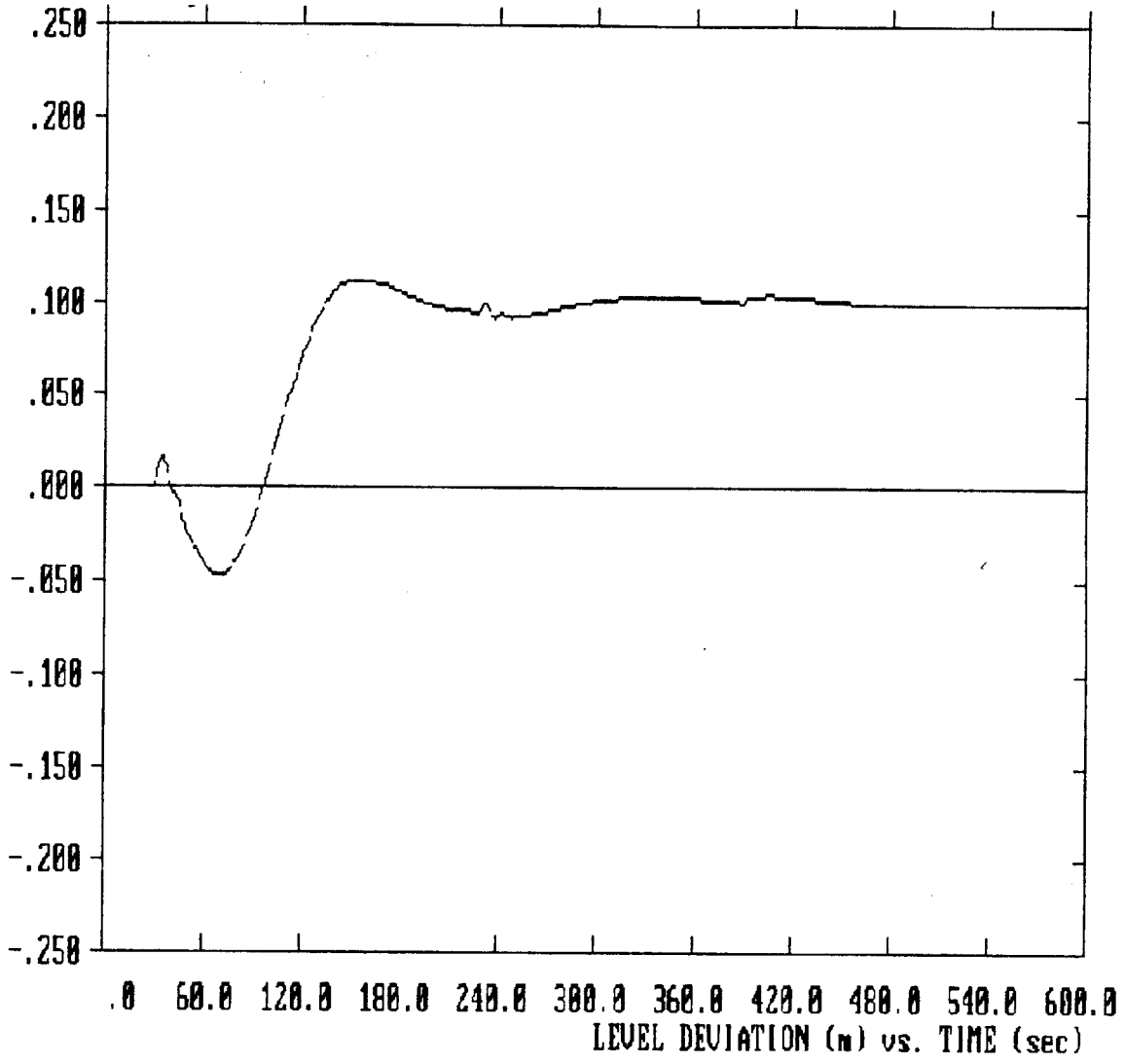

5.2-5 Transient level responses to the reference level step-up (100 mm)

(a) at 10% power

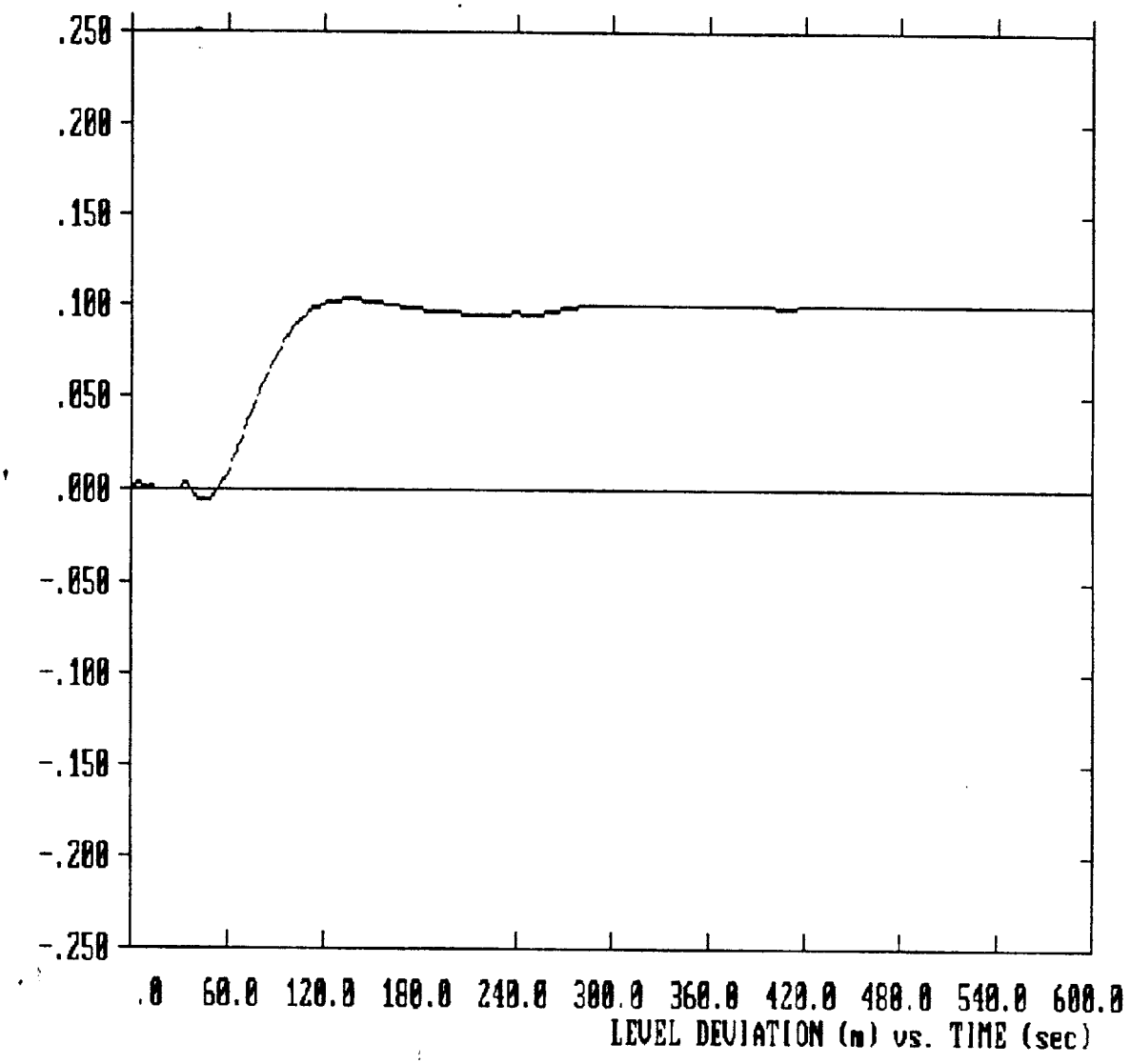
.250
.200
.150
.100
.050
.000
-.050
-.100
-.150
-.200
-.250
.0
60.0
120.0
180.0
240.0
300.0
360.0
420.0
480.0
540.0
600.0
LEVEL DEVIATION (m) vs. TIME (sec)

(b) at 50% power

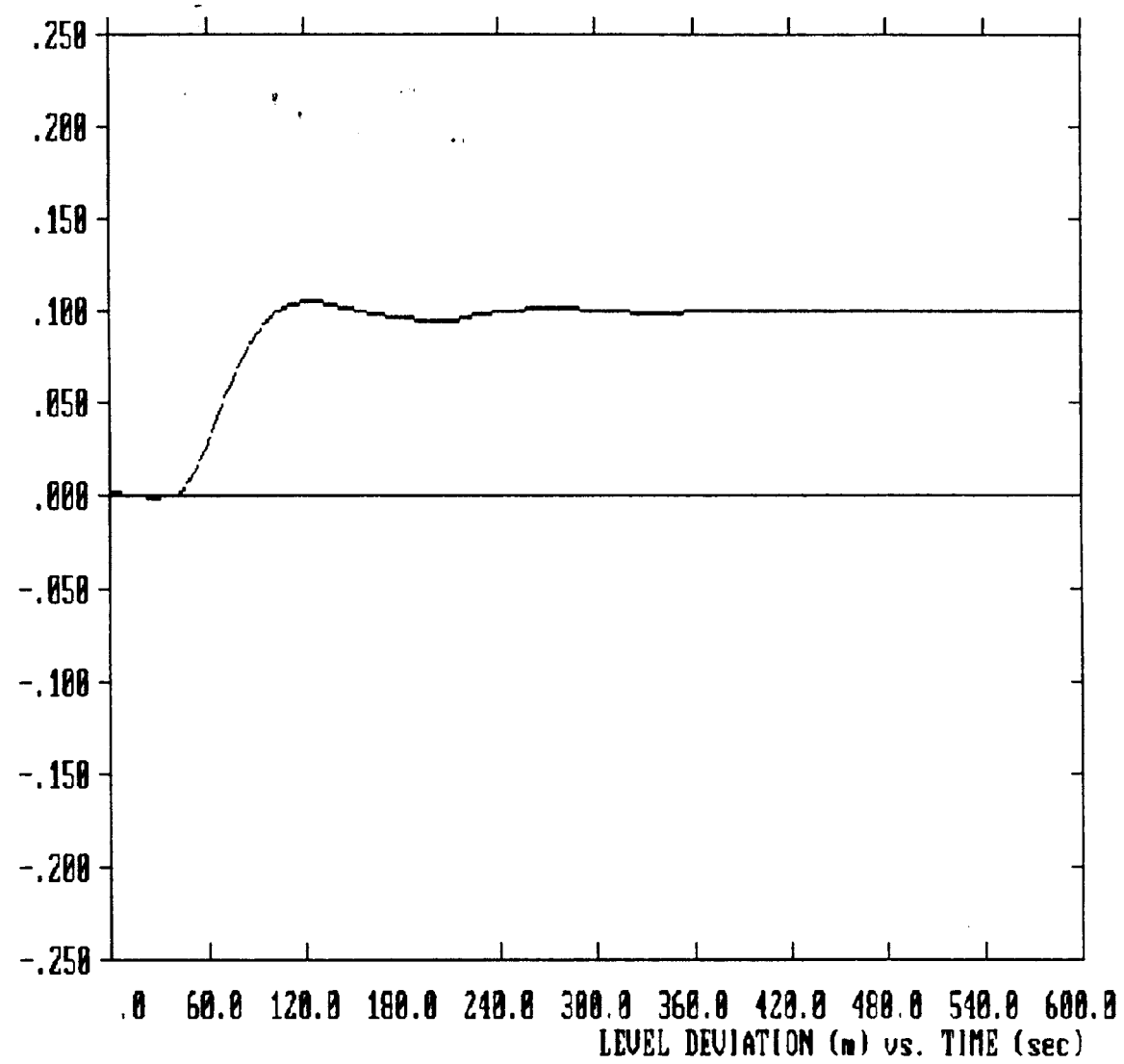
.250
.200
.150
.100
.050
.000
-.050
-.100
-.150
-.200
-.250
.0
60.0
120.0
180.0
240.0
300.0
360.0
420.0
480.0
540.0
600.0
LEVEL DEVIATION (m) vs. TIME (sec)

(c) at 95% power

Chapter 6

SUMMARY, CONCLUSIONS AND RECOMMENDATIONS

6.1 Summary

A good control system for a steam generator water level is of major importance in a pressurized water reactor plant because of its direct impact on plant availability. During plant transients, the level control is complicated by the reverse thermal effects known as shrink and swell. Due to the presence of steam in the tube bundle region, the water level measured in the downcomer temporarily reacts in a reverse manner to water inventory change. These behaviors are accentuated at start-up/low power conditions. In that case, the only true indication for water inventory change is the relationship between steam flow and feed flow. Those flows are, however, too uncertain to be used for control input. It is well-known that controllers traditionally provided do not permit satisfactory automatic level control during start-up/low power conditions. Unsatisfactory performance of automatic level control may either produce a reactor trip or require the operator to take manual control. Either automatic or manual control give a reactor trip rate which is found to be too high.

Efforts to find remedies for these problems have been hindered by the limited capabilities of the current analog controller. The flexibility and computing power of digital controllers makes it possible to accommodate highly sophisticated and advanced algorithms

easily in the software. The range of possible algorithms and solutions to control problems associated with the steam generator water level control is greatly expanded by the use of digital controllers.

The objective of this research is to develop and evaluate a new controller which always ensures a satisfactory automatic control for the steam generator water level from start-up to full power. A big challenge is the treatment of the shrink and swell effects at low power conditions.

A pertinent steam generator model is desired for the following three purposes :

1) to give physical ideas about the steam generator dynamics;
2) to be used for direct incorporation in a controller if it runs fast enough ; and
3) to replace actual plant testing for early evaluation of the controller.

For these purposes, an existing model has been adopted and upgraded in its simulation capability at low power condtions. The model of the tube bundle region was modified for the better simulation of the reverse dynamics due to the shrink and swell effects. To avoid extra computing time due to the modification, the model order remains the same by adding a new dependant variable to the existing state variables. The modification effects were evaluated with a physical interpretation based on transient simulations. It was found that the modification effects might be crucial to the system stability when combined with the controller. We saw that the modification added more

realism to the simulation of the shrink and swell effects and it went in a the desirable direction for the purpose of a new controller design. The simulation results provided by the model were compared to actual plant data. The comparisons provided support for model adequacy.

A mathematical equation was used to represent a conventional controller. In conjunction with the modified steam generator model (non-linear ninth order), the problems encountered by the conventional controller were simulated. To grasp the physical ideas about the nature of problems, a simplified model (linear second order) was deduced through system identification. Based on those physical ideas, possible solutions were proposed and incorporated into a new control equation representing a proposed controller.

The basic approach to the design of the proposed controller is to compensate the level measurement for a calculated component due to the shrink and swell effects. This compensation tends to minimize the reverse indication so disruptive to gainst proper control action. The aim is achieved by the use of two physically-based correction terms and an adaptive adjustment term. The first correction term is the compensation for variation in downcomer level proportional to the calculated change of tube bundle mass. This change is found to be a good measure of the shrink and swell effects. The second correction term accounts for the effect of tube bundle mass change that accompanies change in steady-state operating variables such as power level. The third and final term is an adaptive adjustment to account

for model imperfections. The compensated water level based on these correction terms was found to be less susceptible to the reverse dynamics than the actual level.

The tube bundle mass, which is one of the major variables in the proposed controller, is not measurable but can be made observable using practically available physical sensors. For the on-line estimation of the tube bundle mass, an observer based on the non-linear digital model was developed. The observer was validated for its practical applicability.

The proposed controller was evaluated by the various ways in conjuction with the simulation of existing Westinghous F-type steam generators. First, the physical ideas, on which the proposed controller was based, were validated by looking into the transient responses. Through a sensitivity study, the effectiveness of the proposed correction terms were analytically evaluated and then validated with actual transient simulation. The transient results by the non-linear model showed a good consistency with the analytic expectation based on the linear model. With those studies, the improvements offered by the proposed controller relative to the conventional one were well confirmed.

Next, by applying the proposed controller to a wide spectrum of operating conditions, the performances of the controller were evaluated from the practical point of view. For a long term power increase transient from start-up to full power, the proposed controller showed good performance for the entire range of power.

Water level was settled down within 3 minutes following each 5% power ramp (one minute duration). There were no stability problems. The maximum overshoot in water level occured at low power and was an acceptable magnitude (less than 0.366m). By artificially imposing step changes in reference level, further demonstration of good controller capability was achieved.

6.2 Conclusions

Based on the achievments of the proposed controller, the following conclusions can be drawn :

1) Stability -- It is possible to mitigate or eliminate the stability constraints imposed on the level feedback gains by compensating for the shrink and swell effects on the downcomer level measurement. Such an improvement in stability was proven by an analytic method and then confirmed by simulation using a nonlinear model.

2) Capability -- With stability problems solved, we can set the level feedback gains to the values for the best capability. Even at low power conditions, the proposed controller allows the level feedback gains to be high enough to ensure a fast effective response in counteracting imposed disturbances without any stability problems.

3) Robustness to flow measurements -- With the solution to stability problems and the high level feedback gains, we could eliminate the

contribution of the flow error signals to the control action. Thus the proposed controller became robust (insensitive to flow measurement uncertainties). The satisfactory performance of the controller implied the perfect robustness relative to the flow measurements.

4) Robustness to the design parameters -- Through the sensitivity study of the design parameters for the proposed controller, we found that satisfactory performances were shown over a wide range of parameters. The range was wide enough to assure that the system can tolerate design uncertainties or dynamics changes. Thus the proposed controller was robust or insensitive to variations about the optimum design parameters.

5) Adaptive scheme -- An on-line adaptive scheme was incorporated in the proposed controller to minimize the adverse influence of model imperfections.

6) Achievement of research objective -- The simulation results showed that the proposed controller led to a satisfactory automatic control from start-up to full power including the solution of many of the problems encountered by the existing controller.

6.3 Recommendations

The following recommendations concern possible areas for further research :

1) Shrink and Swell Model -- A good on-line simulation of shrink and swell phenomena is one of the most important contributions to the success of the proposed controller. More efforts should be aimed at physical models of the shrink and swell effects and at related experimental studies.

2) Realistic Features -- For more realism, the digitization effects, sensor noises, measurement uncertainties and actuator disturbances shoud be considered. These practical features are adressed in Appendix [F]. Plant features not yet handled include the actions when switching from the bypass valve to the main valve. They also include possible interactions between the level controller and the pump speed controller.

3) Adaptive Schemes for the controller parameters -- Though the proposed controller has a large robustness to the design parameters, we can, in principle, adjust these parameters in an adaptive manner to achieve better performance. The present study used an off-line basis. A systematic on-line adaptive scheme is desired. That is based on practical measurement capabilities.

4) In-Plant Testing -- For an ultimate evaluation of the feasibility of the proposed controller, in-plant testing should be performed. Before implementation in an actual plant, the testing of the proposed

controller in a plant simulator (and/or in a simplified experimental setup) is desirable.

5) Application to BWR -- We may apply the proposed controller to the feedwater control system of a Boiling Water Reactor plant.

Appendix A

FEED PUMP SPEED CONTROL SYSTEM (from [B1])

The Feed Pump Speed Control System, shown in Fig. A-1, automatically varies the speed of the turbine-driven feedwater pumps in response to changes in secondary plant steam flow. Raising pump speed as steam demand increase produces the following desirable results:

1) Reduced feedwater regulating valve disk and seat erosion.
2) Improved feedwater regulating valve throttling characteristics.

The Feedwater Pump Speed Control System includes a basic comparision circuit consisting of two elements: feed pressure and steam pressure. A summator in the system compares the combined feedwater pump discharge pressure (PT 508) to steam pressure of the main steam header (PT 507). The output of this summator forms an "actual" pressure difference signal ($P_{FEED} - P_{STEAM}$). In the comparision circuit, feed pressure is given an electrically negative signal and steam pressure is given an electrically positive signal. This results in an electrically negative output signal.

The comparision circuit also develops a programmed differential pressure signal. Programmed pressure difference is determined by a portion of the circuit that senses total plant steam flow. The outputs of the four steam flow controlling transmitters are sent to a summing amplifier. The output signal from the summing amplifier is conditioned

within a lag circuit. The time constant associated with this signal conditioner is 120 seconds. This means that the output of summing amplifier is significantly delayed relative to a changing steam flow signal. The overall effect of the lag circuit is to make feed pump speed respond slowly during and after secondary plant transients. After a transient, pump speed will smoothly continue toward a new programmed value. As steam flow increases, the pressure difference between the Main Feedwater System and the Main Steam System is programmed to rise linearly from the no-load value (45 psia).

The actual pressure difference signal should always be electrically negative (feed pressure > steam pressure), while the programmed signal is positive. The signal that is finally sent to the feedwater pump speed master controller is the error signal, (ΔP program - ΔP actual). The master controller is a P.I controller whose theory of operation is similar to that of the total error controller used for the Steam Generator Water Level Control System. The output of the master controller becomes the input for the individual controllers of each of the two turbine-driven feed pumps. Hydraulics are used to throttle steam flow to the feed pump turbines. A complex governing system takes the electrical input received from the individual controller and converts it into a hydraulic-positioning signal, thereby controlling pump speed.

The Feedwater Flow Control System is designed so that volume flow rate can be approximately double without changing the position of the feedwater regulating valve. This is accomplished by raising pump

speed. The following desirable results are obtained by increasing feedwater flow by increasing pump speed in contrast to using feedwater regulating valve position to totally produce an increase:

1) If pump speed is increased, feedwater pressure is significantly higher than it would be if the feedwater regulating valve were opened to increase feedwater flow. Because of this, a sharp increase in steam pressure due to load rejection will not produce an adverse reduction in feed flow.
2) The feedwater regulating valve is allowed to remain near its mid-position. A throttling valve such as the feedwater regulating valve performs in the most stable manner when approximately half the system head loss takes place across the valve.

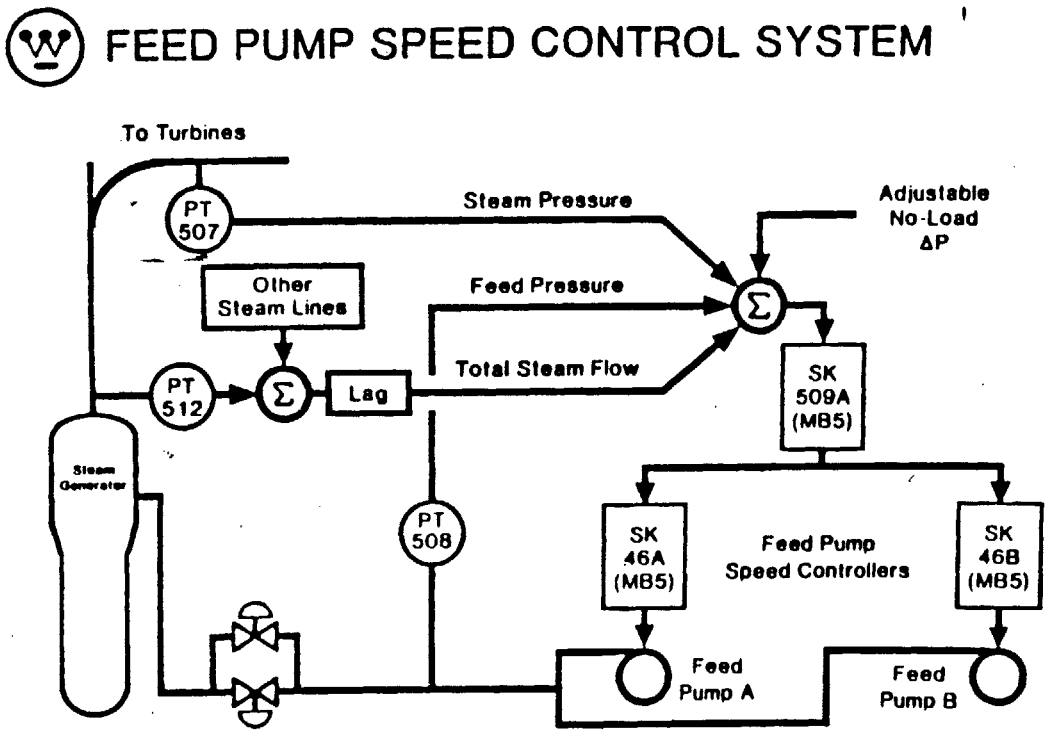

A-1 Feed pump speed control system (from [B1])

Appendix B

DETAILED DESCRIPTION FOR MEASUREMENTS AND ACTUATIONS

(from [B1])

B.1 Level Measurements

The boiling process in the tube bundle region results in a homogeneous mixture of saturated liquid and saturated vapor with no well-defined separation between these two fluid states. This makes liquid level measurement in the tube bundle region an impossibility. However, there is another region that is ideal for sensing steam generator water level. This region, known as the downcomer, is the annular region between the steam generator's inside wall and a shroud surrounding the tubes. The level of the subcooled liquid in this region is an indicator of steam generator water level.

The device used to measure downcomer water level is a differential pressure (D/P) transmitter. The basic internals of such a detector are shown in Fig. B-1. The transmitter operates on the principle that the pressure existing at the bottom of a column of water changes as the height of the water changes. One inlet to the transmitter, "HP" (a high-pressure process connection) is located at the bottom of a column of water (reference leg) whose height is maintained at a constant value. The opposite end of the transmitter, "LP" (a low-pressure process connection) is attached to a column of water whose height may vary -- the downcomer. The transmitter sees a constant high pressure on one of its sides and a variable lower

pressure on the other. The pressure differential is inversely proportional to the height of water in the downcomer and is used to determine the position of an over-range valve shaft. This shaft, in turn, is used to move one end of a flexible member whose opposite end is rigidly fastened. The member is a strain gauge assembly with two pieces of semiconductor material attached. With the over-range shaft in other than the midposition, one piece of material is in compression, while the other is in tension. Compression tends to raise material electrical conductivity, lowering resistance to current flow,while tension has the opposite effect. This imbalance in material resistance can be used to produce a proportional electrical output signal. Measurement of water level with a D/P transmitter could be complicated by operating steam pressure acting on the surface of the water in the downcomer, causing an invalid pressure indication. This potential problem is eliminated by exposing the referece leg to steam pressure, too, cancelling its effect on the transmitter assembly movement.

Each steam generator has five D/P transmitters. Electrical outputs are used for indication, alarm, control, and protection. Each transmitter has its own individual steam generator reference and variable leg taps. Four of the five transmitters provide narrow-range level measurement. The fifth provides wide-range measurement. Both the narrow-range and the wide-range instrument reference leg taps are located at the same elevation, 15.16 m above the steam generator support ring. The narrow-range instrument variable taps are located

10.95 m above the support ring and the wide-range instrument variable tap is located 0.56 m above the support ring. As the terms of "narrow" and "wide" stand for, narrow-range detection supplies 3.66 m of level indication as the full range whereas wide-range detection supplies 14.6 m. Detailed features are shown in Fig. B-2. All four narrow-range detectors on each steam generator provide protection and indication and two of four are used as inputs to the Steam Generator Water Level Control System. For a typical Westinghouse Type F steam generator, the programmed water level for control is set at 50 % of narrow-range from zero to full power and the level set points for protection are 30 % and 80% of narrow-range as the Lo-Lo level and the Hi-Hi level respectively. The wide-range detector is used solely for indication.

B.2 Steam Flow Measurement

Steam flow from each steam generator is measured by sensing the pressure drop that occurs across the flow restrictor of a steam generator. When the electrical output of the D/P transmitter is corrected for steam vapor density, this pressure drop can be used to provide mass flow rate indication. The D/P transmitter used for measuring steam flow are similar to those used for measuring water level.

Each steam generator flow restrictor has two D/P transmitters connected across it. The high pressure taps (upsteam) utilize the reference leg penetrations for two of the four narrow-range level detectors. The low pressure taps (downstream) penetrate the main steam

line just after the restrictor.

A method for density compensation is extremely important if restrictor differential pressure is to be used for steam flow measurement. As plant load increases, two factors that affect mass flow measurement also change -- steam vapor pressure and steam velocity. Steam pressure lowers and steam velocity increases. Velocity increasing causes restrictor ΔP to rise, indicating a similar increase in mass flow rate. At the same time, however, pressure, and thus steam density, has dropped. Unless this effect is electrically compensated for, indicated steam flow will be higher than actual steam flow. The disparity between indicated and actual steam flow would widen as plant load increased to even higher values. For this reason, electrical signal developed by pressure transmitters on the main steam lines are sent to the flow circuits. As steam pressure drops, the compensation signal decreases, keeping indicated flow down to the actual value. Mismatch signals between steam flow and feedwater flow are used for the Steam Generator Water Level Control System and also for the protective system. No mismatch is required for control and the setpoint of flow mismatch for protection is 90 kg/s in a typical plant.

B.3 Steam Pressure Measurement

Steam pressure is measured downstream of each of the four steam generator outlet flow restrictors. Steam pressure is sensed by pressure transmitter, which is shown in Fig. B-3. The type of detector

in the figure is known as a δ - Cell.

Three transmitters are provided on each steam line for various purposes. One use of the electrical signals developed by these transmitters is to compensate the steam flow signal as discussed in the previous section. Only two of the three transmitters are used for this purpose, because only two flow signals are developed for each line. These are also used for control board indication and alarm.

All these three pressure transmitters are used in the Reactor Protection and the Safeguards Actuation System. A low steam pressure of 585 psig from 2/3 pressure transmitters initiates a safety injection signal and a steamline isolation signal. In addition, a steamline isolation signal, which shuts the main steam isolation valves, is generated by a rate/lag, 2/3 coincident circuit. The steamline isolation signal actuates at a trip level of -100 psi (this means an instantaneous drop of 100 psi will cause an isolation signal). The more negative the steam pressure rate, the faster the rate/lag circuit responds. The low steam pressure and high steam pressure rate protective functions are interlocked with the cold leg loop stop valve position. This interlock allows these protective functions to be blocked when performing a cooldown. The setpoints for protection are based on a typical Westinghouse plant.

A fourth transmitter on each steam line is used for automatic control of its respective steam generator power-operated relief valve. In addition, a single detector senses pressure on the combined steam dump bypass header. This measurement is used for steam dump operation,

feed pump speed control, and control board indication.

B.4 Feedwater Pressure Measurement

Feedwater pressure is measured on the feedwater piping common header, between the feedwater heaters and the individual branches to each steam generator. The feedwater pressure transmitter is the same type of pressure transmitter that measures steam pressure. This transmitter's measurement provides a control function input to the feed pump speed control circuit and provides pressure indication on control panel.

B.5 Feedwater Flow Measurement

Feedwater flow to each steam generator is sensed upstream of the steam generator's individual feedwater regulating valve, located just inside the turbine building. The flow element itself is a venturi. The venturi principle of operation takes advantage of the fact that as flow area decreases, velocity increases (kinetic energy increases). This increase in kinetic energy shows up as a pressure (flow energy) decrease. With proper circuit design, the differential pressure between venturi inlet and venturi throat can be used to provide mass flow rate indication. As velocity (and therefore mass flow rate) at the inlet of the venturi increases, the pressure differential across the D/P transmitters goes up by the amount of increase squared. To obtain the flow, the square root of the D/P transmitter signal must be taken. Note that unlike steam flow signals, it is not necessary to

electronically perform any type of density compensation. This is because the assumption that liquid water is incompressible for the range of pressures and temperatures at the feedwater pump discharge is a good one.

Two D/P detectors are connected across each one of the four feedline flow elements. Mismatch signals between steam flow and feedwater flow are used for the Steam Generator Water Level Control System and also for the protective system. No mismatch is required for control and the setpoint of flow mismatch for protection is 90 kg/s in a typical plant.

B.6 Turbine Impulse Chamber Pressure Measurement

Two Bourdon tube transmitters sense turbine steam pressure downstream of the turbine first-stage nozzle block. Since pressure in this region increases with turbine load (even as main steam pressure drops), these detectors can rapidly detect steam power changes. Their sensing point is an ideal location for transmitting a parameter to control and protection circuit, which use program bands that are a function of plant power.

Two impulse chamber pressure transmitters are designated. Either transmitter's signal may be chosen as the impulse pressure input to the Steam Generator Water Level Control System by selector switch. The impulse pressure is used to determine programmed steam generator water level, which is presently set at 50 % for all turbine pressure in a Westinghouse Type F steam generator. The switch also determines which

transmitter will send the turbine impulse pressure signal that is a component of the rod control rate of power change mismatch signal, the rod control T_{Ref} signal.

B.7 Main Feedwater Regulating Valve

An electropneumatic (I/P) converter changes an electrical signal (4 mA to 20 mA) from the total error controller to a signal of proportionally pressurized air. The air is throttled to produce a control air signal. The control air from the converter does not directly act on the feedwater regulating valve diaphragm; instead, it is used to change the position of a small air valve called the positioner. The positioner's air output will go to whatever pressure is required to move the feedwater regulating valve toward the desired position. It is shown in Fig. B-4.

A three-way solenoid valve is located downstream of the positioner. It receives signals from train "A" of the Reactor Protection System. During normal operation it is lined up to allow control air from the positioner to act on a booster relay device. This device amplifies the air signal from the positioner. This is required to supply sufficient pressure to manipulate the feedewater regulating valve's diaphragm. The amplified control air signal acts on the underside of the feedwater regulating valve diaphragm. Increasing air pressure compresses the valve spring and moves the diaphragm upward. This causes further opening of the valve. Decreasing air pressure results in the spring forcing to move the daiphragm downward until the

spring forces and control air forces are balanced. The valve size is 12 inches in diameter.

A deenergized signal to the solenoid actuator of the three-way valve will block air pressure to the feedwater regulating valve diaphragm. At the same time, air pressure acting below the diaphragm will be vented to the atmosphere. The result is rapid (5 second) closure of the feedwater regulating valve.

Indication of feedwater regulating valve position is provided on control panel. An illuminated red light indicates that the valve is off its closed seat, while a green light indicates a fully closed valve.

B.8 Bypass Feedwater Regulating Valve

A bypass line with a bypass feedwater regulating valve is provided around each main feedwater regulating valve. It is shown in Fig. B-5. This valve is designed to operate at plant start-up and low power operations (less than 15 % load), which are outside the range where the main feedwater regulating valve gives optimum response. The bypass valve is 6 inches in diameter. In the fully open position it will pass a maximum of 25 percent of rated steam generator feed flow. The actuation of the bypass valve is similar to the one of the main valve. Because of the relatively small valve size, no booster relay is used.

The bypass valve has automatic and manual features. In automatic, the valve P.I controllers use steam generator water level and

high-auctioneered neutron flux as control inputs. The controller positions the bypass valve to deliever the correct feed flow for the nuclear power level. Indication of the bypass valve position is provided on the Automatic/Manual (A/M) station.

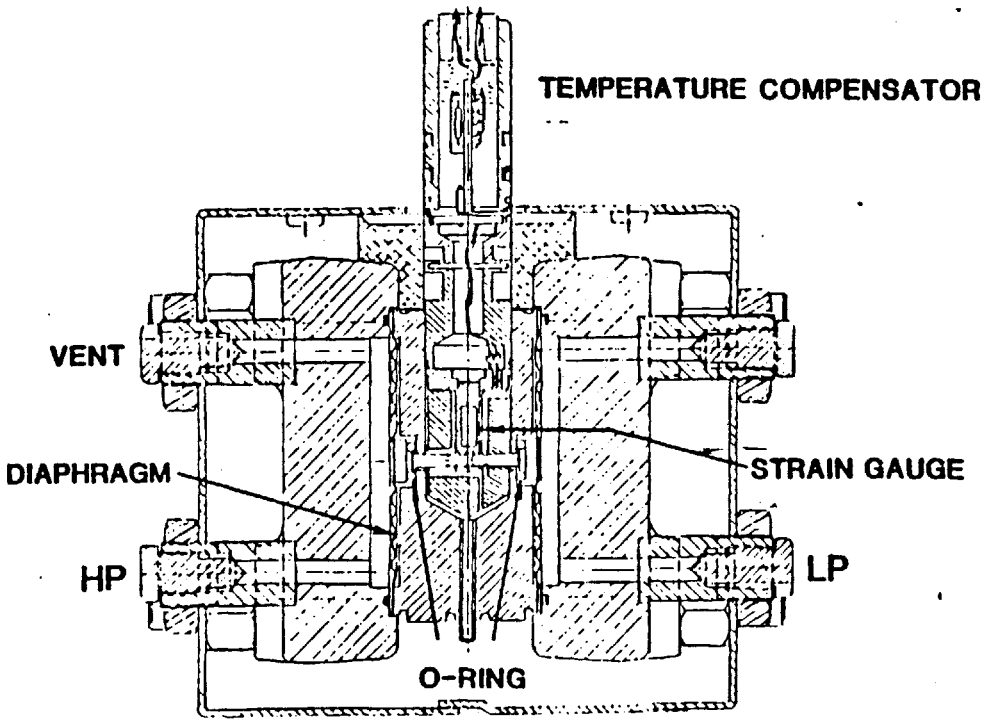

B-1 Internals of differential pressure (D/P) sensor (from [B1])

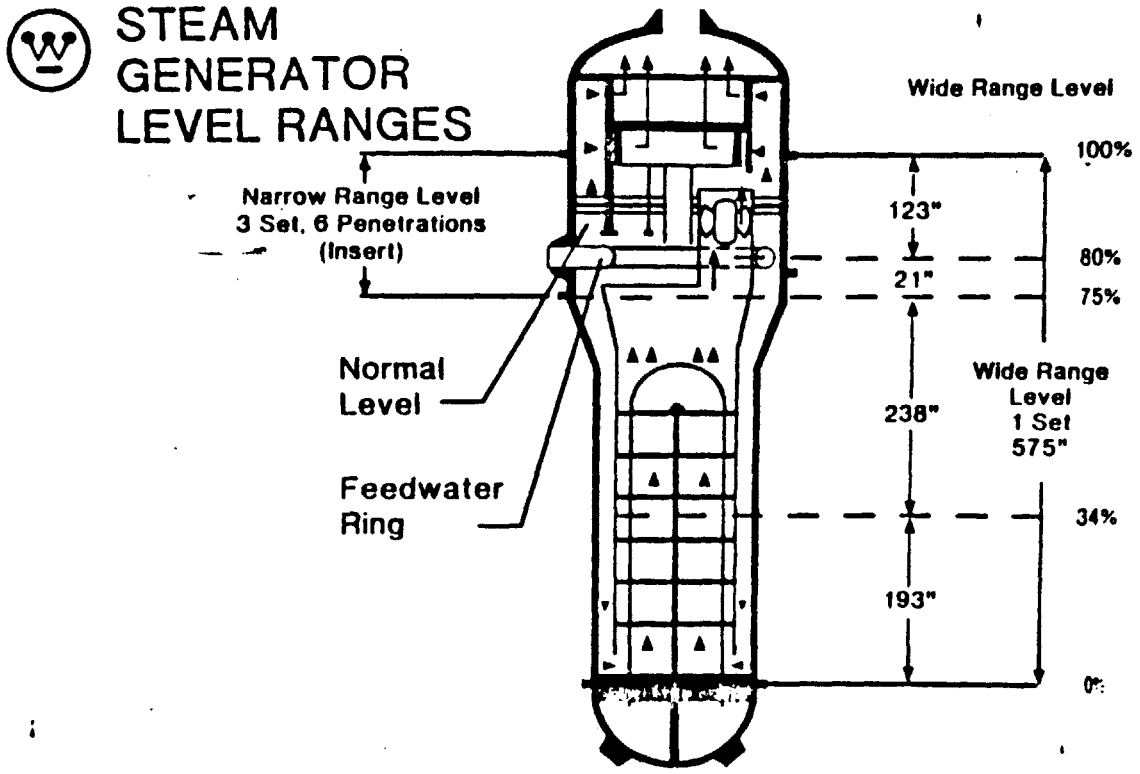

B-2 Steam generator level ranges (from [B1])

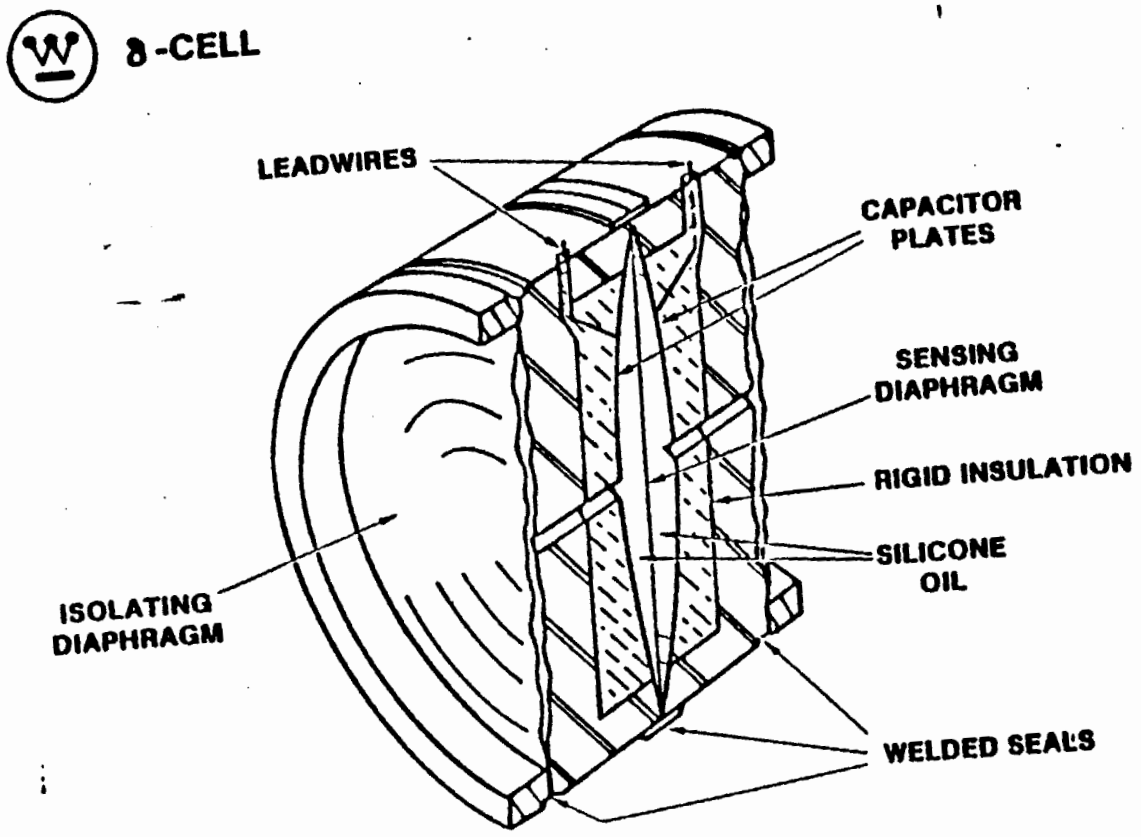

B-3 Internals of pressure sensors (from [B1])

FEEDWATER CONTROL ELECTRO-PNEUMATIC (TYPICAL OF FOUR)

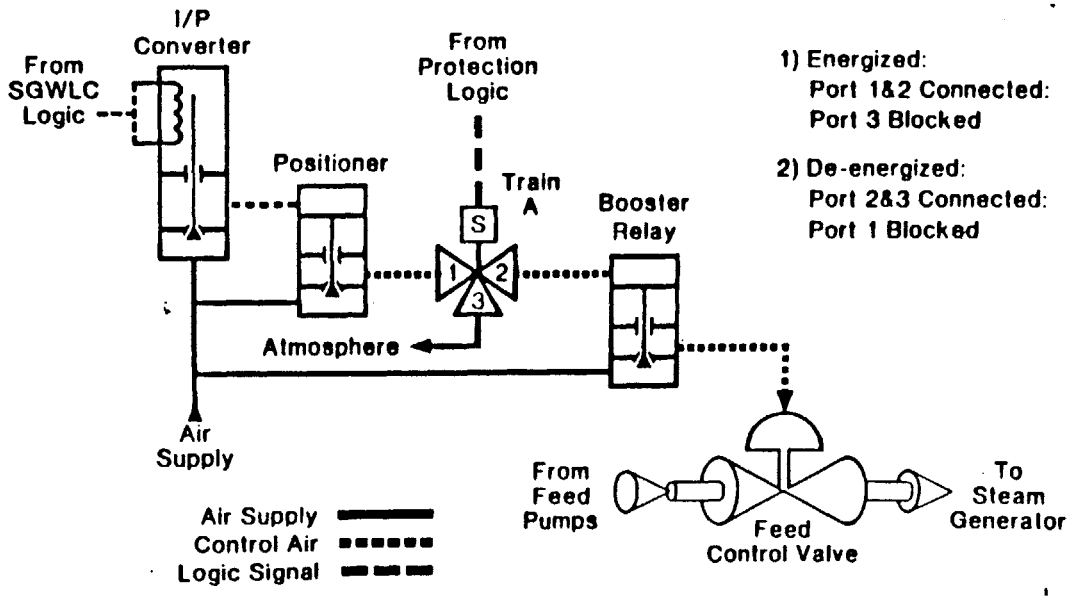

B-4 Actuation with the main feedwater regulating valve

(from [B1])

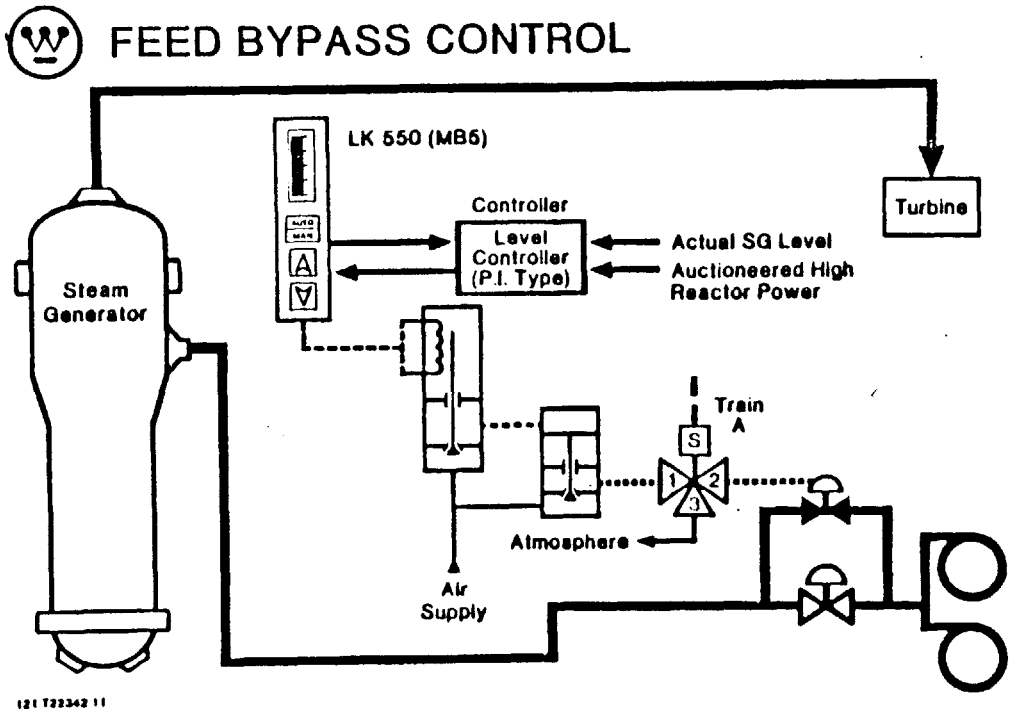

B-5 Actuation with the by-pass feedwater regulating valve (from [B1])

Appendix C

GEOMETRIC MODEL FOR THE STEAM GENERATOR

(Westinghouse Type-F [B1],[W1])

The geometric modeling is to simulate the actual steam generator by using the computer model: The conversion of the actual complex geometry to the equivalant simple geometry. The variation in the geometric modeling may result in the different simulation results.

Fig. C-1 is a schematic of the geometric model for a Westinghouse F-type steam generator showing the nomenclature used in this appendix.

C.1 Tube Bundle Region

As shown in Fig. C-1, the tube bundle region is assigned to the secondary side volume from the top of tube plate to the bottom of transition cone inside the wrapper. The actual geometry is complicated by the bundle of U-tubes. For modeling, this region is simplified to an equivalent cylindrical geometry with the radius R_{TB} and the height L_{TB}. Keeping L_{TB} to the actual height L_4, R_{TB} is calculated. The volume occupied by the U-tube bundle is :

$$V_{OT} = N_t \, (\pi \, d_t^2 / 4) \, \bar{L}_{tube}$$

where

N_t = # of tubes ,

d_t = tube diameter ,

$\bar{L}_{tube}$ = average tube length

$$= A_H / (N_t \pi d_t) \quad , \text{ and}$$

A_H = total heat transfer area

The total volume including V_{OT} is :

$$V_T = \pi R_3^2 L_4$$

Thus, the secondary side tube bundle region volume is :

$$V_{TB} = V_T - V_{OT}$$

Therefore the equivalent radius of the tube bundle region is :

$$R_{TB} = \left(\frac{V_{TB}}{\pi L_{TB}} \right)^{1/2}$$

C.2 Riser

As shown in Fig. C-2 (detailed part of Fig. C-1), the riser is assigned the volume composed of two regions : region 1 is the transition cone ; and region 2 is the swirl vane drain pipes. By the same way in the tube bundle region, the riser is simplified to the equivalent cylinder with the radius R_{Riser} and the height L_{Riser}. Keeping L_{Riser} to the actual height, $L_2 + L_3$, R_{Riser} is calculated. First, the volume of region 1 is :

$$V_1 = \frac{1}{3} \pi L_3 \frac{R_2^3 - R_3^3}{R_2 - R_3}$$

Second, the volume of region 2 is :

$$V_2 = (\pi r_{pipe}^2) (N_{pipe}) L_2$$

where

r_{pipe} = radius of the swirl vane drain pipe

and

N_{pipe} = # of the swirl vane drain pipe

which are derived based on the cross-sectional schematic of the region 2 shown in Fig. C-3.

Thus the volume of the riser is :

$$V_{Riser} = V_1 + V_2$$

Therefore

$$R_{Riser} = \left(\frac{V_{Riser}}{\pi L_{Riser}} \right)^{1/2}$$

C.3 Steam Dome and Downcomer Region

The steam dome and downcomer region is assigned the outside of the tube bundle and riser regions as shown in Fig. C-1. The water

level is calculated based on the geometry of this region. As shown in Fig. C-1, this region is composed of 5 regions with volumes of V_1, V_2, V_3, V_4, and V_5 . Each region has its own cross-sectional area, which is uniform with the region except the region 4. The cross-sectional area and height of each region can be specified by the given physical dimension in Fig. C-1.

A challenge is to estimate the equivalent cross-sectional area of the region 3, at which the water level is measured. This is the outside region of the riser region 2. Using the cross-sectional layout of this region shown in Fig. C-3, the cross-sectional area is :

$$A_3 = \frac{V_3}{L_2}$$

where

$$V_3 = \pi R_1^2 L_2 - (\pi r_{pipe}^2)(N_{pipe} + 1) L_2$$

$N_{pipe} + 1$ = the number of the swirl vane drain pipe including the center pipe

The volumes of the regions are :

$$V_1 = 0 \text{ (reglected)},$$

$$V_2 = (\pi R_1^2) L_1,$$

$$V_3 = A_3 L_2,$$

$$V_4 = \frac{1}{3} \pi L_3 \left(\frac{R_1^3 - R_4^3}{R_1 - R_4} - \frac{R_2^3 - R_3^3}{R_2 - R_3} \right)$$

and

$$V_5 = \pi L_4 (R_4^2 - R_3^2)$$

The water level is calculated as follows :

Let the vapor volume V_V; the water level L_w; and $L_T = L_1+L_2+L_3+L_4$

1) $V_V \leq V_1$:

$$L_w = L_T$$

2) $V_1 < V_V \leq (V_1 + V_2)$:

$$L_w = L_T - (V_V - V_1) / \pi R_1^2$$

3) $(V_1 + V_2) < V_V \leq (V_1 + V_2 + V_3)$ (normal narrow range) :

$$L_w = L_T - L_1 - (V_V - V_1 - V_2) / A_3$$

4) $(V_1 + V_2 + V_3) < V_V \leq (V_1 + V_2 + V_3 + V_4)$:

$$L_w = L_T - L_1 - L_2 - [B - (B^2 - 4AC)^{1/2}]/ 2A$$

where

$$A = \pi d \left(\frac{R_2 - R_3}{L_3} \right) ,$$

$$B = (2 R_2 + d) \pi d \text{ , and}$$

$$C = V_V - V_1 - V_2 - V_3$$

5) $(V_1 + V_2 + V_3 + V_4) < V_V \leq (V_1 + V_2 + V_3 + V_4 + V_5)$:

$$L_w = L_4 - \frac{V_G - V_1 - V_2 - V_3 - V_4}{\pi (R_4^2 - R_3^2)}$$

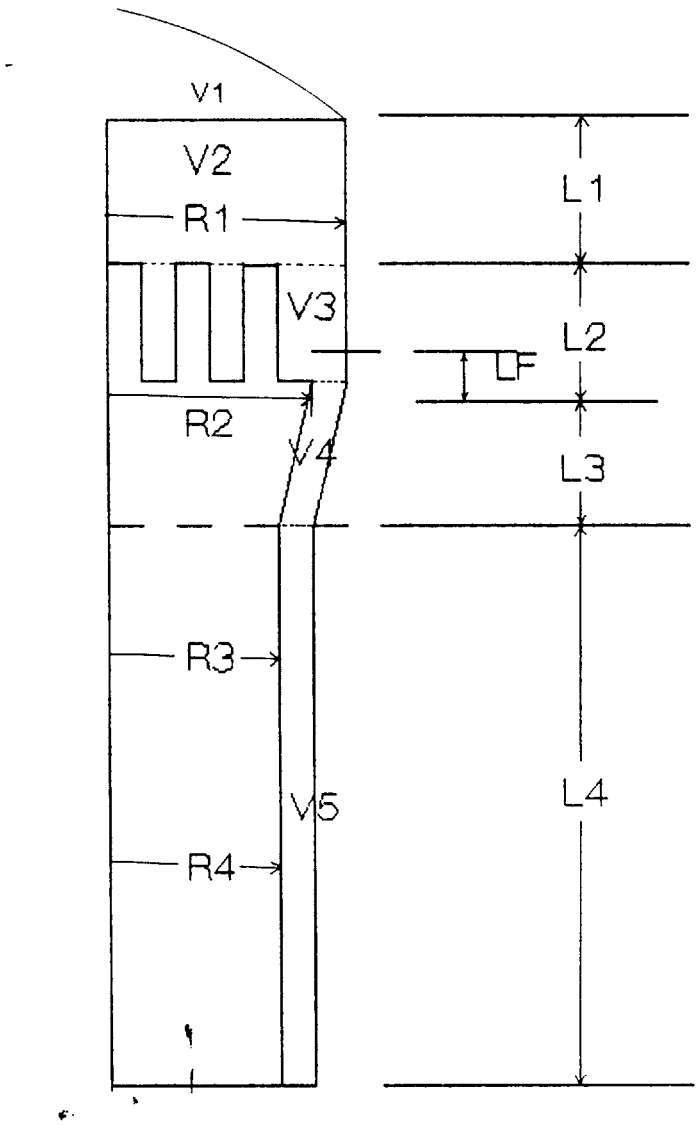

C-1 Steam generator geometrical representation

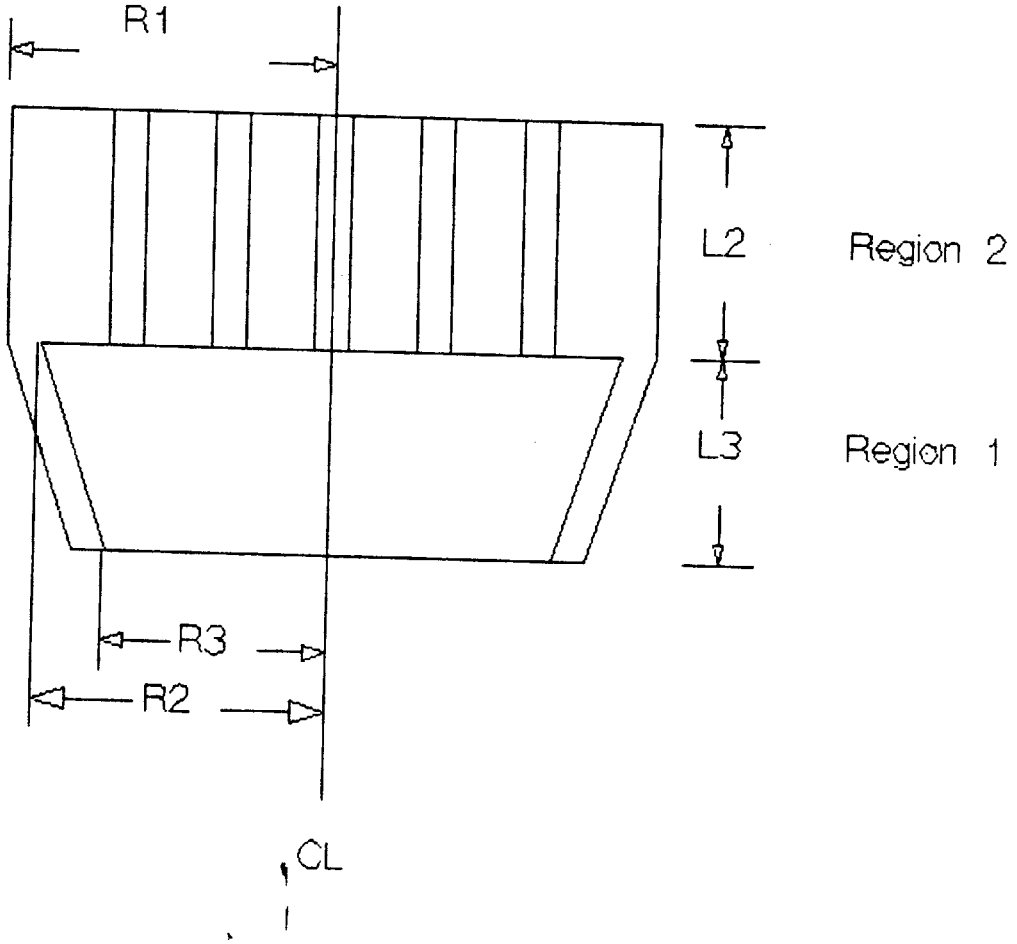

C-2 Riser region model

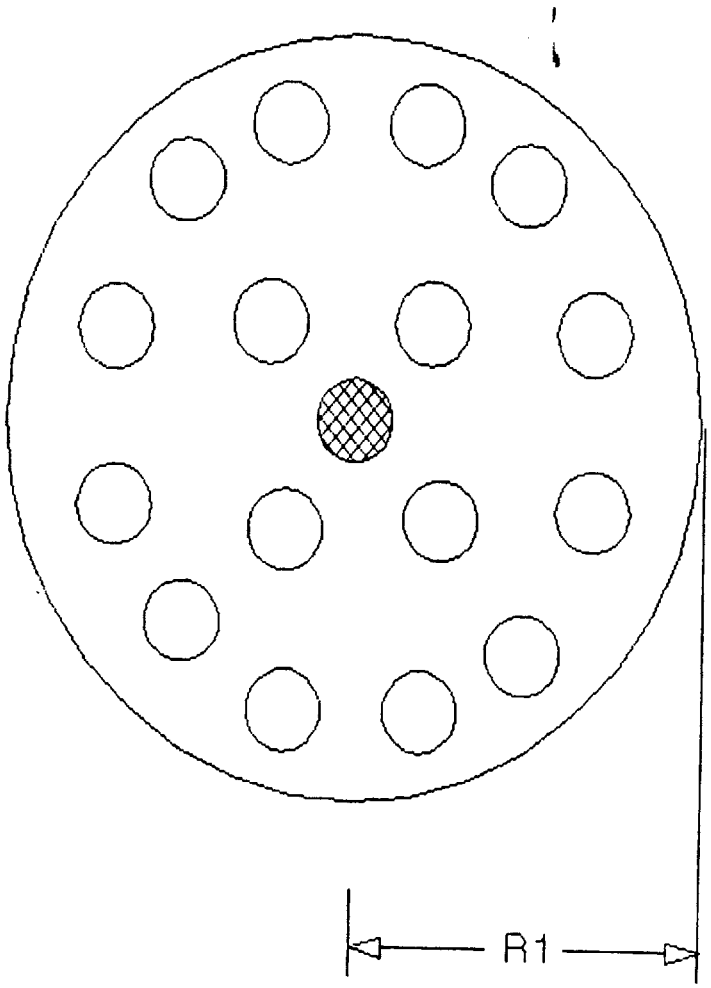

C-3 Riser region layout

Appendix D

SYSTEM IDENTIFICATION

System identification is the experimental approach to process-modeling. In practice, the procedure of system identification is iterative. It starts with transient analysis to select a model structure. The unknown parameters in the model are then estimated with the data obtained from experiments. Based on the results, the model structure can be improved. A typical technique for system identification is the least square method, which determines parameters in the way to minimize the summation of variance between the experiment data and the model-based data.

In this reseach, system identification may be performed to obtain a simplified linear model for the steam generator level dynamics. The simulation results with the detailed non-linear model are used as the experiment data. From the transient response to the step input and some priori physical knowledge, we can deduce a linear model structure as follow :

$$L_w(s) = [G_1/s - G_2 / (1 + \tau_2 s)] W_{fw}(s) \qquad (D\text{-}1)$$

To the step input $W_{fw}(s) = W_{fw} / s$, the transient response is :

$$L_w(t) = [G_1 t - G_2 (1 - e^{-t/\tau 2})] W_{fw} \qquad (D\text{-}2)$$

To determine unknown parameters G_1 , G_2 and τ_2, we may use the least square method as follow :

Determine these parameters in the way to minimize

$$Q = \sum_i (L_{wi} - L_w(t_i))^2 \qquad \text{(D-3)}$$

where

t_i = i-th data point,

L_{wi} = calculated level at t_i with detailed non-linear model,

and

$L_w(t_i)$ = calculated level at t_i with simplified linear model given in Eq. (D-2).

In this case, however, we can easily determine the parameter without using the least square method. The procedures are :

1) As t goes to the infinity, $L_w(t)$ becomes a linear line with a slope $G_1 W_{fw}$. Thus from the long term behavior of level by the detailed non-linear model, we can estimate the value of G_1 (W_{fw} is a known transient input).

2) Then, we can decompose the level response (by the detailed non-linear model) into the linear line $G_1 W_{fw} t$ (the mass capacity term) and the remaining part (the reverse dynamics term). From the remaining part, we can estimate the parameters G_2 and τ_2 as shown in Fig. D-1 (a).

These parameters are functions of power. At various power levels,

the decomposed level responses are shown in Fig. D-1 (a) to (e). The numerical values for these parameters from this system identification are given in Table 4.1-1 .

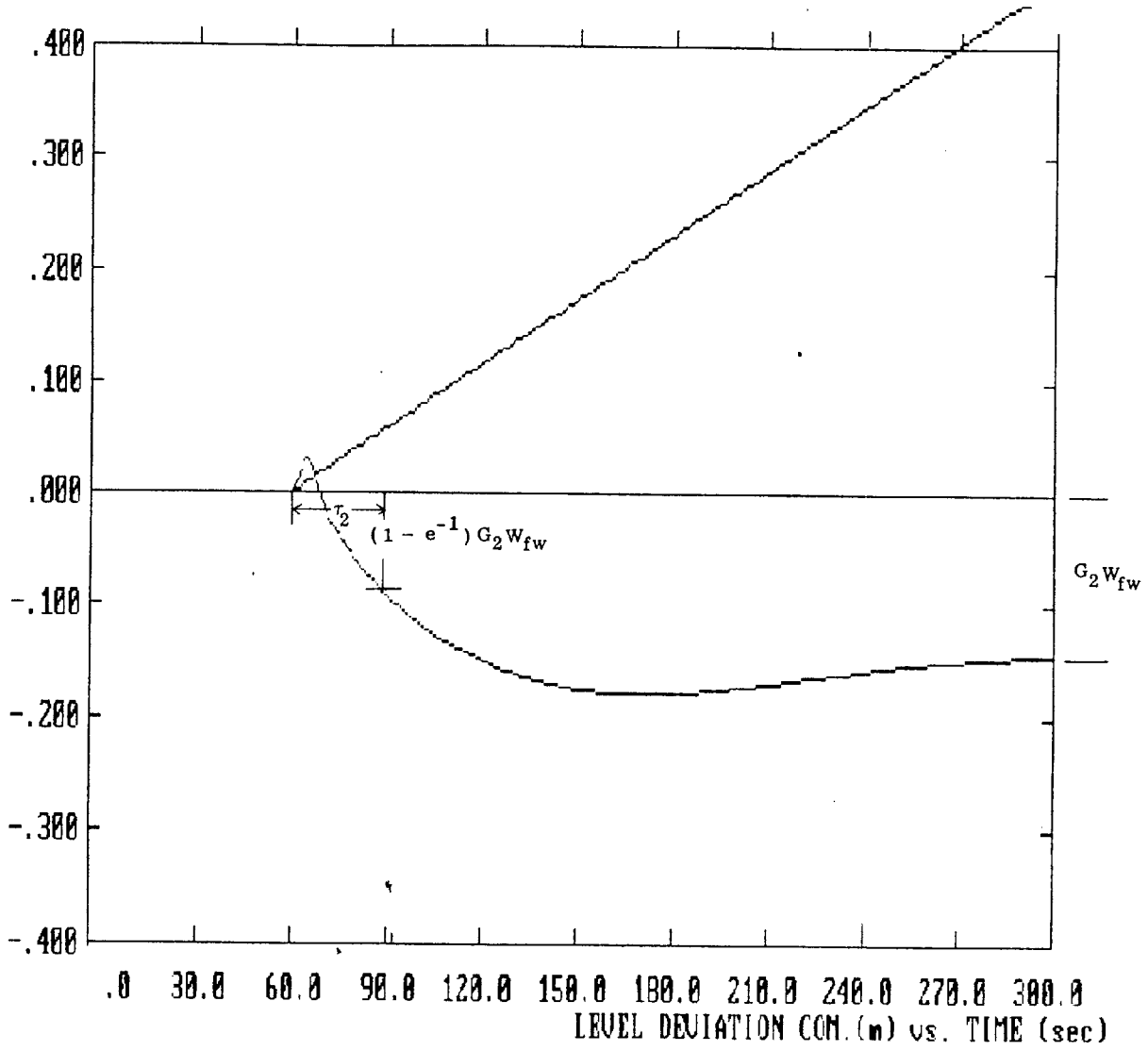

D-1 Decomposed ingredients of water level for the system identification

(a) at 5% power

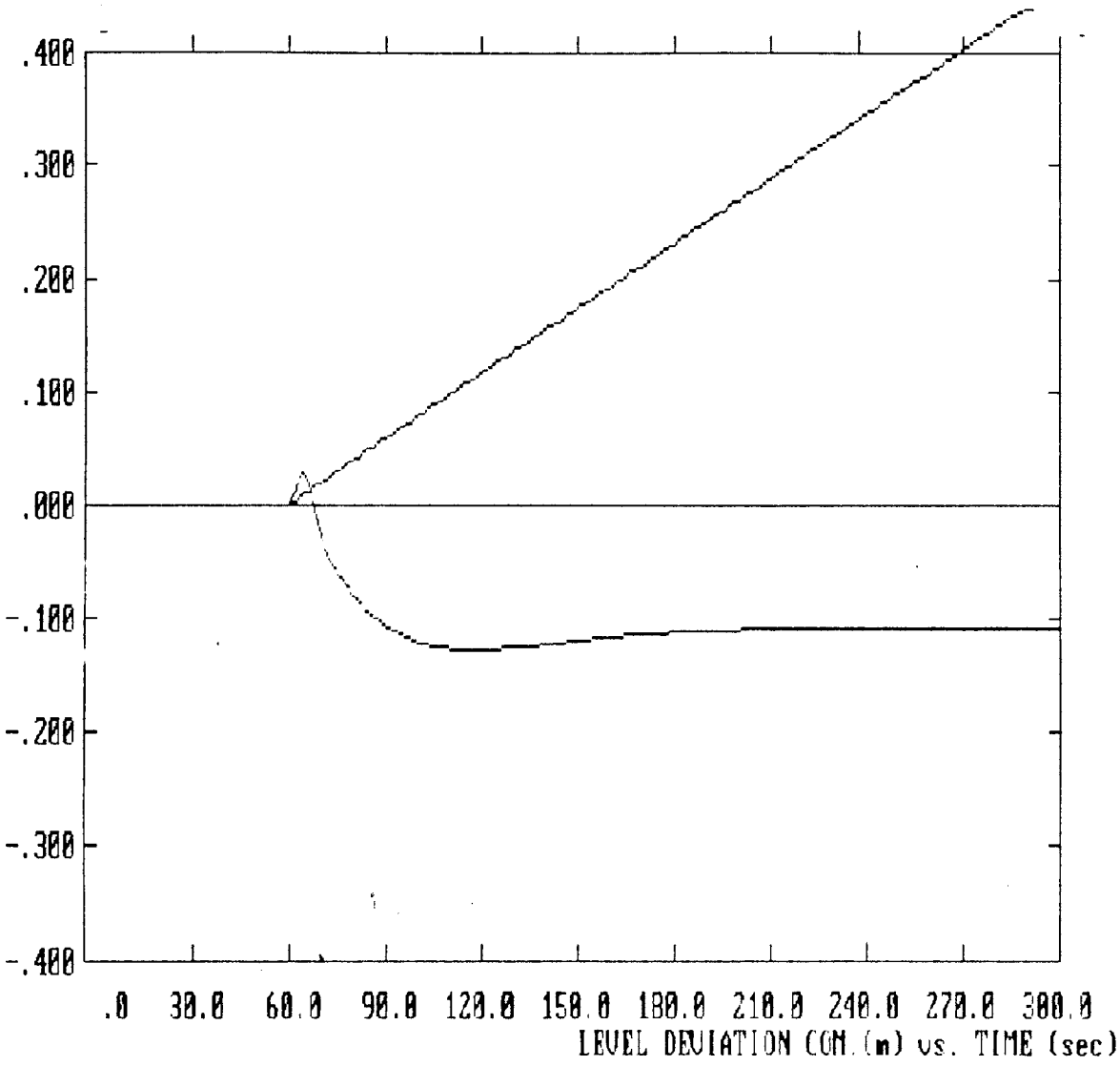
.400
.300
.200
.100
.000
-.100
-.200
-.300
-.400
.0
30.0
60.0
90.0
120.0
150.0
180.0
210.0
240.0
270.0
300.0
LEVEL DEVIATION CON.(m) vs. TIME (sec)

(b) at 10% power

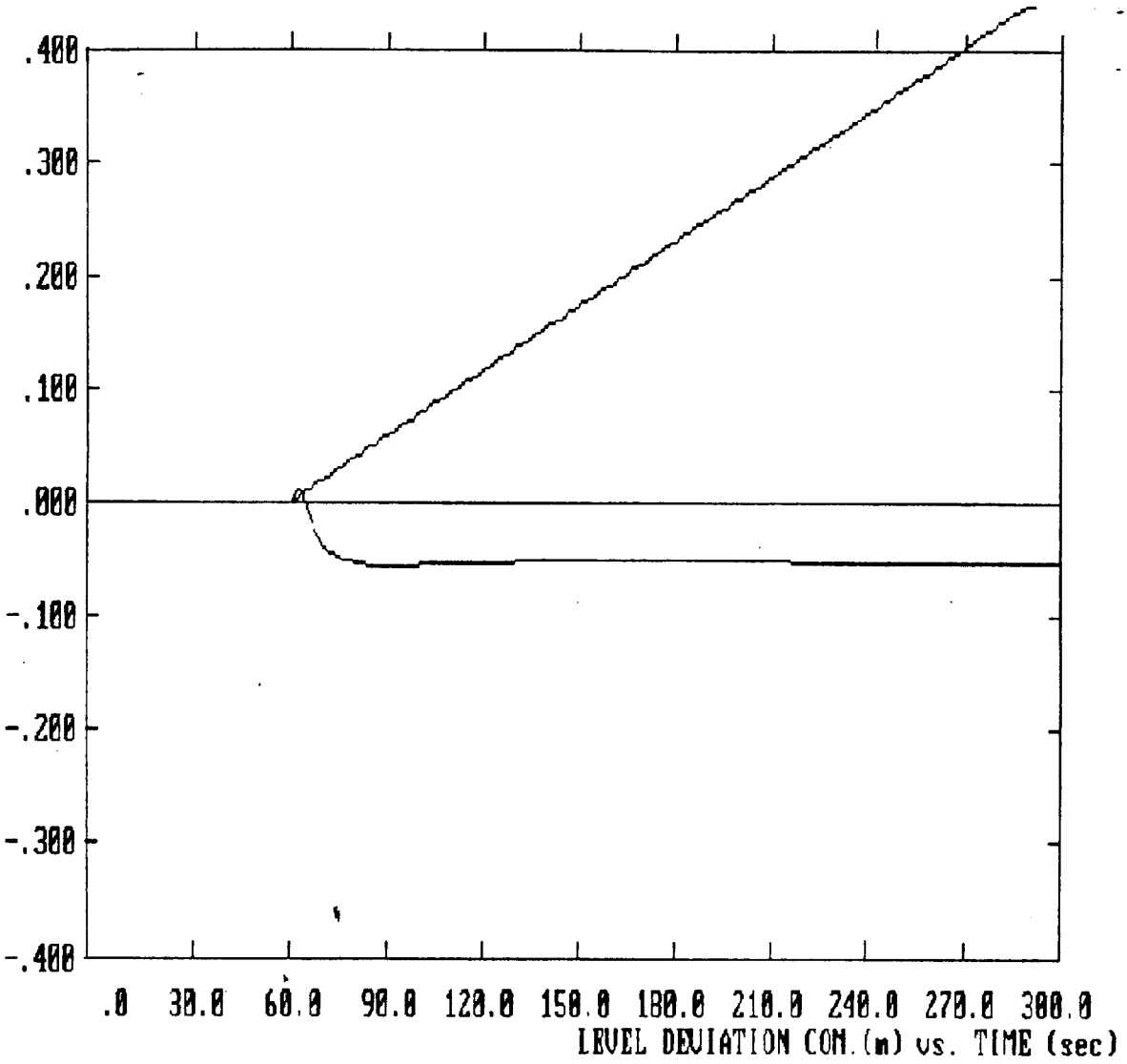
.400
.300
.200
.100
.000
-.100
-.200
-.300
-.400
.0
30.0
60.0
90.0
120.0
150.0
180.0
210.0
240.0
270.0
300.0
LEVEL DEVIATION COM.(m) vs. TIME (sec)

(c) at 30% power

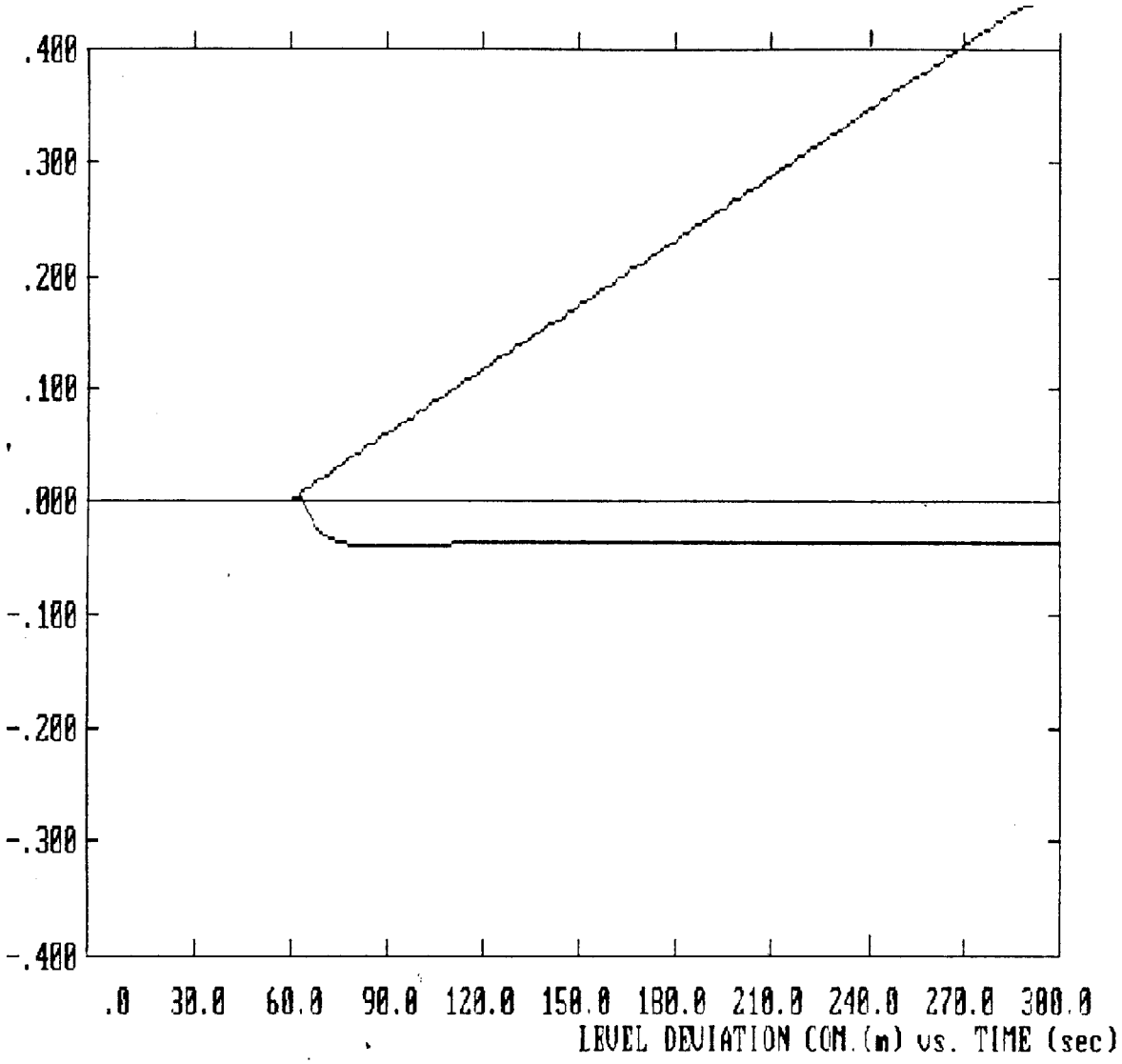
.400
.300
.200
.100
.000
-.100
-.200
-.300
-.400
.0
30.0
60.0
90.0
120.0
150.0
180.0
210.0
240.0
270.0
300.0
LEVEL DEVIATION COM.(m) vs. TIME (sec)

(d) at 50% power

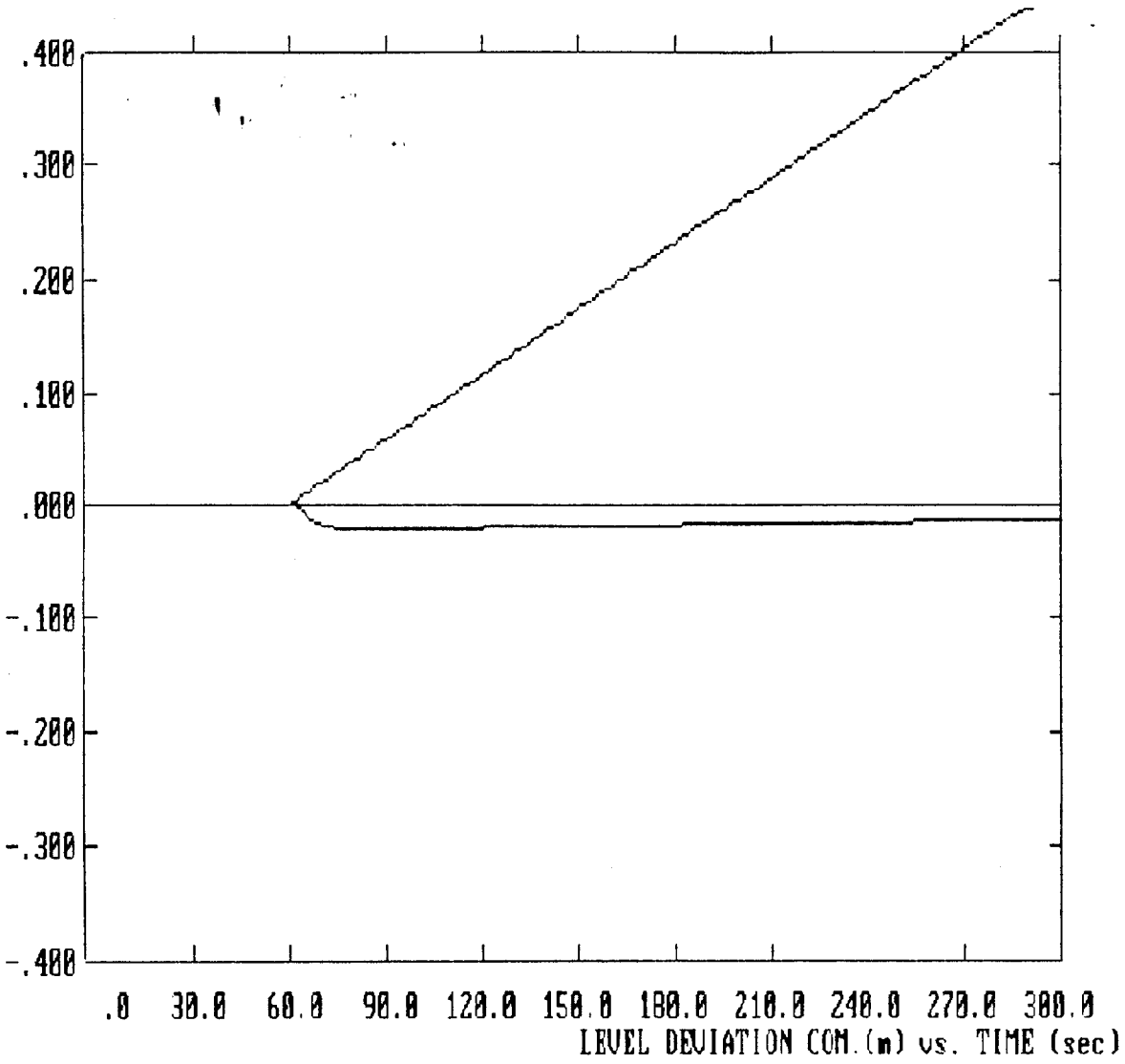
.400
.300
.200
.100
.000
-.100
-.200
-.300
-.400
.0
30.0
60.0
90.0
120.0
150.0
180.0
210.0
240.0
270.0
300.0
LEVEL DEVIATION COM.(m) vs. TIME (sec)

(e) at 95% power

Appendix E

STABILITY ANALYSIS OF LINEAR SYSTEM

In this appendix, are presented two methods for the stability analysis of linear system, which are used in this thesis.

E.1 Routh's Stability Criterion

The Routh's stability criterion is an algebraic procedure for determining whether a polynomial has any zeros in the right half s-plane. It involves examining the signs and magnitudes of the coefficients of the characteristic equation without actually having to determine its roots.

The procedures are to be described by applying to a third-order polynomial equation, which is the same as the characteristic equation of the steam generator level control system with a P.I controller. (See Ref. [O1], [S5], [H2] for general description of the Routh's stability criterion)

The third-order polynomial equation is :

$$a_o s^3 + a_1 s^2 + a_2 s + a_3 = 0$$

1) As a necessary condition for the stability (all roots lie on the left half s-plane), all the coefficient must be positive.
2) If all coefficients are positive, arrange the coefficients of the polynomial in rows and columns according to the following pattern:

s^3	a_o	a_2
s^2	a_1	a_3
s^1	$\frac{a_1 a_2 - a_o a_3}{a_1}$	
s^o	a_3	

The second condition for the stability is that all terms in the first column of the array have positive signs.

3) The necessary and sufficient condition that all roots lie on the left half s-plane is that

a_o, a_1, a_2, and a_3 must be positive and

$a_1 a_2 > a_o a_3$

E.2 The Root-Locus Method

The basic idea behind the root-locus method is that the values of s which make the transfer function around the loop equal to -1 must satisfy the characteristic equation of the system. The root-locus method enables us to find the closed-loop poles from the open-loop poles and zeros with the gain as parameter.

The procedures are to be described by applying to the steam generator level control system with a P.I controller, which has two zeros (z_1, z_2) and three open loop poles (p_1, p_2, p_3). (See Ref. [O2], [S5],[H2] for general description of the root-locus method)

The characteristic equation is :

$$K \frac{(s - z_1)(s - z_2)}{(s - p_1)(s - p_2)(s - p_3)} = -1 \qquad \text{(E-1)}$$

1) Three roots of this equation (closed-loop poles) move from p_1, p_2, and p_3 to z_1, z_2, and the infinity as the gain K increases from 0 to the infinity.

2) Eq. (E-1) can be split into two equations by equating the angles and magnitudes of both sides, respectively.

Angle condition :

$$\angle(s - z_1) + \angle(s - z_2) - \angle(s - p_1) - \angle(s - p_2) - \angle(s - p_3) =$$

$$\pm \pi (2k + 1) \qquad (k = 0,1,2,\cdots)$$

magnitude condition :

$$K |s - z_1| |s - z_2| = |s - p_1| |s - p_2| |s - p_3|$$

The values of s which fulfill the angle and magnitude conditions are the roots of the characteristic equation, or the closed-loop poles. A plot of the points of the complex plane satisfying the angle condition alone is the root locus. The roots of the characteristic equation corresponding to a given value of the gain can be determined from magnitude condition.

Appendix F

PRACTICAL FEATURES

F.1 Digitization Effects

The development of a new controller are based on the premise that the current analog control loop will be replaced with the digital controller. As a common approach usually taken at the conceptual design stage of the digital system, we start with the continuous domain. However, we have to move from the continuos domain to the discrete one ultimately.

The essential elements of a digital controller are samplers and holders. A sampler converts a continuous signal into a train of pulses occuring at the sampling instants 0, T, 2T, $\cdots$, where T is the sampling period. It generates a sequence of discrete input for the digital controller (compter). A holding device converts the sampled signal into a continuous signal, which approxiamtely reproduces the signal applied to a sampler. The simplest holding device converts the sampled signal into one which is constant between two consecutive sampling instants (called a "zero-order holder"). It converts a sequence of discrete output from the digital controller (computer) into a continuos input for the acuation.

For the discrete system, z-tranformation is used as the Laplace transform for the discrete function. That is:

$$Z[\ x^*(t)\ ] = \sum_{k=0}^{\infty} x(kT)\ z^{-k} \qquad \text{(F-1)}$$

with a relation to the Laplace variable s

$$e^{Ts} = z \qquad \text{(F-2)}$$

All analyses used in the continuous system with Laplace tranforms are also applicable to the discrete system with z-transforms. It is only noted that the left half s-plane is equivalent to the inside of a unit circle with its center at the origin in z-plane. Therefore, all poles of the z-transfer function must lie inside the unit circle for the stability.

We also use a P.I control logic in the discrete domain with some approximation. The discrete equivalents of P.I controller is :

$$K_p \left(1 + \frac{1}{T_i\, s} \right) \quad \text{(continuos)}$$

$$\rightarrow \quad K_p \left(1 + \frac{T}{2\, T_i} \frac{1 + z^{-1}}{1 - z^{-1}} \right) \quad \text{(discrete)} \qquad \text{(F-3)}$$

In Eq. (F-3), it is noted that the sampling period T is shown in the discrete system as an additional control parameter. So the selection of the sampling period is another major topic in the digital controller design.

For more detailed information, see Ref. [F1], [A1], and [E1].

F.2 Other Practical Features

For adding more realism, we can consider the sensor noise (Ref. [U1]). The following simple sensor noise model can be incorporated in the controller simulation:

$$y = x + b + r \tag{F-4}$$

where

- y : modeled measurement for the control input,
- x : calculated value by the process simulation
- b : bias (given as a constant value) and
- r : random noise (normal distribution)

As another practical feature, the disturbance due the actuator (valve) non-linearity may be consider. The following model for the actuator disturbance can be incorporated in the controller simulation:

$$W_{fw} = (W_{fwc})^{1+\delta} + W_b \tag{F-5}$$

where

- W_{fw} : actuator output,
- W_{fwc} : actuator input from the controller,
- δ : random variable (normal distribution) accounting for the valve non-linearity

and

- W_b : random bias (normal distribution) accounting for the valve leakage

Time delays due to sensor response, actuation and control algoritm execution must be considered for more realism.

NOMENCLATURE

A	Area (m^2)
E	Energy Content (J)
H	Specific Enthalpy (J/kg)
H'	Specific Enthalpy of Flowing Mixture (J/kg)
I	Inertance (m^{-1})
L	Lengh (m)
M	Mass Content (kg)
p	pressure (Pa)
q_B	Power or Heat Transfer Rate (W)
r	Radius (m)
T	Temperature (oK)
t	Time (s)
U	Specific Internal Energy (J/kg)
u	Velocity (m/s)
V	Volume (m^3)
W	Flowrate (kg/s)
$<\alpha>$	Void Fraction
$\phi_{\ell o}$	Two-Phase Multiplier
ρ	Density (kg/m^3)

Subscripts

fw	Feedwater
ℓ	Liquid
ℓs	Saturated Liquid

n	Riser Outlet
o	Downcomer Exit
p	Parallel-to-Crossflow Transition
r	Riser Inlet
R	Riser
s	Steam
SAT	Saturated
SUB	Subcooled
TB	Tube Bundle
TBC	Tube Bundle Crossflow Region
TBP	Tube Bundle Primary Side
v	Vapor
vs	Saturated Vapor

Controller Related Variables

L_w	Actual Water Level
Y_w	Compensated Water Level
ϵ	Control Error Signal
K_p	Proportional Gain
T_i	Integral Time
s	Laplace Variable
p	pole
z	zero

REFERENCES

[A1] K.J. Åström and B. Wittenmark, Computer Controlled Systems, Prentice-Hall , 1984

[B1] Steve Brown, "NSSS Process Control - Miscellaneous Control/Protection System: SGWLCS Lesson," Northeast Utility Co. , Jun. 1986

[B2] Paul M. Blanch, "Offsite Information System as an Engineering Analysis Tool," Northeast Utility Co., EPRI Seminar, May 1986

[C1] Jung In Choi, " SGLCP (Steam Generator Level Controller Program) Manual," Unpublished Information, N.E.D, MIT, 1987

[D1] E.J. Davison, "On Pole Assignment in Linear Systems with Incomplete State Feedback," IEEE Transactions on Automatic Control, Vol. AC-15, No. 3, 348-351, Jun. 1970

[E1] "Digital Feedwater Controller for a BWR : A Conceptual Design Study," EPRI NP-3323, 1984

[F1] G.F. Franklin and J.D. Powell, Digital Control of Dynamic Systems, Addison-Wesley, 1980

[G1] A. Gautier, et al, "U-Tube Steam Generator Modelling: Application to Level Control and Comparison with Plant Data," Boiler Dynamics and Control in Nuclear Power Station, BNES, London, 1980

[G2] Graham and McRuer, Analysis of Nonlinear Control Systems, Dover Press, 1971

[G3] A. Gelf, Applied Optimal Estimation, MIT Press, MA, 1974

[H1] R. Hocepied, et al, "Automatic Control of the Water Level of

Steam Generators from 0% to 100% of the Load," Nuclear Energy, 17, 133-142, 1978

[H2] Hsu and Meyer, Modern Control Principles and Applications, McGraw-Hill, 1968

[H3] Hahn, Theory and Application of Lyapnunov's Direct Method, Prentice-Hall, 1963

[I1] E. Irving and C. Bihoreaux, "Adaptive Control of Non-Minimum Phase System: Application to the P.W.R. Steam Generator Water Level Control," 19th IEEE Conf. Control and Decision, Albuquerque, NM, Dec. 1980

[I2] E.Irving, et al, "Towards Efficient Full Automatic Operation of the PWR Steam Generator with Water Level Adaptive Control," Boiler Dynamics and Control in Nuclear Power Stations, BNES, London, 1980

[L1] J. Lewins, Nuclear Reactor Kinetics and Control, Pergamon Press, 1978

[L2] Y. Landau, Adaptive Control : The Model Reference Approach, Marcel Dekker, New York, 1979

[N1] Northeast Utility Co., Verbal Communication with Plant Personnel

[O1] K. Ogata, Modern Control Engineering, Prentice-Hall, N.J.,1970

[P1] A. Parry, et al, "Recent Progress in SG Level Control in French PWR Plant," Boiler Dynamics and Control in Nuclear Power Stations, BNES, London, 1985

[R1] B.W. Rhee, "Dynamic Model of a U-Tube Steam Generator for Real Time Simulation," MIT PhD Thesis, 1985

[S1] "Simulator Training Manual," Sequoyah Nuclear Power Plant

[S2] "Unplanned Reactor Trips on SWEC Plants," Unpublished Information, Stone and Webster Electric Co., 1984

[S3] "Operating Plant Evaluation Code", the Stoller Co.

[S4] W.H. Strohmayer, "Dynamic Modeling of Vertical U-Tube Steam Generators for Operational Safety Systems," MIT PhD Thesis (CSDL-778), Aug. 1982

[S5] S.M. Shinners, Modern Control System Theory and Application, Addison-Wesley, 1979

[U1] G. Ueo, "Uncertainty Estimation and Signal Validation for Performance Monitoring of Power Plant Components," MIT PhD Thesis 1986

[W1] "Reference Safety Analysis Report," Westinghouse, Revision 3, Jun. 1972

[W2] "PWR Plant System Manual," Westinghouse

[W3] "Feedwater Control System," Unpublished Information, Westinghouse